

EPA-600/3-83-035

May 1983

A REGIONAL SCALE (1000 KM) MODEL
OF PHOTOCHEMICAL AIR POLLUTION
Part 1. Theoretical Formulation

by

Robert G. Lamb
Meteorology and Assessment Division
Environmental Sciences Research Laboratory
Research Triangle Park, North Carolina 27711

ENVIRONMENTAL SCIENCES RESEARCH LABORATORY
OFFICE OF RESEARCH AND DEVELOPMENT
U.S. ENVIRONMENTAL PROTECTION AGENCY
RESEARCH TRIANGLE PARK, NORTH CAROLINA 27711

EPA-600/3-83-035

May 1983

A REGIONAL SCALE (1000 KM) MODEL
OF PHOTOCHEMICAL AIR POLLUTION
Part 1. Theoretical Formulation

by

Robert G. Lamb
Meteorology and Assessment Division
Environmental Sciences Research Laboratory
Research Triangle Park, North Carolina 27711

ENVIRONMENTAL SCIENCES RESEARCH LABORATORY
OFFICE OF RESEARCH AND DEVELOPMENT
U.S. ENVIRONMENTAL PROTECTION AGENCY
RESEARCH TRIANGLE PARK, NORTH CAROLINA 27711

DISCLAIMER

This report has been reviewed by the Environmental Sciences Research Laboratory, U.S. Environmental Protection Agency, and approved for publication. Mention of trade names or commercial products does not constitute endorsement or recommendation for use.

AUTHORS' AFFILIATION

The author is on assignment with the U.S. Environmental Protection Agency from the National Oceanic and Atmospheric Administration, U.S. Department of Commerce.

PREFACE

The original goal of this work was to develop a specific model of regional scale photochemical air pollution. However, as the work progressed and new developments and ideas continually emerged, the need was seen for a general modeling framework within which the various physical and chemical processes that play important roles could be treated in modular form. This would permit ongoing incorporation into the model of state-of-the-art techniques without the need to overhaul the model each time. The basic framework we have developed for this purpose is based on phenomenological concepts and is presented in Section 2. Most of the subsequent sections develop specific modules for use in implementing a first generation model. Therefore, the techniques presented in those sections should not be viewed as an integral part of the model but rather as one of many possible methods that could be utilized to perform specific functions. Moreover, in a few instances the techniques presented require further development before they can be employed in an operational role. This is particularly true of the mixed layer submodel given in Section 4.1. In short, the reader will find in this report rather exact specifications of the framework of a regional scale model but only rough sketches of some of the components that are required to make the model work. In later parts of this report we will describe the components that we assemble to construct an operational, first generation regional scale model of photochemical air pollution.

As we approach the task of simulating air pollution chemistry and dispersion over multi day 1000 km scale domains, we move into a realm of problems that lies largely beyond the scope of empirical science. The classical definition of turbulence and the empirical data that form the basis of current short range diffusion models are insufficient to treat dispersion and chemistry at long range. As a consequence we must turn to theoretical science to provide the additional information we need and to formulate expressions for the quantities we wish to predict. With this shift from empiricism to theory there arises the somewhat philosophical question of whether the limitations of theoretical science preclude the formulation of a model that can provide the information that regulatory officials require. One way of phrasing this question is this: given perfect emissions data, perfect knowledge of the chemical kinetics, an exact solution to the turbulence closure problem, and an infinitely large and fast computer, could one predict within the limits of accuracy required the quantities needed in regulatory studies? In Sections 6 and 7 we discuss this important question in detail, and we lay the basis for an effort parallel to the model development work that in principle can provide quantitative estimates of the uncertainty, or "error-bounds", associated with the predictions of regional scale models. In the author's view this task is crucial to the meaningful utilization of model predictions in decision making processes.

R. G. Lamb
February 1982

ABSTRACT

A theoretical framework for a multi-day 1000-km scale simulation model of photochemical oxidant is developed. It is structured in a highly modular form so that eventually the model can be applied through straightforward modifications to simulations of particulates, visibility and acid rain.

The model structure is based on phenomenological concepts and consists of three and one-half layers. The interface surfaces separating the layers are functions of both space and time that respond to variations in the meteorological phenomena that each layer is intended to treat. Among the physical and chemical processes affecting passage and distribution of photochemical concentrations that the model is designed to handle are: horizontal transport; photochemistry; nighttime wind shear and the nocturnal jet; cumulus cloud effects; mesoscale vertical motion; mesoscale eddy effects; terrain effects; subgrid scale chemistry processes; natural sources of hydrocarbons, NO_x , and stratospheric ozone; and wet and dry removal processes, e.g., washout and deposition.

The predictability of pollutant concentrations at long range is considered along with such related problems as the parameterization of "mesoscale" diffusion and the design of model "validation" experiments. A basis is established for estimating quantitatively the levels of uncertainty associated with dispersion model predictions.

This report focuses on theoretical aspects of the model and the question of predictability. Results of the model's performance and quantitative assessments of predictability will be presented in subsequent parts of this report.

CONTENTS

Preface	iii
Abstract	v
Figures	viii
Tables	x
Acknowledgments	xi
1. Introduction.	1
2. Derivation of Prognostic Equations for Layers 1, 2, and 3.	18
3. The Interface Surfaces H_i	26
The model's top surface H_3	26
The subsidence inversion base surface, H_2	26
The nocturnal jet top, H_1	27
The surface layer top, H_0	32
4. The Interface Fluxes: F_i	35
Flux across the subsidence inversion base: F_2	36
Equations governing w_2 , $f\theta/\Delta\theta$, and z_2	42
Flux across the jet layer top: F_1	53
Flux across the surface layer top: F_0	62
5. Derivation of Diagnostic Equations for Layer 0.	65
Mass balance equations in $V - \delta V$	71
The flux component F_0 in the case of no cumulus clouds	75
Modifications of F_0 to include effects of cumulus clouds	77
Equations for the cell-averaged and fluctuation concentrations in layer 0.	80
6. The Representation of Atmospheric Motion:	
Winds and Turbulence.	83
A game analogy of diffusion modeling	88
The statistical bases for air pollution modeling	99
The global family of atmospheric states.	100
General considerations.	100
The constraints of physical laws.	103
7. Mesoscale Diffusion; Concentration Predictability; Model "Validation"; and Related Topics.	114
Remarks.	125
The character of diffusion at long range.	125
Parameterization of dispersion.	132
Predictability of concentration at long range	133
Model validation exercises.	136
Predicting impact of future emissions distributions	137

8.	Formulation of Miscellaneous Fields and	
	Model Parameters	139
	Source emissions rates $\langle S \rangle_1$, S	140
	The plume volume fraction, ζ	141
	Turbulence parameters w_* , λ_* , etc on H_0	
	and in Layer 0.	142
	The plume entrainment velocity, v	144
9.	Computer Solution of the Governing Equations	146
	Introduction.	146
	Transformation of the governing equation	148
	Solution of the r equation, (9-5)	154
	Solution of the $\hat{\gamma}$ equation, (9-17).	180
	Solution of the $\gamma'_{(\alpha)n}$ equation, (9-24).	189
10.	Summary of Model Equations	199
References		207
Appendices		
A.	Transformation of the governing equations	
	to curvilinear coordinates	210
B.	Criteria for validity of the steady-state	
	assumption in layer 0.	217
C.	Explicit forms of the b and g matrix elements	
	b_{nm} , g_n that enter in the $\hat{\gamma}$ equation	221

FIGURES

<u>Number</u>		<u>Page</u>
1-1a.	Schematic illustration of the "dynamic" layer structure of the regional scale model and the daytime phenomena each layer is designed to treat	7
1-1b.	Same as 1-1a except nighttime phenomena	8
1-2.	Idealized view of the fate of polluted air parcels in a cumulus humilis topped mixed layer. A, parcel receives emissions; B, it rises and cools; C, saturation occurs producing cloud droplets; D, the parcel descends and dries; and E, it receives new emissions and/or deposits pollutants on surfaces. From E the cycle begins anew.	11
1-3.	Hypothetical case of an urban area in which O_3 and NO are segregated into 16 cells. If this distribution is simulated in a regional model whose cell size is the large outer square, subgrid chemistry phenomena arise.	14
4-1.	Schematic vies of cumulus clouds transporting material aloft from the mixed layer and acting to lower the surface H_2	35
4-2.	Projection of a unit horizontal square on the surface H_2	38
4-3.	Probability density of vertical velocity w_2 near the mixed layer top (H_2) derived from the numerical model of Deardorff (1974).	45
4-4.	Comparison of the true solution of Equation (4-27a) with the approximation (4-27c)	47
4-5.	Schematic illustration of typical temperature, wind speed and mixing ratio profiles over (a) rural and (b) urban areas at night	54
4-6.	Intersection of the surface $z = z_1$, defined by Equation (3-5), with elevated terrain features. A fraction σ_{T1} of the grid cell's horizontal area A is intersected by terrain.	57

4-7.	Coincidence of surfaces H_0 and H_1 with terrain surface. Surface area of H_0 lying on terrain is approximated as $(\sigma_{T0} - \sigma_{T1})A$	64
5-1.	Schematic illustration of Layer 0 and the notation used to describe processes within it	67
5-2.	Partitioning of surface flux into cumulus clouds and Layer 1.	79
6-1.	The global family of possible outcome matrices A resulting from the throw of 3 dice 3 times (see text for more details).	89
6-2.	Number of matrices in the global family with given element sum S	93
6-3.	Illustration of the set Ω of complex functions $u(k, \omega)$ that comprise the global family of fluid flow velocity Fourier Transforms. Set Ξ represents functions that satisfy purely mathematical constraints like Equation (6-15). Set Δ represents functions that satisfy mass continuity relationships, like Equation (6-18); and set π denotes functions that satisfy all other laws like momentum and entropy. Intersection of Δ and π defines the global family Ω of u	106
7-1.	Mapping of the set Ω and W in flow field function space into the set Γ and C in concentration function space for a given source distribution S	117
7-2.	Plot of a hypothetical example of the function $\phi(x_0, t x_s, t')$ for given source location x_s and receptor site x_0 . The function ϕ has unit value inside the shaded regions and is zero everywhere else	121
7-3.	Trajectories of particles emanating from x_s in the ensemble W associated with the single wind observation $\bar{u}(x_0, t) = \bar{u}_0$, where $x_s \approx x_0$	127
7-4.	Plumes from the C ensemble that mark the limits of lateral motion.	134
9-1.	Illustration of the grid, coordinate system, and other parameters on which the 2-D representation (9-46) and (9-47) of the function $r(\eta, \xi)$ is based. . . .	163

9-2a.	Results after 50 time steps from a simulation by the biquadratic scheme of the advection of a conic shaped cloud in a rotating flow. Angular speed of rotation. Angular speed of rotation $\omega = (40\Delta)^{-1}$ and $K_H = 0$	167
9-2b.	Same as 9-2a, except results are after 100 time steps.	168
9-3a.	Same as Figure 9-2a using the bicubic scheme	169
9-3b.	Same as 9-3a, except results are after 100 time steps.	170
9-4.	Comparison of simulations by 3 differencing schemes of the advection of an ellipsoidal cloud in a rotating flow. Panels a-e display different cross-sections of the cloud (indicated in the upper right corner of each panel) after 1 complete rotation of the cloud, 100 time steps in the case of schemes Q and S, 150 steps in the case of Z	173
9-5.	Sample solutions of the $\hat{\gamma}$ equation (9-78).	187
9-6.	Temporal behavior of the reaction system (9-24) for initial species concentrations: (a) $NO = 100$ ppb, $NO_2 = 500$ ppb, $O_3 = 30$ ppb, $O = 10^{-5}$ ppb; and (b) one-tenth the values used in (a). Arrows indicate the time steps used by the model to arrive at concentrations at $t = 100$ s.	195
A-1.	The curvilinear coordinate system used in the model.	210
B-1.	Two-layer system for analysis of the steady-state mixing assumption.	217

TABLES

<u>Number</u>		<u>Page</u>
9-1.	Computer time requirements for the Q, S and Z schemes	179

ACKNOWLEDGMENTS

The model development work reported here was initiated in 1977 by Dr. Kenneth Demerjian through a contract with Systems Applications, Inc. Without his support in the intervening years, this work would not have been possible.

Dr. Robert Papetti reviewed the original derivation of the model equations presented in Section 2 and provided a number of suggestions which lead to a greatly improved set of notation and also to a more elegant formulation of some of the basic mathematical relationships. I am indebted to him for this help and for his interest in this work generally.

In the course of this project I have benefited by discussions on many topics with my colleague, Dr. Francis Binkowski. I would also like to acknowledge the capable assistance of Mr. Chris Mitchell in developing and testing the new differencing schemes presented in Section 9.

Finally, I extend my sincere appreciation to Ms. Barbara Hinton for her patience and stamina in typing and retyping this manuscript and its innumerable equations. My thanks go also to Ms. Sheila Pinkney for her noble efforts in typing the original draft.

SECTION 1

INTRODUCTION

The objective of this study is to develop a model that can guide the formulation of regional emissions control strategies. In this task the model will be called upon to estimate the impact of sources on concentrations in remote regions, to determine the pollution burden that cities impose on distant neighbors, and eventually to analyze quantitatively emissions impacts on acid rain, visibility and fine particulates. We believe that in all these roles the utility and credibility of the model will be determined primarily by the extent to which it accounts for all the governing physical and chemical processes. Accordingly, in this report we will formulate a generalized model that in principle can treat all of the chemical and physical processes that are known, or presently thought, to affect the concentrations of air pollutants over several day/1000 km scale domains. Among these processes are (not necessarily in order of importance):

1. Horizontal transport;
2. Photochemistry, including the very slow reactions;
3. Nighttime chemistry of the products and precursors of photochemical reactions;
4. Nighttime wind shear, stability stratification, and turbulence "episodes" associated with the nocturnal jet;

5. Cumulus cloud effects--venting pollutants from the mixed layer, perturbing photochemical reaction rates in their shadows, providing sites for liquid phase reactions, influencing changes in the mixed layer depth, perturbing horizontal flow;
6. Mesoscale vertical motion induced by terrain and horizontal divergence of the large scale flow;
7. Mesoscale eddy effects on urban plume trajectories and growth rates;
8. Terrain effects, on horizontal flows, removal, diffusion;
9. Subgrid scale chemistry processes--resulting from emissions from sources smaller than the model's grid can resolve;
10. Natural sources of hydrocarbons, oxides of nitrogen (NO_x) and stratospheric ozone (O_3);
11. Wet and dry removal processes (e.g., washout and deposition).

Of the 11 processes listed above, only the first and last have been treated in any detail in the regional scale models of air pollution developed to date. In fact, a review of these models (see, for example, reviews by Drake and Bass in Henderson et al. 1980) reveals that virtually all Eulerian type models are in essence simply expanded urban scale models. They account for the physical processes that are active during daylight hours and within 10 km or so of a source, but they neglect both the processes that are important beyond this distance and those that are active at night.

When this model development work was initiated some 3 years ago, an attempt was made to derive from the observational evidence available at

that time an estimate of the minimum vertical and horizontal resolutions necessary to describe regional scale air pollution phenomena. The aim was to arrive at the best compromise between the restrictions imposed upon the model by computer time and memory limitations and the need to describe as accurately as possible all of the governing processes cited earlier. We reviewed the nitric oxide (NO), O₃ and meteorological data reported in Siple et al. (1977) by the participants of the 1975 Northeast Oxidant Transport Study and made the following observations:

- o Ozone concentrations at an elevation of 2 km are consistently between 40 and 60 ppb regardless of the concentrations below this level. Exceptions occur when the base of the synoptic subsidence inversion is above 2 km. On these occasions, O₃ values at 2 km can reach 80 ppb. This suggests that the top of the model need not be much higher than 2 km (~ 800 mb).
- o After the passage of a cold front and the onset of high pressure in the study area, dry, strong subsidence inversions based between 1700 m and 2000 m frequently occur. Ozone values within these inversions usually appear to be about 50 ppb near the base and to increase upward. Nitric oxide concentrations within the inversion are very lean and are approximately constant with height (see, for example, Siple et al. (1977), Flight 12, Spirals 1 through 3; Flight 6, Spirals 1 through 3). These observations and the extreme dryness of the inversion air indicate that this air might be of stratospheric origin. If so, entrainment of inversion layer air into the mixed layer may result in a contribution of stratospheric O₃ to ground-level oxidant

concentrations. This can be handled in the model by appropriate material fluxes across the inversion base.

- o Nitric oxide is usually uniformly distributed in the mixed layer (the layer between the ground and the base of the subsidence inversion). Exceptions consist chiefly of periods when maximum NO occurs near the ground. Both characteristics can be accommodated in a model that represents the mixed layer with only 2 vertical levels.
- o For the majority of the flights, there is strong evidence of a positive correlation between O_3 concentration and dew point temperature. The latter is a measure of the concentration of water vapor (see Flight 3, Spirals 1 through 6; Flight 8, Spiral 1). This suggests that the bulk of the O_3 observed in the study area is of an anthropogenic origin; if it originated in the stratosphere, there would be a negative correlation between O_3 and dew point. These observations also suggest that estimates of the rate of transport of O_3 and its precursors through the top of the mixed layer by large-scale vertical motion and cumulus clouds can be obtained from estimates of the transport of water vapor in the upper atmosphere by these same processes. The latter estimates can be obtained from surface and rawinsonde meteorological data.
- o When the Boston urban plume spreads out to sea during daylight hours, O_3 concentrations in the plume are usually at a maximum near the sea surface, and they decrease steadily upward (see for example, Flight 2, Spirals 2, 3, 6, 7, 8; Flight 9, Spiral 1).

A plausible explanation of this pattern is that as the warm air moves over the colder water, the layer of air in contact with the water is cooled and thereby stabilized. As this occurs, turbulent motions that otherwise would mix pollutants vertically are attenuated, and rich mixtures of NO_x and hydrocarbons remain at low altitudes. With sufficient sunlight, large quantities of O_3 can be produced in this air. The same type of stabilization occurs at night over land as air in contact with the ground is cooled by long wave radiation, but, in this case, the absence of sunlight results in a net decrease in O_3 concentration. These phenomena play a crucial role in determining the ultimate species concentrations in an aged air mass that has spent part of its life over the sea or over the land at night. To account properly for these processes, the model must possess the ability to simulate the development of these shallow, stable layers adjacent to the ground and the rates of chemical reactions within these layers.

- o Marked changes in wind speed and direction often occur near the interface between surface stable layers and the air mass above and at the interface between the daytime mixed layer and the subsidence inversion. The model must have separate layers to treat each of these regions.

The characteristics of the O_3 distribution described above would require at the very least a 3-level model: one level assigned to the surface layer, a second level to the remainder of the daytime mixed layer, and a third layer atop the mixed layer. The top level would be used in conjunction with the mixed layer to account for downward fluxes of strato-

spheric O_3 as well as upward fluxes of O_3 and its precursors into the subsidence inversion layer above. Material that entered this top layer could be transported by winds aloft to areas outside the modeling region; it could reenter the mixed layer by subsidence or entrainment; it could enter precipitating clouds and be rained out of the atmosphere; or it could undergo chemical transformation. Representing the subsidence inversion, where cumulus clouds often form under stagnant high pressure conditions, the top level of the model could be instrumental in simulating the chemical sink effect of heterogeneous (within cloud droplets) reactions among O_3 , its precursors, and other natural and pollutant species. Including cloud effects in the model would be especially important in simulating sulphur dioxide (SO_2) and sulfates.

Having 3 layers in a model is insufficient in itself to simulate the phenomena we have discussed above. For example, 3 layers of constant thickness are incompatible with the spatial and temporal variability that the radiation inversion and mixed layer thicknesses are known to have. What is needed in the model is 3 "dynamic" layers that are free to expand and contract locally in response to changes in the phenomena they are intended to treat. The model we will develop here possesses this property. Figure 1-1 illustrates the vertical structure of this model and the physical phenomena that each layer is intended to simulate. The surfaces that comprise the interfaces of adjacent layers in our model are variable in both space and time in order that each layer can keep track of the changes that occur in the particular set of phenomena that layer is designed to describe (summarized in Figure 1-1). A consequence of this structure is that the volumes of the grid cells vary in both space and time. By contrast, in

Daytime

Layer Functions

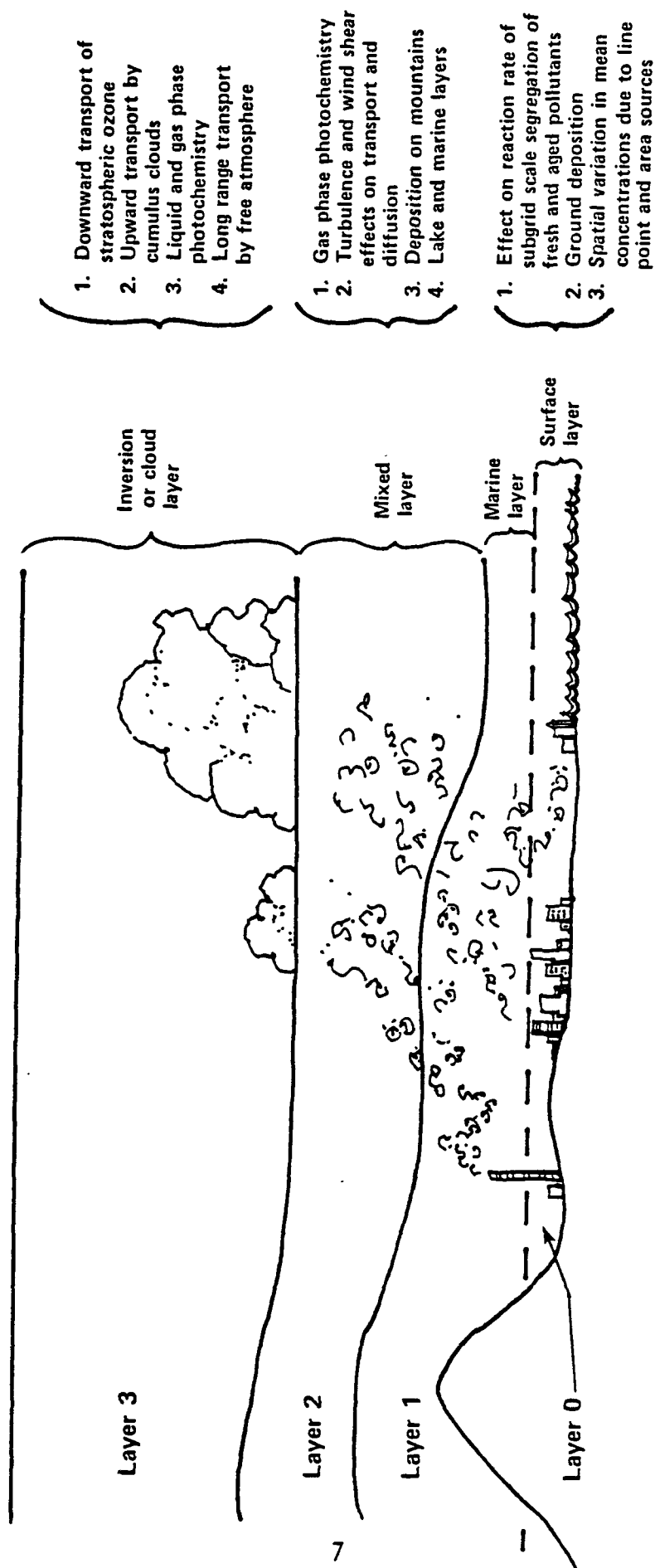


Figure 1-1a. Schematic illustration of the "dynamic" layer structure of the regional scale model and the daytime phenomena each layer is designed to treat.

Nighttime

Layer Functions

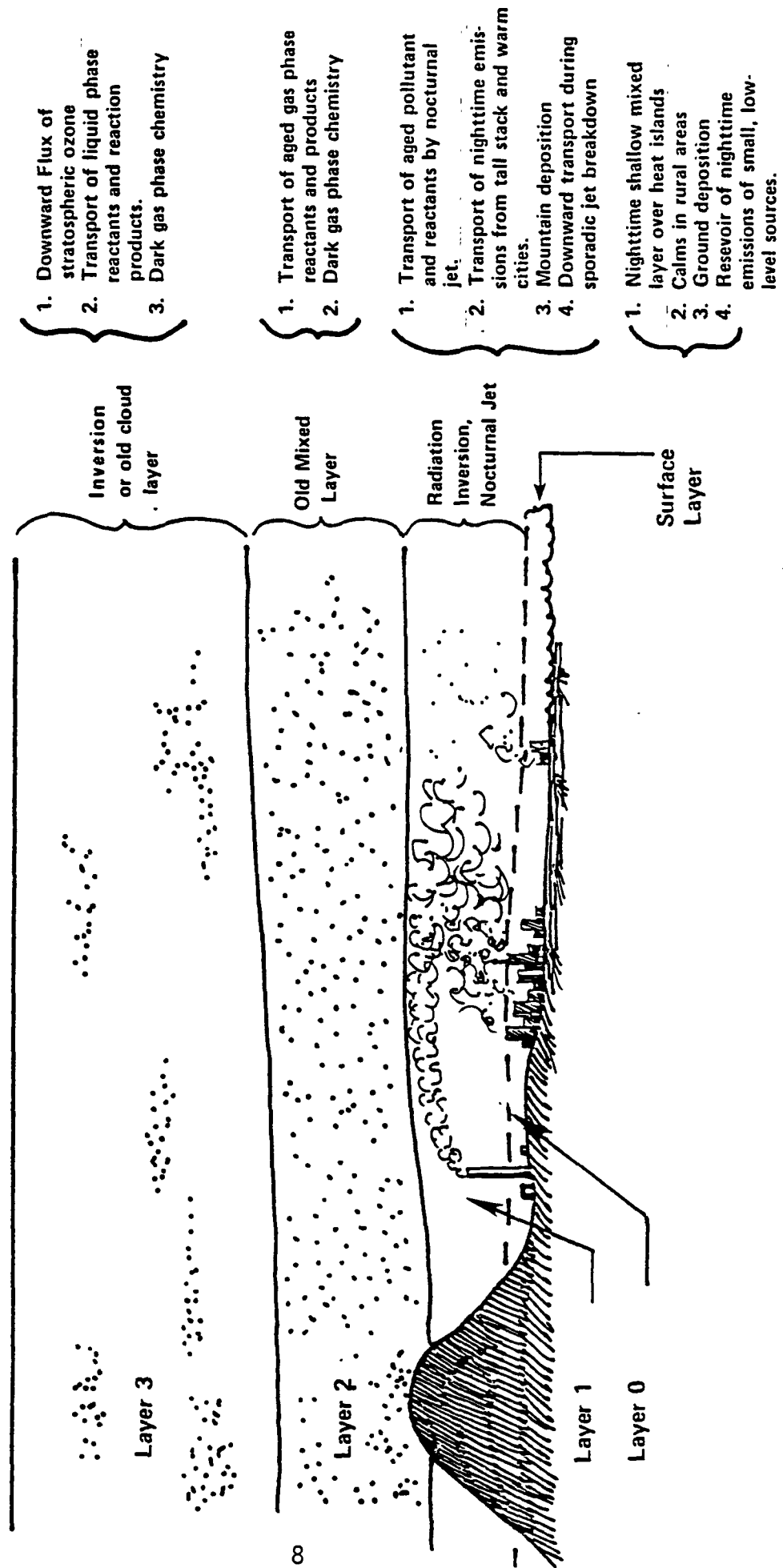


Figure 1-1b. Same as 1-1a except nighttime phenomena.

conventional models the grid network and cell volumes remain fixed and surfaces such as the mixed layer top move through the grid system. In the following several paragraphs, we elaborate on some of the phenomena cited in Figure 1-1 that our model will take into account.

During the day the highest layer shown in Figure 1-1a represents the synoptic scale subsidence inversion, which may or may not contain cumulus clouds. Stratospheric O_3 is transported downward through this layer and anthropogenic O_3 and its precursors can be carried into it by cumulus clouds or penetrative convection, the depth of the penetration being determined mainly by the intensity of the temperature stratification in the inversion and by the scale and intensity of convection in the mixed layer. The base of this layer is normally 1 or 2 km above ground level. Below it pollutants are kept well mixed vertically by turbulent convection. If the winds are strong or the surface heat flux is weak, wind speed and direction may vary appreciably within the first several hundred m above ground. There is usually also a marked difference in the wind speed and direction between the inversion layer and the mixed layer below. Over large lakes and along sea coasts there is frequently a second inversion layer below that generated by synoptic scale subsidence. This lower inversion is produced by sea or lake breeze regimes and it restricts the vertical mixing of pollutants emitted over the water and within several km inland from the water's edge.

Air drawn into young cumulus clouds originates primarily in the lower portion of the mixed layer. Fresh emissions of NO_x and hydrocarbons can be transported by the vertical currents that feed these clouds from ground-level to altitudes well above the top of the mixed layer in one steady, upward motion. In the process little or no mixing with aged pollutants in

the mixed layer occurs. At night, cumulus clouds usually evaporate and, when they do, they leave behind products of liquid phase reactions that can be transported hundreds of km before sunrise.

When the daytime mixed layer is moist enough for cumulus humilis clouds to form at its top, pollutant emissions can undergo a quasi-cyclic series of events that may have a great effect on the chemical fate of pollutants and particularly the formation of aerosol (Figure 1-2). As shown in the figure, the thermals, or vertical jets of warm air, of which cumulus humilis are a part, have their roots near ground-level. Fresh emissions of pollutants that enter a thermal can rise in a steady motion all the way to the top of the mixed layer. Individual clouds mark the locations where air parcels that compose thermals have become saturated and liquid water has formed. In the saturated parcels, air pollution chemistry will be altered by the sudden presence of liquid water and also by the accompanying attenuation of sunlight. The presence of cumulus humilis signifies that the upper layers of the atmosphere are too stably stratified for thermals to penetrate higher, and so in this instance the cloud tops bend over and the air of which they are composed dives back down into the mixed layer (see Figure 1-2). As a saturated parcel descends, it is warmed by compressional heating and eventually the cloud droplets within it evaporate leaving behind the residue of aqueous phase reactions, probably in aerosol form. After some time the parcel will arrive again at ground-level where new emissions may be injected into it, and/or deposition on surfaces may occur; subsequently, the entire process is repeated. The time required for 1 complete cycle would typically be 30-50 min with maybe one-tenth of the time spent in the cloud stage. The chemistry associated with the cycle we have just described could possibly be studied in the laboratory by measuring the composition of initially moist,

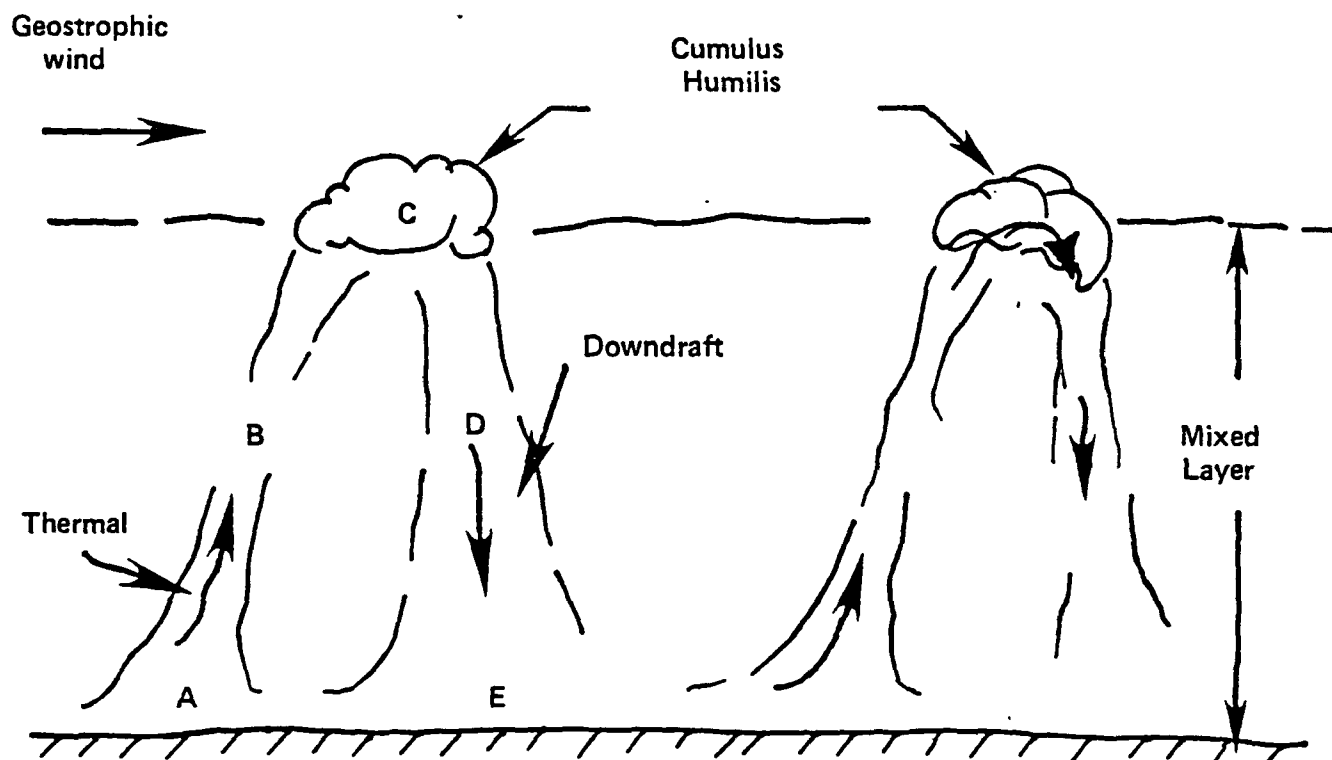


Figure 1.2. Idealized view of the fate of polluted air parcels in a cumulus humilis topped mixed layer. A, parcel receives emissions; B, it rises and cools; C, saturation occurs producing cloud droplets; D, the parcel descends and dries; and E, it receives new emissions and/or deposits pollutants on surfaces. From E the cycle begins anew.

polluted air as it is subjected to a series of expansions and compressions in a cloud-chamber apparatus. The framework of the model that we develop later will allow treatment of this process.

Dramatic changes occur in the mixed layer at night. With onset of surface cooling following sunset, a stable layer of air forms near the ground that quenches the vertical momentum fluxes that give rise to frictional drag on the horizontal flow. With retardation forces eliminated, the wind just above the stable layer accelerates giving rise to the phenomenon known as the nocturnal jet. Wind speeds in the core of the jet, which usually lies between 300 and 500 m above ground, may be 10-15 m/s while at the same time the air is nearly calm at the surface. Emissions from tall stacks and from sources within the urban heat island enter the jet region at night. There they react with aged pollutants from the previous day and are transported considerable distances by the strong flow. The remnant of the previous day's mixed layer above the jet is isolated from the influence of fresh emissions and it moves at a slower speed than air below.

Sporadic episodes of turbulence in the shear layer beneath the nocturnal jet is a mechanism by which O_3 and constituents of urban plumes are brought to ground-level at night. There deposition on surfaces and reactions with emissions of small, low-level sources occur. This sporadic mixing process is perhaps the only mechanism by which the reservoir of aged pollutants aloft can be depleted at night.

One point that we wish to emphasize here is that 1-layer regional scale air pollution models are incapable of simulating the effects on pollutants like O_3 of the vertical segregation of aged and fresh emissions that occur at night. Being cut-off from contact with the ground and fresh NO_x emissions,

O₃ above the nighttime radiation inversion is free to travel great distances before it is mixed vertically by convection the following day. The effect of this nighttime segregation of pollutants is to extend greatly the effective residence times of species like O₃ in the lower troposphere. Consequently, a multi-layered model seems to be essential to simulate accurately the long range transport of photochemical air pollutants.

The horizontal resolution of the model that we now plan to make operational is about 18 km. We want this resolution to be as high as possible to mitigate the effects of subgrid scale concentration fluctuations. Since apparently few modelers are aware of this phenomenon, it is perhaps worthwhile to digress here with an explanation of it.

Suppose we were simulating O₃ concentrations within an urban region covered by the 16 grid cells shown in Figure 1-3. Suppose further that at some instant transport and diffusion ceased leaving NO and O₃ unmixed and partitioned in the manner shown. If NO and O₃ are the only species present, then clearly there will be no change in the concentrations in any of the cells. In this case our model, using the rate equations

$$\frac{d\overline{NO}}{dt} = \frac{d\overline{O_3}}{dt} = -k \overline{NO} \overline{O_3} \quad (1-1)$$

would correctly predict

$$\frac{d\overline{NO}}{dt} = \frac{d\overline{O_3}}{dt} = 0$$

where the overbar denotes an average over any 1 of the 16 cells shown in Figure 1-3.

Suppose now that this same concentration distribution were contained within a single cell (denoted by the heavy outer square in Figure 1-3) of

NO	O ₃	NO	O ₃
O ₃	NO	O ₃	NO
NO	O ₃	NO	O ₃
O ₃	NO	O ₃	NO

Figure 1-3.

Hypothetical case of an urban area in which ozone and NO are segregated into 16 cells. If this distribution is simulated in a regional model whose cell size is the large outer square, subgrid chemistry phenomena arise.

a regional model. Denoting mean values within the regional cells by the tilde (\sim) and using the counterpart of (1-1) we find

$$\frac{d\tilde{NO}}{dt} = \frac{d\tilde{O}_3}{dt} = -k \tilde{NO} \tilde{O}_3 \neq 0 \quad (1-2)$$

Thus, the regional model predicts decay of the O_3 and NO within its cell even though none is occurring. Note that this fictitious decay resulted only from the increase in the horizontal cell size; with the small cells the model simulated properly the absence of chemical reaction.

Obviously, it is the variability of concentrations within the model grid cells (i.e., subgrid scale fluctuations) that is responsible for this problem. In averaging a variable we lose information about its fine scale structure. If this structure is important, as it is in second-order chemical processes (but not first order reactions), and in rain out and washout processes where the spatial extent of the area of precipitation is comparable to or smaller than the grid size, then either the loss of details must be mitigated by keeping the averaging interval to a minimum size or a scheme must be developed to parameterize the fine structure effects. We develop such a scheme in this report (Section 5) and we implement it in Layer 0, which is adjacent to the ground (see Figure 1-1). This layer is treated diagnostically in the governing equations.

There are 3 basic problems that must be overcome to make a model as large and comprehensive as the one we plan to develop operational.

First, the empirical data needed to parameterize some of the physical phenomena cited earlier are not presently available. To remedy this problem, the Atmospheric Modeling Branch of Environmental Sciences Research Laboratory initiated project NEROS to collect during the summers of 1979 and 1980

the meteorological and chemical data required to formulate the model. A second goal of NEROS was to gather the data required to perform comprehensive test runs and validation exercises of the model.

A second problem is limitations of computer storage capacity. To simulate air quality over the Northeastern United States with the horizontal resolution we desire, our model will have roughly 10^4 grid points and it will treat 23 (eventually more) chemical species. Thus, the concentration variables alone will require 250K words of storage and this is just under the working limit of 260K words of memory on EPA's Univac computer. To accommodate a model of the anticipated size we will have to develop special techniques that permit handling the modeling domain in piecewise fashion. This problem is addressed in Section 9 of this report.

Finally, due to the large number of processes that we will attempt to treat, our model will be rather complicated. In order to alleviate the problems that this might cause in operating the model and in making future refinements, we will structure it so that its central core consists solely of a set of algorithms for solving the coupled set of generalized finite difference equations that describe processes in each of its layers. The modeling functions of describing the mixed layer dynamics, topographic effects on wind, chemistry, cloud fluxes, etc., will be handled by a set of special processors that are external to the central model and which feed the model key variables through a computer file. Within this framework the techniques used to describe the various physical processes can be altered without overhauling the model itself. An additional advantage is that execution times are greatly reduced when several runs of a given scenario are to be performed in which only 1 or a few parameter values are altered. Details of the model

system are given in Part II of this report.

In the sections that follow we develop in detail the theoretical bases of the regional model. Operational aspects, refinements, validation exercises and other details will be presented in subsequent volumes of this report.

SECTION 2

DERIVATION OF PROGNOSTIC EQUATIONS FOR LAYERS 1, 2 AND 3

Let c denote the concentration of any pollutant species we wish to model. Its mass continuity equation is

$$\frac{\partial c}{\partial t} + \nabla_H \cdot (c\mathbf{v}) + \frac{\partial}{\partial z} (cw) = S + R - W \quad (2-1)$$

where

∇_H = the horizontal del operator

\mathbf{v} = the horizontal component of the wind,

w = the vertical component of the wind,

S = the source strength function of the species,

R = the net rate of production of c by chemical reaction,

W = the rate of removal by rainout and washout.

Deposition is taken into account by the boundary conditions on (2-1). In cases where c represents a photochemical pollutant, (2-1) is coupled through the reaction term R to the equations governing other pollutant concentrations.

The surfaces separating the model layers will be expressed in the implicit form

$$H_i(x,y,t) = z_i(x,y,t) - z, \quad i = 0,1,2,3 \quad (2-2)$$

The terrain surface will be denoted by z_T and we will allow it to extend up through H_0 and H_1 under certain conditions, which we will define later. Each of the interface surfaces H_n is prescribed later, in Section 3.

Let ϕ be an arbitrary function of (r, t) . We define the mean value ϕ in Layer j ($= 0, 1, 2, 3$) to be

$$\langle \phi(x, y, t) \rangle_j \equiv \frac{1}{V_j} \int_{x-\Delta x}^{x+\Delta x} \int_{y-\Delta y}^{y+\Delta y} \int_{z_{j-1}(x', y', t)}^{z_j(x', y', t)} \phi(x', y', z', t) dz' dy' dx' \quad (2-3)$$

where

$$V_j(x, y, t) = \int_{x-\Delta x}^{x+\Delta x} \int_{y-\Delta y}^{y+\Delta y} \int_{z_{j-1}(x', y', t)}^{z_j(x', y', t)} dz' dy' dx' \quad (2-4)$$

In order to derive from Equation (2-1) the equation governing the mean pollutant concentration $\langle c \rangle_j$ in each layer, it is convenient at this point to introduce some of the properties of time and space derivatives of volume averaged quantities defined by (2-3). Consider first the time derivative $\partial \langle \phi \rangle_j / \partial t$.

From (2-3) we obtain

$$\begin{aligned} \frac{\partial}{\partial t} \langle \phi \rangle_j &= \frac{1}{V_j} \int_A \left[\phi(x', y', z_j, t) \frac{\partial z_j}{\partial t} - \phi(x', y', z_{j-1}, t) \frac{\partial z_{j-1}}{\partial t} \right. \\ &\quad \left. + \int_{z_{j-1}}^{z_j} \frac{\partial \phi}{\partial t} dz' \right] dx' dy' - \frac{\langle \phi \rangle_j}{V_j} \frac{\partial V_j}{\partial t} \end{aligned} \quad (2-5)$$

where $\int_A dx dy$ denotes integration over an area $4\Delta x \Delta y$ centered at (x, y) .

From Equation (2-4), we obtain

$$\frac{\partial V_j}{\partial t} = \int_A \left(\frac{\partial z_j}{\partial t} - \frac{\partial z_j}{\partial t} - 1 \right) dx' dy' \quad (2-6)$$

Let us define the following surface average:

$$\overline{\phi(x,y,t)}^j = \frac{1}{A} \int_{x-\Delta x}^{x+\Delta x} \int_{y-\Delta y}^{y+\Delta y} \phi[x',y',z_j,t] dy' dx' \quad (2-7)$$

where

$$A = 4\Delta x \Delta y \quad (2-8)$$

This is simply the average of ϕ , evaluated on the surface H_j , within the rectangular area A centered at (x,y) . We emphasize that (2-7) is not an average over the projection of A on the surface H_j . Using (2-7) and the abbreviated notation

$$z_j = \partial z_j / \partial t \quad (2-9)$$

we can write (2-6) in the form

$$\frac{\partial V_j}{\partial t} = A(\overline{z_j}^j - \overline{z_j}^{j-1}) \quad (2-10)$$

Then, Equation (2-5) gives

$$\frac{\partial}{\partial t} \langle \phi \rangle_j = \frac{A}{V_j} (\overline{\phi z_j}^j - \overline{\phi z_j}^{j-1}) + \langle \frac{\partial \phi}{\partial t} \rangle_j - \langle \phi \rangle_j \frac{\partial}{\partial t} \ln V_j \quad (2-11)$$

Consider next the space derivatives of $\langle \phi \rangle$:

$$\frac{\partial}{\partial x} \langle \phi \rangle_j = \frac{1}{V_j} [I_j(x + \Delta x) - I_j(x - \Delta x)] - \langle \phi \rangle_j \frac{\partial}{\partial x} \ln V_j \quad (2-12)$$

where

$$I_j(\xi) = \int_{y-\Delta y}^{y+\Delta y} \int_{z_{j-1}(\xi, y', t)}^{z_j(\xi, y', t)} \phi(\xi, y', z', t) dz' dy' \quad (2-13)$$

We can transform Equation (2-12) into more familiar terms by comparing it with

$$\langle \frac{\partial \phi}{\partial x} \rangle_j = \frac{1}{V_j} \int_A \int_{z_{j-1}}^{z_j} \frac{\partial \phi}{\partial x'} dz' dy' dx' \quad (2-14)$$

This equation can be simplified starting with

$$\begin{aligned} \frac{\partial}{\partial x'} I_j(x') &= \int_{y-\Delta y}^{y+\Delta y} [\phi(x', y', z_j, t) \frac{\partial z_j}{\partial x'} - \phi(x', y', z_{j-1}, t) \frac{\partial z_{j-1}}{\partial x'} \\ &\quad + \int_{z_{j-1}}^{z_j} \frac{\partial \phi}{\partial x'} dz'] dy' \end{aligned} \quad (2-15)$$

Combining Equations (2-14) and (2-15), we obtain

$$\langle \frac{\partial \phi}{\partial x} \rangle_j = \frac{1}{V_j} [I_j(x + \Delta x) - I_j(x - \Delta x)] + \frac{A}{V_j} (\phi \frac{\partial z_{j-1}}{\partial x} - \phi \frac{\partial z_j}{\partial x}) \quad (2-16)$$

and substituting from Equation (2-12), we find that

$$\langle \frac{\partial \phi}{\partial x} \rangle_j = \frac{\partial}{\partial x} \langle \phi \rangle_j + \frac{A}{V_j} (\phi \frac{\partial z_{j-1}}{\partial x} - \phi \frac{\partial z_j}{\partial x}) + \langle \phi \rangle_j \frac{\partial}{\partial x} \ln V_j \quad (2-17)$$

By analogy

$$\langle \frac{\partial \phi}{\partial y} \rangle_j = \frac{\partial}{\partial y} \langle \phi \rangle_j + \frac{A}{V_j} (\phi \frac{\partial z_{j-1}}{\partial y} - \phi \frac{\partial z_j}{\partial y}) + \langle \phi \rangle_j \frac{\partial}{\partial y} \ln V_j \quad (2-18)$$

Finally, we see from Equations (2-3) and (2-7) that

$$\begin{aligned} \langle \frac{\partial \phi}{\partial z} \rangle_j &= \frac{1}{V_j} \int_A [\phi(x', y', z_j, t) - \phi(x', y', z_{j-1}, t)] dx' dy' \\ \langle \frac{\partial \phi}{\partial z} \rangle_j &= \frac{A}{V_j} (\bar{\phi}^j - \bar{\phi}^{j-1}) \end{aligned} \quad (2-19)$$

We now have the relationships needed to derive the equations governing $\langle c \rangle_j$. Performing the $\langle \rangle$ averaging on Equation (2-1) and making use of Equations (2-11) and (2-17)-(2-19) we obtain

$$\begin{aligned} \frac{\partial}{\partial t} \langle c \rangle_j &- \frac{A}{V_j} (\bar{cz}_j - \bar{cz}_{j-1}) + \langle c \rangle_j \frac{\partial}{\partial t} \ln V_j + \nabla_H \cdot \langle vc \rangle_j + \frac{\langle uc \rangle_j}{V_j} \frac{\partial V_j}{\partial x} \\ &+ \frac{\langle vc \rangle_j}{V_j} \frac{\partial V_j}{\partial y} - \frac{A}{V_j} (uc \frac{\partial z}{\partial x}^j + vc \frac{\partial z}{\partial y}^j) + \frac{A}{V_j} (uc \frac{\partial z}{\partial x}^{j-1} + vc \frac{\partial z}{\partial y}^{j-1}) \\ &+ \frac{A}{V_j} (\bar{cw}^j - \bar{cw}^{j-1}) = \langle S \rangle_j + \langle R \rangle_j - \langle W \rangle_j \end{aligned} \quad (2-20)$$

where $\underline{v} = (u, v)$. Recall that $z = \partial z / \partial t$.

Collecting terms representing averages over each of the surfaces H_j and H_{j-1} , we can express (2-20) in the more concise form

$$\begin{aligned} \frac{\partial}{\partial t} \langle c \rangle_j + \langle c \rangle_j \frac{\partial}{\partial t} \ln V_j + \nabla_H \cdot \langle vc \rangle_j + \langle uc \rangle_j \frac{\partial}{\partial x} \ln V_j \\ + \langle vc \rangle_j \frac{\partial}{\partial y} \ln V_j = \frac{A}{V_j} [F_j - F_{j-1}] + \langle S \rangle_j + \langle R \rangle_j - \langle W \rangle_j \end{aligned} \quad (2-21)$$

where

$$F_j \equiv c \frac{dH_j}{dt} \quad (2-22)$$

$$\frac{d}{dt} \equiv \frac{\partial}{\partial t} + \underline{v} \cdot \nabla_H + w \frac{\partial}{\partial z} \quad (2-23)$$

$\underline{v} = (u,v)$ and H_j is given by (2-2). Note that F_j is the total flux of the species represented by c across the surface H_j within the area formed by the projection of A , centered at (x,y) , on H_j .

In modeling atmospheric processes over 1000 km scale regions, earth curvative effects must be taken into account. This can be done either by transforming the governing equations into one of the rectilinear projections of the earth, such as polar stereographic, Albers equal area, etc., or by casting the equations in curvilinear coordinates, such as latitude - longitude. In either case the equations acquire a form different from the well-known Cartesian form we have developed above. In Appendix A we give the details of the transformation of Equation (2-21) into a curvilinear frame in which latitude, longitude and elevation are coordinates and the basis vectors point north, east and vertically upward at every point on the earth. We have chosen this frame because it is a natural one from which transformations to any rectilinear system are easily performed. Also, it is the frame in which worldwide meteorological data are reported. In the chosen frame Equation (2-21) takes the form

$$\frac{\partial}{\partial t} \langle c \rangle_j + \langle c \rangle_j \frac{\partial \ln V_j}{\partial t} + \mu_\lambda \frac{\partial \langle uc \rangle_j}{\partial \lambda} + \mu_\phi \frac{\partial \langle vc \rangle_j}{\partial \phi} \quad (2-24)$$

$$\begin{aligned} & \mu_\lambda \langle uc \rangle_j \frac{\partial \ln V_j}{\partial \lambda} + \mu_\phi \langle vc \rangle_j \frac{\partial \ln V_j}{\partial \phi} + \frac{A}{V_j} \left[c \frac{dH}{dt} \right]_j - \overline{c \frac{dH}{dt}}_j \\ & = \langle S \rangle_j + \langle R \rangle_j - \langle W \rangle_j \end{aligned}$$

where μ_λ and μ_ϕ are the metric factors

$$\mu_\lambda = \frac{1}{a \cos \phi}, \quad \mu_\phi = \frac{1}{a}$$

a is the earth's radius at msl; λ is longitude; ϕ is latitude;

v is the north-south wind component; u is the east-west component;

and

$$\frac{d}{dt} \equiv \frac{\partial}{\partial t} + u_{\lambda} \frac{\partial}{\partial \lambda} + u_{\phi} \frac{\partial}{\partial \phi} + w \frac{\partial}{\partial z} \quad (2-25)$$

The product mean terms that enter in (2-24) can be simplified through use of the continuity equation for the atmosphere. In studies of flows that are shallow comparable to the scale height of the atmosphere, the continuity equation can be simplified to the form

$$\nabla \cdot \underline{v} \approx 0 \quad (2-26)$$

(see Haltiner 1971, page 54).

Applying the $\langle \rangle$ averaging operation to this equation we obtain through a process like that described in Appendix A,

$$\begin{aligned} & \mu_{\lambda} \frac{\partial \langle u \rangle_j}{\partial \lambda} + \mu_{\phi} \frac{\partial \langle v \rangle_j}{\partial \phi} + \mu_{\lambda} \langle u \rangle_j \frac{\partial \ln V_j}{\partial \lambda} + \mu_{\phi} \langle v \rangle_j \frac{\partial \ln V_j}{\partial \phi} \\ & + \frac{A}{V_j} \left[\mu_{\lambda} \overline{u \frac{\partial H_j}{\partial \lambda}} + \mu_{\phi} \overline{v \frac{\partial H_j}{\partial \phi}} + w \overline{\frac{\partial H_j}{\partial z}} \right] \\ & - \frac{A}{V_j} \left[\mu_{\lambda} \overline{u \frac{\partial H_j}{\partial \lambda}} + \mu_{\phi} \overline{v \frac{\partial H_j}{\partial \phi}} + w \overline{\frac{\partial H_j}{\partial z}} \right] = 0 \end{aligned} \quad (2-27)$$

In this equation, as in (2-24), the terms under the overbars are evaluated on the surface H_j whose derivative is the product term.

Let us define the flux terms

$$\begin{aligned} \langle u'c' \rangle &= \langle uc \rangle - \langle u \rangle \langle c \rangle \\ \langle v'c' \rangle &= \langle vc \rangle - \langle v \rangle \langle c \rangle \end{aligned} \quad (2-28)$$

applicable to any of the 3 model layers. Note that under these definitions, $\langle u' \rangle$ and $\langle v' \rangle$ are not necessarily zero. Making use of (2-27) and (2-28) we can express (2-24) in the equivalent but more manageable form

$$\begin{aligned}
& \frac{\partial}{\partial t} \langle c \rangle_j + \langle c \rangle_j \frac{\partial \ln V_j}{\partial t} + \mu_\lambda \langle u \rangle_j \frac{\partial \langle c \rangle_j}{\partial \lambda} + \mu_\phi \langle v \rangle_j \frac{\partial \langle c \rangle_j}{\partial \phi} \\
& + \mu_\lambda \langle u'c' \rangle_j \frac{\partial \ln V_j}{\partial \lambda} + \mu_\phi \langle v'c' \rangle_j \frac{\partial \ln V_j}{\partial \phi} + \mu_\lambda \frac{\partial}{\partial \lambda} \langle u'c' \rangle_j \\
& + \mu_\phi \frac{\partial}{\partial \phi} \langle v'c' \rangle_j + \frac{A}{V_j} [F_{j-1,j} - F_{j,j}] = \langle S \rangle_j + \langle R \rangle_j - \langle W \rangle_j \quad (2-29)
\end{aligned}$$

where

$$F_{j,k} \equiv \overline{c_j \underline{v} \cdot \underline{\nabla} H_j} - \langle c \rangle_k \overline{\underline{v} \cdot \underline{\nabla} H_j} + \overline{c_j \frac{\partial H_j}{\partial t}} \quad (2-30)$$

and

$$\underline{\nabla} \equiv \mu_\lambda \frac{\partial}{\partial \lambda} + \mu_\phi \frac{\partial}{\partial \phi} + \frac{\partial}{\partial z}$$

and c_j and \underline{v} denote concentration and velocity, respectively, evaluated on surface H_j . By definition [Equation (2-30)], $F_{j,k}$ is the rate of transport of material c across the surface H_j , to or from Layer k , per unit horizontal area (not unit surface area of H_j) with H_j held fixed in time. Equation (2-29) is the general form of the model equation with which we shall work in the remainder of this report. In the sections that follow, we develop expressions for each parameter that enters in this equation.

SECTION 3

THE INTERFACE SURFACES H_j

We summarized earlier in Figure 1-1 the various roles that each of the models' 4 layers are intended to serve. In this section we will specify functional forms for the layer interface surfaces $H_j(\lambda, \phi, t)$ that we believe are compatible with those roles.

The Model's Top Surface, H_3

There are two conflicting constraints on the surface H_3 . The first is that $z_3(x, y, t)$ must be high enough that no appreciable turbulent or cloud fluxes of material cross it. The second requirement is that the depth of Layer 3, i.e., $z_3 - z_2$, must be small enough that subgrid scale concentration variations within the layer are negligible. To satisfy both these requirements, we will prescribe $z_3(x, y, t)$ based on observations of convective cloud top elevations and on the estimated level z_2 of the "mixed" layer top. Further details will be presented in Part 2 of this report.

The Subsidence Inversion Base Surface, H_2

This is one of the most important parameters in the model; because acting as a barrier (a "leaky" barrier when cumulus clouds are present) to the upward movement of pollutants, the height of H_2 above ground determines the concentration that fresh emissions produce once they become well mixed vertically.

As a consequence, H_2 has an effect both on the rates of slow second order chemical reactions that occur among the constituents of polluted air as it moves over long distances and on the rate of surface deposition. In view of its importance, the surface $H_2(\lambda, \phi, t)$ is treated rather rigorously in the model. We will postpone further discussions of it until Section 4, where we describe in detail the procedure we use to calculate H_2 .

The Nocturnal Jet Top, H_1

We believe that an essential requirement for the model's ability to simulate accurately the long range transport of O_3 is the ability to handle properly the deposition of nighttime emissions of hydrocarbons and NO_x . Preliminary results of aircraft studies performed as part of project NEROS in August, 1979 support our original speculation that nighttime surface emissions are confined primarily to the lower one-quarter of the old daytime mixed layer, and that O_3 and aged precursors reside in the upper three-quarters where they undergo virtually no mixing with the fresh emissions below. It is this segregation of the old and fresh emissions at night that allows O_3 to travel great distances before being scavenged by NO or hydrocarbon. Thus, the surface H_1 should be set just above the level that nighttime emissions reach. This level is probably controlled by the temperature profile of the nocturnal boundary layer, by the wind speed and by the buoyancy flux of the urban plume. One of the objectives of the NEROS field program is to determine just how these factors control the nighttime urban plume rise and spread.

Another role intended for surface H_1 is to represent the barrier to upward diffusion imposed by the weak subsidence inversion associated with

lake and sea breeze regimes. The base of this inversion is lowest over the water, but it slopes upward inland until at some distance from the shore it vanishes altogether. This feature of the boundary layer probably plays an important part in the dispersion of emissions around the Great Lakes and along the Atlantic Coast.

A third role of Layer 1 is to describe the daytime shear layer in which mean transport has a different direction and speed than in the upper part of the mixed layer.

To serve in all these capacities, the surface H_1 should be calculated from the set of equations that describes the nocturnal inversion layer and urban plume rise at night, the lake/sea breeze inversion by day and the shear layer depth. At the present stage of the model development we attempt to describe H_1 rather rigorously under stable conditions but only approximately in neutral and unstable situations. In the former case we prescribe the volume flux η_1 across H_1 , i.e.,

$$\frac{dH_1}{dt} = \eta_1 \quad , \text{ stable conditions .} \quad (3-1a)$$

Using computed values of the fluid velocity (u_1, v_1, w_1) in the stable boundary layer and the estimated value of η_1 , we solve (3-1a) for H_1 during stable conditions. Details are given in Part 2 of this report. During neutral and unstable conditions the methods employed in the stable case do not apply and we rely then on an ad hoc formulation of z_1 itself. The objective is to account for the shear layer depth and terrain effects mentioned above but not the lake/sea breeze inversions. The same ad hoc method is used to describe H_0 under all conditions. We describe the method below.

First, we assume that at any point the vertical velocity w is composed of 2 components: one, w_T , induced by the motion of horizontal flow over terrain features and the other, w_D , arising from turbulence and horizontal divergence of the large scale flow. That is,

$$w = w_T + w_D \quad (3-1b)$$

If the vertical velocity component w_D were zero and the horizontal wind (u, v) were steady, H_1 would be a material surface if

$$\underline{v}_{H1} \cdot \underline{\nabla}_H z_1 = w_{T1} \quad (3-1c)$$

where $\underline{v}_{H1} = (u_1, v_1)$,

$$\underline{\nabla}_H \equiv \mu_\lambda \frac{\partial}{\partial \lambda} + \mu_\phi \frac{\partial}{\partial \phi} \quad (3-1d)$$

and where the subscript "1" denotes evaluation at level z_1 . We can express w_{T1} in the form

$$w_{T1} = A_1(\lambda, \phi, t) [\underline{v}_{H1} \cdot \underline{\nabla}_H z_T] \quad (3-1e)$$

where the term in brackets is a measure of w_{T0} , i.e., vertical speed at the ground surface z_T , and A_1 is an unknown function (which we approximate below). If we express z_1 in the form

$$z_1 = z_T + H_1 \quad (3-1f)$$

where H_1 is the depth of the shear layer over smooth terrain, then we find on substituting this expression and (3-1e) into (3-1c) that in order for z_1 to satisfy (3-1c), H_1 must satisfy

$$\underline{\nabla}_H H_1 + (1 - A_1) \underline{\nabla}_H z_T = 0 \quad (3-1g)$$

Thus, once we have an estimate of A_1 , we can use (3-1f, g) to define a surface H_1 that will satisfy (3-1c).

To approximate A_1 we first define 2 smoothed terrain functions

$$\hat{z}_T(\lambda, \phi) = \frac{1}{25} \int_{x-2.5}^{x+2.5} \int_{y-2.5}^{y+2.5} z_T(x', y') dy' dx' \quad (3-2a)$$

$$\tilde{z}_T(\lambda, \phi) = \frac{1}{2500} \int_{x-25}^{x+25} \int_{y-25}^{y+25} z_T(x', y') dy' dx' \quad (3-2b)$$

where (x, y) are Cartesian coordinates centered at (λ, ϕ) , z_T is local topography elevation (MSL), and distances are measured in kilometers. We next define a rms topography

$$\Sigma_T^2(\lambda, \phi) = \frac{1}{2500} \int_{x-25}^{x+25} \int_{y-25}^{y+25} [\hat{z}_T(x', y') - \tilde{z}_T(x', y')]^2 dy' dx' \quad (3-3)$$

Using Σ_T we define a terrain Froude number F_r by

$$F_r = \frac{U}{2N\Sigma_T} \quad (3-4)$$

where $N^2 = g/\bar{\theta} \frac{d\bar{\theta}}{dz}$ is the Brunt-Vaisala frequency and U is the horizontal wind speed at an elevation Σ_T above the level \tilde{z}_T . According to Godowitch et al. (1979), nighttime inversions over rural areas around St. Louis were observed to have intensities of between 10 and 20°K per kilometer. Thus, we will adopt $N = 0.33 \text{ s}^{-1}$ as a representative value for use in our modeling studies of the Northeastern United States.

Hunt et al. (1978) found in laboratory studies that stably stratified fluid tends to move horizontally rather than over an isolated hill of

moderate slope when the Froude number is less than 0.3. Based on this finding we propose as an interim approximation

$$A_k = \exp \left[- \left(\frac{1}{2F_r} \right)^2 - (H_k/3z_T)^2 \right] \quad , k = 1 \text{ or } 0; \quad (3-5)$$

and F_r is given by Equation (3-4) with

$$N = \begin{cases} 0.03 \text{ s}^{-1}, & \text{nighttime hours} \\ 0.0 \text{ s}^{-1}, & \text{daytime} \end{cases} \quad (3-6)$$

The last term in brackets in Equation (3-5) is intended to account for the decrease in the amplitude of vertical velocity with height that is associated with flow over obstacles. We expect that H_1 will have a value of about 300 m. Thus, terrain features smaller than about 50 m will have virtually no influence on the slope of z_1 .

In summary, during stable conditions we prescribe

$$\frac{dH_1}{dt} = \eta_1 \quad , \text{ stable conditions}; \quad (3-7a)$$

where η_1 is a function given in Part 2 of this report; and under neutral and unstable daytime hours we define

$$z_1 = \bar{z}_T + H_1 \quad (3-7b)$$

where H_1 satisfies

$$\nabla_H H_1 + (1 - A_1) \nabla_H \bar{z}_T = 0 \quad (3-7c)$$

in the interior of the model domain and has the value of the shear layer depth at the boundaries. With A_1 given by (3-5) we assume that z_1 satisfies

$$\nabla_H H_1 \cdot \nabla_H z_1 = w_{T1} \quad (3-7d)$$

In this case we have

$$\frac{dH_1}{dt} = \eta_1 = \frac{\partial z_1}{\partial t} - w_{D1} \quad , \text{ neutral and unstable} \quad (3-7e)$$

Thus, in stable conditions η_1 is prescribed and z_1 is computed, and conversely in neutral and unstable conditions.

All our assumptions regarding z_1 are speculative and are intended to serve only as a first order estimate of the effects of topography on the vertical transport of pollutants. More refined representations of the surface H_1 that are consistent with the roles that Layer 1 serves in the model can be incorporated as they become available without having to overhaul the model (see Part 2 of this report). Further discussions of the surface z_1 and its roles will be given in Section 4.

The Surface Layer Top, H_0

The 2 main roles of Layer 0 are to treat the subgrid scale concentration fluctuation effects on chemical reactions and to parameterize surface removal processes. Both phenomena are confined to a relatively shallow layer next to the ground. Therefore, it is possible through a judicious design to formulate the Layer 0 equations in a way that does not require additional computer storage. In other words, the Layer 0 equations can be written in a diagnostic form in which concentrations in Layer 0 are expressed in terms of concurrent concentrations in Layer 1, surface source emission rates and the like. The details will be given later. The only restriction on such a formulation is that the total mass flux of material through the top surface of any Layer 0 cell be much larger than that through its sidewalls. If L denotes the horizontal cell size and H_0 the depth of Layer 0, then we require

$$\frac{\text{Vertical Flux}}{\text{Horizontal Flux}} \sim \frac{\sigma_w L^2}{\bar{u} L H_0} \gg 1 \quad (3-8)$$

where σ_w is the effective turbulence velocity on the top surface of Layer 0 and \bar{u} is the mean flow speed within the cell. This condition is satisfied if

$$L/H_0 \gg \bar{u}/\sigma_w \quad (3-9)$$

The velocity ratio on the right side of this expression is typically of the order of 10 or less throughout the depth of convective mixed layers. In stably stratified flows over flat terrain, it varies from a value of about 10 a few meters above the ground to a value of several hundred near the top of the nocturnal boundary layer (roughly 100 m).

Thus, using a grid cell $L \sim 20$ km we can let H_0 be as large as 100 m during the day (this will allow us to encompass the bulk of the subgrid scale concentrations variations) but at night we will have to limit H_0 to about 30 m.

Since we will neglect horizontal motions in Layer 0, we must define H_0 so that there is no net transport of air across it. That is

$$\overline{v_0 \cdot \nabla H_0} = 0 \quad (3-10)$$

To meet this condition, we will assume that the average divergent component of the vertical velocity, i.e., \bar{w}_0 [see (3-1a)] is zero at $z = z_0$, rather than at $z = \tilde{z}_T$, and we will define z_0 so that it follows approximately the terrain induced flow, that is,

$$w_{T0} = \mu_\lambda u_0 \frac{\partial z_0}{\partial \lambda} + \mu_\phi v_0 \frac{\partial z_0}{\partial \phi} \quad (3-11)$$

where w_{T0} is the component of w at z_0 induced by flow over terrain. We

can satisfy this requirement and at the same time fulfill the constraints on the depth of Layer 0 defined above by making z_0 similar to z_1 in form, namely

$$z_0(\lambda, \phi, t) = \tilde{z}_T(\lambda, \phi) + H_0(t) \quad (3-12)$$

where A_0 is given by (3-5), H_0 satisfies

$$\nabla_H H_0 + (1 - A_0) \nabla_H \tilde{z}_T = 0 \quad (3-13)$$

in the interior of the model domain and on the boundaries has the value

$$H_0(t) = \begin{cases} 75, & t_{SR} + 3 < t < t_{SS} \\ 75 - (t - t_{SS}) \cdot 15, & t_{SS} \leq t \leq t_{SS} + 3 \\ 30 + (t - t_{SR}) \cdot 15, & t_{SR} \leq t \leq t_{SR} + 3 \\ 30, & \text{otherwise} \end{cases} \quad (3-14)$$

where t_{SS} and t_{SR} denote the hours of sunset and sunrise, respectively.

In later versions of the model a different formulation of the top surface of Layer 0 can be adopted if the present one is found to be unacceptable. The modular structure of our model mentioned earlier permits changes of this type to be performed with a minimum of effort.

SECTION 4

THE INTERFACE FLUXES: $F_{j,k}$

In this section we derive explicit forms for the interface fluxes $F_{j,k}$ that enter in the governing equations (2-29) of each of the model's layers.

Flux Across the Model's Top Surface: $F_{3,3}$

We concluded in the previous section that the elevation z_3 of the top surface H_3 of the model must be a prescribed function. In this case (2-30) gives (see also 2-2, 2-22 and 2-23)

$$\begin{aligned} F_{3,3} &\equiv \overline{c \mathbf{v} \cdot \nabla H_3} - \langle c \rangle_3 \overline{\mathbf{v} \cdot \nabla H_3} + c \frac{\partial H_3}{\partial t} \\ &= c_3 \frac{dH_3}{dt} - \langle c \rangle_3 \left[\frac{dH_3}{dt} - \frac{\partial z_3}{\partial t} \right] \end{aligned} \quad (4-1)$$

where c_3 denotes concentration on the given surface H_3 . We will assume that

$$c_3 = \begin{cases} \langle c \rangle_3 & , \text{ if } \frac{dH_3}{dt} \leq 0 \\ c_\infty & , \text{ otherwise} \end{cases} \quad (4-2)$$

where c_∞ is the concentration of species c in the free atmosphere above the model domain. Combining (4-1) and (4-2), we obtain

$$F_{3,3} = \begin{cases} \langle c \rangle_3 \frac{\partial z_3}{\partial t} & , \text{ if } \frac{dH_3}{dt} \leq 0 \\ (c_\infty - \langle c \rangle_3) \frac{dH_3}{dt} + \langle c \rangle_3 \frac{\partial z_3}{\partial t} & , \text{ otherwise} \end{cases} \quad (4-3)$$

This approximation of $F_{3,3}$ assumes implicitly that there is no turbulent flux of material across H_3 . No error should be introduced by this assumption if, as we intend, H_3 is above the top of the mixed layer and above the top of any convective clouds that might be present.

Flux Across the Subsidence Inversion Base: $F_{2,2}$ and $F_{2,3}$

We have defined H_2 as the base of the synoptic scale subsidence inversion. During daylight hours this surface marks the top of the region known as the mixed layer in which, due to the action of convection, moisture and pollutant concentrations become approximately uniformly distributed vertically. Observations have shown that potential temperature, water vapor mixing ratio, and often pollutant concentration change abruptly at the mixed layer top. Based on this knowledge we shall assume, following Lilly (1968), that all 3 of these variables have discontinuities on H_2 . This approximation will be used below to derive the expressions both for the pollutant fluxes across H_2 and for the spatial and temporal variations in H_2 itself.

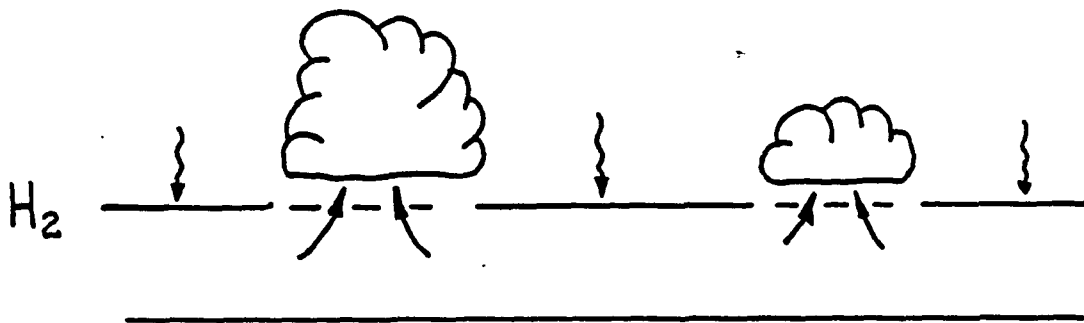


Figure 4-1. Schematic view of cumulus clouds transporting material aloft from the mixed layer and acting to lower the surface H_2 .

We consider the general situation depicted schematically in Figure 4-1 in which cumulus clouds transport heat, moisture, and pollutants through the mixed layer top into the cloud layer above. The upward motion in the clouds produces a compensatory downward velocity between clouds that acts to lower the mixed layer top.

On H_2 we assume that the concentration c_2 at any point is given by

$$c_2 = \begin{cases} c_c & , \text{beneath cumulus clouds} \\ \langle c \rangle_2 + c'_2 & , \text{between clouds} \end{cases} \quad (4-4)$$

where c_c is the concentration of species c in the updrafts feeding cumulus clouds in the given grid cell. This variable is a function of space and time and will be evaluated later in this section.

Let H_{2+} be a surface parallel to H_2 that is just high enough that the dry thermals that overshoot level z_2 between cumulus clouds cannot reach it. On H_{2+} we assume that the local concentration c_{2+} is given by

$$c_{2+} = \begin{cases} c_c & , \text{beneath cumulus clouds} \\ \langle c \rangle_3 & , \text{between clouds} \end{cases} \quad (4-5)$$

The latter expression is a result of our choosing H_{2+} high enough that there are no fluctuations in concentration on this surface due to the turbulent convection below.

Let σ_c denote the fraction ($0 \leq \sigma_c < 1$) of any given cell area A covered by cumulus clouds. Spatial and temporal variability of σ_c will be allowed but not explicitly stated.

For mathematical convenience we will express $F_{2,2}$ and $F_{2,3}$ in the form

$$F_{2,k} \equiv F_2 - \langle c \rangle_k \overline{v_{2,k} \cdot \nabla H_2} \quad (4-6)$$

where

$$F_2 \equiv \overline{c_2 \frac{dH_2}{dt}} \quad (4-7a)$$

and

$$\frac{d}{dt} \equiv \frac{\partial}{\partial t} + \underline{v}_2 \cdot \underline{\nabla} \quad (4-7b)$$

and \underline{v}_2 is the velocity vector measured on H_2 . Using (4-7b) and (4-7a) we obtain

$$F_{2+} \equiv \overline{c_{2+} \frac{dH_{2+}}{dt}} = \frac{1}{A} \left[\int_{\sigma_c} c_c \frac{dH_{2+}}{dt} da + \int_{1-\sigma_c} \langle c \rangle_3 \frac{dH_{2+}}{dt} da \right] \quad (4-8)$$

where the first integral is over the portion of H_{2+} beneath cumulus clouds and the last integration is over the remaining area within a grid cell. Assuming that there is negligible variation in c_c from cloud to cloud within any grid cell, and that spatial variations of $\langle c \rangle_3$ within any cell are small, we can reduce (4-8) to

$$F_{2+} = \sigma_c \bar{c}_c \overline{\frac{dH_{2+}}{dt}}^c + (1 - \sigma_c) \langle c \rangle_3 \overline{\frac{dH_{2+}}{dt}}^e \quad (4-9)$$

where $\overline{\quad}^c$ represents a mean value over the portion of H_{2+} beneath clouds and $\overline{\quad}^e$ represents a mean value over the environment between clouds within any grid cell.

Through a process similar to that leading to Equation (4-9), we obtain for the flux F_2 on H_2 :

$$F_2 = \frac{1}{A} \left[\int_{\sigma_c} c_c \frac{dH_2}{dt} da + \int_{1-\sigma_c} (\langle c \rangle_2 + c_2^1) \frac{dH_2}{dt} da \right] \quad (4-10)$$

$$= \sigma_c \bar{c}_c \overline{\frac{dH_2}{dt}}^c + (1 - \sigma_c) \left[\langle c \rangle_2 \overline{\frac{dH_2}{dt}}^e + c_2^1 \overline{\frac{dH_2}{dt}}^e \right] \quad (4-11)$$

Continuity of material flux across H_2 and the assumption that the distance separating H_2 and H_{2+} is small require that

$$F_2 = F_{2+} \quad (4-12)$$

Thus, equating (4-9) and (4-11) and noting that since H_2 and H_{2+} are parallel,

$$\frac{dH_2}{dt} = \frac{dH_{2+}}{dt} \quad (4-13)$$

we obtain

$$\langle c \rangle_3 \frac{dH_2}{dt} e = \langle c \rangle_2 \frac{dH_2}{dt} e + c_2' \frac{dH_2}{dt} e \quad (4-14)$$

By definitions (2-2) and (4-7b) the downward mass flux of air across the moving surface H_2 (i.e., measured by an observer at a fixed point on surface H_2) is

$$F = A\rho \frac{dH_2}{dt} \quad (4-15)$$

where ρ is the air density on H_2 , A is the area of the projection of a unit horizontal square on H_2 (see Figure 4-2), and F is the total downward mass flux through area A . It follows

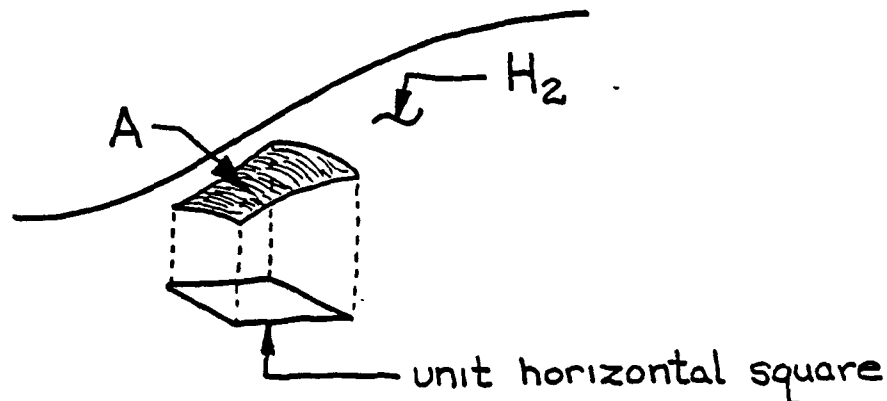


Figure 4-2. Projection of a unit horizontal square on the surface H_2 .

from (4-15) that $\rho \, dH_2/dt$ is the downward mass flux of air per unit horizontal area, rather than unit area of H_2 . Therefore, the last term on the right hand side of (4-14) is the mean downward mass flux relative to H_2 that includes the effects of mean vertical fluid motion, mean motion of surface H_2 and turbulent convection.

For notational convenience we will write

$$f_c \equiv \overline{c_2' \frac{dH_2}{dt}}^e \quad (4-16)$$

Substituting this into (4-14) we get

$$\overline{\frac{dH_2}{dt}}^e = f_c / \Delta c \quad (4-17a)$$

where

$$\Delta c = \langle c \rangle_3 - \langle c \rangle_2 \quad (4-17b)$$

An important point to note here is that $\langle c \rangle_3$ in this last expression is used as a measure of the concentration on surface H_{2+} [see (4-5)] which penetrating convective elements do not reach. This fact will be used later when we develop an approximation for f_c and the rate equation governing H_2 .

The analyses that led up to (4-17a) are applicable also to other scalar quantities, such as potential temperature θ . This fact and (4-17a) indicate that

$$f_c / \Delta c = f_\theta / \Delta \theta \quad (4-17c)$$

where

$$f_\theta = \overline{\theta_2' \frac{dH_2}{dt}}^e \quad (4-17d)$$

and

$$\Delta \theta = \langle \theta \rangle_3 - \langle \theta \rangle_2 \quad (4-17e)$$

As in the case of concentration, $\langle \theta \rangle_3$ is treated as a known quantity and is used here as a measure of θ at the level just above the altitude of the highest reaching convective parcels from the mixed layer, or equivalently, the level where the turbulent heat flux becomes zero. Since it is $f_\theta/\Delta\theta$ that we will parameterize later, we shall take advantage of (4-17c) and substitute it for $f_c/\Delta c$ from here on.

The surface H_2 is smooth in that it is not deformed abruptly within individual cumulus clouds. As a result (4-17a) is equivalent to

$$\frac{\partial \bar{z}_2}{\partial t} + \overline{v_{2H} \cdot \nabla_H z_2} - \bar{w}_e = + f_\theta/\Delta\theta \quad (4-18)$$

where \bar{w}_e is the mean vertical velocity over the environment between cumulus clouds.

By definition, the mean vertical fluid velocity \bar{w}_2 at any instant on H_2 is

$$\bar{w}_2 = \sigma_c \bar{w}_c + (1 - \sigma_c) \bar{w}_e \quad (4-19)$$

where \bar{w}_c is the mean upward velocity in cumulus clouds in the given cell. This expression and (4-18) yield

$$\frac{\partial \bar{z}_2}{\partial t} + \overline{v_{2H} \cdot \nabla_H z_2} = \frac{\bar{w}_2 - \sigma_c \bar{w}_c}{1 - \sigma_c} + f_\theta/\Delta\theta \quad (4-20)$$

The flux $F_{2,2}$ [see (4-6)] may now be expressed using (4-9), (4-12), (4-13), (4-18) and assumptions invoked above concerning the variations of H_2 within the horizontal scale of a single grid:

$$\begin{aligned} F_{2,2} = & \sigma_c \bar{c}_c \left[\frac{\bar{w}_2 - \bar{w}_c}{1 - \sigma_c} + f_\theta/\Delta\theta \right] + \langle c \rangle_3 (1 - \sigma_c) f_\theta/\Delta\theta \\ & - \langle c \rangle_2 \left[\frac{\sigma_c}{1 - \sigma_c} (\bar{w}_2 - \bar{w}_c) + f_\theta/\Delta\theta - \frac{\partial \bar{z}_2}{\partial t} \right] \end{aligned} \quad (4-21a)$$

and by similar means we obtain from (4-6)

$$F_{2,3} = \sigma_c \left[\frac{\bar{w}_2 - \bar{w}_c}{1 - \sigma_c} + f_{\theta}/\Delta\theta \right] (\bar{c}_c - \langle c \rangle_3) + \langle c \rangle_3 \frac{\partial \bar{z}_2}{\partial t} \quad (4-21b)$$

Except for \bar{c}_c all of the independent variables in (4-21) are inter-related [see, for example, (4-20)]. Thus, to obtain meaningful estimates of $F_{2,k}$ we must derive these variables from their governing equations. This task is undertaken in the following subsection.

Equations governing \bar{w}_2 , $f_{\theta}/\Delta\theta$, and z_2

First, let us derive an approximation for f_{θ} . From its definition (4-17d) we have

$$f_{\theta} = - \overline{\theta_2' w_R} \quad e \quad (4-22a)$$

where

$$w_R = w_2 - \partial z_2 / \partial t - v_{2H} \cdot \nabla_H z_2 \quad (4-22b)$$

is the vertical component of fluid relative to H_2 ; and

$$\theta_2' = \theta_2 - \langle \theta \rangle_2 \quad (4-22c)$$

where θ_2 is potential temperature on surface H_2 [cf. (4-4)]. A plausible assumption regarding θ_2 is

$$\theta_2 = \begin{cases} \langle \theta \rangle_2 & , \text{ if } w_R \geq 0 \\ \langle \theta \rangle_2 + \Delta\theta' & , w_R < 0 \end{cases} \quad (4-23)$$

Since fluid that descends through H_2 originates somewhere between levels H_2 and H_{2+} , the fluctuation $\Delta\theta'$ in (4-23) must lie in the range

$$0 < \Delta\theta' < \Delta\theta \quad (4-23a)$$

where $\Delta\theta$ is given by (4-17e). Thus, the ratio

$$\tau \equiv \Delta\theta' / \Delta\theta \quad (4-23b)$$

has a value in the range

$$0 < \tau < 1 \quad (4-23c)$$

that is determined by the complex dynamic processes that occur within the thin layer at the base of the inversion layer where penetrating thermals are entraining the warm inversion layer air and carrying it down into the mixed layer below. The value of τ is also affected by our choice of the surface H_2 . We chose H_{2+} so that it was in the stable layer of fluid above the mixed layer where spatial variations in temperature associated with turbulent mixing are not present. Thus, if we select H_{2+} as the lowest surface on which this condition is satisfied, then H_{2+} is uniquely defined. But H_2 is not so clearly established. We have required only that it be "near" enough to H_{2+} that we can equate the instantaneous material fluxes across H_2 and H_{2+} [see (4-12)]. There is probably a range of separations in which flux equality holds to good approximation, and hence there may be a range of values of τ . Later we will have to specify the turbulent velocity variance σ_w on H_2 and when this is done we will in effect have determined this surface and with it a unique value for τ .

An approximation that we shall make use of throughout our analyses of the interfacial fluxes is that averages over the horizontal extent of any surface within a grid cell, which we have been denoting by the overbar, are equivalent to ensemble (or statistical) averages. This assumption is certainly reasonable given that the grid cells of interest to us are about 20 km on a side and that the scales of convective turbulence are comparable

to the mixed layer depth, about 2 km. Here we shall extend this assumption to include averages over the environment between cumulus clouds represented by the overbar and superscript "e" in (4-22a). The validity of this approximation requires that the fractional coverage σ_c of cumulus clouds be less than about 0.5.

With this assumption, (4-22a) can be written

$$f_\theta = - [\theta'_2 \int_0^\infty w_R p(w_R) dw_R + \theta'_2 \int_{-\infty}^0 w_R p(w_R) dw_R] \quad (4-24)$$

where $p(w_R)$ is the probability density of vertical velocity w_R relative to H_2 , as defined by (4-22b). Combining (4-22c), (4-23) and (4-24) we get

$$f_\theta = - \Delta\theta' \int_{-\infty}^0 w_R p(w_R) dw_R \quad (4-24a)$$

where $\Delta\theta'$ is given by (4-17e).

Figure 4-3 shows the probability density of the vertical velocity w_2 at the inversion base H_2 as given by the numerical model of Deardorff (1974). It indicates that to good approximation, w_2 has a Gaussian density, that is,

$$p_2(w_2) = \frac{1}{\sqrt{2\pi} \sigma_w} \exp \left(-\frac{(w_2 - \bar{w}_2)^2}{2\sigma_w^2} \right) \quad (4-25)$$

where \bar{w}_2 is the mean vertical velocity at H_2 , due to subsidence, and σ_w is the variance, which is proportional to the turbulent energy at H_2 . Since the 2 last terms on the right side of (4-22b) are deterministic variables, it can be shown that $p(w_R)$ is also Gaussian with mean

$$\bar{w}_R = \bar{w}_e - \partial \bar{z}_2 / \partial t - \overline{v_{2H} \cdot \nabla_H \bar{z}_2} \quad (4-25a)$$

and variance σ_w , the same as that of w_2 . The \bar{w}_e term enters this

ALTITUDE = 1100 M \approx MIXED LAYER TOP

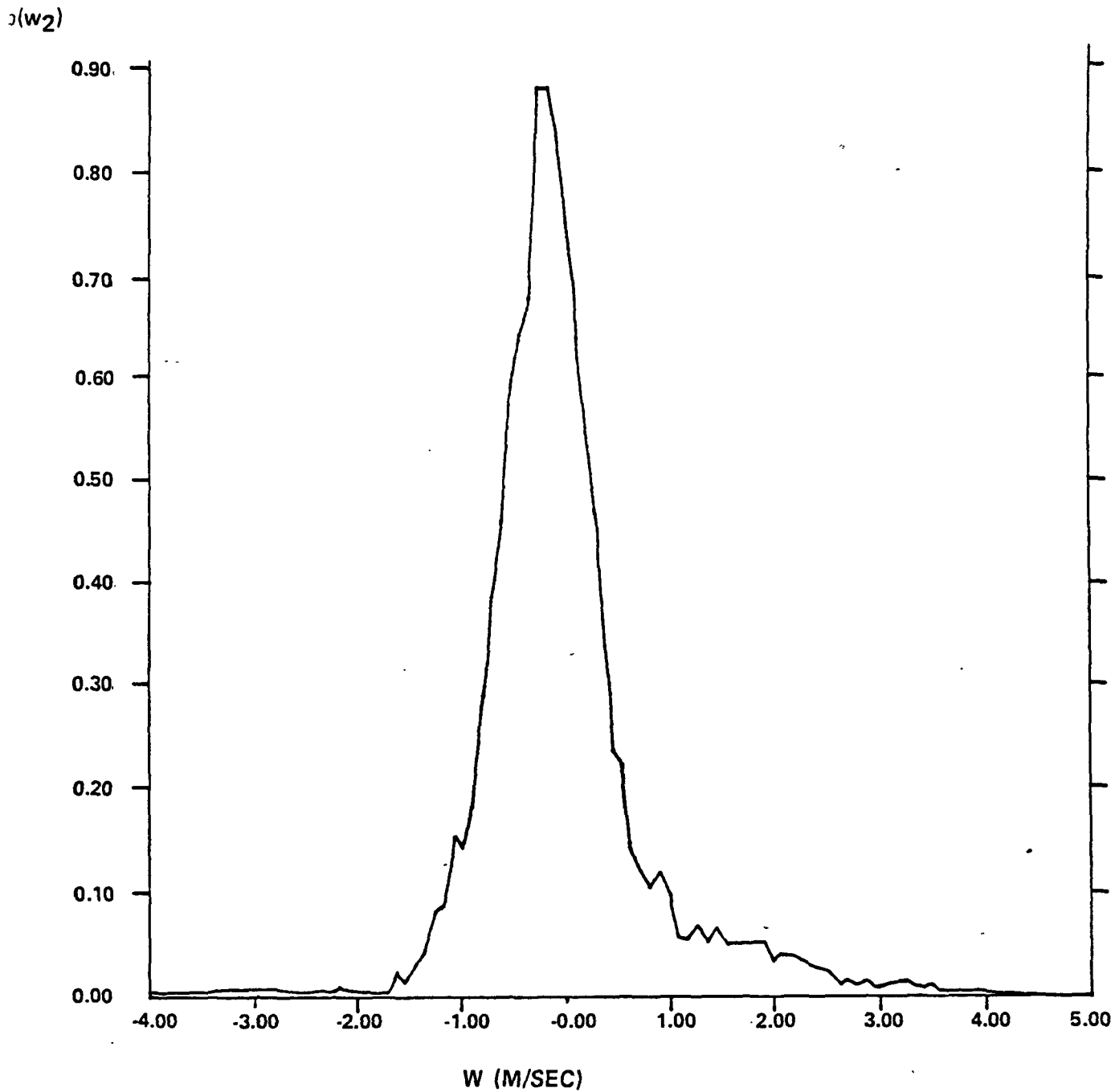


Figure 4-3. Probability density of vertical velocity w_2 near the mixed layer top (H_2) derived from the numerical model of Deardorff (1974) .

expression because we are averaging over the cumulus free environment only, as indicated by (4-22a).

The Gaussian form permits the integral in (4-24a) to be evaluated analytically. We get

$$f_{\theta} = -\Delta\theta' \left[\frac{\bar{w}_R}{2} \left(1 - \operatorname{erf} \left(\frac{\bar{w}_R}{\sqrt{2} \sigma_w} \right) \right) - \frac{\sigma_w}{\sqrt{2\pi}} \exp \left(-\frac{\bar{w}_R^2}{2\sigma_w^2} \right) \right] \quad (4-26)$$

where erf denotes the error function [see (4-23)]. Combining (4-25a) and (4-18) we obtain

$$-\bar{w}_R = f_{\theta}/\Delta\theta$$

and upon introducing (4-26) we get after some rearrangement of terms

$$J [1 - \pi/2 (1 + \operatorname{erf} J)] = \frac{T}{2\sqrt{\pi}} \exp(-J^2) \quad (4-27a)$$

where

$$J = -\frac{\bar{w}_R}{\sqrt{2} \sigma_w} \quad (4-27b)$$

The solution $J(T)$ of the transcendental equation (4-27a) in the interval $0 \leq T < 0.9$ is approximated closely by

$$J(T) \doteq \frac{T}{3.37 - 0.86T - 1.46T^2} \quad 0 \leq T < 0.9 \quad (4-27c)$$

This relationship is plotted with the exact solution of (4-27a) in Figure 4-4. Thus, from (4-27b), (4-25a) and (4-19) we obtain the mixed layer growth rate equation

$$\frac{\partial \bar{z}_2}{\partial t} + \frac{v_{2H} \cdot \nabla_H \bar{z}_2}{\bar{z}_2} = \frac{\bar{w}_2 - \sigma_c \bar{w}_c}{1 - \sigma_c} + \sqrt{2} \sigma_w J(T) \quad (4-28a)$$

and

$$f_{\theta}/\Delta\theta = f_c/\Delta c = \sqrt{2} \sigma_w J(T) \quad (4-28b)$$

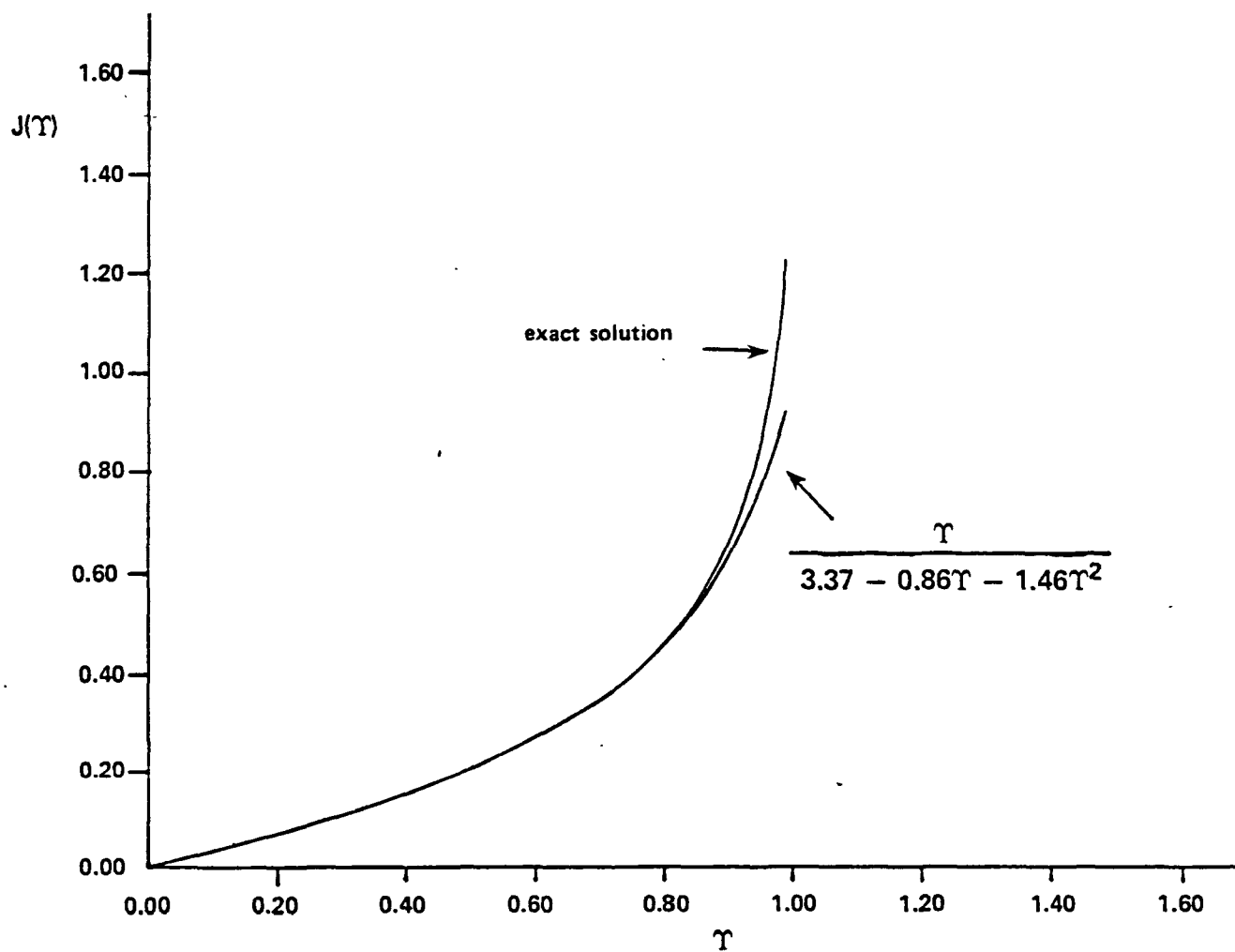


Figure 4-4. Comparison of the true solution of equation (4-27a) with the approximation (4-27c).

The vertical velocity fluctuations on H_2 are generated by convection within the mixed layer below. Hence, it seems reasonable to assume, as is often done, that σ_w is proportional to the convective velocity scale w_* :

$$\sigma_w = \alpha w_* \quad (4-29a)$$

where

$$w_* = (g/\theta \overline{(w'\theta')}_0 h)^{1/3} \quad (4-29b)$$

Here θ is the mean potential temperature in the mixed layer:

$$\theta(\lambda, \phi, t) = \frac{a^2 \cos \phi}{Ah} \int_{\lambda-\Delta\lambda}^{\lambda+\Delta\lambda} \int_{\phi-\Delta\phi}^{\phi+\Delta\phi} \int_{\hat{z}_T(\lambda', \phi', t)}^{z_2(\lambda', \phi', t)} \theta(\lambda', \phi', t) d\phi' d\lambda' dz \quad (4-30a)$$

$A = 4\Delta\lambda\Delta\phi a^2 \cos \phi$ is the grid cell area;

h is the mean mixed layer depth in the cell,

$$\begin{aligned} h(\lambda, \phi, t) &= \frac{a^2 \cos \phi}{A} \int_{\lambda-\Delta\lambda}^{\lambda+\Delta\lambda} \int_{\phi-\Delta\phi}^{\phi+\Delta\phi} \int_{\hat{z}_T(\lambda', \phi', t)}^{z_2(\lambda', \phi', t)} dz d\phi' d\lambda' \\ &= \overline{z_2} - \hat{z}_T \end{aligned} \quad (4-30b)$$

$\overline{(w'\theta')}_0$ is the kinematic heat flux at the ground; g is gravity and α is a constant. Laboratory investigations of Willis and Deardorff (1974) and numerical model results of Deardorff (1974) indicate that the value of α is about 0.4.

The heat equation, which governs θ , is of the same form as (2-29) so we have at once

$$\begin{aligned} \frac{\partial \theta}{\partial t} + \frac{\theta}{h} \frac{\partial h}{\partial t} + \langle \underline{v}_H \rangle_M \cdot \nabla_H \theta + \frac{1}{h} \langle \underline{v}_H' \theta' \rangle_M \cdot \nabla_H H_2 \\ + \nabla_H \cdot \langle \underline{v}_H' \theta' \rangle_M = \frac{1}{h} \left[\overline{\theta_2 \frac{dH_2}{dt}} - \overline{\theta_2 \underline{v}_2 \cdot \nabla_H H_2} \right. \\ \left. - \overline{\theta_T \frac{dH_T}{dt}} + \overline{\theta_T \underline{v}_T \cdot \nabla_H H_T} \right] \end{aligned} \quad (4-30c)$$

where

$$\langle \underline{v}_H' \theta' \rangle_M = \langle \underline{v}_H \theta \rangle_M - \langle \underline{v}_H \rangle_M \theta \quad (4-30d)$$

Here $\langle \underline{v}_H \rangle_M$ denotes the mean horizontal wind in the mixed layer, θ_2 and \underline{v}_2 are the potential temperature and wind vector on H_2 , H_T represents the ground surface where $\theta = \theta_T$, and $\langle \underline{v}_H' \theta' \rangle$ is defined by (2-28).

The last term on the righthand side of (4-30c) is identically zero because the ground is a material surface. The third term on the right side of this expression is just the kinematic heat flux at the ground, namely

$$-\theta_T \frac{dH_T}{dt} = (\overline{w' \theta'})_0 \equiv f_{\theta S} \quad (4-31)$$

Comparing the first 2 terms on the righthand side of (4-30c) with (4-6), which is the definition of F_2 , we see that the sum of these terms is equivalent to (4-21), but with $\langle c \rangle_2$ replaced by θ ; $\langle c \rangle_3 - \langle c \rangle_2$ replaced by $\Delta\theta$ [see (4-17b) and (4-17e)]; and with \bar{c}_c replaced by

$$\bar{\theta}_c = \xi \theta \quad (4-32)$$

where $\xi \geq 1$ (assuming that the ground surface is warmer than the mean temperature θ of the mixed layer). Substituting these results into (4-30c) we obtain

$$\begin{aligned} h \frac{\partial \theta}{\partial t} + h \langle \underline{v}_H \rangle_M \cdot \nabla_H \theta + \langle \underline{v}_H' \theta' \rangle_M \cdot \nabla_H H_2 + h \nabla_H \cdot \langle \underline{v}_H' \theta' \rangle_M \\ = \sigma_c \frac{(\bar{w}_2 - \bar{w}_c)}{1 - \sigma_c} \theta (\xi - 1) - \sqrt{2} \sigma_w J(T) [\theta (1 - \sigma_c \xi) \\ - (1 - \sigma_c)(\Delta\theta + \theta)] + f_{\theta S}. \end{aligned} \quad (4-33)$$

In order to close the system of equations (4-33) and (4-28a) we need an expression for $\Delta\theta$. Inasmuch as this is the difference between $\langle \theta \rangle_3$, the potential temperature at a level just above the highest penetrating thermals

(i.e., at the lowest level where θ is free of spatial and temporal fluctuations) and θ , the mixed layer mean temperature, we propose that

$$\Delta\theta = \Gamma\Delta h \quad (4-34)$$

where Γ is the temperature lapse rate above z_2 ,

$$\Gamma = \partial\theta/\partial z \quad , \quad z > \overline{z_2} \quad (4-35)$$

and Δh is the distance above z_2 that thermals penetrate.

To estimate Δh we assume that at the level $z_2 + \Delta h$ of maximum overshoot,

$$g\Delta\rho\Delta h = \rho w^2$$

where ρ is the density of thermals at level z_2 , $\Delta\rho$ is the difference between their density and that of the environment at $z_2 + \Delta h$, and w is the effective upward speed of thermals at z_2 . Approximating $\rho/\Delta\rho$ by $\theta/\Delta\theta$, we get

$$\Delta h = \frac{\theta}{\Delta\theta} \frac{w^2}{g}$$

or

$$(\Delta\theta)^2 = \Gamma\theta w^2/g \quad (4-36)$$

In the case of a horizontally homogeneous atmosphere (4-28a) reduces to

$$\frac{\partial h}{\partial t} = \frac{\overline{w_2} - \sigma_c \overline{w_c}}{1 - \sigma_c} + \sqrt{2} \sigma_w J(\rho) \quad (4-37)$$

and (4-30c) yields [see (2-21), (4-6) and (4-21)]

$$\frac{\partial}{\partial t} (h\theta) = \sigma_c \theta \frac{\overline{w_2} - \overline{w_c}}{1 - \sigma_c} + \sqrt{2} \sigma_w J(\rho) [\theta + (1 - \sigma_c)\Delta\theta] + f_{\theta s} \quad (4-38)$$

where

$$\sigma_w = \alpha \left(\frac{g}{\theta} h f_{\theta s} \right)^{1/3} \quad (4-38a)$$

$$\Delta\theta = [\Gamma\theta/g]^{1/2} \beta \sigma_w \quad (4-38b)$$

Here β is the ratio of the velocity w at H_2 of the deepest penetrating thermals and σ_w . Clearly $\beta \geq 1$. Also, in deriving (4-38) we assumed that

the parameter ξ in (4-32) is unity.

We have performed preliminary tests of the model equations (4-37,38) using data from the Wangara experiments for validation. These tests have shown that the accuracy of the model is so sensitive to the choice of the parameter τ that accurate results cannot be achieved with current approximations of this parameter, as originally hoped. Therefore, based on the findings of Artaz and Andre (1980) who tested a number of mixed layer entrainment models against observed data, we will adopt the simple empirical formulation

$$\sqrt{2} \sigma_w J(\tau) = \frac{1.4 f_{\theta s}}{\tau h} (= - f_{\theta} / \Delta \theta) \quad (4-38c)$$

At this point we have developed methods for determining the values of all independent variables in the expression for the flux F_2 across H_2 (4-21) except the material concentration \bar{c}_c entering cumulus clouds. We consider this variable next.

Cumulus clouds are initiated by convective thermals, or updrafts, in the mixed layer which in turn are generated and sustained by the surface heat flux. We noted in the Introduction that the roots of the updrafts that feed young cumulus clouds extend down into a relatively shallow layer of air next to the ground. There they can collect fresh emissions of NO_x and hydrocarbons and can transport them within a period of a few min into the clouds above. This phenomenon is potentially quite important to the photochemistry of the mixed layer because it is a mechanism by which fresh emissions are somewhat selectively removed. It is also important to the photochemistry of the atmosphere above the mixed layer because pollutants are injected into this layer only after experiencing the saturated environment within the clouds themselves.

The depth of the cumulus roots, and hence the quantities of fresh pollutants that can be removed, diminishes as the clouds grow. This occurs because the shadows of the growing clouds attenuate the surface heat flux until at some point continued cloud growth can be sustained only by the latent energy of condensation within the clouds themselves. If the atmosphere is conditionally unstable and there is a sufficient supply of moisture in the mixed layer, cumulus clouds eventually become self sustaining. Once this occurs and the surface heat flux has been diminished to very low levels, the updrafts feeding each cloud probably drain most of their air from upper levels of the mixed layer, and with it more aged pollutants than those found near the ground.

We will attempt to parameterize these cloud effects in our model by allowing cumulus clouds to draw a fraction ψ of their air from Layer 0. The remaining portion will be taken from Layer 2. Keep in mind that concentrations in Layers 1 and 2 tend toward the same values during well mixed daytime conditions. The fraction ψ will be made a function of time to reflect the changes (discussed above) that occur in the life cycle of the cloud updraft. The form of the cloud updraft concentration parameter \bar{c}_c follows at once:

$$\bar{c}_c = \begin{cases} (1-\psi)\langle c \rangle_2 & , \text{ in } F_{2,2} \text{ formula;} & (4-39a) \\ (1-\psi)\langle c \rangle_2 + \psi[\xi c' + (1-\xi)c] & , \text{ in } F_{2,3} \text{ formula.} & (4-39b) \end{cases}$$

The term in brackets in (4-39b) is the concentration in Layer 0. It will be discussed in detail later. The differences in the expression for \bar{c}_c for Layers 3 and 2 as indicated in (4-39) are the result of transport of material from Layer 0 directly into Layer 3 without any intermediate mixing in Layers 1 and 2. Thus, the net loss of material from Layer 2 to Layer 3 is

as specified by (4-39a); but the gain by Layer 3 is the loss of Layer 2 plus the portion of the loss of Layer 0 that enters cumulus updrafts. Further consideration of this partitioning of material will be necessary later when we derive $F_{0,0}$ and $F_{0,1}$.

Flux across the jet layer top: $F_{1,1}$ and $F_{1,2}$

In Section 3, we defined H_1 to be just above the tops of nighttime urban plumes, typically about 300 m above ground-level. In the present version of the model, H_1 will be maintained at approximately this same level during the day [see Equations (3-5) - (3-7) for the mathematical definition of H_1], but eventually we plan to modify this formulation to allow Layer 1 to handle additionally the marine layers associated with lake and sea breeze regimes.

A discussion here of some of the characteristics of the nocturnal boundary layer that fall within the bounds of Layer 1 will help provide the rationale for the flux formulation $F_{1,k}$ that follows.

Figure 4-5 compares typical temperature mixing ratio and wind speed profiles measured over rural and urban areas of St. Louis near dawn on summer days. The top of the surface radiation inversion is at about 300 m above ground level (AGL) at both sites. However, over the city there is a shallow mixed layer approximately 100 m deep. At both sites the mixing ratio decreases with height up to a point near the top of the inversion where it becomes approximately constant. Its value at this point is comparable to that observed in the mixed layer the previous day. This suggests that nighttime mixing of air between ground-level, the source of moisture, and the upper levels of the radiation inversion is weak, particularly over

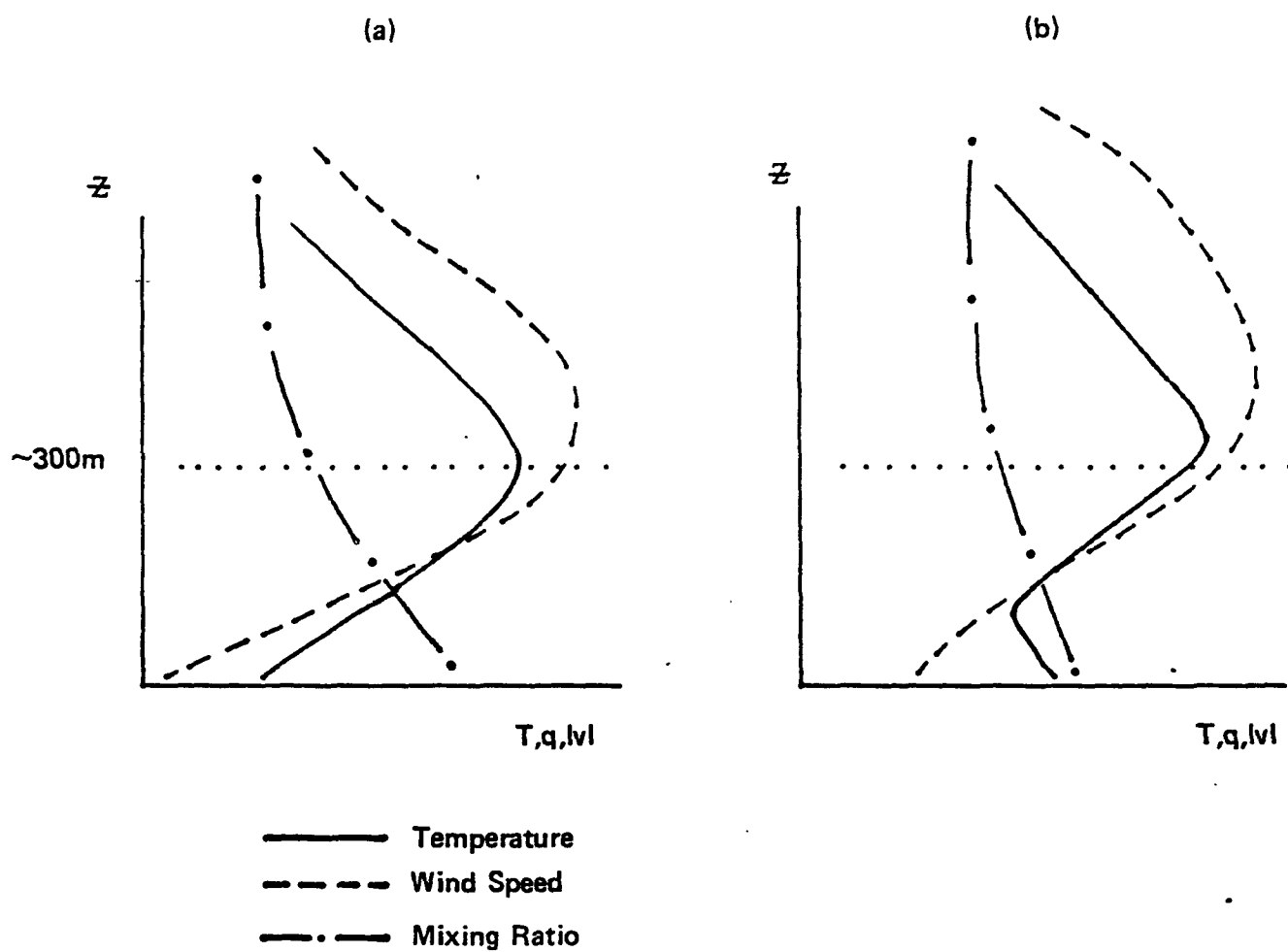


Figure 4-5. Schematic illustration of typical temperature, wind speed, and mixing ratio profiles over (a) rural and (b) urban areas at night .

rural areas where the largest vertical gradients in the mixing ratios are observed.

We have mentioned earlier that vertical fluxes of heat momentum and drier air are often observed in rural areas at night during brief, sporadic episodes of turbulence that are believed to be caused by the growth and subsequent breakdown of waves in the nocturnal jet's shear layer. The jet is evident in both sets of soundings in Figure 4-5 as the wind speed maximum that occurs at about the top of the surface inversion layer. It is not known whether these sporadic downward excursions of air are confined to a shallow layer adjacent to the ground or whether they extend well up above the jet itself. Telford et al. (1976) speculated on the basis of aircraft observations that nighttime exchanges of air take place within layers 300 - 400 m thick at all levels up to about 1000 m. This is not supported by vertical O_3 profiles measured over St. Louis near sunrise (Evans 1979). These data reveal the rather common occurrence of an O_3 maximum in the core of the nocturnal jet. If deep mixing of air occurs as suggested by Telford et al., O_3 maxima such as these could not persist through the night. One of the goals of NEROS will be to determine the vertical extent of nighttime mixing processes. This information is essential to the development of reliable regional scale oxidant models. Because if frequent exchanges of air do occur between ground-level and layers above the top of the nocturnal inversion, the maximum possible transport distance of O_3 will be considerably smaller than if deep mixing does not take place. Whatever the nature of the mixing happens to be, we should be able to treat it in the model through a suitable formulation of the flux term $F_{1,k}$.

A feature of H_1 not discussed in Section 3 that will affect the flux formulation is that with z_1 defined by (3-7), it is possible in regions of rough terrain for hills to extend up through the surface $z = z_1$.

Figure 4-6 illustrates a hypothetical case. We will denote by $\sigma_{T1}(\lambda, \phi, t)$ the fraction of the horizontal area A of the grid cell centered at (λ, ϕ) that is formed by the intersection of terrain with the surface $z = z_1$ at time t . This possibility requires that the definition of the top surface H_1 of Layer 1 be modified as follows:

$$H_1(\lambda, \phi, t) = \begin{cases} z_1(\lambda, \phi, t) - z & , \quad \text{if } z_1(\lambda, \phi, t) > \hat{z}_T(\lambda, \phi) \\ \hat{z}_T(\lambda, \phi) - z & , \quad \text{otherwise} \end{cases} \quad (4-40a)$$

$$(4-40b)$$

where z_1 is given by Equation (3-7).

Using notation like that employed earlier in formulating $F_{2,k}$ [see Equations (4-6) and (4-7)], we can express $F_{1,k}$ in the form

$$F_{1,k} = c_1 \overline{\frac{dH_1}{dt}} - \langle c \rangle_k \overline{v_1 \cdot \nabla H_1} \quad (4-40c)$$

where c_1 and v_1 denote values measured on surface H_1 , and the overbar represents, as before, an average over the area A of a grid cell. To evaluate (4-40c), we will divide the overbar averages into 2 parts: one over the area $\sigma_{T1}A$ intersected by terrain and the other over the remaining area $(1 - \sigma_{T1})A$.

Over the former, the first term in (4-40c) is the deposition flux onto the ground surfaces that extend into Layer 2. We will parameterize this flux by $\beta \langle c \rangle_2$, where β is the deposition velocity of species c . Over this same area the last term in (4-40c) is identically zero; because by virtue of (4-40b), H_1 is coincident with the terrain surface where it extends into

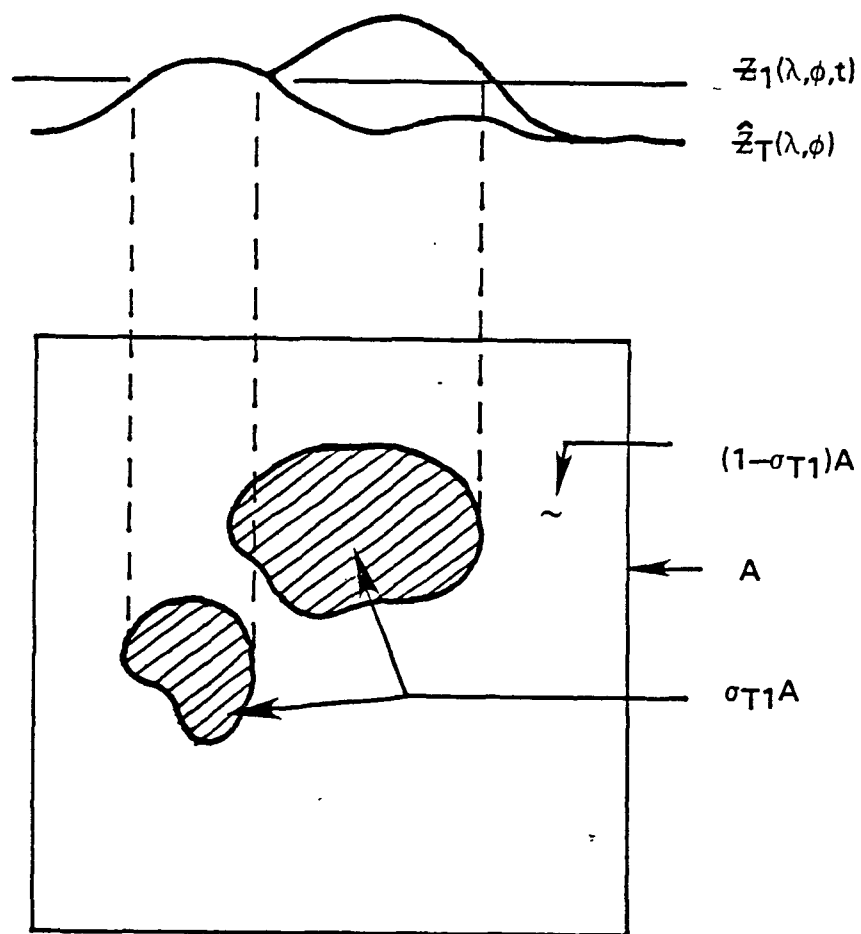


figure 4-6.

Intersection of the surface $z = z_1$, defined by Eq. (3-5), with elevated terrain features. A fraction σ_{T1} of the grid cell's horizontal area A is intersected by terrain.

Layer 2 and hence there it is a material surface. Thus, the component of $F_{1,k}$ over the area $\sigma_{T1}A$ is

$$F_{1,k})_{\sigma_{T1}} = \begin{cases} \sigma_{T1} \beta \langle c \rangle_2 & , \text{ if } k = 2 ; \\ 0 & , \text{ if } k = 1 . \end{cases} \quad (4-41a)$$

$$F_{1,k})_{1-\sigma_{T1}} = (1 - \sigma_{T1}) \left[c_1 \overline{\frac{dH_1}{dt}} - \langle c \rangle_k (\overline{v_1 \cdot \nabla H_1}) \right] \quad (4-41b)$$

where $\underline{v}_1 = (u_1, v_1, w_1)$. By design

$$\frac{dH_1}{dt} = \eta_1$$

where η_1 is a given function in stable conditions (see 3-7a) and

$$\eta_1 = \dot{z}_1 - w_{D1}$$

in neutral and unstable situations. Consequently, (4-41b) becomes

$$F_{1,k})_{1-\sigma_{T1}} = (1 - \sigma_{T1}) \cdot \begin{cases} \overline{c_1 \eta_1} - \langle c \rangle_k (\overline{\eta_1} - \dot{z}_1) & , \text{ stable ;} \\ \overline{c_1 (\dot{z}_1 - w_{D1})} + \langle c \rangle_k \overline{w_{D1}} & , \text{ neutral and unstable .} \end{cases} \quad (4-41c)$$

To approximate the terms in this equation that apply to unstable conditions, we must take into account the effects of cumulus clouds that transport material across H_1 from Layer 0 to Layer 3. The zones occupied by these roots on surface H_1 contribute nothing to air exchanges between Layers 1 and 2. Given that the cumulus updraft velocity is $\overline{w_c}$, that a fraction σ_c of the cell area A is covered by cumulus clouds, and that a fraction ψ of the cumulus flux is from Layer 0, we see that the "excluded" area for air exchanges between Layers 1 and 2 across H_1 contains a total volume flux

$$\psi \sigma_c \overline{w_c} A. \quad (4-41d)$$

We can express the total area of the excluded zones in terms of the frequency distribution $p(w)$ of vertical velocity on H_1 (i.e., all components of w_1 except that induced by terrain w_{T1}).

If we assume that the horizontal area A of a cell is large enough that spatial averages of velocity over it are equivalent to ensemble averages, it follows from the definition of the probability density $p(w)$ that the fraction of A covered by vertical velocity in the range w to $w + dw$ is $p(w)dw$.

Keep in mind that we are concerned at the moment with unstable cases and with the component of $F_{1,k}$ through the area $(1 - \sigma_{T1})A$ of H_1 (see 4-41c). Thus, it follows from (4-41d) and the properties of $p(w)$ discussed above that in the region $(1 - \sigma_{T1})A$ of H_1 that contributes to $F_{1,k}$, vertical velocity w_{D1} is in the range $-\infty < w_{D1} \leq w_m$, where w_m is the value that satisfies

$$\int_{w_m}^{\infty} w_{D1} p(w_{D1}) p w_{D1} = \frac{\psi \sigma_c \bar{w}_c}{(1 - \sigma_{T1})} \quad (4-41e)$$

In summary, we assume that all regions of H_1 in which the instantaneous vertical velocity is greater than w_m do not contribute to $F_{1,k}$ because they are part of cumulus updrafts that are transporting material directly from Layer 0 to Layer 3.

Looking now at the first two terms on the righthand side of (4-41c) and keeping in mind that w_{D1} includes turbulent velocity fluctuations, we have

$$\overline{c_1 \dot{z}_1} - \overline{c_1 w_{D1}} = - \overline{c_1 w_{R1}} \quad (4-42a)$$

where

$$w_{R1} = w_{D1} - \dot{z}_1 \quad (4-42b)$$

is the vertical component of the instantaneous fluid velocity relative to surface H_1 . As a first order approximation we shall assume that the concentration c_1 at any point on H_1 is equal to $\langle c \rangle_1$ if the relative speed w_{R1} at that point is positive and that $c_1 = \langle c \rangle_2$ if the local speed $w_{R1} \leq 0$.

That is

$$c_1 = \begin{cases} \langle c \rangle_1 & , \text{ if } w_{R1} > 0 \\ \langle c \rangle_2 & , \text{ if } w_{R1} \leq 0 \end{cases} \quad (4-42c)$$

This and the assumption that spatial averages over $(1 - \sigma_{T1})A$ are equivalent to ensemble averages lead to

$$\overline{c_1 w_{R1}} = \langle c \rangle_2 \int_{-\infty}^0 w_{R1} p(w_{R1}) dw_{R1} + \langle c \rangle_1 \int_0^{w_m - z_1} w_{R1} p(w_{R1}) dw_{R1} \quad (4-42d)$$

Averaging (4-42b) we obtain

$$\overline{w_{R1}} = \int_{-\infty}^{\infty} w_{R1} p(w_{R1}) dw_{R1} = \overline{w_{D1}} - z_1 \quad (4-42e)$$

With this we can reduce (4-42d) to

$$\begin{aligned} \overline{c_1 w_{R1}} - \langle c \rangle_1 \overline{w_{D1}} &= (\langle c \rangle_2 - \langle c \rangle_1) \int_{-\infty}^0 w_{R1} p(w_{R1}) dw_{R1} - \langle c \rangle_1 [z_1 + \\ &\quad \int_{w_m - z_1}^{\infty} w_{R1} p(w_{R1}) dw_{R1}] \end{aligned} \quad (4-42f)$$

For simplicity we will assume that the probability density of w_{D1} is Gaussian with mean $\overline{w_{D1}}$ and variance σ_{w1}^2 . Note that

$$p(w_{R1}) = p_D(w_{R1} + z_1)$$

where p_D denotes the density of w_{D1} (see 4-42b). In this case we find with the aid of (4-41e) that the term in brackets in (4-42f) is

$$\omega_1 \equiv \dot{z}_1 + \int_{w_m - \dot{z}_1}^{\infty} w_{R1} p(w_{R1}) dw_{R1} = \frac{\psi \sigma_c \bar{w}_c}{1 - \sigma_{T1}} + \frac{\dot{z}_1}{2} [1 + \operatorname{erf} \left(\frac{w_m - \bar{w}_{D1}}{\sqrt{2} \sigma_{w1}} \right)] \quad (4-42g)$$

and that

$$\omega_{1m} \equiv \int_{-\infty}^0 w_{R1} p(w_{R1}) dw_{R1} = \bar{w}_{R1} - \frac{\sigma_{w1}}{\sqrt{2\pi}} \exp \left(-\frac{\bar{w}_{R1}^2}{2\sigma_{w1}^2} \right) \quad (4-42h)$$

$$- \frac{\bar{w}_{R1}}{2} \left[1 + \operatorname{erf} \left(\frac{\bar{w}_{R1}}{\sqrt{2} \sigma_{w1}} \right) \right]$$

where \bar{w}_{R1} is given by (4-42e) and where

$$\operatorname{erf}(x) = \frac{2}{\sqrt{\pi}} \int_0^x e^{-t^2} dt \quad (4-43)$$

(Under this definition, $\operatorname{erf}(\infty) = 1$.)

Applying a similar analysis to the stable case, where w_{R1} then plays the role of $-\eta_1$ (compare 4-41c and 4-42a) we find that in general $F_{1,k}$ can be expressed in the form

$$F_{1,k} = \sigma_{T1} \beta \langle c \rangle_k \delta_{k2} + (1 - \sigma_{T1}) [\langle c \rangle_1 \omega_1 + (\langle c \rangle_1 - \langle c \rangle_2) \omega_{1m} + (\langle c \rangle_k - \langle c \rangle_1) \bar{w}_{D1}] \quad (4-44)$$

where

$$\omega_1 = \begin{cases} \text{Equation 4-42g, neutral and unstable conditions;} \\ \dot{z}_1, & \text{stable case;} \end{cases} \quad (4-44a)$$

$$\omega_{1m} = \begin{cases} \text{Equation 4-42h, neutral and unstable conditions;} \\ -\bar{\eta}_1, & \text{stable case;} \end{cases} \quad (4-44b)$$

$$\bar{w}_{D1} = \begin{cases} \text{given} & , \text{ neutr : and unstable ;} \\ w_1 + w_{1m} & , \text{ stable ;} \end{cases} \quad (4-44c)$$

and $\delta_{mn} = 1$ if $m = n$; $= 0$ otherwise.

The variance σ_{w1} of the vertical velocity component w_D on surface H_1 is caused only by turbulence. Kaimal et al. (1976) found from field studies that in the daytime mixed layer,

$$\sigma_w^2 \cong 0.4 w_*^2 \quad (4-45)$$

throughout the upper 80 percent of the mixed layer. [Here w_* is the convective velocity scale defined by (4-29b)]. Surface H_1 in our model lies in this region most of the time.

Values of σ_w at the level of H_1 are not as well known under stable nighttime conditions. Pending the outcome of the NEROS nighttime studies of vertical mixing, we will assume that under stable conditions at the ground, there is no turbulence at the altitude of H_1 (approximately 300 m). In summary, we will assume on surface H_1

$$\sigma_{w1} = \begin{cases} 0.6 w_* , L < 0 \\ 0 & , \text{ otherwise} \end{cases} \quad (4-46)$$

where L is the local Obukhov length scale.

Flux Across the Surface Layer Top: $F_{0,0}$ and $F_{0,1}$

Several factors complicate the form of $F_{0,k}$. One is that in regions of rough terrain, not all of surface H_0 is common to both Layer 0 and 1; part of it lies on terrain (see Figure 4-7). Another complicating factor is that part of the volume flux that leaves Layer 0 may enter cumulus clouds

rather than Layer 1. A third factor is that to parameterize the subgrid scale chemistry, which is one of the main roles of Layer 0, we require different flux forms for each pollutant species. The last 2 factors will be treated in the next section where we formulate the Layer 0 equations in detail. Here we will develop the gross form of the $F_{0,k}$ expression and consider the terrain effects cited above.

The general form of $F_{0,k}$ is the same as for all the other layers [see Equation (2-30)]

$$F_{0,k} = F_0 - \langle c \rangle_k \overline{\mathbf{v}_0 \cdot \nabla H_0} \quad (4-47)$$

By design of surface H_0 , the last term in this expression is identically zero [see Equation (3-10)]. The remaining term is the total downward mass flux of species c , across H_0 per unit horizontal area.

Referring to Figure 4-7, we will assume that an area $(\sigma_{T0} - \sigma_{T1})$ of the horizontal projection of surface H_0 lies on terrain. (Note that due to the natural slopes of terrain, within any grid cell σ_{T0} is always greater than σ_{T1} .)

Assuming as before that the deposition flux can be approximated in terms of layer-averaged concentrations, we have

$$F_{0,k} = (\sigma_{T0} - \sigma_{T1}) \beta \langle c \rangle_k \delta_{k1} + (1 - \sigma_{T0}) F_0 \quad (4-48)$$

where F_0 is the mass flux through the portion of H_0 common to both Layers 0 and 1, β is the deposition velocity of species c , and δ_{mn} is the Kronecker delta defined earlier following (4-44). In the next section we formulate F_0 .

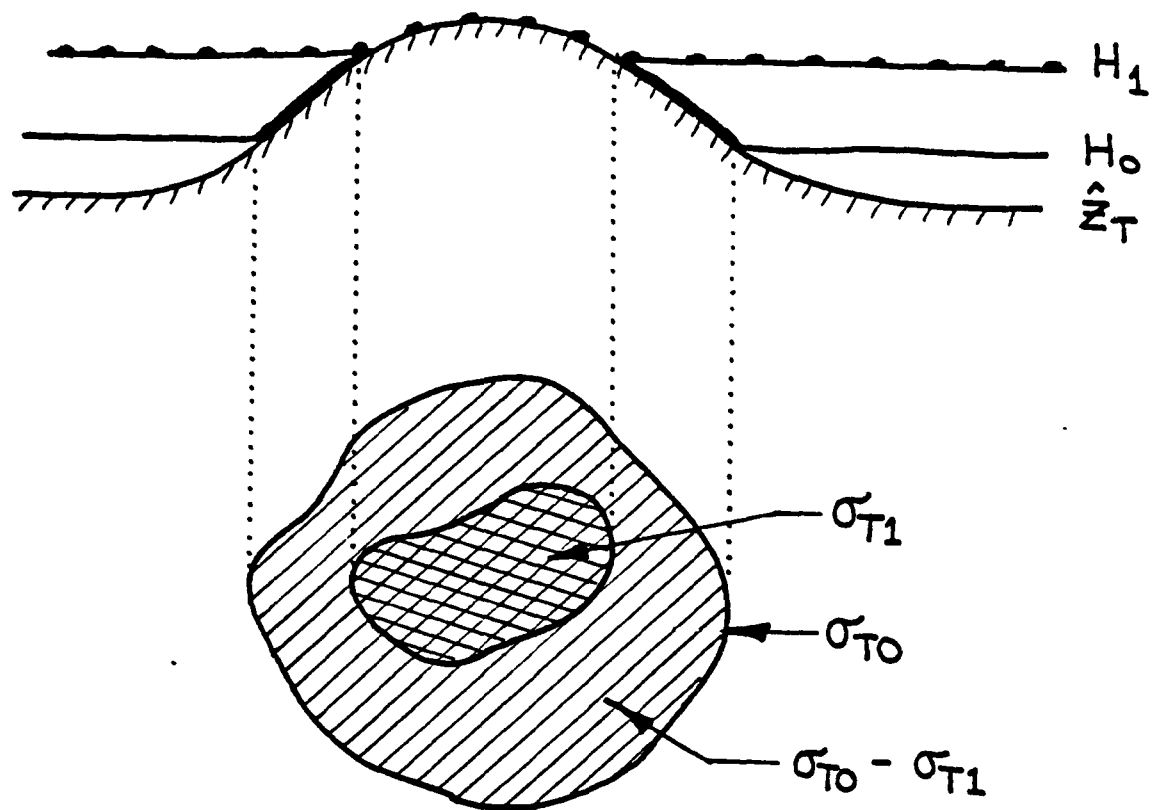


Figure 4-7. Coincidence of surface H_0 and H_1 with terrain surface. Surface area of H_0 lying on terrain is approximated as $(\sigma_{T0} - \sigma_{T1})A$.

SECTION 5

DERIVATION OF DIAGNOSTIC EQUATIONS FOR LAYER 0

The aim of this section is to develop a scheme for parameterizing the physical and chemical processes cited in the Introduction that occur within about 100 m of the ground. Among these are the effects on chemical reaction rates of the spatial segregation of pollutant concentrations that result from the injections of material from point and line sources; the stagnation of surface emissions in the calm surface layer of air over rural areas and in mountain valleys at night; and the deposition of pollutants on vegetation and other surfaces.

A basic constraint on the design of this scheme will be that it has a diagnostic form; that is one that does not require computer storage in addition to that taken by the other 3 layers of the model. (Appendix B describes the constraints on the thickness of Layer 0 that allow the use of diagnostic, rather than prognostic, equations to treat this layer.) With this type of formulation, conditions in Layer 0 are expressed in terms of current conditions in Layer 1 immediately above and local, independent parameters such as emission rates, deposition velocity and the like. In essence Layer 0 is simply a sophisticated lower boundary condition of Layer 1. Indeed, since horizontal transport is negligibly small within Layer 0, it is only through the vertical material flux F_0 that the effects of events in this layer are propagated to distant places.

An added feature of the scheme we develop is that it provides an estimate of the magnitude of spatial variations in concentration in Layer 0. This feature is particularly valuable in comparing cell-averaged concentrations that the model predicts with values observed at fixed point monitoring sites.

For simplicity we will formulate the scheme initially for the case in which cumulus clouds are not present. Once this basic form is established it will be a relatively straightforward task to generalize it to include cumulus cloud root effects.

The flux component F_0 is given by [cf. Equations (4-47) and (4-48)]

$$F_0 = c_0 \frac{dH_0}{dt} = -c_0(w_0 - \dot{z}_0)$$

This follows from (4-47) and the definition of H_0 . Thus, to parameterize F_0 we must work with the fluid velocity

$$w_{r0} = w_0 - \dot{z}_0 \quad (5-1)$$

relative to surface H_0 . Here, w_0 is the vertical component of turbulent velocity fluctuations on H_0 . Its mean value is $\bar{w}_0 = \bar{w}_{D0} = 0$, by previous assumption.

Some of the special notation that we will use to develop mathematical relationships are defined schematically in Figure 5-1. Also illustrated is a line source plume which we will use as an example in developing the physical basis for the scheme.

Let λ_- represent the fraction of surface H_0 that is in descending air relative to H_0 at any moment and let λ_+ denote the corresponding area covered by stationary and ascending air. If $p_{r0}(w)$ represents the probability density of w_{r0} [given by Equation (5-1)] then

$$\lambda_+ = \int_0^{\infty} p_{r0}(w) dw \quad (5-2a)$$

and

$$\lambda_- = 1 - \lambda_+ \quad (5-2b)$$

Let w_- be the mean value of $|w_{r0}|$ in the regions of descent (i.e., where $w_{r0} < 0$), and let w_+ denote the mean relative speed of ascending fluid. In terms of p_{r0} we have

$$w_+ = \int_0^{\infty} w p_{r0}(w) dw \quad (5-3a)$$

$$w_- = - \int_{-\infty}^0 w p_{r0}(w) dw \quad (5-3b)$$

In a later section we will prescribe forms for p_{r0} from which λ_- , λ_+ , w_- , and w_+ can be evaluated.

The area marked δA in Figure 5-1 is formed by the intersection of the line source plume with the surface H_0 . Since the source is at ground level, fluid within δA must on the average be ascending. We assume then that

$$\frac{\delta A}{\lambda_+ A} = \xi, \quad 0 \leq \xi \leq 1 \quad (5-4)$$

where

$$A = a^2 \cos \phi \Delta \lambda \Delta \phi \quad (5-5)$$

In words, it is assumed that on the surface H_0 the plumes of all sources in Layer 0 are confined to zones of ascending fluid. Once these emissions reach the cells above the lowest layer, thorough mixing of all pollutants is assumed to result so that in all fluid descending through H_0 concentrations are uniformly distributed.

Fluxes through the side walls of cells within Layer 0 are negligible, as a consequence of our definition of H_0 [see the discussion preceeding

(3-8)], compared to those through the surface H_0 and will be neglected.

Within each cell of Layer 0, we distinguish between 2 domains: δv , the volume occupied by all emissions of sources in that cell and $V - \delta v$, the region outside δv (see Figure 5-1). Here V is the volume of the lowest cell,

$$V = a^2 \cos \phi \int_{\lambda - \Delta \lambda}^{\lambda + \Delta \lambda} \int_{\phi - \Delta \phi}^{\phi + \Delta \phi} \max\{[z_0(\lambda', \phi', t) - z_T(\lambda', \phi')], 0\} \quad (5-6a)$$

It is convenient to define also an effective cell depth

$$\Delta z_0 \equiv V/A_0 \quad (5-6b)$$

and

$$A_0 \equiv (1 - \sigma_{T_0}) a^2 \cos \phi \Delta \lambda \Delta \phi \quad (5-6c)$$

Within the restrictions of assumptions introduced above, the only source of fluid in $V - \delta v$ is subsidence through the surface H_0 . However, there are 3 avenues by which fluid leaves this domain. One is by direct transport back through the cell top, that is, through an area $(1 - \xi)\lambda_+ A$. A second path of escape is turbulent entrainment into the plume volume δv . Finally, pollutant species can leave $V - \delta v$ by deposition on the ground surface. Chemical reactions within $V - \delta v$ are neglected because in view of the origin of fluid in this domain, pollutants there are somewhat aged and, consequently, the ratios of their concentrations are probably close enough to their chemical equilibrium values that little reaction occurs during the brief time that species are in residence.

Fluids enter the domain δv by entrainment from $V - \delta v$ and from pollutant sources, and they leave by chemical removal and by ascent through an area $\xi\lambda_+ A$ of the top of the cell. (Note that by definition of δv , all source emissions are injected directly into this volume.) For species such

as O_3 and NO , chemical processes within δv are expected to be rapid because the concentrations of these pollutants are greatly disturbed from their chemical equilibrium values by the fresh injections of NO_x . We believe that O_3 , NO and NO_2 are the only species that are sufficiently reactive to be affected by subgrid scale concentration variations (SSV), as it exists within δv . Accordingly, we shall assume in this study that only O_3 and NO undergo significant conversion within δv and that, moreover, the rate of reaction between these species is infinite. All other pollutants will be treated as pseudo-inert substances inasmuch as the time scales of their reactions are much larger than the characteristic residence time of material within Layer 0.

Our plan now is to write the mass balance equations for each of the pollutant species in δv and $V - \delta v$ and, from these, to formulate the desired expressions for the net material fluxes through H_0 and the mean pollutant concentrations in Layer 0. For these purposes, it is convenient to introduce the following special notations:

- $\dot{M}(x\downarrow)$ = net downward mass flow rate (mass/time) of given species x across H_0 into $V - \delta v$,
- $\dot{M}(x\downarrow)$ = mass flow rate of species x into the ground surface in $V - \delta v$ by deposition,
- $\dot{M}(x\uparrow_1)$ = mass flow rate of x from $V - \delta v$ into δv by entrainment,
- $\dot{M}(x\rightarrow^*)$ = mass rate of removal of species x in δv by chemical reaction,
- $\dot{M}(x\uparrow)$ = net upward mass flow rate of x across H_0 from δv ,
- $\langle x \rangle_1$ = average concentrations of species x in Layer 1 in the cell atop the given cell of Layer 0,

\bar{x} = average concentration of species x in $V - \delta v$,

\bar{x}' = average concentration of species x in δv .

Many of the terms listed above are illustrated in Figure 5 1.

A. Mass Balance Equations in $V - \delta v$

Consider first the mass balance of O_3 . We have

$$\dot{M}(O_{3+}) = \dot{M}(O_{3 \rightarrow 1}) + \dot{M}(O_{3 \downarrow}) \quad (5-7)$$

Straightforward analysis gives

$$\dot{M}(O_{3+}) = w_- \lambda_- A \langle O_3 \rangle_1 - O_3 w_+ (1 - \xi) \lambda_+ A \quad (5-8)$$

$$\dot{M}(O_{3 \rightarrow 1}) = v \delta a O_3 \quad (5-9)$$

In the last equation, v is the entrainment velocity of fluid into δv and δa is the effective surface area of δv . We use the approximation

$$\delta a = \frac{\delta v}{\Delta z_0} \quad (5-10)$$

where δv denotes the total volume of the domain δv . It is convenient at this point to introduce a final parameter,

$$\zeta = \frac{\delta v}{A \Delta z_0} \quad (5-11)$$

This is the fraction ($0 \leq \zeta < 1$) of the lowest cell occupied by source emissions. (Note that $\zeta \neq \delta v/V$ unless $\sigma_{T_0} = 0$.)

For the deposition mass flow rate of O_3 in $V - \delta v$, we assume

$$\dot{M}(O_{3 \downarrow}) = \beta_{O_3} A O_3 (1 - \zeta) \quad (5-12)$$

where β_{O_3} is the deposition velocity of O_3 . The factor $(1 - \zeta)$ in Equation (5-12) is intended to account for the fact that the domain $V - \delta v$ does not necessarily cover the entire ground surface. We assume that a fraction

ζ of it is covered by δv .

Substituting Equations (5-8), (5-9) and (5-12) into Equation (5-7) and making use of the relationship

$$v\zeta = w_+\lambda_+\xi \quad (5-13)$$

imposed by conservation of mass, we obtain

$$O_3 = \frac{w_-\lambda_- \langle O_3 \rangle_1}{w_+\lambda_+ + (1 - \zeta)\beta_{O_3}} \quad (5-14)$$

By analogy with this relationship, we obtain

$$NO = \frac{w_-\lambda_- \langle NO \rangle_1}{w_+\lambda_+ + (1 - \zeta)\beta_{NO}} \quad (5-15)$$

$$NO_2 = \frac{w_-\lambda_- \langle NO_2 \rangle_1}{w_+\lambda_+ + (1 - \zeta)\beta_{NO_2}} \quad (5-16)$$

and in general

$$X = \frac{w_-\lambda_- \langle X \rangle_1}{w_+\lambda_+ + (1 - \zeta)\beta_X} \quad (5-17)$$

B. Mass Balance Equations in δv

For O_3 , we have

$$\dot{M}(O_{3 \rightarrow 1}) = \dot{M}(O_{3 \rightarrow *}^{\downarrow}) + \dot{M}(O_{3 \rightarrow \downarrow}^{\downarrow}) + \dot{M}(O_{2 \rightarrow \uparrow}^{\downarrow}) \quad (5-18)$$

The first term of this equation was given earlier:

$$\dot{M}(O_{3 \rightarrow 1}) = v\delta a O_3 \quad (5-19)$$

The deposition term is given by Equation (5-6)

$$\dot{M}(O_{3 \rightarrow \downarrow}^{\downarrow}) = \beta_{O_3} \zeta A O_3^{\downarrow} \quad (5-20)$$

and the upward mass flow by

$$\dot{M}(O_{3 \rightarrow \uparrow}^{\downarrow}) = w_+\lambda_+\xi O_3^{\downarrow} A \quad (5-21)$$

The chemical removal term $\dot{M}(O_{3 \rightarrow *}^{\downarrow})$ is somewhat more complicated. Under the

assumption adopted previously that NO and O_3 react infinitely rapidly in δv , it is clear that ozone will be destroyed in δv at the same rate at which NO is produced by sources. But the rate of destruction of O_3 cannot exceed the rate $\dot{M}(O_3 \rightarrow \star)$ at which it is entrained into δv no matter how large the NO emission rate might be. Let \tilde{S}_{NO} represent the NO emission rate averaged over the lowest cell in units of moles/area. Then from the considerations cited above, we conclude

$$\dot{M}(O_3' \rightarrow \star) = \begin{cases} O_3 v \delta a & \text{if } \tilde{S}_{NO} > v \zeta O_3 \\ \tilde{S}_{NO} A & \text{otherwise} \end{cases} \quad (5-22)$$

Substituting Equations (5-19) through (5-22) into Equation (5-18) and simplifying, we obtain

$$O_3' = \begin{cases} 0 & \text{if } \tilde{S}_{NO} > v \zeta O_3 \\ \frac{O_3 v - \frac{\tilde{S}_{NO}}{\zeta}}{\beta O_3 + v}, & \text{otherwise} \end{cases} \quad (5-23)$$

The mass balance equation for NO in δv is

$$\dot{M}(NO \rightarrow \star) + \tilde{S}_{NO} A = \dot{M}(NO' \rightarrow \star) + \dot{M}(NO' \downarrow) + \dot{M}(NO' \uparrow) \quad (5-24)$$

All of the terms here can be written down immediately based on information supplied above:

$$\dot{M}(NO \rightarrow \star) = NO v \delta a, \quad (5-25)$$

$$\dot{M}(NO' \uparrow) = NO' w_{+} \lambda_{+} \xi A \quad (5-26)$$

$$\dot{M}(NO' \downarrow) = \beta_{NO} NO' \zeta A \quad (5-27)$$

$$\dot{M}(NO' \rightarrow \star) = \begin{cases} O_3 v \delta a & \text{if } \tilde{S}_{NO} > v \zeta O_3 \\ \tilde{S}_{NO} A & \text{otherwise} \end{cases} \quad (5-28)$$

Combining these expressions with Equation (5-24), we obtain

$$NO' = \begin{cases} \frac{\frac{\tilde{S}_{NO}}{\zeta} + v(NO - O_3)}{\beta_{NO} + v} & \text{if } \tilde{S}_{NO} > v\zeta O_3 \\ \frac{vNO}{\beta_{NO} + v}, & \text{otherwise} \end{cases} \quad (5-29)$$

The mass balance equation for NO_2 is

$$\dot{M}(NO_{2 \rightarrow 1}) + \tilde{S}_{NO_2} A + \dot{M}(O_3 \rightarrow *) = \dot{M}(NO_{2 \uparrow}') + \dot{M}(NO_{2 \downarrow}') \quad (5-30)$$

Note that we have neglected the loss of NO_2 due to photolysis. Following procedures like those used above we obtain

$$NO_2' = \begin{cases} \frac{NO_2 v + O_3 v + \frac{\tilde{S}_{NO_2}}{\zeta}}{\beta_{NO_2} + v} & \text{if } \tilde{S}_{NO} > v\zeta O_3 \\ \frac{NO_2 v + \frac{\tilde{S}_{NO_2} + \tilde{S}_{NO}}{\zeta}}{\beta_{NO_2} + v}, & \text{otherwise} \end{cases} \quad (5-31)$$

One of the assumptions we made earlier is that all pollutant species except O_3 and NO react too slowly to undergo significant chemical transformation during the brief time they are in the lowest layer (Layer 0).

Let x' represent the mean concentration of 1 of these species in δv .

Its mass balance equation then has the form

$$\dot{M}(x_{\rightarrow 1}) + \tilde{S}_x A = \dot{M}(x'_{\downarrow}) + \dot{M}(x'_{\uparrow}) \quad (5-32)$$

which reduces after analyses like those performed earlier to

$$x' = \frac{xv + \frac{\tilde{S}_x}{\zeta}}{\beta_x + v} \quad (5-33)$$

Recall that χ can be obtained from Equation (5-17).

C. The flux component F_0 in the case of no cumulus clouds

We can now formulate the flux component F_0 that enters in the general expression (4-48) for the total flux $F_{0,k}$. Let $F_0(O_3)$ be the net downward flux of O_3 through H_0 over a horizontal area A . That is,

$$F_0(O_3) = \frac{1}{A} [\dot{M}(O_3^+) - \dot{M}(O_3^-)] \quad (5-34)$$

which reduces with the aid of (5-8) and (5-21) to

$$F_0(O_3) = w_{-\lambda_-} \langle O_3 \rangle_1 - O_3 w_{+\lambda_+} (1 - \xi) - w_{+\lambda_+} \xi O_3^1 \quad (5-35)$$

Making use of Equations (5-14) and (5-23), we obtain finally

$$F_0(O_3) = w_{-\lambda_-} \langle O_3 \rangle_1 - O_3 w_{+\lambda_+} (1 - \xi) - \begin{cases} 0 & \text{if } \tilde{S}_{NO} > v \zeta O_3 \\ \frac{O_3 v^2 \zeta - \tilde{S}_{NO} v}{\beta_{O_3} + v} & \text{otherwise} \end{cases} \quad (5-36)$$

where

$$O_3 = \frac{w_{-\lambda_-} \langle O_3 \rangle_1}{w_{+\lambda_+} + (1 - \zeta) \beta_{O_3}} \quad (5-37)$$

Note that Equations (5-36) and (5-37) give the flux in terms of the predicted mean concentration $\langle O_3 \rangle_1$ in the cell above Layer 0, the NO emissions rate in Layer 0, and other quantities, all of which are specified.

With the NO flux $F_0(NO)$ defined in the same manner as Equation (5-34), we obtain through a process similar to that leading to Equation (5-37):

$$F_o(NO) = \langle NO \rangle_1 w_- \lambda_- \left[\frac{(1 - \zeta) \beta_{NO} + w_+ \lambda_+ \xi}{(1 - \zeta) \beta_{NO} + w_+ \lambda_+} \right]$$

$$- \begin{cases} \frac{\tilde{S}_{NO} + v\zeta(NO - O_3)}{1 + \frac{\beta_{NO}}{v}} & \text{if } \tilde{S}_{NO} > v\zeta O_3 \\ \frac{v\zeta NO}{1 + \frac{\beta_{NO}}{v}}, & \text{otherwise} \end{cases} \quad (5-38)$$

where

$$NO = \frac{\langle NO \rangle_1 w_- \lambda_-}{w_+ \lambda_+ + (1 - \zeta) \beta_{NO}} \quad (5-39)$$

and O_3 is given by Equation (5-37).

The NO_2 flux is found to be

$$F_o(NO_2) = \langle NO_2 \rangle_1 w_- \lambda_- \left[\frac{(1 - \zeta) \beta_{NO_2} + w_+ \lambda_+ \xi}{(1 - \zeta) \beta_{NO_2} + w_+ \lambda_+} \right]$$

$$- \begin{cases} \frac{v\zeta(NO_2 + O_3) + \tilde{S}_{NO_2}}{1 + \frac{\beta_{NO_2}}{v}} & \text{if } \tilde{S}_{NO} > v\zeta O_3 \\ \frac{v\zeta NO_2 + \tilde{S}_{NO_2} + \tilde{S}_{NO}}{1 + \frac{\beta_{NO_2}}{v}}, & \text{otherwise} \end{cases} \quad (5-40)$$

where

$$NO_2 = \frac{\langle NO_2 \rangle_1 w_- \lambda_-}{w_+ \lambda_+ + (1 - \zeta) \beta_{NO_2}} \quad (5-41)$$

and O_3 is given by Equation (5-37).

Finally, for all pollutants x other than NO , O_3 , and NO_2 , we have

$$F_O(x) = \langle x \rangle_1 w_- \lambda_- \left[\frac{(1 - \zeta) \beta_x + w_+ \lambda_+ \xi}{(1 - \zeta) \beta_x + w_+ \lambda_+} \right] - \frac{v \zeta x + \tilde{S}_x}{1 + \frac{\beta_x}{v}} \quad (5-42)$$

where

$$x = \frac{\langle x \rangle_1 w_- \lambda_-}{w_+ \lambda_+ + (1 - \zeta) \beta_x} \quad (5-43)$$

D. Modifications of F_O to include effects of cumulus clouds.

When cumulus clouds are present overhead, they pull a volume flux

$$F_{cu} = \psi \sigma_c V_c A \quad (5-44)$$

from Layer 0. Here

$$V_c = - \frac{\bar{w}_2 - \bar{w}_c}{1 - \sigma_c} - f_\theta / \Delta \theta \quad (5-45)$$

[see Equations (4-15), (4-20) and (4-20a)]. The upward volume flux through the top of Layer 0 is

$$w_+ \lambda_+ (1 - \sigma_{T0}) A \quad (5-46)$$

This follows from the definitions of w_+ and λ_+ . Obviously, the cumulus flux F_{cu} cannot exceed that given by (5-46), so we must limit the values we assign to ψ by

$$\psi \leq \frac{w_+ \lambda_+ (1 - \sigma_{T0})}{\sigma_c V_c} \quad (5-47)$$

We must impose this restriction on ψ at all times and at all points in space during model simulation.

Figure 5-2 illustrates the partitioning of the cumulus cloud flux. Of the upward volume flux through H_0 a fraction α given by

$$\alpha = \frac{\psi \sigma_c V_c}{w_+ \lambda_+ (1 - \sigma_{T0})} \quad (5-48)$$

is destined for cumulus clouds. The remainder enters Layer 1. Thus, when clouds are present, the flux component F_0 , which is the net downward flux into Layer 0 from Layer 1, has the form

$$F_0(x) = \frac{1}{A} \{ \dot{M}(x+) - [\dot{M}(x+) - \dot{M}_c(x+)] - [\dot{M}(x'++) - \dot{M}_c(x'++)] \} \quad (5-49)$$

where \dot{M}_c represents mass flux into clouds. Modifying Equations (5-36), (5-38) and (5-40) in this manner we obtain the final forms of the flux component F_0 for use in Equation (4-48):

$$F_0(O_3) = \langle O_3 \rangle_1 w_- \lambda_- - O_3 w_+ \lambda_+ (1 - \xi) (1 - \alpha) - (1 - \alpha) \cdot \begin{cases} 0, & \text{if } \tilde{S}_{NO} > v \zeta O_3 \\ \frac{O_3 v^2 \zeta - \tilde{S}_{NO} v}{\beta_{O_3} + v}, & \text{otherwise} \end{cases} \quad (5-50)$$

where O_3 is given by (5-37);

$$F_0(NO) = \langle NO \rangle_1 w_- \lambda_- - NO w_+ \lambda_+ (1 - \xi) (1 - \alpha) - (1 - \alpha) \cdot \begin{cases} \frac{\tilde{S}_{NO} + v \zeta (NO - O_3)}{1 + \beta_{NO}/v}, & \text{if } \tilde{S}_{NO} > v \zeta O_3 \\ \frac{v \zeta NO}{1 + \beta_{NO}/v}, & \text{otherwise} \end{cases} \quad (5-51)$$

where NO is given by (5-39);

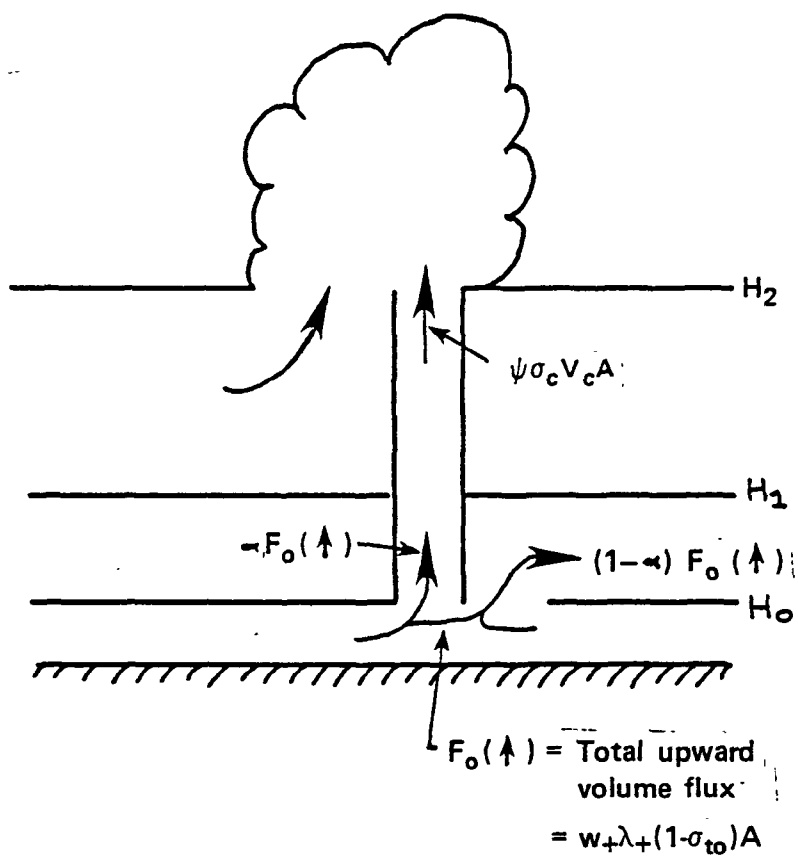


Figure 5-2. Partitioning of surface flux into cumulus clouds and Layer 1 .

$$F_0(NO_2) = \langle NO_2 \rangle_1 w_{-} \lambda_{-} - NO_2 w_{+} \lambda_{+} (1 - \xi) (1 - \alpha)$$

$$-(1 - \alpha) \cdot \begin{cases} \frac{v \xi (NO_2 + O_3) + \tilde{S}_{NO_2}}{1 + \beta_{NO_2}/v} & \text{if } \tilde{S}_{NO} > v \xi O_3 \\ \frac{v \xi NO_2 + \tilde{S}_{NO_2} + \tilde{S}_{NO}}{1 + \beta_{NO_2}/v}, & \text{otherwise} \end{cases} \quad (5-52)$$

where NO_2 is given by 5-41;

$$F_0(x) = \langle x \rangle_1 w_{-} \lambda_{-} - x w_{+} \lambda_{+} (1 - \xi) (1 - \alpha) - (1 - \alpha) (v \xi x + \tilde{S}_x) (1 + \beta_x/v)^{-1} \quad (5-53)$$

where x is given by (5-43).

E. Equations for the cell averaged and fluctuation concentrations in Layer 0.

The average concentration of species x over the volume V of a cell in Layer 0 is

$$\langle x \rangle_0 = \frac{1}{V} \int_V x \, dv \quad (5-54)$$

where V is given by (5-6a). The assumed uniformity of concentrations within each of the two domains $V - \delta v$ and δv of each cell leads to

$$\langle x \rangle_0 = (1 - \hat{\xi}) x + \hat{\xi} x' \quad (5-55)$$

where

$$\hat{\xi} = \xi / (1 - \sigma_{T_0})$$

Using this equation and those given earlier for O_3 , O_3' , NO , and so on, we obtain the following:

$$\langle O_3 \rangle_o = \begin{cases} (1 - \hat{\zeta})O_3 & \text{if } \tilde{S}_{NO} > v\zeta O_3 \\ O_3 \left[1 - \frac{\beta_{O_3} \hat{\zeta}}{\beta_{O_3} + v} \right] - \frac{\tilde{S}_{NO}(\hat{\zeta}/\zeta)}{\beta_{O_3} + v} & \text{otherwise} \end{cases} \quad (5-56)$$

where O_3 is given by Equation (5-37);

$$\langle NO \rangle_o = NO \left[1 - \frac{\beta_{NO} \hat{\zeta}}{\beta_{NO} + v} \right] + \begin{cases} \frac{\tilde{S}_{NO}(\hat{\zeta}/\zeta) - \hat{\zeta}vO_3}{\beta_{NO} + v} & \text{if } \tilde{S}_{NO} > v\zeta O_3 \\ 0 & \text{otherwise} \end{cases} \quad (5-57)$$

where NO is given by Equation (5-39);

$$\langle NO_2 \rangle_o = NO_2 \left[1 - \frac{\beta_{NO_2} \hat{\zeta}}{\beta_{NO_2} + v} \right] + \frac{\tilde{S}_{NO_2}(\hat{\zeta}/\zeta)}{\beta_{NO_2} + v}$$

$$+ \begin{cases} \frac{O_3 v \hat{\zeta}}{\beta_{NO_2} + v} & \text{if } \tilde{S}_{NO} > v\zeta O_3 \\ \frac{\tilde{S}_{NO}(\hat{\zeta}/\zeta)}{\beta_{NO_2} + v} & \text{otherwise} \end{cases} \quad (5-58)$$

and NO_2 is given by Equation (5-41);

$$\langle X \rangle_o = \frac{\langle X \rangle_1 w_{\lambda_-} [v + (1 - \hat{\zeta})\beta_X]}{v + \beta_X [w_{\lambda_+} + (1 - \hat{\zeta})\beta_X]} + \frac{\tilde{S}_X(\hat{\zeta}/\zeta)}{\beta_X + v} \quad (5-59)$$

As we noted earlier, it is not necessary to evaluate the concentration formulas [Equations (5-56) through (5-59)] at every time step and in every grid

cell. In the computer program these equations are coded as a subroutine that is called only at those times and sites where ground-level concentration estimates are needed. Concurrent evaluations of the root-mean-square concentration variation σ_x within selected cells of Layer 0 are also performed. In terms of the concentrations x and x' defined earlier, σ_x is given by

$$\sigma_x^2 = \hat{\xi}(1 - \hat{\xi})(x - x')^2 \quad (5-60)$$

This expression can be applied to any of the pollutant species. For example, the rms ozone concentration can be obtained by substituting (5-37) for x and (5-23) for x' in (5-60).

No other air pollution model predicts quantities like σ_x , but information about mean concentration variations within grid cells, such as σ_x provides, is of value in estimating concentration extrema, in assessing the magnitude of modeling errors from comparisons of predicted cell averaged concentrations with values measured at fixed monitoring sites within those cells, and in studies where subgrid scale concentrations fluctuations play an important role.

SECTION 6

THE REPRESENTATION OF ATMOSPHERIC MOTION: WINDS AND TURBULENCE

In classical studies of short-range dispersion, atmospheric motion is assumed to consist of 2 rather distinct components: a large scale, uniform (in space and time) flow (the so-called "mean" or "transport" wind); and small scale spatial and temporal fluctuations in the flow known as turbulence. The latter are generated by 2 physical processes: the transformation into kinetic energy of potential energy acquired by the fluid when its lower boundary is heated (so-called buoyancy generated turbulence); and small scale motions associated with the instability or rolling-up of vortex sheets produced on rigid surfaces by viscous effects (so-called shear generated turbulence). It has been found from observations over flat, uniform terrain that if the "mean" wind is represented by a time average of the instantaneous velocity over a period of about 30 min, that time averaged variances, covariances, etc., of the corresponding turbulent velocity fluctuations acquire universal forms when properly scaled with the speed of the "mean" wind, the depth h of the fluid in which turbulence is confined, and properties at the lower boundary, namely the surface roughness and heat flux.

It is perhaps these universal characteristics that have given rise to the common notion that turbulence, and turbulent diffusion in particular, are intrinsic properties of atmospheric flow. This premise underlies the common practice in air pollution models of representing the mean or transport wind

by a mathematical expression fit to hourly averaged wind observations and parameterizing the effects of small scale wind fluctuations by dispersion coefficients or an eddy diffusivity whose values are taken from empirical data. One of the purposes of this section is to emphasize that this is not a sound method of representing atmospheric motion in regional dispersion models. Our principal objective here will be to formulate a conceptual and mathematical basis for representing fluid motion that not only is consistent with the classical definitions of transport and turbulence associated with boundary layer diffusion studies at short range but also is applicable to simulations of dispersion over arbitrarily large scales.

Consider for a moment the universality of the structure noted above of turbulence defined in the classical sense. When a fluid of given depth is forced by some uniform, external agent to flow over an "infinite", flat, uniform surface of given roughness and temperature, the states accessible to the velocity, pressure and temperature of the fluid comprise only that limited region of the phase space of these fields whose members satisfy all the external constraints and physical laws jointly. It is in part the limited domain of accessible states that is manifest in the tendency for time-averaged quantities in idealized boundary flows to exhibit universal forms; and in essence it is the quantification of the properties of those states that is the objective of boundary layer turbulence studies.

Now in regional scale fluids the physical laws involved are the same but the external constraints are different. The driving force of the fluid is not uniform or steady; the bounding surface is not infinite, flat, or uniform; the effective depth of the flow is not fixed; etc. Under these conditions the accessible states of the fluid motion comprise a much

different region of phase space whose members can not be characterized solely by properties of the states accessible to the idealized boundary flow. The existence of a broader set of possible flow fields in these conditions is evident in a superficial way in the fact that a set of discrete, wind observations collected over a regional scale area do not uniquely define a flow field. Indeed, when one attempts to fit a continuous field to discrete data using some objective analysis technique, one finds that each technique produces a different field. The ability of any technique to fit a single function to a given set of data is a result of the imposition by that technique of additional constraints on the system. In most cases these added constraints are artificial and have no relevance to the "physics" of the system. One also finds that the flow field derived from a set of data varies as the number of locations of the observation sites changes. In short, the mean or transport flow fields commonly used in regional scale diffusion models are not unique.

This brings into question the practice of parameterizing the dispersive effects of small scale velocity fluctuations using empirical expressions that are completely independent of the data used to represent the "mean" wind. If the flow field is decomposed into a "mean" and a "turbulent" part, then for a given flow the character of the "turbulence" will change if one alters the description of the "mean" flow, as, for example, by the incorporation of additional wind data into the analysis. Recent studies such as that of Carras and Williams (1981) have measured the spread of point source plumes out to distances of 1000 km from the source and expressed the spread as a function of travel time or distance. Many long range transport models utilize these data to estimate the width of a plume, and flow fields fit to hourly averaged wind data in the model domain to estimate the centerline.

This practice is simply an extrapolation of the concepts employed in the empirical Gaussian model of short-range dispersion, and as we shall show, it is not supported by theory.

That a basic problem exists in the current methods of treating diffusion in regional scale simulations is evident in the following paradox, of which apparently few modelers are aware.

In implementing K-theory in long range diffusion models, Taylor's (1922) statistical theory of turbulence is usually invoked to support the premise that for large-scale diffusion the eddy diffusivity is proportional to the variance of the turbulence velocity, $\overline{u'^2}$ say, times the Lagrangian integral time scale T_L of the turbulence, thus,

$$K \sim T_L \overline{u'^2} \quad (6-1)$$

Since T_L is not an easily measureable quantity, its value is usually inferred from diffusion data [see, for example, Draxler (1976)]. However, the integral time scale T_L of a stochastic process is nonzero only if the energy spectrum of the process has finite amplitude in the limit as the frequency $\omega \rightarrow 0$ (we show this in Section 7). But the zero frequency component of atmospheric motion is contained not in the "turbulence" but in the time averaged wind \bar{u} which is used to describe the "mean" flow. Consequently, the integral time scale of "turbulence" as it is defined implicitly in regional models should always be zero! The existence of this paradox is an indicator that basic features of existing diffusion models are not well defined.

The questions and problems that we have cited above have come to the forefront as the scope of diffusion models has been expanded from the micro scale to the regional scale, and beyond. Short-range diffusion studies have been based heavily on empiricism and in this way theoretical questions of

definition have been largely avoided. For example, the Gaussian plume formula has been the mainstay of short-range dispersion analyses for many years. Being an empirical relationship (based largely on diffusion data collected during the Prairie Grass experiments), the plume formula provides quite well defined concentration estimates (approximately 10 min averages at fixed points in space) in terms of well specified input parameters. Unfortunately, there does not exist a comparable empirical basis for regional scale modeling, although we might add that there is some weak evidence that such a basis might actually exist, at least for chemically inert material. Specifically, the success of the Gaussian model in predicting 10-30 min averaged concentrations out to 1 km from a point source is apparently due to the small scatter in 30 min averaged concentrations that one finds from one observation to another conducted under the same flow conditions. And this small scatter is apparently attributable to a gap in the turbulence energy spectrum (Van der Hoven, 1957) at periods of about 1 h. It turns out that there is another gap in the spectrum at periods of the order of 90 days, and this suggests that perhaps there exists a regional scale counterpart of the empirical Gaussian model that would provide estimates of seasonally averaged concentrations out to 1000 km from a source in terms of certain seasonally averaged meteorological fields. Demonstrating the viability of such a model would require a large scale dispersion experiment conducted over a period of at least 1 year.

It is imperative now that unresolved theoretical aspects of the representation of atmospheric motion in diffusion models be addressed. We attempt that in this section. By this effort we hope to derive sound definitions of transport and turbulence and at the same time lay the basis for answering the following closely related questions which have great relevance

to the utility of pollution models in regulatory decision-making roles:

- (1) What aspects of pollutant concentrations are models capable of predicting?
- (2) Given our present state of knowledge, what are the theoretical limits on the accuracy with which these quantities can be predicted (assuming perfect emissions data, chemical information, etc.)?
- (3) How does one assess the accuracy of a given model?

A Game Analogy of Diffusion Modeling

In order to help convey some of the basic ideas that we introduce later, we present in this section a simple game analogy that possesses many features in common with the diffusion modeling problem but which are less abstract. Our game involves the throwing of 3 dice 3 times to produce a 3x3 matrix of, for example, numbers A . (We consider 3 throws of 3 dice, rather than a single throw of 9 dice, as a way of retaining space-time features). We assume for simplicity that the faces of each of the 3 dice are marked with an integer from the set 1, 2, 3, 4, 5 and 6. In this case the matrix A is a member of the family of $6^9 = 10,077,696$ matrices illustrated in Figure 6-1. We will call this the global family of matrices because it contains all matrices that are consistent with the fundamental definition of the system: 3 dice with faces marked 1, 2, 3, 4, 5 or 6 thrown 3 times. Every realization of this system must be a member of the global family shown in Figure 6-1, regardless of whether the dice involved are "loaded", or whether some were accidentally stamped with the same number on more than one face, or how the dice are thrown, etc. These details are characteristics

$$\begin{array}{c}
 A_n \\
 n=1 \quad \begin{pmatrix} 1 & 1 & 1 \\ 1 & 1 & 1 \\ 1 & 1 & 1 \end{pmatrix} \\
 \\
 =2 \quad \begin{pmatrix} 2 & 1 & 1 \\ 1 & 1 & 1 \\ 1 & 1 & 1 \end{pmatrix} \\
 \\
 \vdots \\
 \\
 =10,077,696 \quad \begin{pmatrix} 6 & 6 & 6 \\ 6 & 6 & 6 \\ 6 & 6 & 6 \end{pmatrix}
 \end{array}$$

Figure 6-1. The global family of possible outcome matrices A resulting from the throw of three dice three times (see text for more details) .

of the specific system (i.e., the actual dice used in a particular instance, the throwing method, etc.). For reasons that will become clear later, to maintain a proper analogy with diffusion modeling we cannot restrict specific details of the system beyond the 3 basic requirements given earlier. In other words, in our game the choice of the dice, the throwing method, etc., are optional, so long as there are only 3 dice thrown 3 times with faces marked with 1 of the integers, 1, 2, 3, 4, 5 or 6.

Suppose that a set of dice has been selected and is thrown. We ask is it possible to predict in advance the outcome matrix A ? The determinism that we associate with physical law leads us to believe that we could predict A if we knew all the physical details of the dice, their exact positions at the beginning of the throw, etc. But like so many natural phenomena, these details are so numerous and intricate that they are outside the scope of our capabilities of quantitative observation. And without precise knowledge of the initial state of a system, physical laws are powerless as predictors.

This is one of the key points that we wish to emphasize in this section. We believe that one of the debilitating practices of atmospheric diffusion modeling as it is now applied to large scales is the employment of physical laws in deterministic roles when the observational data are too crude to warrant it. In the next subsection we argue that under these conditions, a more natural role for physical law is that of delineating the class or family of possible atmospheric states (such as the family of A matrices defined above). We will postpone further discussion of this point until later in this section.

Lacking ability to predict the specific matrix \underline{A} that will result on any outcome of our dice game, we next pursue the question of whether there is not some attribute of each \underline{A} that is so prevalent in the family of \underline{A} 's that nearly all members possess it, or at least a value near some one value. In seeking such an attribute, we consider only those that are analogous to properties of interest in the diffusion modeling counterpart that we introduce later. Here the space-time character of our \underline{A} matrix will be of value. Let's assume that each column in \underline{A} represents the numbers on each of the 3 dice on 1 of the 3 roles and is roughly analogous to 3 spatial points at a fixed time. Similarly, each row of \underline{A} contains the 3 outcomes of each of the 3 successive roles and we will regard it as analogous to temporal variation at a fixed space point.

Within this frame of view the attribute "the sum of the 9 elements of \underline{A} " is the analogue of a space-time average of a single realization or outcome of \underline{A} and therefore it is a property of interest. Suppose we scan down the family of \underline{A}_n shown in Figure 6-1 and compute the sum S_n of the 9 elements of each member, viz.,

$$S_n = \sum_{i=1}^3 \sum_{j=1}^3 a_{ijn} \quad (6-2)$$

where a_{ijn} are the elements of \underline{A}_n .

We find that the sums S_n lie in the range $9 \leq S_n \leq 54$ for all n . Only 1 of the \underline{A}_n has the sum 9, namely the member $n=1$; and only the last member has the sum 54. Nine members have the sum 10 and 9 possess the sum 53. But an inordinate 767,394 have the sum 31 and the same number have the sum 32. In fact, over one-half of the entire family have sums that are within ± 10 percent of the family mean sum 31.5; and almost 90 percent have sums

within ± 20 percent of the family mean. The full distribution of sums S_n is plotted in Figure 6-2. (We add in passing that since the profile shown in Figure 6-2 is simply a property of the set of numbers illustrated in Figure 6-1, we can argue that the Gaussian shape of this profile is attributable to the "geometry" of the number system. Perhaps this is why sufficient conditions for the occurrence of the Gaussian distribution, as set forth by the Central Limit Theorem, are so weak.)

The tight clustering of the sums S_n about the family mean value suggests that even though we cannot predict which of the matrices A_n will occur on any occasion, we can predict with respectable accuracy what the sum of its elements will be, provided that there is nothing inherent in the dice, the throwing method, etc., that causes preferential occurrence of those matrices whose sums are farthest from the family mean value. Thus, we are back to the problem of predictability or, more generally, causality. What we lack is information about the "mechanism" that selects from the family of A matrices the ones we actually observe when a given set of dice are rolled.

Philosophically, one might argue that there is no causal "mechanism", that the outcomes of A that we observe are simply revelations of the unfolding of time. However, this point of view does not aid our understanding or conceptualization of the problem so we will postulate a "mechanism" that is consistent with observation. Specifically, we imagine that for every set of dice, throwing method, surface, etc., there exists a well balanced wheel and pointer with the family numbers n shown in Figure 6-1 inscribed on the circumference of the wheel. Before each throw (i.e., 3 throws of the 3 dice), the wheel is spun (by "mother nature") and the number n indicated by the pointer when the wheel stops determines the matrix A that we observe on that throw.

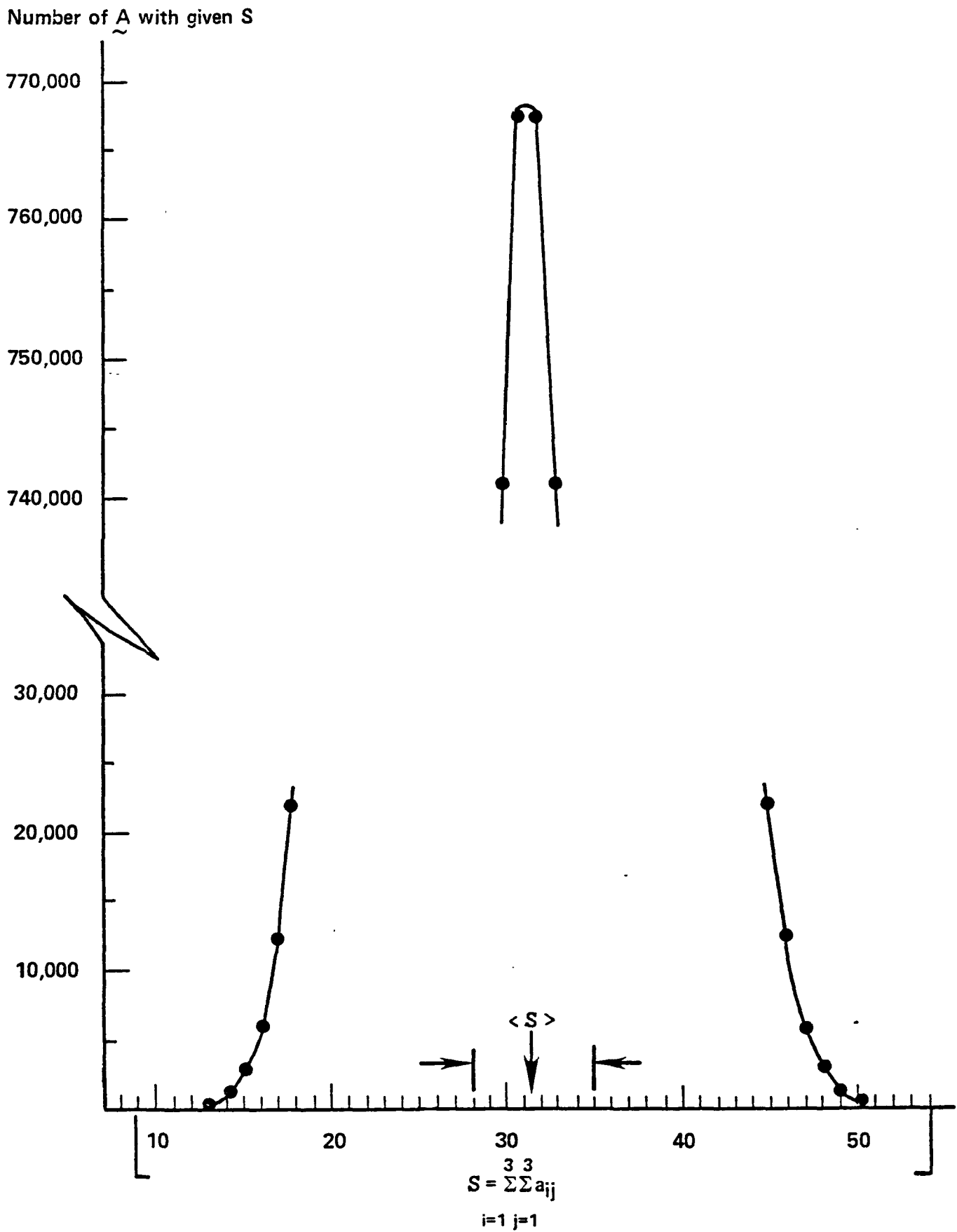


Figure 6-2. Number of matrices in the global family with given element sum S .

Now there are many ways to arrange the numbers n on the wheel. The simplest is to include all the numbers, $n=1,2,\dots, 10,077,696$ and to allocate equal angles of arc to each. This configuration is the one we would associate with "fair" dice games in which any one of the possible outcomes (A) is as "likely" to occur as any other. Another possible arrangement of the numbers is to include them all but to allocate more space to some numbers than to others. This would represent a game in which the dice were "loaded". Yet another possibility is to exclude some numbers n altogether. For example, if due to some manufacturing flaw 1 of the 3 dice had had a "5" stamped on the face that should be marked "6", our corresponding "causal wheel" would not contain the numbers n of Figure 6-1 that denote matrices with 6's in row 2, say; and those numbers that represent matrices with 5's in row 2 would have twice the space allocations as the others.

Our wheel concept is quite crude but we believe that it provides an easy way to conceptualize the link between the purely mathematical aspects of the problem, such as the family of possible states of the system (or sample space as it is usually referred to in probability theory), and the sequence of system states that we would actually observe with a particular system (e.g., set of dice, throwing method, etc.). Also, in the context of the wheel the probability of occurrence of a given matrix A_n is simply

$$\text{Prob}(A_n) = \frac{\lambda_n}{2\pi} \quad (6-3)$$

where λ_n is the arc length in radians allocated to member n .

In statistical analyses one deals with ensembles of the function or variable in question. We can produce an ensemble of A 's by spinning the wheel many times and listing the A 's that result. One of the important

purposes that an ensemble serves is to provide information about which members of the global family of states is included on the wheel and the relative space allocated to each (i.e., their probabilities).

In some instances we do not need to know anything about the "causal wheel". For example, if we are designing a system and are concerned about the occurrence of certain states that violate some safety criteria, and if we are able to define the global family of possible states as we have done in Figure 6-1 for the dice game, then there is no need for information about the wheel if the states of concern are not members of the family. In most cases, however, the violating states are members of the global family and the problem is then one of estimating how frequently they will occur during operation of the system. (The ultimate goal of the present study is the estimation of the frequency of violation of air quality standards.) In these situations information about probabilities is essential.

In this connection 2 important points must be made. The first is that theoretical knowledge is generally incapable of describing exactly which family members are on the wheel and how they are apportioned space. We can only infer this information from observations, namely from an ensemble as defined earlier. The second point, which is somewhat contradictory of the first, is that the exact collection and layout of numbers on the wheel cannot be determined from observation.

To see this, suppose we had a perfectly balanced wheel with the numbers $n=1,2,\dots,N=10,077,696$ arranged at equal intervals around its rim. Since there exists no force to cause the wheel to stop on each of the N numbers once and only once in N spins, an ensemble of N numbers produced by N spins might not contain some of the n . Obviously, we would be wrong if we inferred

from this ensemble that the missing n were not present on the wheel. It is this same freedom of the action of the wheel that makes it impossible to predict the frequency with which given states of a system will occur.

For example, our intuition tells us that throwing 9 dice and having them all come up 6's (the last member of the A family of Figure 6-1), is a "rare" event. Yet if the dice are "fair", this event is just as likely as any of the others. Thus, all of the outcomes are equally rare so a "rare" event occurs on every outcome of the throw! It follows that there is no reason for "rare" events to occur infrequently. In the language of hydrologists, the "hundred year flood" may occur several years in succession. Consequently, all we can do is base decisions on the expected frequencies of events, and then to hope that we're lucky!

The expected frequency of the all-6 matrix of Figure 6-1 in a fair game is 1 in 10,077,696 games. If, in some hypothetical game, the player won \$10 on every throw that the all-6 matrix did not come up but was beheaded the first time it did, one could "expect" to make a million dollars a year at this game for 100 years before suffering the ultimate loss. But there is nothing in the universe to prevent the all-6 matrix from coming up the very first game! Similarly, we can "expect" the sum S of the dice to differ from 31.5 by no more than ± 20 percent in only 1 game in 10. But there is nothing to prevent exceedance in 10 successive games. Our purpose in elaborating on these basic concepts is partly to emphasize the limits on the knowledge that we can hope to acquire about the future behavior of natural systems. We especially want to emphasize that the notion of determinism that underlies current thinking and practices in air pollution modeling and in the expectations that regulatory officials have in the utility of model pre-

dictions is unsupportable. Another purpose is to lay the bases for the general approach to diffusion modeling that we present in the next subsection.

Before proceeding we need to introduce a few more concepts and then to summarize all that we have presented in this section.

We first define a subset of the global family of states as the collection of all members that have some given property in common. For example, we can speak of the subfamily of A 's that have 1's along their main diagonal (there are 6^6 members of this subfamily); or the subfamily whose element sum $S = 18$ (there are 22,825 members of this subfamily); etc.

The ensemble mean of a parameter is obtained by generating an infinite ensemble of system states (e.g., A 's) in the manner described earlier, and averaging the parameter values collected from each member of the ensemble. We denote ensemble averages by angle brackets $\langle \rangle$.

Intuitively, one can see that the ensemble mean can be computed from the global family by weighting the parameter value associated with each member of the family by the probability of that member, as defined in Equation (6-3). For example, the ensemble mean of the matrix element sum S_n discussed earlier is

$$\langle S \rangle = \frac{10,077,696}{\sum_{n=1} \text{Prob}(A_n)} S_n \quad (6-4)$$

(In the remainder of this report the ensemble average $\langle \rangle$ and the cell average $\langle \rangle_j$ can be distinguished by the presence or absence of the subscript.)

If S represents the sum of the elements of the matrix A that occurs on a given throw, then as we have already discussed, S is not predictable but $\langle S \rangle$ is. Thus, it is of interest to know how far to "expect" S to fall from

the ensemble mean value $\langle S \rangle$. Denoting the difference by

$$\epsilon = S - \langle S \rangle \quad (6-5)$$

we see that the ensemble mean square value of ϵ is

$$\langle \epsilon^2 \rangle = \frac{10,077,696}{\sum_{n=1} \text{Prob}(A_n)} (S_n - \langle S \rangle)^2 \quad (6-6)$$

If $\langle \epsilon^2 \rangle^{\frac{1}{2}}$ is a small fraction of $\langle S \rangle$, then within the ensemble the values of S are clustered around $\langle S \rangle$ and we can expect values near $\langle S \rangle$ to occur frequently. (The distribution of S_n shown in Figure 6-2 is an example.) This measure of the range of likely values is one of the easiest to determine and is used widely in statistical analyses.

In this section we have distinguished between 2 inherent aspects of natural systems: the global family of possible states of the system, and the "causal wheel" which we shall use here to conceptualize the agent that causes particular states to occur on particular occasions when observing a particular system. A precise description of the global family (or sample space) can often be derived from the fundamental features of the system. We did this earlier for the case of a system of dice. However, a quantitative description of the causal wheel is generally not derivable and can only be inferred from actual observations of the system's behavior. The property of concern is embodied in the concept of probability, which we defined in Equation (6-3) in terms of our wheel. Having defined the global family and estimated the probability of its various members, we can then calculate ensemble mean values as in Equations (6-4) and (6-6) above. If our description of the global family and its member's probabilities are accurate, we can extract certain ensemble statistics from this information that will delineate bounds within which given system's parameter values can be expected to fall

with given frequency. These expected frequencies represent averages over an infinite period of observation and may differ greatly from those seen during a finite period of observation, even when the information used to make the expected frequency estimates is exact. The important point is that the parameter value itself is not predictable. The best that can happen is that the interval over which 90 percent of the values are expected to occur is so narrow that, on average, 90 percent of the observed values differ negligibly from the prediction.

The Statistical Bases for Air Pollution Modeling

The quantities of pollutants and their precursors emitted into the atmosphere and the times and places where they are released are variables that, for the most part, are controlled by man. In fact, it is this control that is to be exercised to achieve concentration levels that are in compliance with air quality standards. But once material is airborne, its fate is determined jointly by atmospheric motion, chemistry and other processes that are neither controllable nor observable (quantitatively) in their entirety. Like the dice discussed earlier, atmospheric motion obeys known physical laws but the information needed about the state of the atmosphere to apply these laws in a predictive role is far beyond our capabilities to acquire. Consequently, the joint effects of atmospheric motion, chemistry, etc., on pollutant concentration must be treated in a statistical manner like that employed earlier with the dice game. Our first step, then, is to define the global family of possible atmospheric states.

The Global Family of Atmospheric States

1. General considerations

Let \mathcal{D} denote the spatial region in which pollutants are to be modeled and let T represent the period of interest. Let $\hat{u}(\underline{x}, t)$ represent the instantaneous fluid velocity at any point (\underline{x}, t) in space. Then, by expressing atmospheric motion in the truncated form

$$\underline{u}(\underline{x}, t) = \begin{cases} \hat{u}(\underline{x}, t), & \text{if } \underline{x} \in \mathcal{D} \text{ and } 0 \leq t \leq T \\ 0, & \text{otherwise} \end{cases} \quad (6-7)$$

we can represent \underline{u} by the complex Fourier transform

$$\underline{u}(\underline{x}, t) = \frac{1}{(2\pi)^{n+1}} \int \int \underline{U}(\underline{k}, \omega) e^{i(\underline{k} \cdot \underline{x} + \omega t)} d\underline{k} d\omega \quad (6-8)$$

where n is the spatial dimensionality of the modeling region ($n=1, 2$, or 3); \underline{U} is the complex Fourier transform of \underline{u} ; \underline{k} is the wave number vector; ω is the angular frequency; and the integrations are over all \underline{k} and ω space. By definition of \underline{U} the inverse transform of (6-8) is

$$\underline{U}(\underline{k}, \omega) = \int_{\mathcal{D}} \int_0^T \underline{u}(\underline{x}, t) e^{-i(\underline{k} \cdot \underline{x} + \omega t)} dt d\underline{x} \quad (6-9)$$

Consider for the moment the case where \mathcal{D} is one dimensional. Equation (6-8) reduces to

$$u(x, t) = \frac{1}{(2\pi)^2} \int \int U(k, \omega) e^{i(kx + \omega t)} d\omega dk \quad (6-10)$$

where now u , U , and x and k are scalar variables. We can imagine the integrals in (6-10) to be the limits of sums, namely

$$u(x,t) = \frac{1}{(2\pi)^2} \lim_{\Delta k \Delta \omega \rightarrow 0} \sum_{n=-\infty}^{\infty} \sum_{m=-\infty}^{\infty} \hat{u}_{mn} e^{i(k_n x + \omega_m t)} \Delta \omega \Delta k \quad (6-11)$$

where $k_n = n\Delta k$, $\omega_m = m\Delta \omega$ and \hat{u}_{nm} are elements of the matrix \hat{u} . In words, given a one dimensional domain \mathcal{D} and time period T , we can represent any velocity fields $u(x,t)$ in that region by a matrix \hat{u} using Equation (6-11) and its 1-D counterpart, Equation (6-9). For each possible velocity distribution $u(k,t)$ there exists a matrix \hat{u} , and conversely.

Note that the matrices \hat{u} are analogous to the A used in the previous section to represent the possible states of the system of dice. Our reason for working with \hat{u} rather than the velocity itself is that the former provides a much more concise way of representing continuous functions, especially when they are to be approximated by a finite set of discrete data.

In order to illustrate important points, it is necessary to work with at least 2-D fluids. Therefore, considering a two dimensional flow, we adopt the notations

$$\underline{u}(\underline{x},t) = [u(\underline{x},t), v(\underline{x},t)] \quad (6-12a)$$

$$\underline{x} = (x,y) \quad (6-12b)$$

$$\underline{u}(\underline{k},\omega) = [u(\underline{k},\omega), v(\underline{k},\omega)] \quad (6-12c)$$

$$\underline{k} = (k_x, k_y). \quad (6-12d)$$

Then, from Equation (6-8) we have

$$u(\underline{x},t) = \frac{1}{(2\pi)^3} \int \int u(\underline{k},\omega) e^{i(\underline{k} \cdot \underline{x} + \omega t)} d\omega d\underline{k} \quad (6-13a)$$

$$v(\underline{x},t) = \frac{1}{(2\pi)^3} \int \int v(\underline{k},\omega) e^{i(\underline{k} \cdot \underline{x} + \omega t)} d\omega d\underline{k} \quad (6-13b)$$

In the case of the dice game we were able to define the entire family of possible states \underline{A} using only the definition of the system. To some extent we can do that with the fluid system. First, we note that since \underline{u} is a real function, the transform \underline{u} , which is complex, must satisfy certain conditions. One of these is found by taking the complex conjugate of (6-9). We get

$$\underline{u}^*(\underline{k}, \omega) = \int_D \int_0^T \underline{u}(\underline{x}, t) e^{-i(\underline{k} \cdot \underline{x} + \omega t)} dt d\underline{x} \quad (6-14)$$

where \underline{u}^* denotes the complex conjugate. Comparing (6-14) and (6-9) we see that

$$\underline{u}^*(\underline{k}, \omega) = \underline{u}(-\underline{k}, -\omega) \quad (6-15a)$$

$$\text{Also} \quad \underline{u}^*(-\underline{k}, -\omega) = \underline{u}(\underline{k}, \omega) \quad (6-15b)$$

Multiplying (6-15a) by (6-15b) we find that

$$|\underline{u}(-\underline{k}, -\omega)| = |\underline{u}(\underline{k}, \omega)| \quad (6-16a)$$

$$|\underline{v}(-\underline{k}, -\omega)| = |\underline{v}(\underline{k}, \omega)| \quad (6-16b)$$

In words, the amplitudes of the complex Fourier transforms must be even functions of \underline{k} and ω in order for the fluid velocity components to be real functions. Thus, the global family of transforms \underline{u} is comprised of only complex functions that satisfy Equations (6-15) and (6-16).

Strictly speaking this condition and any others that arise from the realness of \underline{u} are the only conditions that we should impose on the definition of the global family. The constraints imposed by physical law should be looked upon as properties of our causal wheel inasmuch as they are the re-

sults of observations of the natural world. (This is the view we held earlier in defining the global family of outcomes \underline{A} of the dice game.) Indeed, fluid flows that violate 1 or more of the so-called physical laws may be possible but have such small probabilities that they have never been observed. This philosophical argument notwithstanding, we shall proceed to include physical law in the definition of the global family of velocity transforms \underline{u} .

2. The constraints of physical laws

Physical laws have the effect of imposing certain relationships among the elements of each member of the \underline{u} family. We will illustrate this here considering only the mass continuity law in its incompressible form, and the momentum law, both in the context of a 2-D fluid. Later we will consider a more general case.

The continuity law is

$$\frac{\partial u}{\partial x} + \frac{\partial v}{\partial y} = 0 \quad (6-17)$$

Substituting (6-13a) and (6-13b) into this equation and performing the differentiation, we get

$$k_x u(k_x, k_y, \omega) + k_y v(k_x, k_y, \omega) = 0 \quad (6-18)$$

Thus, any function $\underline{u} = (u, v)$ that does not satisfy both (6-15) and (6-18) is not a member of the global family. All other \underline{u} , of which there are infinitely many, are eligible members.

The momentum law in 2 dimension, and somewhat simplified, can be expressed in the form

$$\frac{\partial \eta}{\partial t} + \frac{\partial}{\partial x}(u\eta) + \frac{\partial}{\partial y}(v\eta) = \kappa \frac{\partial^2 \eta}{\partial x^2} + \kappa \frac{\partial^2 \eta}{\partial y^2} \quad (6-19)$$

where η is the vorticity defined by

$$\eta = \frac{\partial v}{\partial x} - \frac{\partial u}{\partial y} \quad (6-20)$$

and κ represents molecular viscosity. Denoting the transform of η by $N(\underline{k}, \omega)$, we find from (6-19)

$$\begin{aligned} i\omega N(\underline{k}, \omega) + i \int \int N(\underline{k}', \omega') [k_x u(\underline{k} - \underline{k}', \omega - \omega') \\ + k_y v(\underline{k} - \underline{k}', \omega - \omega')] d\underline{k}' d\omega' = -\kappa(k_x^2 + k_y^2) N(\underline{k}, \omega) \end{aligned} \quad (6-21a)$$

and from (6-20) we obtain

$$N(\underline{k}, \omega) = i[k_x v(\underline{k}, \omega) - k_y u(\underline{k}, \omega)] \quad (6-21b)$$

Any complex function $\underline{u} = (u, v)$ that does not satisfy all of the relationships, (6-21), (6-16) and (6-15) is not a member of the global family of fluid velocity transforms. In atmospheric studies we deal with a 3-dimensional fluid that is heated and cooled and that contains water. In this instance to describe the state of the system we need in place of the vector (u, v) used in the preceeding example a 6-dimensional vector $(u, v, w, \rho, \theta, q)$, where (u, v, w) are the fluid velocity components, ρ is the fluid density, θ its temperature, and q the mass of water vapor per mass of air. If we let \underline{u} represent this 6-D vector, or its equivalent, in Fourier space, then in the manner illustrated above we could derive from the conservation laws of momentum, mass and energy the relationships that define the global family of \underline{u} . Let's call this family Ω . The details of its definition, corresponding to Equation (6-18) and (6-21), are not important at this point and we can think of it simply as the intersection in function space of those subsets of \underline{u} each of whose members satisfies one of the physical laws.

This is illustrated schematically in Figure 6-3.

The set Ω represents all possible fluid motions. Specifying the fluid (i.e., its viscosity, heat capacity, etc.) and suitable initial and boundary conditions effects the selection from Ω of a single function that describes the exact state of the fluid system in space-time under the conditions prescribed. This is the essence of determinism, but it is generally unachievable in practice for the same reason that the outcome of the throw of a set of dice is not deterministic: the initial and boundary conditions cannot be determined with adequate resolution.

When we specify the initial and boundary conditions of a fluid, we do so only in some macro sense. That is, we say that a surface is "smooth" but on the microscale it is very rough. Similarly, we say that a fluid is initially "at rest", but on the microscale the fluid is in a constant state of agitation (this is evident in Brownian motion). Generally speaking, in low Reynolds number flows the state of the system is insensitive to microscale details in the initial and boundary conditions. In this class of problems a macro-specification of the initial and boundary conditions determines the macro state of the system uniquely. The analogous situation with the dice is having a set that is so "loaded", that despite differences in the way the dice are held or tossed, every throw results in the same outcome matrix A . In effect, the causal wheel has only 1 system state on it.

The same is not true at high Reynolds numbers. It is found, for example, that as the pressure gradient driving fluid through a pipe is steadily increased, a "critical" Reynolds number is eventually reached at which the flow field suddenly changes from the organized, Hagen-Poiseuille state

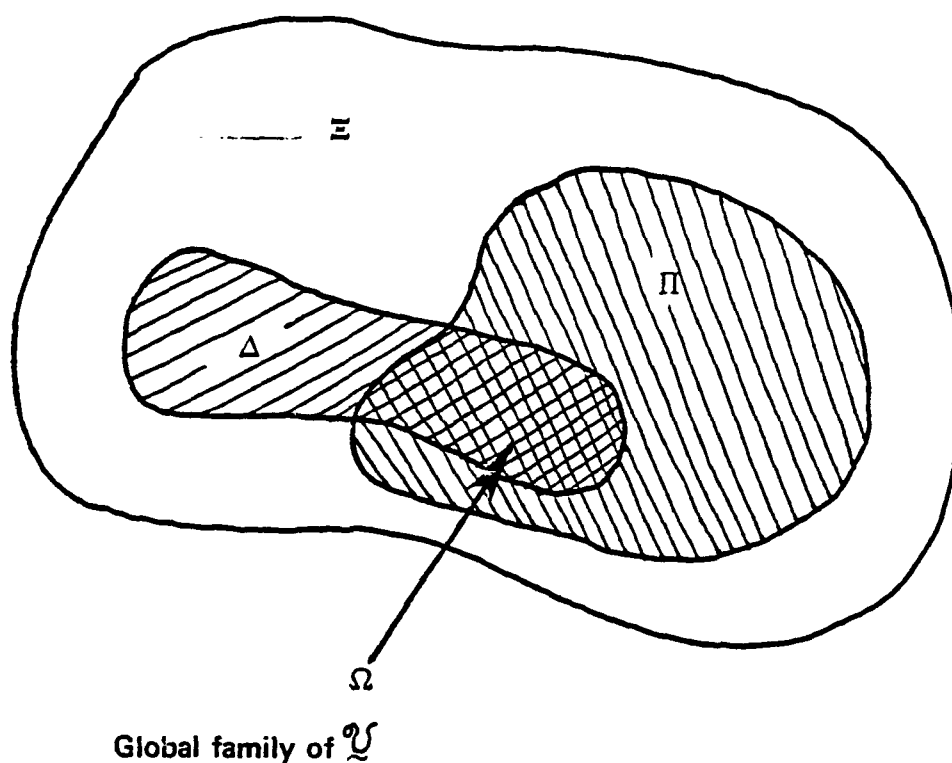


Figure 6-3. Illustration of the set Ω of complex functions $\underline{u}(k, \omega)$ that comprise the global family of fluid flow velocity Fourier Transforms. Set Ξ represents functions that satisfy purely mathematical constraints like Eq. (6-15). Set Δ represents functions that satisfy mass continuity relationships, like Eq. (6-18); and set Π denotes functions that satisfy all other laws like momentum and entropy. Intersection of Δ and Π defines the global family Ω of \underline{u} .

characteristic of the low Reynolds number regime into a chaotic state known as turbulence. No matter how many times the experiment is repeated, the state of the fluid after the onset of turbulence is different and it differs from one pipe to another. In these cases the flow is so sensitive to small scale details in the initial state of the fluid and the boundaries that specification of only macro properties of the initial and boundary conditions is only adequate to delineate the subset of Ω to which the fluid state u belongs, but not the exact state u itself (the causal wheel now contains a subset of Ω rather than a single member). Let's call this set W . We can illustrate the differences among the members of W and something of the nature of the set W itself with the following analogous problem in free convection.

Imagine a closed air chamber with thermally insulated walls and top and with a bottom made of a high resistance metal that becomes hot when an electrical current is made to flow through it. And imagine that a velocity probe is placed at some arbitrary, fixed location inside the chamber.

Suppose now that after waiting several days for the air inside the chamber to reach a "state of rest", an electrical current were applied to the bottom of the chamber and simultaneously recording of the signal from the velocity probe were begun. We would expect that after some brief interval the velocity would depart from its initial value of zero and would vary in an erratic manner from that time on. Let's suppose that in this first experiment the velocity is recorded for 1 h and after that the heating current is switched off.

Suppose that after waiting many days for the heat injected into the chamber in the first experiment to escape and for the air to return once again to a "state of rest" the same experiment were repeated. Our intuition

tells us that the initial portion of the velocity record made this second time might coincide with that made in the first experiment, but in time the 2 records would diverge and would differ in a "random" way for all later times.

Since it is axiomatically assumed that fluids obey physical laws (whether those laws are represented accurately by the mathematical equations currently used is another matter) and that the solutions of the equations that express those laws are unique functions of the initial and boundary conditions, the only way the velocity records collected in our hypothetical experiments could differ would be for the initial, or less likely, the boundary conditions to be different in the 2 cases. (Actually, to the author's knowledge an experiment of this type has never been conducted, so the conclusion that the velocity would differ from one outcome to the next is only speculation. We look upon this simply as a "thought experiment" that illustrates the nature of an ensemble of flow fields.)

Our statement that the air in the chamber is initially "at rest" is a macro-specification of the velocity distribution that does not uniquely determine the precise mathematical state $\underline{v}(\underline{r}, t_0)$. In fact, there exists an innumerable set of functions $\underline{v}(\underline{r}, t_0)$, ($\underline{r} \in \mathcal{D}$, where \mathcal{D} is the space inside the chamber) each of which is consistent with the criteria, implicit or otherwise, that define the macrostate "fluid at rest". Let's call this set of functions I . Then under our premise each member of I maps through the equations that represent physical laws into a set W of functions $\underline{v}(\underline{r}, t)$, $\underline{r} \in \mathcal{D}$, $t_0 \leq t < \infty$. Thus, W represents the subset of the global family Ω of velocity fields that is delineated by the conditions that define our chamber experiment and it is the members of the set W that our velocity probe

samples. Since there is no known mechanism that would tend to cause any member of I to occur more frequently than any of the other members of the set, then each velocity field in W is equally likely to occur and hence W is also the ensemble of flow fields.

As in the dice game, there is no way of determining which member of I characterizes the air in the chamber at the beginning of any experiment and therefore there is no way of predicting the outcome $\underline{v}(\underline{r}, t)$. We can only hope to determine properties of the ensemble W .

If the angle brackets $\langle \rangle$ denote an ensemble average and \underline{r}_0 represents the location of the velocity probe in the chamber, then $\langle \underline{v}(\underline{r}_0, t) \rangle$ and $\langle \underline{v}^2(\underline{r}_0, t) \rangle$ are the mean and mean square velocities, averaged over infinitely many experiments, that we could expect to observe.

Since the bounds on the subset W are determined by the parameters that define our experiment, namely the dimensions of the chamber, the rate at which heat is injected into it, physical properties of air, and the roughness of the chamber walls, all ensemble mean quantities must be functions of these variables. The aim of turbulence theory is to predict these relationships.

Two important points should be noted here. The first is that the "ensemble" of flow fields is determined by the conditions that define the problem. In the present example these include: thermally insulated, smooth-walled air chamber with bottom heated uniformly at a specified rate; fluid initially at rest; etc. In typical atmospheric boundary layer studies the defining conditions include: flat infinite surface of given roughness length z_0 and heat flux H_0 ; friction velocity u^* (which is a surrogate for the pressure gradient that drives the flow); etc.

The second point is that in conventional turbulence studies the conditions that define the ensemble are usually "external" parameters such as those just listed rather than "internal" parameters that we define below. Perhaps the purpose for this is that once the relationships between ensemble averaged state variables and the external parameters have been determined, those expressions can be used to predict averaged values in other similar, but quantitatively different, situations.

In regional scale air pollution studies we are generally not interested in prognostic capabilities of this sort. We consider the flow fields in the region of interest to be fixed, in a climatological sense, and we attempt to determine how air quality in that region would change if the source emissions were altered in a prescribed way. Furthermore, external parameters are not readily definable in these problems because there are no walls or tops on the airshed of interest, the earth's surface is not uniform, etc. In these cases the conditions that define the flow fields are measurements of "internal" parameters such as wind velocity, temperature, pressure, and so on. Therefore, these data must define the ensemble of flow fields. And as we show in the next section, they define in turn the corresponding ensemble of concentration fields associated with a given source distribution.

To define the ensemble in terms of "internal" parameters, let's assume that in the space-time domain (\mathcal{D}, T) of interest we have available observations of the horizontal wind components (u, v) , temperature θ , etc., sites x_1, x_2, \dots, x_N . Suppose further that these data are in the form of moving time averages:

$$\bar{u}_n(t) = \frac{1}{2T} \int_{t-T}^{t+T} u(\underline{x}_n, t') dt' \quad , \quad n=1, \dots, N \quad (6-22a)$$

$$\bar{\theta}_n(t) = \frac{1}{2T} \int_{t-T}^{t+T} \theta(\underline{x}_n, t') dt' \quad , \quad n=1, \dots, N \quad (6-22b)$$

etc. Let's assume also that in addition to the N surface monitoring stations there are M upper air soundings made at locations $\underline{x}_{N+1}, \underline{x}_{N+2}, \dots, \underline{x}_{N+M}$ that give averages of winds, temperature and dewpoint over small vertical intervals Δz :

$$\bar{u}_m^z(z, t) = \frac{1}{\Delta z} \int_{z - \Delta z/2}^{z + \Delta z/2} u(\underline{x}_m, y_m, z', t) dz' \quad (6-23a)$$

$m = N+1, \dots, N+M$

$$\bar{\theta}_m^z(z, t) = \frac{1}{\Delta z} \int_{z - \Delta z/2}^{z + \Delta z/2} \theta(\underline{x}_m, y_m, z', t) dz' \quad (6-23b)$$

$m = N+1, \dots, N+M$

etc. Since the functions on the lefthand side of (6-22) and (6-23) are given (from the measurements), this set of equations constitutes a system of integral equations in the unknown flow fields $\underline{u}(\underline{x}, t)$, $\theta(\underline{x}, t)$, and so on. We now define the ensemble W of velocity fields associated with the space (\mathcal{D}, T) and observations $\bar{u}_n(t)$, $\bar{\theta}_n(t)$, etc in this space as the set of functions $\underline{u}(\underline{x}, t)$, $\theta(\underline{x}, t)$, etc $(\underline{x}, t) \in (\mathcal{D}, T)$ that satisfies jointly the system of Equations (6-22, 23) and the following set of equations that represents physical laws:

$$\frac{d\underline{V}}{dt} = - \frac{1}{\rho} \nabla p - \underline{f} \times \underline{V} + \underline{F}_H \quad (6-24a)$$

$$\frac{\partial p}{\partial z} = - \rho g \quad (6-24b)$$

$$\frac{\partial \rho}{\partial t} = - \nabla \cdot (\rho \underline{V}) \quad (6-24c)$$

$$(c_\ell \ell + c_p) \frac{d\theta}{dt} = \frac{1}{\rho} \frac{dp}{dt} - L \frac{dq}{dt} + Q \quad (6-24d)$$

$$\frac{dq}{dt} = \frac{q_s \theta}{p} \left[\frac{LR - c_p R_v \theta}{c_p R_v \theta^2 + q_s L^2} \right] \frac{dp}{dt} \delta \quad (6-24e)$$

where

$$\delta = \begin{cases} = 1, & \text{if } \frac{dp}{dt} < 0 \text{ and } q \geq q_s \\ = 0, & \text{if } \frac{dp}{dt} \geq 0 \text{ or } q < q_s \end{cases}$$

In Equation (6-24), $\underline{V} = (u, v)$; $\underline{\nabla} = \underline{i} \frac{\partial}{\partial x} + \underline{j} \frac{\partial}{\partial y}$

$$\frac{d}{dt} = \frac{\partial}{\partial t} + \underline{V} \cdot \underline{\nabla} + w \frac{\partial}{\partial z}$$

p is pressure; ρ is density; θ is temperature; f is the Coriolis parameter; F_H is the friction term which is expressible approximately in terms of \underline{V} and other parameters and generally is significant only in the lowest 2 km of the atmosphere; q is the specific humidity and q_s the saturation specific humidity, which is a function of θ and p ; ℓ is the concentration of liquid water; c_p and c_ℓ are the specific heats of air at constant pressure and water, respectively; R and R_v are the gas constants for air and water vapor, respectively; g is gravity; Q is the rate of heat loss or gain by radiation processes or precipitation; and L is the latent heat of vaporization, or sublimation, whichever applies.

In our earlier discussion we defined the set Ω (see Figure 6-3) to be the set of $(u, v, w, \rho, \theta, q)$ that satisfy physical laws, namely the set of equations (6-24). Thus, by imposing the additional constraints (6-22, 23) we reduce the set of states $(u, v, w, \rho, \theta, q)$ accessible to the system to a subset of Ω , namely the subset we call W . By contrast, the classical approach is to specify certain initial and boundary conditions in place of

(6-22), (6-23) that in principle reduce the set of accessible states to a single member of Ω . But as we discussed earlier, in the domain of Ω associated with "turbulent" flows, specifications of the initial and boundary conditions that provide only a macro-description rather than point details are only adequate to delineate a subset of systems states.

The observations \bar{u}_n , etc., that enter in Equations (6-22) and (6-23) reduce the number of possible flow states from the set Ω to the subset W for exactly the same reason that knowledge of the outcome after each roll of 1 of the 3 dice in the earlier game would reduce the number of possible matrices A from the global set of 6^9 matrices to a subset of 6^6 . These reductions effect an improvement in the certainty with which we can describe events that have already taken place. Indeed, in the case where all the dice are observed or where flow variables are measured everywhere in space-time, the subset W of possible states is reduced to a single member of the global set Ω . However, observations obviously do not exist for events that have not yet taken place, and therefore in attempting to predict future states of the fluid or outcomes A of the dice, the set of possible states is the ensemble set which may be identical to the global set Ω . As we pointed out earlier, the purpose of observations is to provide us with a knowledge of the ensemble set and the probabilities of its members. We return to this point in Section 7.

In Part II of this report we will show how (6-22), (6-23) and (6-24) are used to derive an ensemble of cell-averaged flow fields and cell layer heights from which the regional model can generate the associated ensemble of pollutant concentrations distributions, and we will begin to answer the 3 basic questions raised at the beginning of this section.

SECTION 7

MESOSCALE DIFFUSION; CONCENTRATION PREDICTABILITY; MODEL "VALIDATION"; AND RELATED TOPICS

To derive the equations that describe the fate of pollutants in each of the model's 3 layers, we started from the mass continuity equation (2-1) which involves the instantaneous, point fluid velocity \underline{v} . The final form (2-29) of the model equations governing the cell-averaged species concentrations in each layer contain the subgrid "eddy" flux terms

$$\begin{aligned}\langle u'c' \rangle_j &\equiv \langle uc \rangle_j - \langle u \rangle_j \langle c \rangle_j \\ \langle v'c' \rangle_j &\equiv \langle vc \rangle_j - \langle v \rangle_j \langle c \rangle_j\end{aligned}\tag{7-1}$$

where $\langle \rangle_j$ denotes a cell average in layer j , $j=0,1,2,3$; u and v denote the components of the horizontal fluid velocity \underline{u} ; and primed quantities represent deviations of the local, point value from the cell averaged value $\langle \rangle_j$.

In the previous section we showed that from a discrete set of observations of meteorological variables in a domain (\mathcal{D}, T) , one can determine the velocity field $\underline{v} = (u, v, w)$ in that domain to within only a set of functions W . To each member of this set there exists a $\langle u'c' \rangle_j$ and $\langle v'c' \rangle_j$ for each distribution of species sources. Thus, our first task in this section will be to express these subgrid eddy fluxes in terms of $\langle \underline{v} \rangle_j$ and $\langle c \rangle_j$. Following that we will address the 3 questions raised at the beginning of Section 6, which involve the relationship between the set of $\langle c \rangle_j$ associated with the

set W of meteorological fields and the concentrations that one could expect to measure under the meteorological conditions implicit in W . Finally, we will look at whether the concepts we presented in the previous section are consistent with the concepts of turbulent diffusion that form the basis of the classical theories of microscale dispersion.

For simplicity we will approximate the subgrid eddy flux terms in the gradient transfer form

$$\langle u'c' \rangle_j = - K_j \mu_\lambda \frac{\partial}{\partial \lambda} \langle c \rangle_j \quad (7-2a)$$

$$\langle v'c' \rangle_j = - K_j \mu_\phi \frac{\partial}{\partial \phi} \langle c \rangle_j \quad (7-2b)$$

with the eddy diffusivity K_j given simply by

$$K_{1,2} = \begin{cases} 0.1w_*h, & \text{if } L < 0 \\ 0, & \text{otherwise} \end{cases} \quad (7-3a)$$

$$K_3 = \sigma_c \bar{w}_c h \quad (7-3b)$$

where w_* is the convective velocity scale, defined by (4-29b); h is the mixed layer depth, or the elevation above ground of the top surface of Layer 2; L is the Obukhov length; σ_c is the fractional sky coverage of cumulus clouds; and \bar{w}_c is the mean updraft speed in cumulus clouds. Higher order approximations than (7-2) could be written for the flux terms, but the advantage in accuracy gained by these is not commensurate with the level of computational effort required to implement them. Moreover, we believe that the envelope of particle trajectories corresponding to supergrid components $\langle \underline{v} \rangle_j$ of the members of the set W is much broader at regional scale travel distances than the spread of a plume due to subgrid scale velocity fluctuations in a single member of W . One of the tasks that will be performed as part of the NEROS field studies will be to assess the accuracy of Equations (7-2) and (7-3).

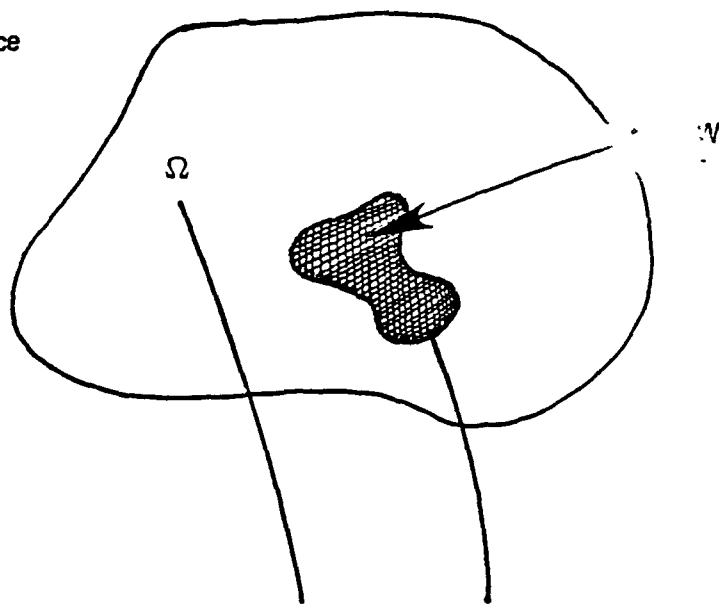
Figure 7-1 illustrates that for a given distribution $\underline{S}(\underline{x}, t)$ of sources of J material species, that is, $\underline{S}(\underline{x}, t) = [S_1(\underline{x}, t), \dots, S_J(\underline{x}, t)]$, the principle of mass conservation, which is represented in the present model by the system of Equation (2-29), effects the unique mapping of each member of the global family Ω of fluid states into a set Γ of functions in concentration space. And each member of the subset W of Ω maps into a subset C of Γ . If there is no process under the observed flow conditions that define W [see (6-22), (6-23)] that would tend to favor the occurrence of any particular members of W over others, then we must assume that each member of W is equally probable and, therefore, that each member of C is equally probable. Since there are infinitely many functions in the set W , the probability of occurrence of any 1 of them is infinitesimally small. This fact precludes our predicting the precise concentration distribution that will result in a given situation and therefore, as in the case of the dice game, we must examine the members of C to determine whether they possess some property (like the sum of the elements a_{ijn} of the matrices \underline{A}_n that make up the ensemble of dice game outcomes) whose value can be expected to lie close to some predictable value, regardless of the member of C that actually occurs.

Consider the time-averaged value of each member of $c(\underline{x}, t)$ of C at a given point \underline{x}_0 :

$$\bar{c}(\underline{x}_0, t) = \frac{1}{2T} \int_{t-T}^{t+T} c(\underline{x}_0, t') dt' \quad , \quad c \in C \quad (7-4)$$

where $\underline{x}_0 \in \mathcal{D}$, $T \leq t \leq T - T$, and T is an arbitrary time interval. (In order to avoid awkward notation, we will use c in this section to represent the members $\langle c \rangle_j$ of C).

Flow field phase space



Law of mass conservation
(Eq. (2-29) with $\underline{S}(\underline{x}, t)$ given)

Concentration phase space

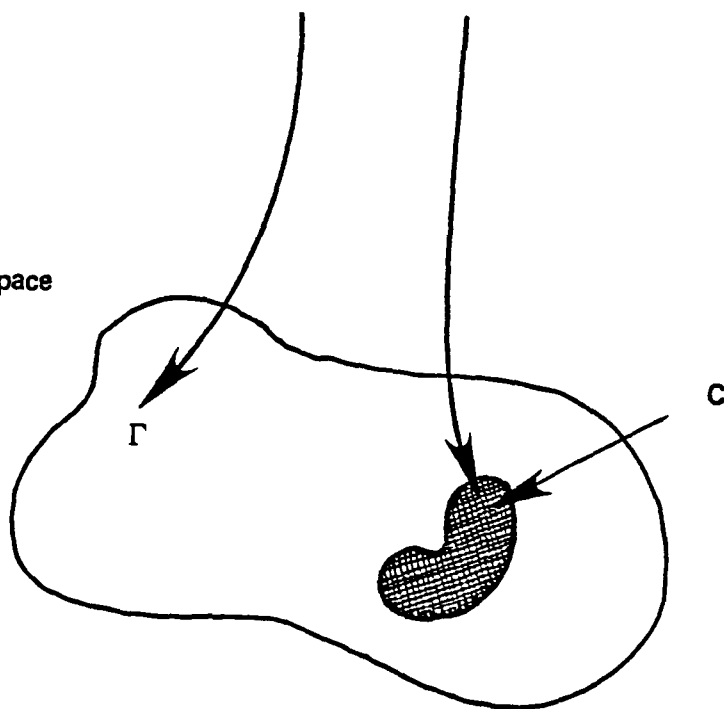


Figure 7-1. Mapping of the set Ω and W in flow field function space into the sets Γ and C in concentration function space for a given source distribution \underline{S} .

By virtue of the assumption that the members of C are equally probable, we obtain by averaging (7-4) over the set C the ensemble time averaged concentration

$$\langle \bar{c}(x_0, t) \rangle = \frac{1}{2T} \int_{t-T}^{t+T} \langle c(x_0, t') \rangle dt' \quad (7-5)$$

Keep in mind that $\langle \bar{c} \rangle$ is the mean value of all possible time averaged concentrations \bar{c} that could occur for a given source distribution S under the discrete set of observed meteorological variables in (6-22), (6-23) that define W.

Let

$$\varepsilon(x_0, t) = \bar{c}(x_0, t) - \langle \bar{c}(x_0, t) \rangle \quad (7-6)$$

denote the difference between the time averaged value \bar{c} of any member of the ensemble and the (predictable) ensemble mean value $\langle \bar{c} \rangle$. Squaring Equation

(7-6) we get

$$\begin{aligned} \varepsilon^2(x_0, t) = & \frac{1}{4T^2} \int_{t-T}^{t+T} \int_{t-T}^{t+T} c(x_0, t') c(x_0, t'') dt' dt'' \\ & - \frac{\langle \bar{c}(x_0, t) \rangle}{T} \int_{t-T}^{t+T} c(x_0, t') dt' + \langle \bar{c}(x_0, t) \rangle^2 \end{aligned} \quad (7-7)$$

Averaging this expression over the ensemble C we obtain

$$\begin{aligned} \langle \varepsilon^2(x_0, t) \rangle = & \frac{1}{4T^2} \int_{t-T}^{t+T} \int_{t-T}^{t+T} \langle c(x_0, t') c(x_0, t'') \rangle dt' dt'' \\ & - \langle \bar{c}(x_0, t) \rangle^2 \end{aligned} \quad (7-8)$$

Note that $\langle \varepsilon \rangle = 0$.

The value of $\langle \epsilon^2 \rangle$ provides a measure of how closely the time averaged concentration \bar{c} at x_0 can be expected to lie to the predictable ensemble mean value $\langle \bar{c} \rangle$.

From the Tchebycheff inequality of statistics, we find that with $\langle \epsilon \rangle = 0$ the fraction λ of the ensemble population whose values \bar{c} are within $\pm \epsilon_0$ of $\langle \bar{c} \rangle$ is

$$\lambda \geq 1 - \frac{\langle \epsilon^2 \rangle}{\epsilon_0^2} \quad (7-9)$$

In words, in a large number of predictions the average frequency with which the observed time average concentration $\bar{c}(x_0, t)$ exceeds the predicted value $\langle \bar{c}(x_0, t) \rangle$ by an amount larger than some fixed value ϵ_0 decreases as $\langle \epsilon^2 \rangle$ decreases. Thus, our next task is to relate $\langle c(x, t) \rangle$ and $\langle c(x, t)c(x, t') \rangle$, the quantities needed to compute $\langle \epsilon^2 \rangle$ and $\langle \bar{c} \rangle$, to the known ensemble properties of W.

Lamb (1975) has shown that for materials that are chemically inert or undergo only first order reactions (i.e., the function R in (2-29) is a linear function), the ensemble mean concentration is given by

$$\langle c(x, t) \rangle = \int \int_0^t p(x, t | x', t') S(x', t') dt' dx' \quad (7-10)$$

and

$$\begin{aligned} \langle c(x, t)c(x, t') \rangle = & \int \int_0^t \int_0^{t'} p_2(x, t; x, t' | x'', t'', x''', t''') \\ & S(x'', t'') S(x''', t''') dt'' dt''' dx'' dx''' \end{aligned} \quad (7-11)$$

where S is the source strength function of the material species whose concentration is c.

In Equations (7-10) and (7-11) the functions p and p_2 are Lagrangian properties of the ensemble W , and hence it is these functions that link the properties of W and those of C for given S .

The function p is called the single particle displacement probability density and is defined for chemically inert material by

$$p(\underline{x}, t | \underline{x}', t') = \langle \phi(\underline{x}, t | \underline{x}', t') \rangle / \delta v \quad (7-12)$$

Here, δv denotes the (small) sample volume centered at \underline{x} , $\langle \rangle$ denotes averaging over W ; and ϕ is defined for each $\underline{v}(\underline{x}, t)$ in W by

$$\phi(\underline{x}, t | \underline{x}', t') = \begin{cases} 1, & \text{if } \underline{v}(\underline{x}, t) \text{ is such that a particle released} \\ & \text{at } (\underline{x}', t') \text{ is in } \delta v \text{ centered at } \underline{x} \text{ at time } t \\ 0, & \text{otherwise} \end{cases} \quad (7-13)$$

In the case of a point source of strength $S(t)$ located at \underline{x}_0 ,

$$S(\underline{x}, t) = S(t) \delta(\underline{x} - \underline{x}_0)$$

we obtain on combining (7-10) and (7-12)

$$\langle c(\underline{x}, t) \rangle = (\delta v)^{-1} \int_0^t S(t') \langle \phi(\underline{x}, t | \underline{x}_0, t') \rangle dt' \quad (7-14)$$

It is instructive at this point to comment on the function ϕ and the physical significance of the forms it takes.

With the source location \underline{x}_s and receptor site \underline{x}_0 given, we can plot ϕ as a function of t and t' . Figure 7-2 illustrates a hypothetical case. Referring to the figure, we point out that a particle that leaves \underline{x}_s at time t_1 enters the sample volume δv at \underline{x}_0 at time t_1 and exits at time $t_1 + \Delta t$. The value of the time integral of ϕ , which plays a role in (7-14), is also indicated.

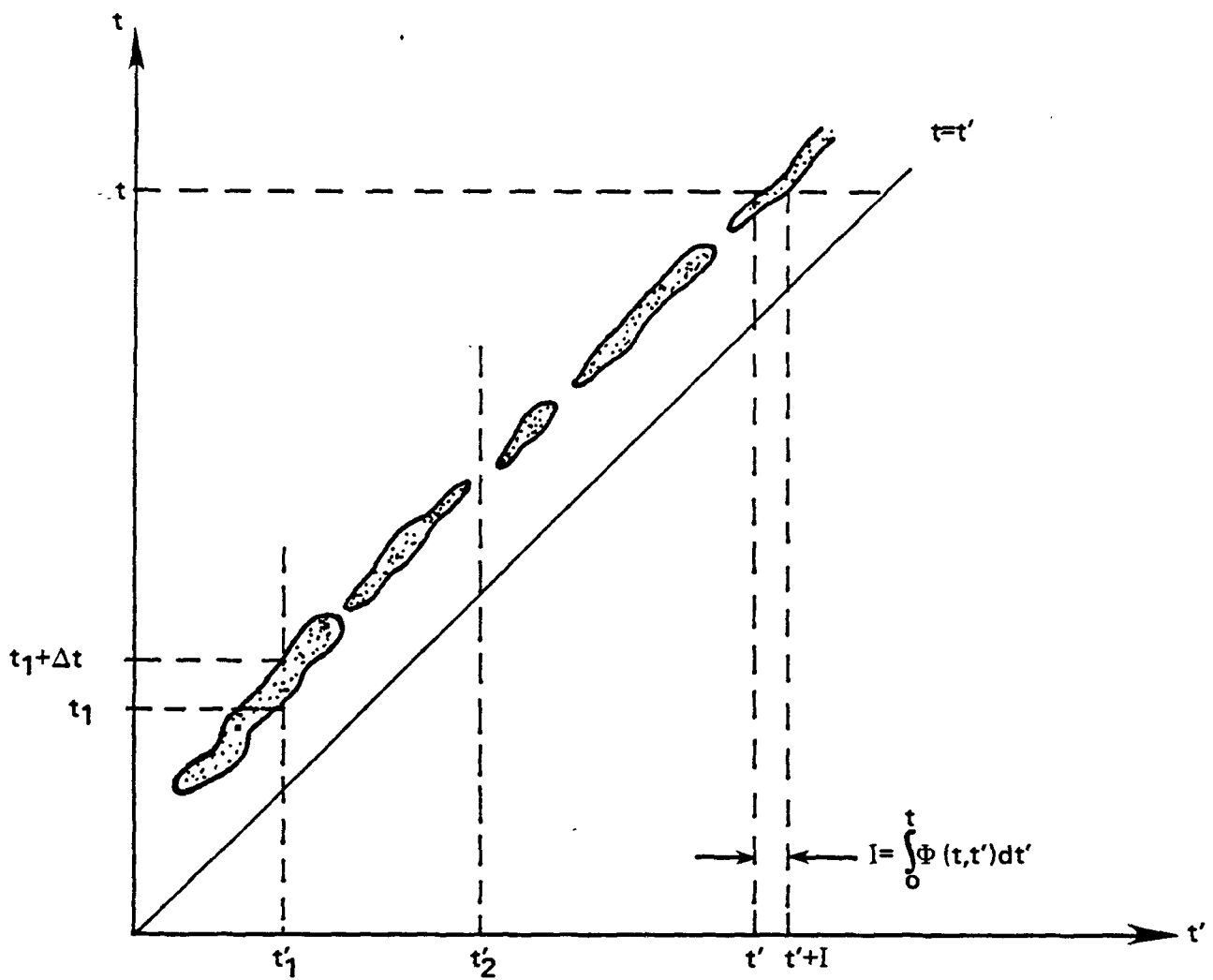


Figure 7-2. Plot of a hypothetical example of the function $\phi(x_0, t | x_s, t')$ for given source location x_s and receptor site x_0 . The function ϕ has unit value inside the shaded regions and is zero everywhere else.

If x_s is one of the points at which the meteorological data that enter in the definition of W are collected, we can expect the functions ϕ corresponding to each member W to have the same general features. By contrast, if x_s and x_o are far from a meteorological station, there will generally be large variations in the form of ϕ from one member of the ensemble to another. (The reasons for this and its ramifications on model predictions are discussed under Remarks later in this section.)

If the plots of all ϕ within W are superposed and averaged at each point (t, t') , we obtain the function $\langle \phi(x_o, t | x_s, t') \rangle$ needed in (7-14) to compute $\langle c(x_o, t) \rangle$. If the distribution of $\langle \phi \rangle$ is aligned parallel to the line $t = t'$ and if its width and amplitude are constant along its length, then ϕ is a statistically stationary function. In this case it is easy to see that

$$\left\langle \int_0^t \phi(t, t') dt' \right\rangle = \langle \Delta t \rangle \quad (7-15)$$

where $\langle \Delta t \rangle$ is the average time spent by a particle released at any time t' in δv (cf. Figure 7-2). If, under these conditions, the source strength is also steady in time, say $S(t) = S_o$, we have the simple result

$$\langle c(x, t) \rangle = \frac{S_o}{\delta v} \langle \Delta t \rangle \quad (7-16)$$

In essence, it is this simple expression that the Gaussian plume formula approximates in an empirical way.

The assumption of stationarity is applied almost routinely in turbulent diffusion studies partly because it simplifies the mathematics. But it is not hard to see by visualizing the shapes of $\phi(t, t')$ that various flows would produce that stationarity is generally not applicable in regional modeling studies. In these cases calculation of $\langle c \rangle$ must be based on (7-13) and

(7-10) rather than equations like (7-16) that assume stationarity.

The function p_2 that enters in (7-11) is called the two-particle displacement probability density and is defined as follows:

$$p_2(\underline{x}, t; \underline{x}, t' | \underline{x}'' , t''; \underline{x}''' , t''') = \langle \phi_2(\underline{x}, t; \underline{x}, t' | \underline{x}'' , t''; \underline{x}''' , t''') \rangle / (\delta v)^2 \quad (7-17a)$$

Here, as in the definition of p (see 7-12), the angle brackets $\langle \rangle$ denote averaging over W ; δv is the sample volume centered at \underline{x} ; and ϕ_2 is defined for any $\underline{v}(\underline{x}, t)$ in W by

$$\phi_2(\underline{x}, t; \underline{x}, t' | \underline{x}'' , t''; \underline{x}''' , t''') = \begin{cases} 1, & \text{if } \underline{v}(\underline{x}, t) \text{ is such that a} \\ & \text{particle released at } (\underline{x}'', t'') \\ & \text{and one released at } (\underline{x}''', t''') \\ & \text{are found at } (\underline{x}, t) \text{ and } (\underline{x}, t'), \\ & \text{respectively:} \\ 0, & \text{otherwise} \end{cases} \quad (7-17b)$$

For a single point source the autocorrelation $\langle c(\underline{x}, t) c(\underline{x}, t') \rangle$ is derivable from the contracted form $\phi_2(\underline{x}, t; \underline{x}, t' | \underline{x}_s, t''; \underline{x}_s, t''')$. This function contains 4 independent variables for given \underline{x} and \underline{x}_s and is much more difficult to visualize than ϕ .

To summarize briefly the points made thus far, we have argued in the previous section that a discrete set of meteorological observations, as given in (6-22), (6-23), in a given space-time domain (\mathcal{D}, T) is adequate to specify the flow field $\underline{v}(\underline{x}, t)$ to within only a set of functions W . For a given source distribution S , each member of the set W maps through the species mass conservation equation [e.g., (2-29)], onto a function element of a subset C in concentration space. Since it is impossible to say which member of W actually describes the state of the fluid in (\mathcal{D}, T) under the discrete set of conditions specified, it is impossible to predict the precise concentration distribution that would occur under those conditions for given S . As in the

dice analogy, we can only hope that there exists some property, say $g(c)$, such that $g(c) \approx \langle g(c) \rangle$ for nearly all $c \in C$. Here $\langle g(c) \rangle$ is the mean value of $g(c)$ over the set C (or the ensemble mean), and it is a quantity that, in principle, can be calculated for any $g(c)$. We showed that if $g(c)$ is the moving time average defined by (7-4), then a fraction λ of the members of C possess $g(c) = \bar{c}$ values that are within $\pm \epsilon_0$ of the set mean value $\langle \bar{c} \rangle$, where ϵ_0 is an arbitrary interval and λ is given by (7-9).

At this point we have answered the first question raised at the end of the introduction to Section 6 and we have obtained partial answers to the other 2 questions. Specifically, we have shown that for a given source distribution S and a given set of meteorological observations, a model can delineate the set of functions C to which the actual concentration distribution $c(x,t)$ resulting from those conditions belongs, but not the function c itself. From the model generated function set C , one can compute the set, or ensemble, mean values of c such as the first and second moments given by (7-10) and (7-11) and from these one can specify the frequency with which actual concentration can be expected to fall within a given interval of values in a large number of observations. The width of this interval [see (7-9)] is a measure of the "predictability" of the concentration and it is determined by the properties of the set C . These in turn are determined by S and the set of meteorological data that define W . Thus, "validating" a model is tantamount to testing whether observed concentrations fall within the interval specified with the frequency specified and, if not, whether the failure can be attributed to sampling fluctuation. Note that from the standpoint of

regulatory needs the utility of a model is measured partly by the width of the interval in which a majority of observations can be expected to fall. If the width of the interval is very large, the model may provide no more information than one could gather simply by guessing the expected concentration. An important task in this regard is the "inverse" problem of specifying the density and type of meteorological data that are needed to achieve a given level of concentration predictability. We will consider these topics again later in this section.

The conventional approach to turbulent diffusion modeling is to formulate equations for $\langle c \rangle$ and possibly higher moments that yield these quantities directly. By contrast, the approach we are following here is to generate members of the ensemble set C and then to compute the set mean values $\langle c \rangle$, etc., by averaging the individual members. In the author's view, this is the only approach that can produce accurate estimates of ensemble mean values, because the closure problem that must be overcome to compute $\langle c \rangle$, $\langle c^2 \rangle$, etc., directly is made virtually insurmountable by the combination of the nonlinearity of the chemistry and the large time and space scales of atmospheric motion. In Part II of this report we will describe our progress in implementing this approach.

Remarks

1. The character of diffusion at long range.

In this subsection we would like to examine the classical definition of turbulence employed in microscale dispersion analyses from the perspective of the mathematical set definition we are proposing here. Our main aims are to examine the cause of the paradox described in the introduction to Section

6 that results when the classical definition is applied to long range diffusion and to determine whether this paradox is reconciled by our definition of "turbulence".

Consider the frequent situation in microscale studies where only a single wind observation site exists, at \underline{x}_0 , and a single point source of material is located nearby at \underline{x}_s . Under our definition, this observation establishes through (6-22), with $N=1$, and (6-24) a set of functions W that contains the field $\underline{v}(\underline{x}, t)$ that describes the actual fluid velocity in the domain (\mathcal{D}, T) in which the observations were made. Suppose that the observation at \underline{x}_0 is a moving time average, as defined by (7-4).

If we were to superpose the trajectories originating at $\underline{x}_s (= \underline{x}_0)$ derived from each flow field in W , we might obtain a pattern like that illustrated in Figure 7-3. The spread of these trajectories is what we regard as "turbulent diffusion".

Since each member of W satisfies (6-22), all trajectories have the same general direction, namely that of $\overline{\underline{u}}(\underline{x}_0, t)$, near the source; but farther downstream there is increasing freedom in the direction that the flow there, and hence the trajectories, can take and still satisfy (6-22). For example, on occasions when the wind vector is $\overline{\underline{u}}_0$ at \underline{x}_0 , the flow can turn cyclonically downstream while on other occasions, with an identical flow at \underline{x}_0 , it may turn anticyclonically. Without more information than simply the wind vector at \underline{x}_0 , there is no way to say which direction the trajectories will take. Indeed, it appears obvious from this perspective that the spread of trajectories far from the source is affected by large scales of motion that one normally associates with transport.

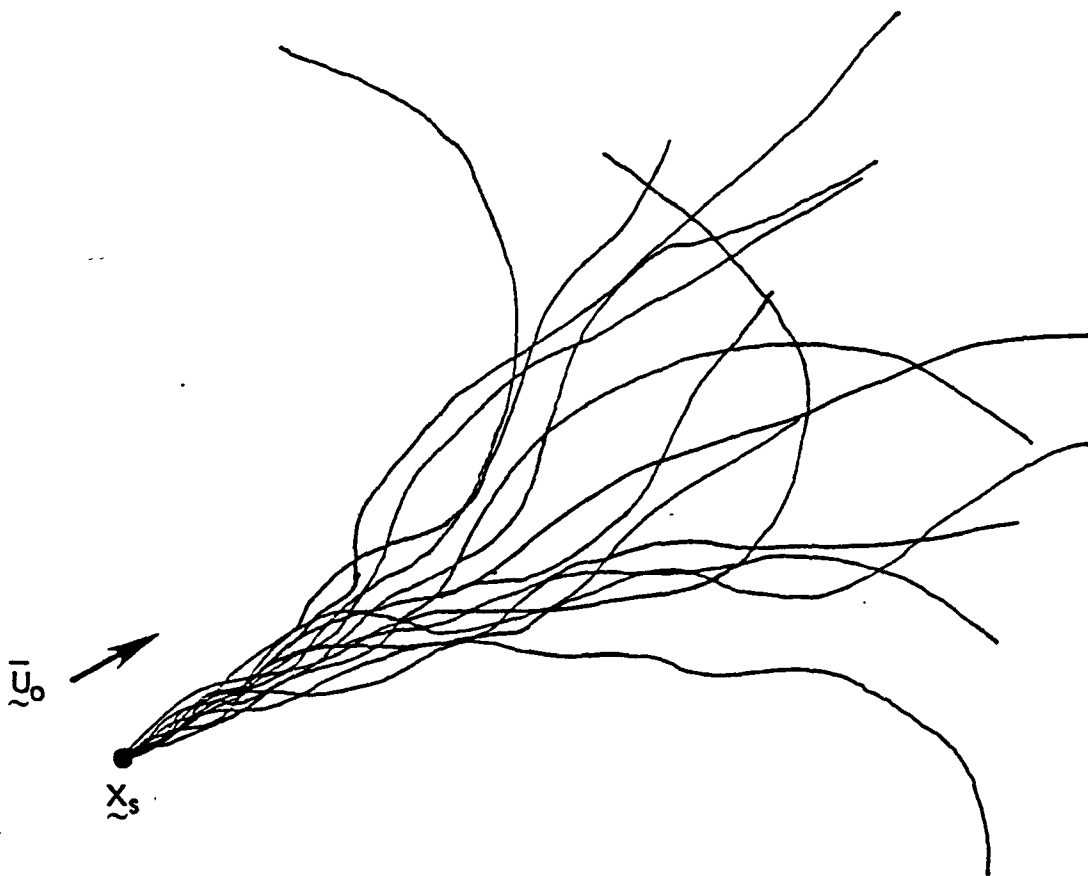


Figure 7-3. Trajectories of particles emanating from x_s in the ensemble W associated with the single wind observation $\bar{u}(x_0, t) = \bar{u}_0$, where $x_s = x_0$.

We can verify this important point by analyzing the problem mathematically. We will show that with "turbulence" defined in the classical way, its spectrum is an implicit function of distance from the site at which the observation used to define the "mean wind" is made. In the present example we are assuming that a wind observation is made at the single location \underline{x}_0 and it provides the moving time averaged velocity

$$\bar{u}_0(t) = \frac{1}{2T} \int_{t-T}^{t+T} u(\underline{x}_0, t') dt' \quad (7-18)$$

where $u(\underline{x}, t)$ represents the instantaneous velocity at (\underline{x}, t) . Expressing u in terms of its complex Fourier transform defined by (6-8) we have

$$u(\underline{x}, t) = \frac{1}{(2\pi)^4} \int \int u(\underline{k}, \omega) e^{i(\underline{k} \cdot \underline{x} + \omega t)} d\underline{k} d\omega \quad (7-19)$$

where u is the complex transform at wave number \underline{k} and frequency ω . Combining (7-18) and (7-19), we get

$$\bar{u}_0(t) = \int \int u(\underline{k}, \omega) \frac{\sin \omega T}{\omega T} e^{i(\underline{k} \cdot \underline{x}_0 + \omega t)} d\underline{k} d\omega \quad (7-20)$$

For notational convenience we will assume that the factor $(2\pi)^{-4}$ is absorbed in u .

Since u is a real function, we must have

$$u(\underline{x}, t) = \int \int u^*(\underline{k}, \omega) e^{-i(\underline{k} \cdot \underline{x} + \omega t)} d\underline{k} d\omega \quad (7-21)$$

where u^* is the complex conjugate of u . Thus the product of u measured at 2 points separated in space-time by (δ, τ) is

$$\underline{u}(\underline{x}, t) \underline{u}(\underline{x} + \underline{\delta}, t + \tau) = \int \int \int \int \underline{u}(\underline{k}, \omega) \underline{u}^*(\underline{k}', \omega') e^{i(\underline{k} \cdot \underline{x} + \omega t) - i[(\underline{k}') \cdot (\underline{x} + \underline{\delta}) + \omega'(t + \tau)]} d\underline{k} d\underline{k}' d\omega d\omega' \quad (7-22)$$

Averaging this product over the ensemble W defined by the observation at \underline{x}_0 [and (6-22) and (6-24)], we have

$$\langle \underline{u}(\underline{x}, t) \underline{u}(\underline{x} + \underline{\delta}, t + \tau) \rangle = \int \int \int \int \langle \underline{u}(\underline{k}, \omega) \underline{u}^*(\underline{k}', \omega') \rangle e^{i(\underline{k} - \underline{k}') \cdot \underline{x} - i\underline{k}' \cdot \underline{\delta} + i(\omega - \omega')t - i\omega'\tau} d\underline{k} d\underline{k}' d\omega d\omega' \quad (7-23)$$

By definition if the set W of velocity fields is homogeneous and stationary, then.

$$\langle \underline{u}(\underline{x}, t) \underline{u}(\underline{x} + \underline{\delta}, t + \tau) \rangle = \underline{R}(\underline{\delta}, \tau) \quad (7-24)$$

That is, the set average of the velocity product depends on the separation $(\underline{\delta}, \tau)$ of the velocity observations but not on the location (\underline{x}, t) in (\mathcal{D}, T) at which the pair of observations are made. Comparing (7-23) and (7-24) we see that stationarity and homogeneity can exist only if

$$\langle \underline{u}(\underline{k}, \omega) \underline{u}^*(\underline{k}', \omega') \rangle = \underline{\Psi}(\underline{k}, \omega) \delta(\underline{k} - \underline{k}') \delta(\omega - \omega') \quad (7-25)$$

where $\delta(\)$ is the Dirac delta function. Combining (7-23, 24, and 25) we get

$$\underline{R}(\underline{\delta}, \tau) = \int \int \underline{\Psi}(\underline{k}, \omega) e^{-i(\underline{k} \cdot \underline{\delta} + \omega \tau)} d\underline{k} d\omega \quad (7-26)$$

Now under the classical definition, the turbulent velocity component at an arbitrary point (\underline{x}, t) is

$$\underline{u}'(\underline{x}, t) \equiv \underline{u}(\underline{x}, t) - \overline{\underline{u}}_0(t) \quad (7-27)$$

Thus,

$$\begin{aligned} \underline{u}'(\underline{x}, t) \underline{u}'(\underline{x} + \underline{\delta}, t + \tau) &= [\underline{u}(\underline{x}, t) - \overline{\underline{u}}_0(t)] [\underline{u}(\underline{x} + \underline{\delta}, t + \tau) \\ &\quad - \overline{\underline{u}}_0(t + \tau)] \end{aligned} \quad (7-28)$$

Taking the ensemble average of this expression and making use of (7-25) we obtain

$$\begin{aligned}
 \langle \underline{u}'(\underline{x}, t) \underline{u}'(\underline{x} + \underline{\delta}, t + \tau) \rangle &= \int \int \Psi(\underline{k}, \omega) [e^{-i(\underline{k} \cdot \underline{\delta} + \omega \tau)} \\
 &\quad - \frac{\sin \omega T}{\omega T} e^{i \underline{k} \cdot (\underline{x} - \underline{x}_0) - i \omega \tau} \\
 &\quad - \frac{\sin \omega T}{\omega T} e^{i \underline{k} \cdot \underline{\delta} + i \underline{k} \cdot (\underline{x} - \underline{x}_0) + i \omega \tau} \\
 &\quad + (\frac{\sin \omega T}{\omega T})^2 e^{-i \omega \tau}] d\underline{k} d\omega
 \end{aligned} \tag{7-29}$$

Evaluating this expression at $\underline{\delta} = \tau = 0$ we obtain the spectral representation of the turbulent energy at (\underline{x}, t) :

$$\begin{aligned}
 \langle u'^2(\underline{x}, t) \rangle &= \int \int \Psi(\underline{k}, \omega) [1 - 2 \frac{\sin \omega T}{\omega T} e^{i \underline{k} \cdot (\underline{x} - \underline{x}_0)} \\
 &\quad + (\frac{\sin \omega T}{\omega T})^2] d\underline{k} d\omega
 \end{aligned} \tag{7-30}$$

This expression shows clearly that while the fluid velocity \underline{u} is stationary and homogeneous, "turbulence" defined by (7-27) is only stationary -- its energy $\langle u'^2 \rangle$ is a function of distance $\underline{x} - \underline{x}_0$ from the wind monitoring site. It is easy to see in (7-30) that as the distance from \underline{x}_0 increases, progressively larger scales of the velocity \underline{u} become embodied in \underline{u}' .

If we evaluate (7-30) at the wind measurement site \underline{x}_0 , we obtain the conventional description

$$\langle u'^2(\underline{x}_0, t) \rangle = \int \int \Psi(\underline{k}, \omega) [1 - \frac{\sin \omega T}{\omega T}]^2 d\underline{k} d\omega \tag{7-31}$$

which conceals the inhomogeneous character of \underline{u}' .

It is the inhomogeneity of \underline{u}' that is responsible for the dispersion paradox described in Section 6. To show this we evaluate (7-29) for $\underline{\delta} = 0$ and use the result in the definition of the Eulerian integral time scale T_E :

$$T_E \equiv \frac{1}{\langle u'^2 \rangle} \int_0^\infty \langle u'(t)u'(t+\tau) \rangle d\tau \quad (7-32)$$

Upon making use of the relationship

$$\frac{1}{2\pi} \int_{-\infty}^\infty e^{-i\omega t} dt = \delta(\omega) \quad (7-33)$$

we obtain

$$T_E(\underline{x}) = \frac{2\pi}{\langle u'^2(\underline{x}) \rangle} \int 2\Psi(\underline{k}, 0) [1 - e^{i\underline{k} \cdot (\underline{x} - \underline{x}_0)}] d\underline{k} \quad (7-34)$$

This expression shows that at the point \underline{x}_0 where the properties of turbulence are measured, the integral time scale T_E is identically zero. And it is from this result and the assumption that the Lagrangian time scale T_L is related to T_E by

$$T_L = \text{CONSTANT} \cdot T_E \quad (7-35)$$

that the aforementioned dispersion paradox arises.

Eq. (7-34) reveals that the observed spreading of a plume at long range is due to increasingly larger scales of motion, scales that are considered part of the "transport" or "mean" wind at \underline{x}_0 . Consequently, if one infers values for T_L from atmospheric data and then uses these values in a regional model in which wind observations are made at multiple sites, the result will be that certain scales of motion are treated twice, once in the transport flow and once (implicitly) in the turbulent diffusivity that is based on T_L . We consider this problem next.

2. Parameterization of dispersion

If we increase the number of flow observation sites in (\mathcal{D}, T) from 1, as in the example above, to N , the set of equations (6-22), (6-23) and (6-24) that defines the set W of flow fields acquires a different form and hence a new set W of flows applies. Let W_1 and W_2 represent the sets of flow fields corresponding to a single flow observation, as in Figure 7-3, and to 2 observations, respectively. Suppose that in the case of 2 measurement sites, one is located at the same site \underline{x}_0 as the monitor in the single observation set, and that the other is located at \underline{x}_1 downwind of \underline{x}_0 . Then the sets of trajectories, associated with the sets W_1 and W_2 will differ. For example, those trajectories in W_1 that pass through \underline{x}_1 but which have a speed and/or direction at \underline{x}_1 that is inconsistent with the observation at \underline{x}_1 are not members of W_2 . Thus, the addition of a second flow observation has effectively altered the character of dispersion. This example illustrates that dispersion is an artifact of our observations, rather than an intrinsic property of the atmosphere, and it must be treated in this manner when attempting to approximate it.

The proper way to estimate the functional form of an effective eddy diffusivity for use in a diffusion equation model is the following.

First, calculate $\langle c \rangle$ for the ensemble of concentration distributions associated with the set W of flow fields. Second, define the transport wind field to be the ensemble mean wind $\langle \underline{u}(\underline{x}, t) \rangle$ in W . Finally, using the known $\langle c \rangle$ and $\langle \underline{u} \rangle$ solve the diffusion equation "in reverse" (i.e., the inverse problem for the diffusivity $K(\underline{x}, t)$). Lamb and Durran (1978) illustrate this process.

In problems involving nonlinear chemistry, the eddy diffusivity derived by this procedure would be an implicit function of the source distribution \underline{S} used to generate the concentration ensemble C , and therefore the model would not be applicable to problems with different source distributions. For this reason, we propose to generate the ensemble properties of concentration like $\langle c \rangle$ from a set of functions approximating C rather than from an ad hoc model of the ensemble mean .

3. Predictability of concentration at long range

We have emphasized in this section that for a given set of meteorological conditions and a given source distribution \underline{S} , one can determine the concentration distribution $c(\underline{x}, t)$ that would result to within only a set of functions $C(c \in C)$. Therefore, in order to utilize a model in decision making processes, it is necessary to know how much variation exists among the members of C . For if the variation is large and each member of C is equally likely to occur, then the information provided by the model has little or no practical value.

In Equation (7-6) we defined a parameter ϵ that provides, through Equation (7-8) and (7-9), an estimate of how closely the time-averaged members \bar{c} of C are clustered around the set mean value $\langle \bar{c} \rangle$. Using this parameter, we will illustrate briefly below that the scatter of $\bar{c}(\underline{x}, t)$ about $\langle \bar{c}(\underline{x}, t) \rangle$ increases as the distance $\underline{x} - \underline{x}_S$ from the source increases (assuming $\underline{x}_S \approx \underline{x}_0$, the wind observation site).

Referring to Figure 7-4, let's assume that the 2 plumes shown represent the extreme lateral deviation from the x axis of all plumes in the C ensemble. By "plume", we mean the superposition of particle trajectories originating

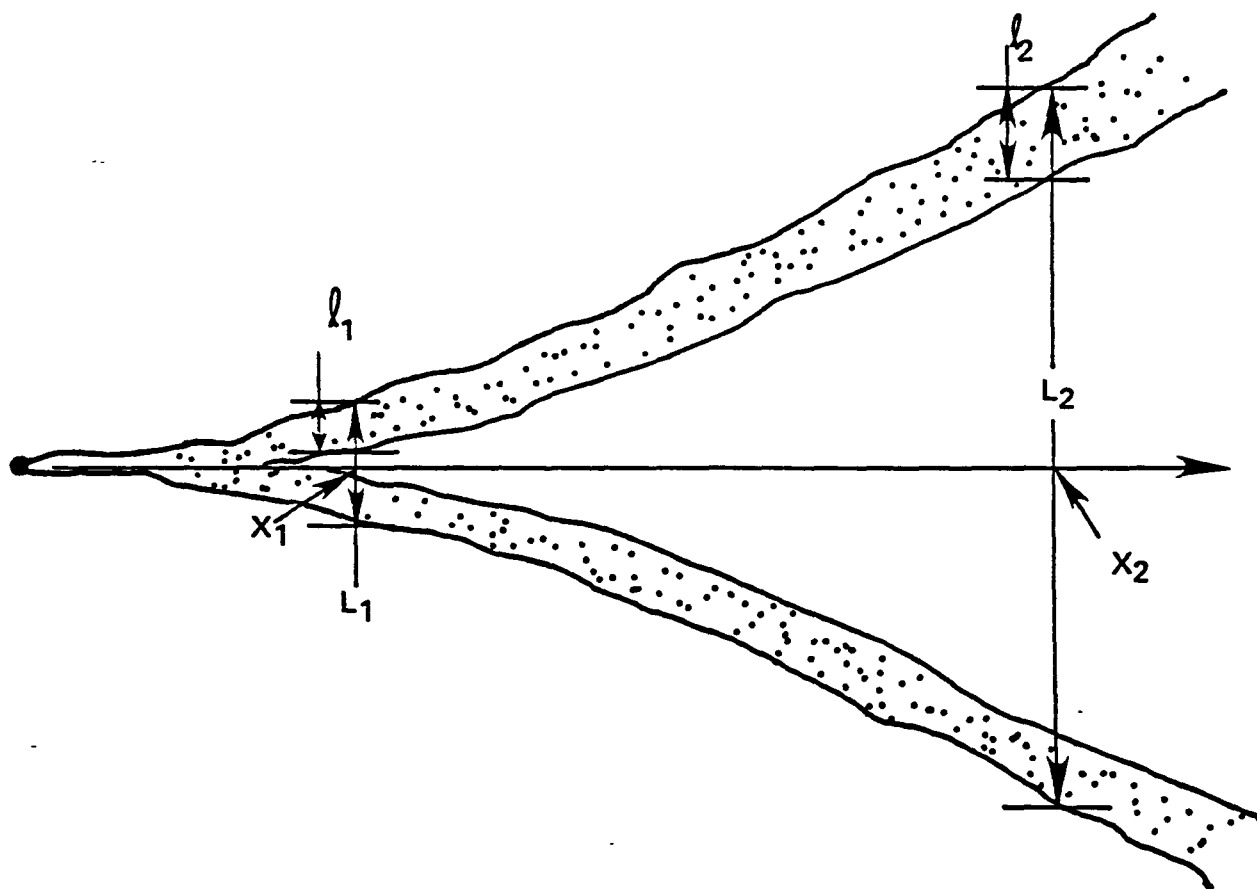


Figure 7-4. Plumes from the C ensemble that mark the limits of lateral motion. .

continually at the source over some small time interval for each $u(x,t)$ in W . Thus, the plume envelopes in the figure represent the locus of travel of the particles released during this small time period. Also, the plumes shown assume that C is an ensemble in which a wind observation site is located at the source but that no other observations are available.

For simplicity, we will assume that the concentration correlation has the form

$$\langle c(t)c(t + \tau) \rangle = \begin{cases} \langle c^2 \rangle, & \tau \leq T \\ \langle c \rangle^2, & \tau > T \end{cases} \quad (7-36)$$

where T is arbitrary and independent of t and x . Assuming that within C , plumes are equally distributed over the lateral ranges L_1 and L_2 shown in Figure 7-4, and their width ℓ is nearly the same within C for a fixed x , we obtain by straightforward calculations based on the definition of ensemble averaging

$$\begin{aligned} \langle c_1^2 \rangle &= \langle c_1 \rangle^2 L_1 / \ell_1 \\ \langle c_2^2 \rangle &= \langle c_2 \rangle^2 L_2 / \ell_2. \end{aligned} \quad (7-37)$$

Now from (7-36) and (7-8) (and assuming stationarity) we obtain

$$\langle \epsilon^2 \rangle = \frac{T}{T} \left(2 - \frac{T}{T} \right) (\langle c^2 \rangle - \langle c \rangle^2) \quad (7-38)$$

where, it will be recalled, ϵ is the difference between an observed concentration averaged over the moving interval T , or equivalently a member \bar{c} of C , and the corresponding predicted ensemble mean value $\langle \bar{c} \rangle$. Making use of (7-37) and assuming $\ell_1 = \ell_2 = \ell$, we get

$$\frac{\langle \epsilon_2^2 \rangle}{\langle \bar{c}_2 \rangle^2} = \frac{\langle \epsilon_1^2 \rangle}{\langle \bar{c}_1 \rangle^2} \left(\frac{L_2 - \ell}{L_1 - \ell} \right) \quad (7-39)$$

Thus, for the same averaging time T , concentrations measured at x_2 can be expected to differ from the mean value at that site by a larger fractional margin than at the point x_1 closer to the source. Judging from the Prairie Grass data, on which the empirical Gaussian plume formula is based, we expect that for points x_1 within 1 km of a source, the scatter in 15 min averaged concentrations \bar{c} is relatively small if meteorological conditions are steady over comparable time periods. However, according to (7-39) the scatter in similar measurements made at a site x_2 farther from the source will be greater by an amount proportional to the square root of the ratio of the plume envelope widths L measured at sites x_1 and x_2 . This result is consistent with our earlier finding, Equation (7-34), that the local integral time scale of turbulence increases with distance from the flow observation site x_0 .

If the flow were stationary, the scatter in \bar{c} measurements at x_2 would be smaller for concentrations averaged over longer time intervals than 15 min. But atmospheric flows are not stationary over arbitrarily long periods. The alternative to reducing the spread of \bar{c} about $\langle \bar{c} \rangle$ is to restrict the spread L within the flow ensemble W . This would require a redefinition of W using additional meteorological observations at sites in the vicinity of the source. For example, it is easy to see that with an additional wind observation near x_2 , the spread of trajectories in the new W ensemble would be less in general than in the single station ensemble shown in Figure 7-4 because some trajectories in the latter would be eliminated by the constraint of the observation at x_2 .

4. Model validation exercises

Our discussion in the preceding subsection illustrates the natural deviation between observations and model predictions that is not attribu-

table to model error. The proper way to establish whether the model assumptions and data are correct is to examine the frequency with which observed values satisfy (7-9). If the observed frequencies differ from that predicted by (7-9) by an amount that is not likely to be due to sampling fluctuations, the modeling hypotheses must be judged to be in error. Obviously, we can find an interval $2\epsilon_0$ centered at $\langle \bar{c} \rangle$ within which all observations will lie. But as we pointed out earlier, if the size of the interval in which a majority of the observations can be expected to fall exceeds some value, the model is worthless.

5. Predicting impact of future emissions distributions

Currently the method of judging the effectiveness of proposed emissions control strategies is to predict concentration levels that proposed sources would produce under so-called "worst case" meteorological conditions. Within the context of the approach we have developed here, this entails defining the ensemble W for the set of "worst case" meteorological conditions and then computing $\langle \bar{c} \rangle$ and $\langle \epsilon^2 \rangle$ for the proposed source distribution $S(x,t)$. However, since meteorology and the source distribution jointly affect concentrations, the concept of "worst case" meteorology is not well defined. Furthermore, the flow regime associated with a past pollution episode might have such a low probability that its expected frequency of occurrence is, say, once in a century. A more meaningful approach, therefore, would be to compute $\langle c \rangle$ and $\langle \epsilon^2 \rangle$ for the ensemble C associated with the flow ensemble W where W is the union of the sets W_i , $i=1,2,\dots,N$, each of which is defined by Equations (6-22), (6-23) and (6-24) from meteorological observations in (\mathcal{D}, T_i) , $i=1,2,\dots,N$; and the T_i are a collection of time intervals selected from the period in which climatological records are available for the modeling region

D. By this definition \mathcal{W} is an estimate of the flow ensemble set, referred to at the end of Section 6, which forms the basis for predicting future states of a system.

SECTION 8

FORMULATION OF MISCELLANEOUS FIELDS AND MODEL PARAMETERS

Model parameters not yet considered will be discussed in this section and possible techniques for deriving them will be described. Chemical kinetics schemes will not be treated in this report because no particular scheme is an integral part of this model. Rather, the chemical mechanism is a peripheral component that can be interchanged as desired. A number of kinetics schemes are currently used in various urban modeling studies and in the course of our regional modeling work we plan to utilize several of them in comparative studies. At the time of this writing we are performing operational tests of the regional model computer code and for these purposes we have implemented the Demerjian-Schere (1979) mechanism that simulates 36 reactions among 23 chemical species.

Deposition Velocity, β .

Following Wesley and Hicks (1977) we shall express the deposition velocity β of each species in terms of the deposition resistance r_s :

$$\beta(\lambda, \phi, t; n) = 0.4u_* [\ln(10/z_0) + 2.6 + 0.4u_*r_s - \psi_c]^{-1} \quad (8-1)$$

where the surface roughness z_0 and friction velocity u_* are functions of (λ, ϕ, t) and the resistance r_s is a function of space and time and the pollutant n . The function ψ_c in (8-1) is an empirical function given by

$$\psi_c = \exp[.598 + .39 \ln(-10/L) - .09 [\ln(-10/L)]^2] \quad (8-2)$$

and L is the Obukhov length at (λ, ϕ, t) .

The surface roughness $z_0(\lambda, \phi)$ is prepared from land use data. The resistances r_s are functions of both land use and time of day. The methods we used to formulate both these variables are described in Part II.

Source Emission Rates $\langle S \rangle_1, \tilde{S}$

The stationary source emissions inventory will be prepared in such a manner that the information necessary to make plume rise calculations will be available for the set of sources that together are responsible for 50 percent of the total emissions of a particular pollutant in the modeling region. Given the stack parameters and a plume rise estimate for each hour of the simulation, the emissions of this set of sources will be partitioned between $\langle S \rangle_1$ and \tilde{S} , depending on whether the estimated effective plume height is above or below H_0 .

The emissions of all remaining stationary sources and those from mobile sources will be included in \tilde{S} . It is important to note that $\langle S \rangle_1$ is a volume source, that is, it has units of mass per volume per time, and it represents uniform emission rate of pollutant from each point within a single grid cell. By contrast, \tilde{S} is an area source -- units of mass per area per time. Emissions from the 10 or so largest point sources in the modeling domain (all power plants) will be handled separately and treated by a puff type model embedded within the regional scale model. Special treatment of these sources is necessary because the injection of material into the upper layers of the model in the form of slender, highly concentrated plumes can cause enormous subgrid scale chemistry effects at altitudes where there is currently no provision in the model to treat them. Moreover,

these sources can cause large subgrid scale variations in ground-level concentrations that the grid model alone cannot resolve.

The Plume Volume Fraction, ζ

This parameter was introduced in the Layer 0 formulation as part of the scheme to treat subgrid scale chemistry associated with low level point and line sources. It was defined in (5-11) as the volume fraction of any Layer 0 grid cell occupied by plumes from point and line sources within that cell.

As in (5-6) let Δz_0 represent the depth of a Layer 0 cell whose horizontal area is A . In the surface layer of the atmosphere we can assume to good approximation that the relative rate of expansion of a point source plume is proportional to the friction velocity u_* and that the centroid of the plume rises at about the same rate. Hence, the centroid of a surface source plume reaches the top of Layer 0 in a time

$$\tau \sim \Delta z_0 / u_* \quad (8-3)$$

and it has a diameter σ there of order $u_* \tau = \Delta z_0$. The volume δv of a single point source plume in Layer 0 is thus

$$\delta v \sim (\Delta z_0)^3 \quad (8-4)$$

If there are ρ point sources per unit area, then

$$\zeta = \frac{\rho \delta v}{A \Delta z_0} \sim \rho (\Delta z_0)^2 \quad (8-5)$$

This expression is not valid if many of the point source plumes overlap. In fact, since $\zeta \leq 1$ by definition, we see that the total number N of point sources in any grid cell must satisfy

$$N < \frac{A}{(\Delta z_0)^2}$$

in order for (8-5) to be a consistent approximation. In our case where $A \sim 400 \text{ km}^2$ and $\Delta z_0 < 100\text{m}$, Equation (8-5) is consistent as long as there are many fewer than about $4 \cdot 10^4$ point sources within any grid cell.

Suppose there is a total length L of nonoverlapping line source plumes in a given cell. The volume fraction of these plumes, derived by the same analyses used for the point sources, is

$$\zeta \sim \frac{L \Delta z_0}{A} \quad (8-6)$$

When both point and line sources are present we shall assume that

$$\zeta = \rho (\Delta z_0)^2 + \frac{L \Delta z_0}{A} \quad (8-7)$$

where ρ and L are values derived from the source inventory. A much more detailed method of approximating ζ is given in Lamb (1976).

Turbulence Parameters w_- , λ_- , etc., on H_0 and in Layer 0.

In Equation (5-2a) we introduced the probability density $p_{r_0}(w)$ of vertical velocity relative to surface H_0 . In this section we shall derive values for the parameters λ_- , λ_+ , w_- and w_+ that stem from p_{r_0} [see Equations (5-2) and (5-3)] by assuming that the turbulent velocity fluctuations at the level of surface H_0 have a Gaussian density, viz

$$p(w_0) = \frac{1}{\sqrt{2\pi}\sigma_{w_0}} \exp \left(- \frac{w_0^2}{2\sigma_{w_0}^2} \right) \quad (8-8)$$

Implicit in this expression is the earlier assumption that the mean vertical motion \bar{w}_{D_0} at the level of H_0 is everywhere and at all times zero. Since

the velocity of surface H_0 is z_0 , it follows from (5-1) and (8-8) that the density $p_{r_0}(w)$ is

$$p_{r_0}(w) = \frac{1}{\sqrt{2\pi}\sigma_{w_0}} \exp \left[-\frac{(z_0 + w)^2}{2\sigma_{w_0}^2} \right] \quad (8-9)$$

Thus, from (5-2a) and (8-9) we get

$$\lambda_+ = \frac{1}{2} \left[1 - \operatorname{erf} \left(\frac{z_0}{\sqrt{2}\sigma_{w_0}} \right) \right] \quad (8-10)$$

where $\operatorname{erf}(\cdot)$ is defined by (4-43); and from (5-2b)

$$\lambda_- = 1 - \lambda_+ \quad (8-11)$$

Using (5-3a) and (8-8) and making use of the integral equivalence (4-42h), we obtain

$$-w_- = -z_0 - \frac{\sigma_{w_0}}{\sqrt{2\pi}} \exp \left(-\frac{z_0^2}{2\sigma_{w_0}^2} \right) + \frac{z_0}{2} \left[1 - \operatorname{erf} \left(\frac{z_0}{\sqrt{2}\sigma_{w_0}} \right) \right] \quad (8-12)$$

and from (5-3a)

$$w_+ = \frac{\sigma_{w_0}}{\sqrt{2\pi}} \exp \left(-\frac{z_0^2}{2\sigma_{w_0}^2} \right) - \frac{z_0}{2} \left[1 - \operatorname{erf} \left(\frac{z_0}{\sqrt{2}\sigma_{w_0}} \right) \right] \quad (8-13)$$

The speed z_0 of surface H_0 is obtained directly from the definition of H_0 [see (2-2) and (3-12)]. The variance $\sigma_{w_0}^2$ of turbulent velocity fluctuations is estimated from the following expression proposed by Binkowski (1979):

$$\sigma_{w_0}^2 = u_*^2 \left(\frac{\phi_m - \xi}{1.2 f_m} \right)^{2/3} \quad (8-14)$$

where

$$\xi = \frac{\Delta z_0}{L}$$

and u_* is the friction velocity. All of the terms appearing in (8-14) will

be described in detail in Part II.

The Plume Entrainment Velocity, v

We use as a measure of the plume entrainment rate the rms spread rate of particle pairs in the surface layer. Using similarity theory, Batchelor (1950) showed that in homogeneous turbulence the rate of expansion of a cloud is

$$\overline{L^2} = c_1 \epsilon^{2/3} \ell_0^{2/3} \tau^2 \quad (8-15)$$

where

c_1 = a constant of order unity,

ϵ = the energy dissipation rate of the turbulence,

τ = the travel time of the cloud,

ℓ_0 = the initial cloud size,

$\overline{L^2}$ = the mean square diameter after a time τ .

Deardorff and Peskin (1970) have shown that Equation (8-15) is also valid for shear flows, such as that characteristic of the lowest layer in our study. Defining

$$v = \frac{d}{dt} \overline{L^2}^{1/2} \quad (8-16)$$

and making use of Equation (8-15), we obtain

$$v = c_1^{1/2} (\epsilon \ell_0)^{1/3} \quad (8-17)$$

Combining this expression with the surface layer formulation of ϵ given by Wyngaard and Cote (1971), namely

$$\epsilon = \frac{u_*^3}{kz} (1 + 0.5 |z/L|^{2/3})^{3/2} \quad (8-18)$$

where k is the von Karman constant ($= 0.4$) and L is the Obukhov length, we get

$$v = \frac{c_1^{1/2}(\ell_0)^{1/3}}{(zk)^{1/3}} u_* (1 + 0.5|z/L|^{2/3})^{1/2} \quad (8-19)$$

where c_1 is a constant of order unity. If we take the release height z of the cloud to be $z = \ell_0$ (which is not unreasonable for motor vehicle emissions) and ℓ_0 to be approximately 1 m, then the term in bracket in Equation (8-19) has a value near unity for values of L typical of urban regions, consequently,

$$v = \alpha u_* \quad (8-20)$$

where α is a constant that we assume for the time being to be 1.

Rainout and Washout Processes

The term W on the righthand side of the general model equation (2-1) represents the scavenging rate of pollutant species c by precipitation processes. We can express it in the form

$$W = \Lambda c \quad (8-21)$$

where c is the material concentration and Λ is the scavenging coefficient. The latter is a function of many variables among which are rainfall rate, gas solubility, and in the case of aerosols, size distribution. McMahon and Denison (1979) have summarized the few measurements of Λ available to date and attempts to relate Λ theoretically to some of the parameters cited above. We will postpone further consideration of wet removal processes until a later report; because in the near-term oxidant studies that are of concern to use, the meteorological regimes of interest are generally not associated with precipitation.

SECTION 9

COMPUTER SOLUTION OF THE GOVERNING EQUATIONS

Introduction

The differential equations that we formulated in the previous sections to describe concentrations in each of the model's 3 layers cannot be solved in general without the use of a large computer. If a digital machine is employed, each of the concentration and input parameter fields must be represented in discrete value form. In this case it is also customary to model the governing differential equations by a system of finite difference equations. There are countless methods of generating finite difference analogues of differential equations but many of them do not preserve essential properties of the differential equations that are important in simulating physical phenomena.

For example, in modeling regional scale air pollution it is not possible in practice to represent the concentration fields in discrete form with sufficient spatial resolution to resolve all of the major variations in the concentration distribution. In some finite difference representations of the advection equation, this limited resolution gives rise to the well known phenomenon of pseudo-diffusion, which is not present in the true advection process.

Another source of potential trouble in applying a conventional method to our set of equations is the large vertical concentration gradients that can arise. In the atmosphere, there are extended periods (usually the nighttime hours) when vertical fluxes of material are very small. During these periods very large vertical gradients in concentration can arise, and these lead in a simulation model to large surges of material from one layer to another once the physical processes that produce interlayer exchanges begin. With many finite difference expressions, large transients of this kind can cause computational instability.

Finally, the multitude of chemical reactions that make up the photochemical air pollution phenomenon possess an extremely wide range of characteristic time scales. A common method of mitigating the problems that this disparity of scales causes the computer simulation is to adopt the steady-state approximation for the fastest of the reactions. The effect of this approach is to "hardwire" a particular chemical kinetics parameterization scheme into the model. Consequently, it is virtually impossible to examine alternative representations of the chemistry and hence the utility of the model as a research tool is diminished.

In this section we seek to develop ways of generating approximate solutions of the governing equations that avoid the problems just cited. We hope to achieve this in 2 ways. First, we will express the governing equations in an alternate form that permits the advection, vertical flux and chemistry phenomena to be treated separately and in modular forms. This will allow the computer version of the model to have sufficient flexi-

bility that various numerical schemes can be utilized without having to overhaul the entire code. Second, we will develop numerical techniques for treating advection, vertical fluxes and chemistry that are well suited to handling the specific problems that arise in regional scale modeling. These schemes are developed later in this section following a modification of the governing equations.

Transformation of the Governing Equations

The differential equations that describe concentrations within each of the model's 3 layers take the general form

$$\frac{\partial c_n}{\partial t} + Lc_n + ac_n + F_n = S_n + R_n \quad n=1,2,3 \quad (9-1)$$

(see Section 10) where $c_n = \langle c \rangle_n$. Here L is the linear advection and diffusion operator (which for illustration purposes only we write in the K-theory form)

$$L \equiv u \frac{\partial}{\partial x} + v \frac{\partial}{\partial y} - \frac{\partial}{\partial x} K_H \frac{\partial}{\partial x} - \frac{\partial}{\partial y} K_H \frac{\partial}{\partial y} \quad (9-2)$$

S_n is the source emissions in layer n ; R_n represents all chemical reactions in this layer; and F_n is a function involving concentrations in layers $m \neq n$ that describes material fluxes from one layer to another.

Our intent here is to restructure (9-1) so that the advection, vertical flux and chemistry processes are decoupled and treatable separately. This suggests looking for a product solution

$$c_n = \gamma_n \Gamma_n \quad (9-3)$$

Substituting this into (9-1), dropping the subscript temporarily for notational convenience, collecting terms in γ and Γ , and assuming that spatial variations in K_H are of a much larger scale than those in $\langle c \rangle_n$, we obtain

$$\begin{aligned} & \Gamma \left[\frac{\partial \gamma}{\partial t} + u \frac{\partial \gamma}{\partial x} + v \frac{\partial \gamma}{\partial y} - K_H \frac{\partial^2 \gamma}{\partial x^2} - K_H \frac{\partial^2 \gamma}{\partial y^2} + a\gamma \right] \\ & + \gamma \left[\frac{\partial \Gamma}{\partial t} + u \frac{\partial \Gamma}{\partial x} + v \frac{\partial \Gamma}{\partial y} - K_H \frac{\partial^2 \Gamma}{\partial x^2} - K_H \frac{\partial^2 \Gamma}{\partial y^2} \right] \\ & - 2K_H \frac{\partial \gamma}{\partial x} \frac{\partial \Gamma}{\partial x} - 2K_H \frac{\partial \gamma}{\partial y} \frac{\partial \Gamma}{\partial y} + F = S + R \end{aligned} \quad (9-4)$$

Suppose that we set the first group of terms in brackets equal to $(-F + R)/\Gamma$ and the second group of bracketed terms equal to S/γ . Then if Γ is the solution of the equation

$$\frac{\partial \Gamma}{\partial t} + u \frac{\partial \Gamma}{\partial x} + v \frac{\partial \Gamma}{\partial y} - K_H \frac{\partial^2 \Gamma}{\partial x^2} - K_H \frac{\partial^2 \Gamma}{\partial y^2} = 0 \quad (9-5)$$

with initial conditions

$$\Gamma(r, t_0) = c(r, t_0) \quad (9-6)$$

and boundary conditions identical to those on Eq. (9-1); and if γ is the solution of

$$\frac{\partial \gamma}{\partial t} + u \frac{\partial \gamma}{\partial x} + v \frac{\partial \gamma}{\partial y} - K_H \frac{\partial^2 \gamma}{\partial x^2} - K_H \frac{\partial^2 \gamma}{\partial y^2} + a\gamma = (-F+S+R)/\Gamma \quad (9-7)$$

with initial conditions

$$\gamma(r, t_0) = 1 \quad (9-8)$$

we see that $c = \gamma\Gamma$ satisfies Eq. (9-1) and its initial and boundary conditions for a period $t_0 < t < t_0 + \Delta T$. The magnitude of ΔT is determined by the rate at which spatial variations in γ arise. Note that Γ has units of concentration while γ is dimensionless. Note also that by construction,

γ is initially uniform in space. However, according to (9-7) horizontal variations in γ are generated by inhomogeneities in the vertical fluxes F of material, in the rate R of chemical processes, and in the source strengths S . Once horizontal gradients in γ have been generated, the last two terms on the left side of (9-4), which effectively couple γ to Γ , became finite and $c = \gamma\Gamma$ is no longer an exact solution of (9-1). (γ and Γ are also coupled through the chemistry term R , which we treat later.)

Working within this limitation on ΔT , we can use Γ , as given by (9-5) and (9-6), and γ , given by (9-7) and (9-8), to obtain approximate solutions of the differential equation (9-1) at discrete intervals ΔT forward in time. The procedure is as follows. First, we use the initial concentration distribution $c(\underline{r}, t_0)$ in (9-6) to solve (9-5) for Γ at time $t = t_0 + \Delta T$. Note that Γ is independent of emissions, chemistry and vertical material fluxes. Concurrently, we solve (9-7) and (9-8) for γ at time $t = t_0 + \Delta T$. We then form the approximate solution

$$c(\underline{r}, t_0 + \Delta T) = \gamma(t_0 + \Delta T)\Gamma(\underline{r}, t_0 + \Delta T) \quad (9-9)$$

We now use this expression in (9-6) to solve for Γ at time $t_0 + 2\Delta T$. The equations governing γ , (9-7) and (9-8), have the same form during this second time interval except $\Gamma(\underline{r}, t_0 + \Delta T)$ is used for Γ in (9-7). This process can be continued indefinitely in time provided that the size of the interval ΔT is kept within the limits discussed above.

At this point we have succeeded in splitting the basic model equation into 2 parts, one of which is independent of the emissions, chemistry and vertical fluxes. This component is given by Equations (9-5) and (9-6) and it can be treated by any suitable 2-dimensional numerical scheme without regard to the complicating effects of chemistry.

The second part of the solution γ is affected by emissions, vertical fluxes and chemistry and we wish now to split this component into 2 subparts which account for these processes separately.

As before, we shall try a product solution of (9-7) and (9-8); but first it is convenient to exploit the smallness of the horizontal gradients in γ during each interval ΔT and write (9-7) in approximate form

$$\frac{\partial \gamma}{\partial t} + a\gamma + F/\Gamma = R/\Gamma + S/\Gamma \quad (9-10)$$

where γ now pertains to arbitrary, local regions of space in which F , R , and Γ have prescribed values. A better approximation is obtained by dropping only the second order derivatives and translating to a system moving with the fluid. In this case $\partial\gamma/\partial t$ in (9-10) becomes $d\gamma/dt$.

It is necessary now to resume the use of subscripts to denote the model layer. We then have from (9-10)

$$\frac{\partial \gamma_n}{\partial t} + a_n \gamma_n + \frac{1}{h_n \Gamma_n} [F_{n-1,n} - F_{n,n}] = R_n/\Gamma_n + S_n/\Gamma_n \quad (9-11)$$

where $F_{n,m}$ is the flux across surface H_n to or from Layer m , and h_n is the local thickness of layer n . The flux $F_{n,k}$ can be written in the general form

$$F_{n,k} = \sum_{m=1}^3 [b'_{knm} c_m] + g'_n \quad (9-12)$$

Thus, let

$$(F_{n-1,n} - F_{n,n})/h_n - S_n + a_n c_n = b_{n1} c_1 + b_{n2} c_2 + b_{n3} c_3 - g_n \quad (9-13)$$

Combining this and (9-11) we get

$$\frac{\partial \gamma_n}{\partial t} + b_{n1}^* \gamma_1 + b_{n2}^* \gamma_2 + b_{n3}^* \gamma_3 = g_n/\Gamma_n + R_n/\Gamma_n \quad (9-14)$$

where

$$b_{nm}^* = b_{nm} \Gamma_m / \Gamma_n \quad (9-15)$$

Note that the term a_n , which appears in (9-11), is absorbed into the coefficient b_{nn} .

We look now for a product solution of (9-14) of the form $\gamma_n = \hat{\gamma}_n \gamma_n'$ in which the component γ_n' represents the chemical processes and $\hat{\gamma}_n$ describes the effects of vertical material fluxes and sources on γ_n . Substituting the proposed solution into (9-14) and collecting terms we have

$$\begin{aligned} \gamma_n' \left[\frac{\partial \hat{\gamma}_n}{\partial t} + b_{n1}^* \hat{\gamma}_1 \gamma_1' / \gamma_n' + b_{n2}^* \hat{\gamma}_2 \gamma_2' / \gamma_n' + b_{n3}^* \hat{\gamma}_3 \gamma_3' / \gamma_n' - \frac{g_n}{\Gamma_n \gamma_n'} \right] \\ + \hat{\gamma}_n \left[\frac{\partial \gamma_n'}{\partial t} - \frac{R_n}{\Gamma_n \hat{\gamma}_n} \right] = 0 \end{aligned} \quad (9-16)$$

The chemistry-free component $\hat{\gamma}_n$ is therefore the solution of

$$\frac{\partial \hat{\gamma}_n}{\partial t} + b_{n1}^{**} \hat{\gamma}_1 + b_{n2}^{**} \hat{\gamma}_2 + b_{n3}^{**} \hat{\gamma}_3 = g_n / (\Gamma_n \gamma_n') \quad (9-17)$$

with initial condition

$$\hat{\gamma}_n(t_0) = 1 \quad (9-18)$$

and

$$b_{nm}^{**} = b_{nm} \frac{\Gamma_m \gamma_m'}{\Gamma_n \gamma_n'} \quad (9-19)$$

Similarly, the component γ_n' that handles the effects of chemistry satisfies

$$\frac{\partial \gamma_n'}{\partial t} = \frac{R_n}{\Gamma_n \hat{\gamma}_n} \quad (9-20)$$

with initial condition

$$\gamma'_n(t_0) = 1 \quad (9-21)$$

We must solve (9-20) and (9-21) for each of the pollutant species present in each layer. For species α , we have

$$\frac{\partial \gamma'_{(\alpha)n}}{\partial t} = \frac{R_{(\alpha)n}}{\Gamma_{(\alpha)n} \gamma_{(\alpha)n}} \quad (9-22)$$

with $\gamma'_{(\alpha)n} = 1$ for all α and n . For bimolecular reactions of the form prevalent in photochemical air pollution, $R_{(\alpha)n}$ can be written

$$R_{(\alpha)n} = \sum_{i=1}^I \sum_{j=i}^I k_{\alpha ij} \langle c_{(i)} c_{(j)} \rangle_n \quad (9-23)$$

where I is the total number of species present and where $\langle \rangle_n$ denotes a cell average in Layer n , as used throughout the analyses in this report [(see (2-3)]. We discussed in Section 5 the existence of subgrid scale variations in the concentration fields and pointed out that they are probably most pronounced near the ground where they are generated by the highly inhomogeneous field of sources. Based on this assumption and motivated by the need to keep the mathematical structure of the model tractable, we developed a scheme for parameterizing the subgrid scale concentration variation effects in the lowest layer of the model, Layer 0, but we chose for simplicity to neglect subgrid scale phenomena in the other layers ($n = 1, 2, 3$). In keeping with this assumption we will assume that the product averaged term in (9-23) can be approximated by

$$\langle c_{(i)} c_{(j)} \rangle_n = \langle c_{(i)} \rangle_n \langle c_{(j)} \rangle_n$$

Combining this with the product solution form $c = \hat{\Gamma} \gamma'$ we obtain finally

$$\frac{\partial \gamma'(\alpha)_n}{\partial t} = \sum_{i=1}^I \sum_{j=1}^I k_{\alpha ij}^* \gamma'(i)_n \gamma'(j)_n \quad (9-24)$$

where

$$k_{\alpha ij}^* = k_{\alpha ij} \frac{\Gamma(i)_n \Gamma(j)_n \hat{\gamma}(i)_n \hat{\gamma}(j)_n}{\Gamma(\alpha)_n \hat{\gamma}(\alpha)_n} \quad (9-25)$$

with initial condition

$$\gamma'(\alpha)_n(t_0) = 1, \text{ all } \alpha \text{ and } n \quad (9-26)$$

Note that (9-24) is a coupled system of I nonlinear ordinary differential equations. Solving this system for γ' for each species, in each layer, and at each grid point of the model domain we obtain 1 of the 3 factors in the solution $\langle c \rangle_n = \gamma' \hat{\gamma} \Gamma$. The second factor $\hat{\gamma}$ is derived from the solution of the system of 3 linear ordinary differential equations (9-17) for each pollutant at each grid point. And the final component Γ is obtained by numerical solution of Equation (9-5) for each pollutant and within each layer over the entire modeling region.

Numerous techniques already exist for treating each of these 3 sets of equations but we seek new ways of treating them that possibly are better suited to our specific modeling needs. In the sections below we develop these alternative methods of solving the Γ , $\hat{\gamma}$, and γ' equations given above [(9-5), (9-17), and (9-24), respectively].

Solution of the Γ Equation, (9-5)

In formulating the equation for Γ , (9-5), from equation (9-4), we collected only those terms that describe horizontal transport and diffusion.

Chemical processes, vertical dispersion and emissions were relegated to the γ equation. As a result (9-5) is a linear, homogeneous partial differential equation with a solution of the form

$$r(\underline{r}, t) = \int \underline{r}(\underline{r}', t_0) p(\underline{r}, t | \underline{r}', t_0) d\underline{r}' \quad (9-27)$$

where p is the Green's function of (9-5). In the present instance we have

$$p(x, y, t | x', y', t_0) = \frac{1}{2\pi\sigma^2} \exp\left[-\frac{1}{2\sigma^2} (x-x'-\bar{x})^2 - \frac{1}{2\sigma^2} (y-y'-\bar{y})^2\right] \quad (9-28)$$

where

$$\sigma^2 = 2K_H(t - t_0) \quad (9-29a)$$

$$\bar{x}(t) = \int_{t_0}^t u[x' + \bar{x}(t'), y' + \bar{y}(t'), t'] dt' \quad (9-29b)$$

$$\bar{y}(t) = \int_{t_0}^t v[x' + \bar{x}(t'), y' + \bar{y}(t'), t'] dt'. \quad (9-29c)$$

We wish to emphasize that (9-5) is a specific form of the general equation

$$\frac{\partial r}{\partial t} + Lr = 0 \quad (9-30)$$

where L is an operator describing the transport and diffusion processes. The solution form (9-27) still applies except in this case p is the Green's function of (9-30). For reasons discussed in the previous section, we use K-theory in our model to describe subgrid scale turbulence only; ensemble average material fluxes, associated with the flows in W , are estimated in a direct manner that does not require the gradient transfer assumption. Thus, for each member of the flow ensemble W , the effects on cell averaged concentration $\langle c \rangle_j$, $j=1,2,3$, of subgrid scale variations in the velocity and concentration fields are approximated by the gradient transfer expression (7-2) with the diffusivity K_H given by (7-3).

Keep in mind that Equation (9-5) and its initial condition (9-6) apply only to discrete-time intervals. If t_0 and t_1 denote the beginning and end of one of these intervals, solution of (9-5) and (9-6) yields $r(t_1)$. Within the same interval the γ equation (9-7), (9-8) is solved concurrently to give $\gamma(t_1)$. The product $c(t_1) = r(t_1)\gamma(t_1)$ then serves as the initial condition (9-6) for r in the next time interval $t_1 \rightarrow t_2$ [cf. (9-6)]. We will use the general solution (9-27) as the basis of a scheme for deriving r at the required time intervals.

In the computer model we will represent $\Gamma(r, t_n)$ on a fixed grid network. A grid system that moves with the wind would yield more accurate descriptions of the time evolution of Γ but such networks pose problems operationally, particularly at the boundaries of the region and when the wind fields are horizontally divergent, as they are in the problems of interest to us. Thus, in the present study we will utilize a fixed grid network.

Let the coordinates of the lattice point (I,J) be given by

$$x = I\Delta x$$

$$y = J\Delta y$$

where $(\Delta x, \Delta y)$ is the grid mesh dimension; and let

$$t_n = n\Delta t$$

denote the elapsed time between the initial instant t_0 and the end of the n -th time interval. Since (9-27) is applicable to any interval for which the initial value of Γ is known, we have

$$\Gamma(I\Delta x, J\Delta y, n\Delta t) = \int_{-\infty}^{\infty} \int_{-\infty}^{\infty} \Gamma(x', y', t_{n-1}) p(I\Delta x, J\Delta y, t_n | x', y', t_{n-1}) dx' dy' \quad (9-31)$$

To evaluate this expression we must express $\Gamma(x,y,t_{n-1})$ as a continuous, rather than a discrete, function. Regardless of whether we use polynomials or trigonometric functions to represent the discrete set of $\Gamma(t_{n-1})$ values, the integrals that result in (9-31) with p given by (9-28) can be evaluated analytically to yield algebraic expressions for $\Gamma(t_n)$ at each grid point. We can illustrate this most easily by considering a one dimensional problem.

In this case the counterpart of (9-31) is

$$\Gamma(I\Delta x, n\Delta t) = \int_{-\infty}^{\infty} \Gamma(x', (n-1)\Delta t) \left(\frac{1}{\sqrt{2\pi\sigma}} \right) \exp \left[-\frac{1}{2\sigma^2} (x-x'-u\Delta t)^2 \right] dx' \quad (9-32)$$

We have assumed here that the time interval Δt is small enough that (9-29b) and (9-29c) reduce to the form

$$\bar{x} = u\Delta t \quad (9-33a)$$

$$\bar{y} = v\Delta t \quad (9-33b)$$

This assumption is adopted here to keep the math simple. In our general scheme, \bar{x} and \bar{y} are calculated from (9-29) and this gives the method an "upstream" characteristic that ensures unconditional computational stability.

The exponential term in (9-32) has a maximum value at the point

$$x' = \bar{x} = x - u\Delta t = I\Delta x - u\Delta t \quad (9-34)$$

and it has values significantly different from zero over an interval $\Delta x' \approx 4\sigma$ centered at this point. These facts indicate that the continuous functional representation we use for $\Gamma[x', (n-1)\Delta t]$ should be most accurate within the interval $\bar{x} - 2\sigma \leq x' \leq \bar{x} + 2\sigma$.

Let $\tilde{x}_K = K\Delta x$ denote the grid point (on which the Γ values are stored) that is nearest to the point \bar{x} given by (9-34), and let

$$\xi = \tilde{x}_K - \tilde{x} = (K - I)\Delta x + u\Delta t \quad (9-35)$$

denote the separation between points \tilde{x}_K and \tilde{x} . By virtue of the definition of \tilde{x}_K we have

$$|\xi| \leq \Delta x/2 \quad (9-36)$$

Introducing the new coordinate

$$\eta = x' - \tilde{x}_K = x' - \tilde{x} - \xi \quad (9-37)$$

into (9-32) we have

$$\bar{\Gamma}(I\Delta x, n\Delta t) = \int_{-\infty}^{\infty} \Gamma(\eta + \tilde{x}_K, (n-1)\Delta t) \left(\frac{1}{\sqrt{2\pi}\sigma} \right) \exp \left[-\frac{(\eta + \xi)^2}{2\sigma^2} \right] d\eta \quad (9-38)$$

Suppose now that we represent $\Gamma[x', (n-1)\Delta t]$ by a quadratic expansion about the point \tilde{x}_K ; that is,

$$\Gamma(x', (n-1)\Delta t) = a + b(x' - \tilde{x}_K) + c(x' - \tilde{x}_K)^2 \quad (9-39)$$

In terms of the grid point values of Γ , the coefficients of the expansion (9-39) are found to be

$$a = \Gamma_{K,n-1} \quad (9-40a)$$

$$b = \frac{1}{2}[\Gamma_{K+1,n-1} - \Gamma_{K-1,n-1}] \quad (9-40b)$$

$$c = \frac{1}{2}[\Gamma_{K+1,n-1} + \Gamma_{K-1,n-1} - 2\Gamma_{K,n-1}] \quad (9-40c)$$

where

$$\Gamma_{K,n-1} = \Gamma(K\Delta x, (n-1)\Delta t) \quad (9-41)$$

Substituting (9-39) into (9-38) we get

$$\bar{\Gamma}_{I,n} = \int_{-\infty}^{\infty} (a + b\eta + c\eta^2) \left(\frac{1}{\sqrt{2\pi}\sigma} \right) \exp \left[-\frac{(\eta + \xi)^2}{2\sigma^2} \right] d\eta \quad (9-42)$$

The integral here is one of the many tabulated by Gradshteyn and Ryzhik (1965). (Note that it is equivalent to the expression for the moments of a normal random variable.) Thus, we are able to reduce (9-42) to the simple, closed form

$$\Gamma_{I,n} = a - \xi b + (\sigma^2 + \xi^2)c. \quad (9-43)$$

Making use of (9-40) we have

$$\begin{aligned} \Gamma_{I,n} &= \Gamma_{K,n-1} + \frac{\xi}{2} [\Gamma_{K+1,n-1} - \Gamma_{K-1,n-1}] \\ &= \frac{1}{2}(\sigma^2 + \xi^2) [\Gamma_{K+1,n-1} + \Gamma_{K-1,n-1} - 2\Gamma_{K,n-1}] \end{aligned} \quad (9-44)$$

where ξ is given by (9-35) and $\sigma^2 = 2K_H \Delta t$.

An interesting aspect of (9-44) is that if we set $K = I$ (and if $\sigma^2 = 0$), then $\xi = u\Delta t$ and we have the well known Lax-Wendroff finite difference approximation of the advection equation, which was derived originally by a method different from the one we have used.

The Lax-Wendroff scheme is known to be computationally stable only if $|u| \leq \Delta x / \Delta t$. From the perspective of the method we have used to derive (9-44), it is easy to see why this criterion must be satisfied. If $|u|$ exceeds $\Delta x / \Delta t$ and yet we use $K = I$, as is done in the Lax-Wendroff scheme, we introduce a systematic error into the calculations by representing Γ in the vicinity of $x' = K\Delta x$ by a quadratic expansion about the distance point $x' = I\Delta x$.

It appears that the method we have introduced above to derive difference schemes inherently guarantees stability, consistency, and certain conservation properties. This ability combined with its ease of application to multi-dimensional problems makes this procedure particularly useful in model development. Numerous finite difference schemes are available for

1-dimensional problems but many lose their stability, consistency and conservation properties when applied straightforwardly to several dimensions. For example, Leith (1965) showed that if the Lax-Wendroff representation of the space derivatives is applied with forward time differencing to the 2-D advection equation

$$\frac{\partial c}{\partial t} + u \frac{\partial c}{\partial x} + v \frac{\partial c}{\partial y} = 0 \quad (9-45)$$

the resulting finite difference approximation is unconditionally unstable. The stability properties possessed by 1-dimensional schemes can be preserved in several dimensions by using either the alternating direction or the time splitting techniques. Both of these methods are very popular but they are not well suited to our needs. The principal difficulty is that both methods require that the dependent variables at each grid point be treated twice (3 times in 3-D simulations) in order to advance these variables to the next time level. Thus, if the available computer memory is not large enough to accomodate the entire model domain (our model exceeds the memory capacity of EPA's Univac 1182 by a sizeable margin) costly I/O operations are necessary to implement these schemes. The most desirable difference scheme is one that allows small portions of the model domain to be processed at a time, particularly subregions small enough to fit within the high-speed memory of the computer; and that require only 1 sweep of the entire domain to advance the dependent variables 1 time level. Difference schemes generated by the above method possess these properties.

Thus far, we have developed a series of 3 schemes using this technique each of which is applicable to 2-dimensional equations, specifically (9-5). Each permits the dependent variables to be stepped forward in time in a

spatially piecewise fashion. These schemes have differing orders of accuracy but each is unconditionally stable and the computer memory requirements of each is independent of the size of the modeling region or the number of dependent variables. We illustrate below the derivation of the lowest order 2-D scheme and comparative results obtained from test studies conducted with it and the next higher order schemes in the sequence.

Recall in the earlier demonstration of the method using a 1-dimensional problem that we expanded the dependent variable Γ in a quadratic series about the point \bar{x} , given by Equation (9-34), where the Green's function p [see Equations (9-31) and (9-32)] has its maximum value. To derive an analogous 2-D scheme we proceed in the same way except in place of the quadratic approximation (9-39) we use the 2-D, biquadratic expansion

$$\begin{aligned} \Gamma(\eta, \xi) = & A_{00} + A_{10}\eta + A_{01}\xi + A_{11}\eta\xi + A_{20}\eta^2 + A_{02}\xi^2 + A_{21}\eta^2\xi \\ & + A_{12}\eta\xi^2 + A_{22}\eta^2\xi^2 \end{aligned} \quad (9-46)$$

where (η, ξ) are the space variables (x, y) transformed as in (9-37). The coefficients A_{nm} in (9-46) can be determined using the Lagrange interpolating polynomial

$$\Gamma(\eta, \xi) = \sum_{m=1}^3 \sum_{n=1}^3 (\Gamma'_{nm} \frac{\prod_{j=1}^3 (\eta - \eta_j) \prod_{k=1}^3 (\xi - \xi_k)}{\prod_{j=1}^3 (\eta - \eta_j) \prod_{k=1}^3 (\xi_m - \xi_k)}) \quad (9-47)$$

where

$$\begin{aligned} \eta_1/\Delta x &= \xi_1/\Delta y = -1 \\ \eta_2 &= \xi_2 = 0 \\ \eta_3/\Delta x &= \xi_3/\Delta y = 1 \end{aligned} \quad (9-48)$$

and $\Gamma'_{nm} = \Gamma(K\Delta x + \eta_n, L\Delta y + \xi_m, N\Delta t)$. Here $(K\Delta x, L\Delta y)$ denotes the grid point nearest $[(I\Delta x - u\Delta t), (J\Delta y - v\Delta t)]$ where the Green's function (9-28) has its maximum value [see (9-34) and the ensuing discussion]. This and other aspects of the representation (9-46) and (9-47) of $\Gamma(n, \xi)$ are illustrated in Figure 9-1.

Using (9-46) and a procedure similar to that which led to (9-38) we obtain

$$\Gamma(I\Delta x, J\Delta y, (n+1)\Delta t) = \frac{1}{2\pi\sigma^2} \sum_{n=1}^3 \sum_{m=1}^3 A_{mn} \int_{-\infty}^{\infty} \int_{-\infty}^{\infty} \left(\frac{\eta'}{\Delta x}\right)^m \left(\frac{\xi'}{\Delta y}\right)^n \phi_{\eta'}(\alpha_0, \sigma^2) \phi_{\xi'}(\beta_0, \sigma^2) d\eta' d\xi' \quad (9-49)$$

where

$$\begin{aligned} \eta' &= \eta\Delta x & \xi' &= \xi\Delta y \\ \alpha_0 &= (I-K)\Delta x - u\Delta t \end{aligned} \quad (9-50a)$$

$$\beta_0 = (J-L)\Delta y - v\Delta t \quad (9-50b)$$

and

$$\begin{aligned} \phi_{\eta'}(\alpha_0, \sigma^2) &= \exp\left[-\frac{(\eta' - \alpha_0)^2}{2\sigma^2}\right] \\ \phi_{\xi'}(\beta_0, \sigma^2) &= \exp\left[-\frac{(\xi' - \beta_0)^2}{2\sigma^2}\right] \end{aligned}$$

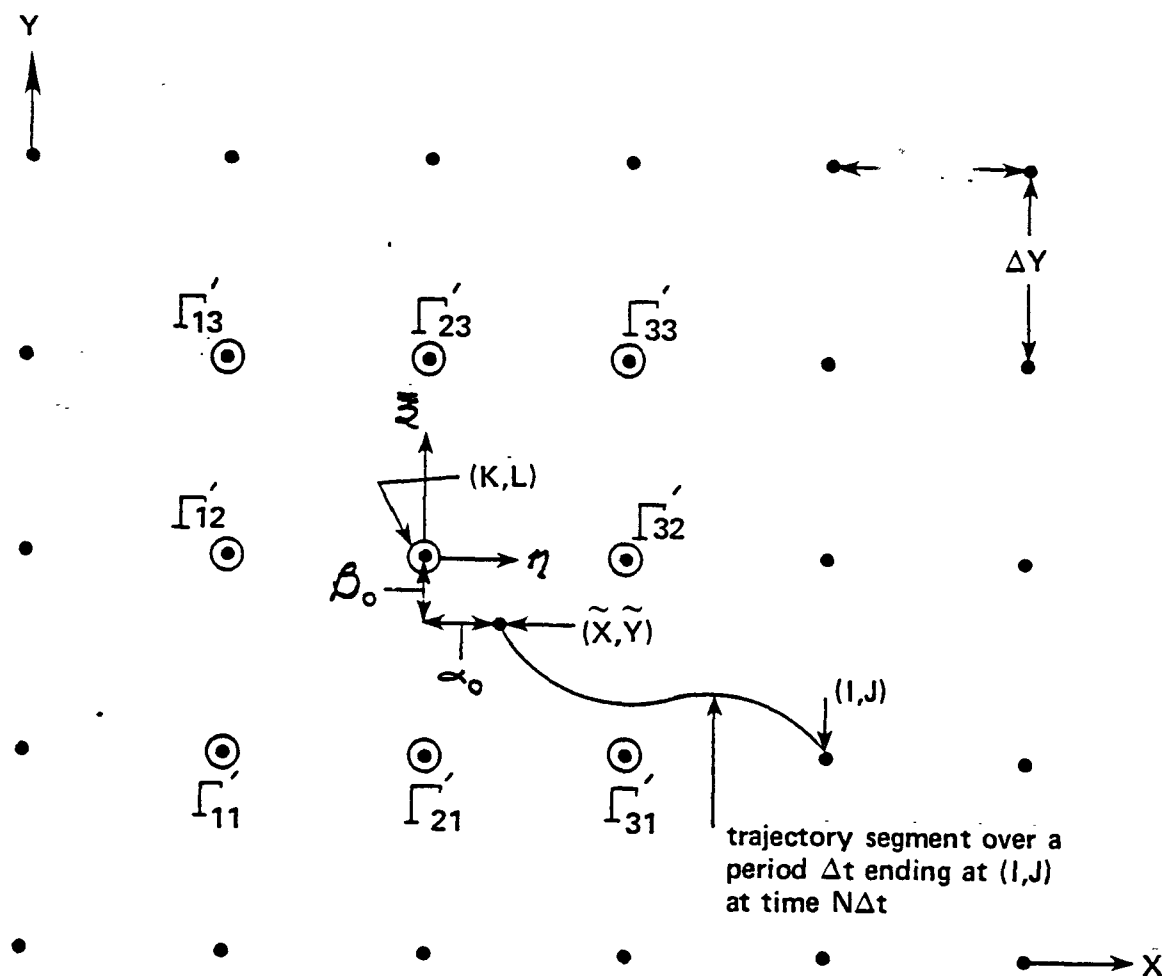


Figure 9-1.

Illustration of the grid, coordinate system, and other parameters on which the 2-D representation (9-46, 47) of the function $\Gamma(\eta, \xi)$ is based.

The integrals in (9-49) can be evaluated analytically. We get

$$\frac{1}{2\pi\sigma^2} \int_{-\infty}^{\infty} \int_{-\infty}^{\infty} \left(\frac{\eta'}{\Delta x}\right)^m \left(\frac{\xi'}{\Delta y}\right)^n \phi_{\eta'}(\alpha_0, \sigma^2) \phi_{\xi'}(\beta_0, \sigma^2) d\eta' d\xi' =$$

	$n = 0$	$n = 1$	$n = 2$
$m = 0$	1	$\frac{\beta_0}{\Delta y}$	$\frac{\beta_0^2 + \sigma^2}{(\Delta y)^2}$
$m = 1$	$\frac{\alpha_0}{\Delta x}$	$\frac{\alpha_0 \beta_0}{\Delta x \Delta y}$	$\frac{\alpha_0 (\beta_0^2 + \sigma^2)}{\Delta x (\Delta y)^2}$
$m = 2$	$\frac{\alpha_0^2 + \sigma^2}{(\Delta x)^2}$	$\frac{(\alpha_0^2 + \sigma^2) \beta_0}{(\Delta x)^2 \Delta y}$	$\frac{(\alpha_0^2 + \sigma^2)(\beta_0^2 + \sigma^2)}{(\Delta x \Delta y)^2}$

Making use of these results in (9-49) we obtain

$$\begin{aligned} r(I\Delta x, J\Delta y, (n+1)\Delta t) = & A_{00} + \frac{A_{10}\alpha_0}{\Delta x} + \frac{A_{01}\beta_0}{\Delta y} + \frac{A_{11}\alpha_0\beta_0}{\Delta x\Delta y} \\ & + \frac{A_{21}(\alpha_0^2 + \sigma^2)\beta_0}{(\Delta x)^2\Delta y} + \frac{A_{12}\alpha_0(\beta_0^2 + \sigma^2)}{\Delta x(\Delta y)^2} \quad (9-51) \\ & + \frac{A_{20}(\alpha_0^2 + \sigma^2)}{(\Delta x)^2} + \frac{A_{02}(\beta_0^2 + \sigma^2)}{(\Delta y)^2} + \frac{A_{22}(\alpha_0^2 + \sigma^2)(\beta_0^2 + \sigma^2)}{(\Delta x\Delta y)^2} \end{aligned}$$

The coefficients A_{nm} are found from (9-46) and (9-47) to be

$$\begin{aligned} A_{00} &= F/2 \\ A_{10} &= (M-C)/4 \\ A_{01} &= E/2 \\ A_{11} &= (H-B)/4 \end{aligned} \quad (9-52)$$

$$A_{21} = (B - 2E + N)/4$$

$$A_{12} = (G - A)/4$$

$$A_{20} = (C - 2F + M)/4$$

$$A_{02} = D/2$$

$$A_{22} = (A - 2D + G)/4$$

where

$$A = r'_{11} - 2r'_{12} + r'_{13}$$

$$B = r'_{13} - r'_{11}$$

$$C = 2r'_{12}$$

$$D = r'_{21} - 2r'_{22} + r'_{23} \quad (9-53)$$

$$E = r'_{23} - r'_{21}$$

$$F = 2r'_{22}$$

$$G = r'_{31} - 2r'_{32} + r'_{33}$$

$$H = r'_{33} - r'_{31}$$

$$M = 2r'_{32}$$

The other 2 difference schemes that we have developed are derived in exactly the same way as the biquadratic scheme (9-51) above except they are based on bicubic and biquintic expansions, respectively, of the r field. Whereas (9-51) uses r values at 9 points to estimate $r(I, J, n+1)$ [note that there are 9 terms on the right side of (9-51)], the bicubic scheme employs 16 points and the biquintic scheme 36 points. The last scheme requires more computer time to operate than either of the 2 lower order schemes, but by streamlining the algebraic operations executed by the computer

code, we have reduced the CPU time requirements of the biquintic scheme to levels of the same order of magnitude as the time required by other difference schemes in current use. We will show this later.

Because they are based on odd ordered polynomials, both the bicubic and biquintic schemes possess much different (and more desirable) properties than the biquadratic (9-51). We illustrate several of these in Figures 9-2 and 9-3 where we show the results of a simulation of a conic-shaped r distribution advected by a flow in counter-clockwise, solid body rotation about the center of the square model domain. The angular speed of fluid rotation is $\omega = (40\Delta t)^{-1} \text{ s}^{-1}$ and the eddy diffusivity $K_H = 0$. The initial r distribution is

$$r(x,y,0) = \begin{cases} 1 - R/4\Delta & , \text{ if } R \leq 4\Delta \\ 0 & , \text{ otherwise} \end{cases} \quad (9-54)$$

where $R = [(x - 21\Delta x)^2 + (y - 15\Delta y)^2]^{1/2}$ and we assume $\Delta x = \Delta y = \Delta$. The results of our solution of Equation (9-5) in a $30\Delta \times 30\Delta$ domain using the parameter and initial values given above are shown in Figures 9-2a,b and 9-3a,b. The former displays the results after 50 and 100 steps using the biquadratic scheme and Figure 9-3a,b exhibits the corresponding solution given by the bicubic scheme. In both cases $\Delta = 1 = \Delta t$.

An obvious deficiency of the biquadratic scheme seen in Figures 9-2a,b is its generation of "ripples" of positive and negative r values that appear as a "wake" behind the moving conical cloud. Actually, the amplitude of the ripples is exaggerated in the Figure by the heavy contours and tick marks drawn along the lines of $r = 0$. Within the regions of negative r , the amplitudes are mostly of the order of -0.02 ; but there is a region of $r = -0.1$ immediately behind the cloud that has deepened to $r = -0.13$ after 100 time steps.

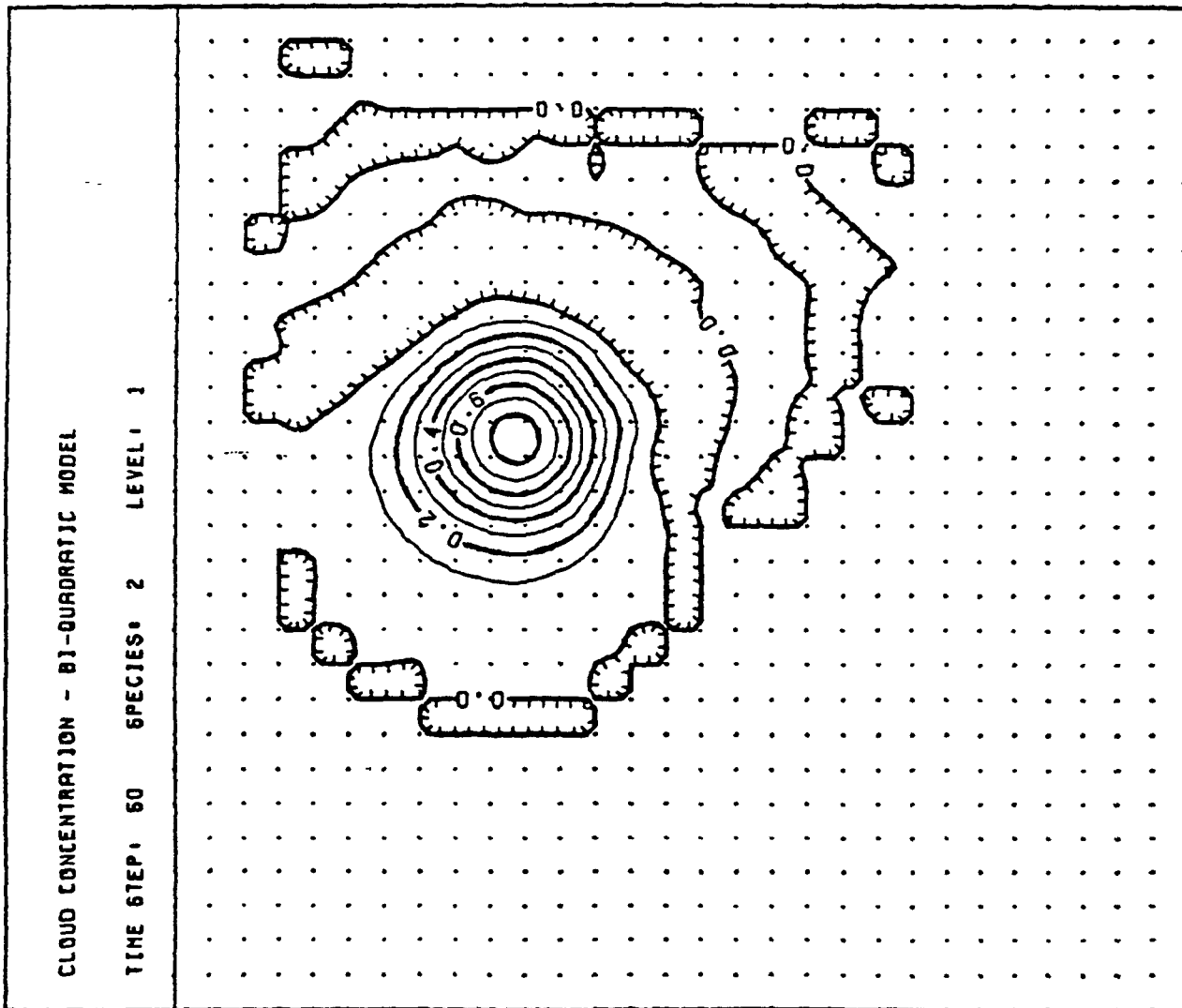


Figure 9-2a.

Results after 50 time steps from a simulation by the biquadratic scheme of the advection of a conic shaped cloud in a rotating flow. Angular speed of rotation $\omega = (40\Delta)^{-1}$ and $K_H = 0$.

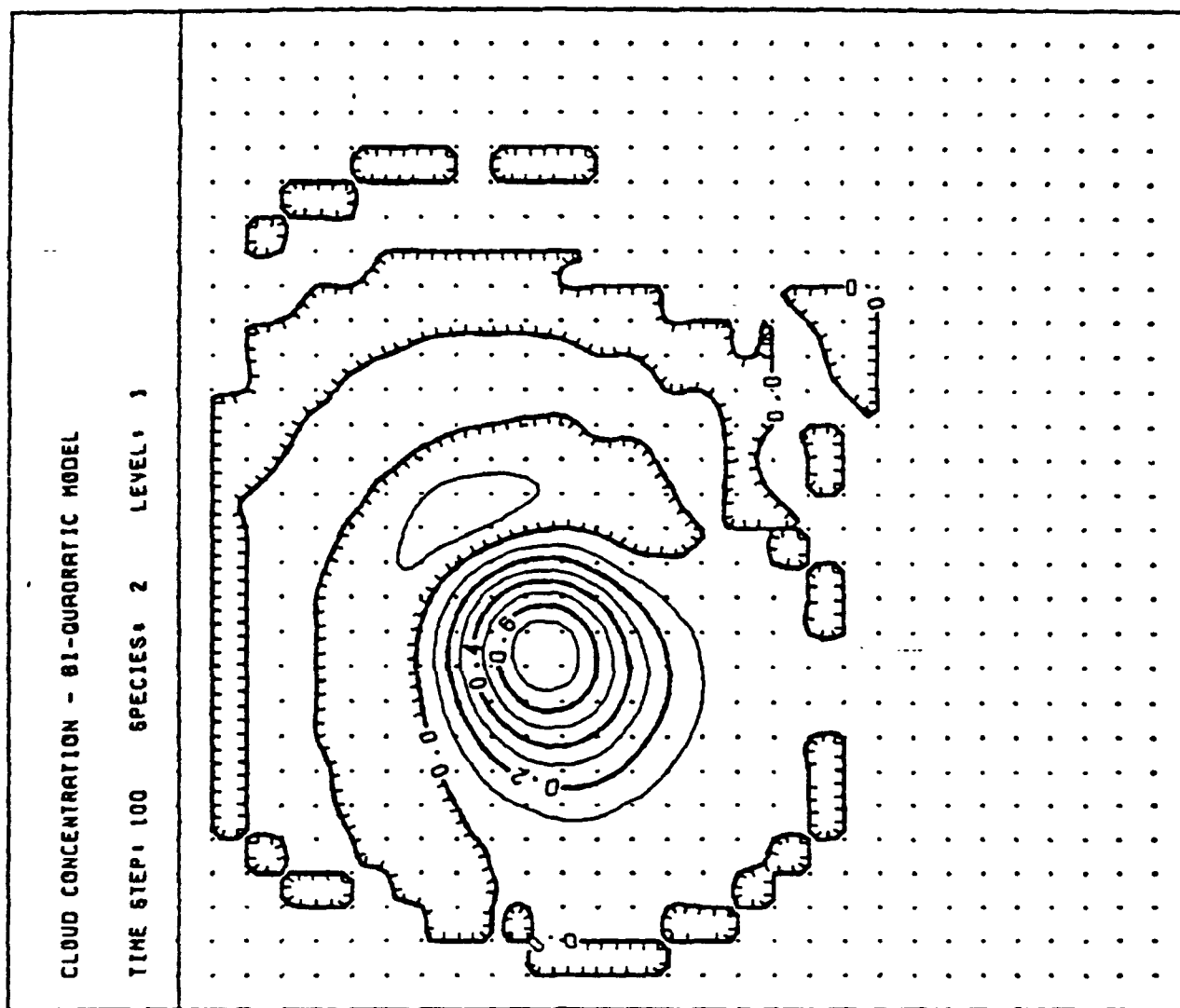


Figure 9-2b. Same as 9-2a, except results are after 100 time steps .

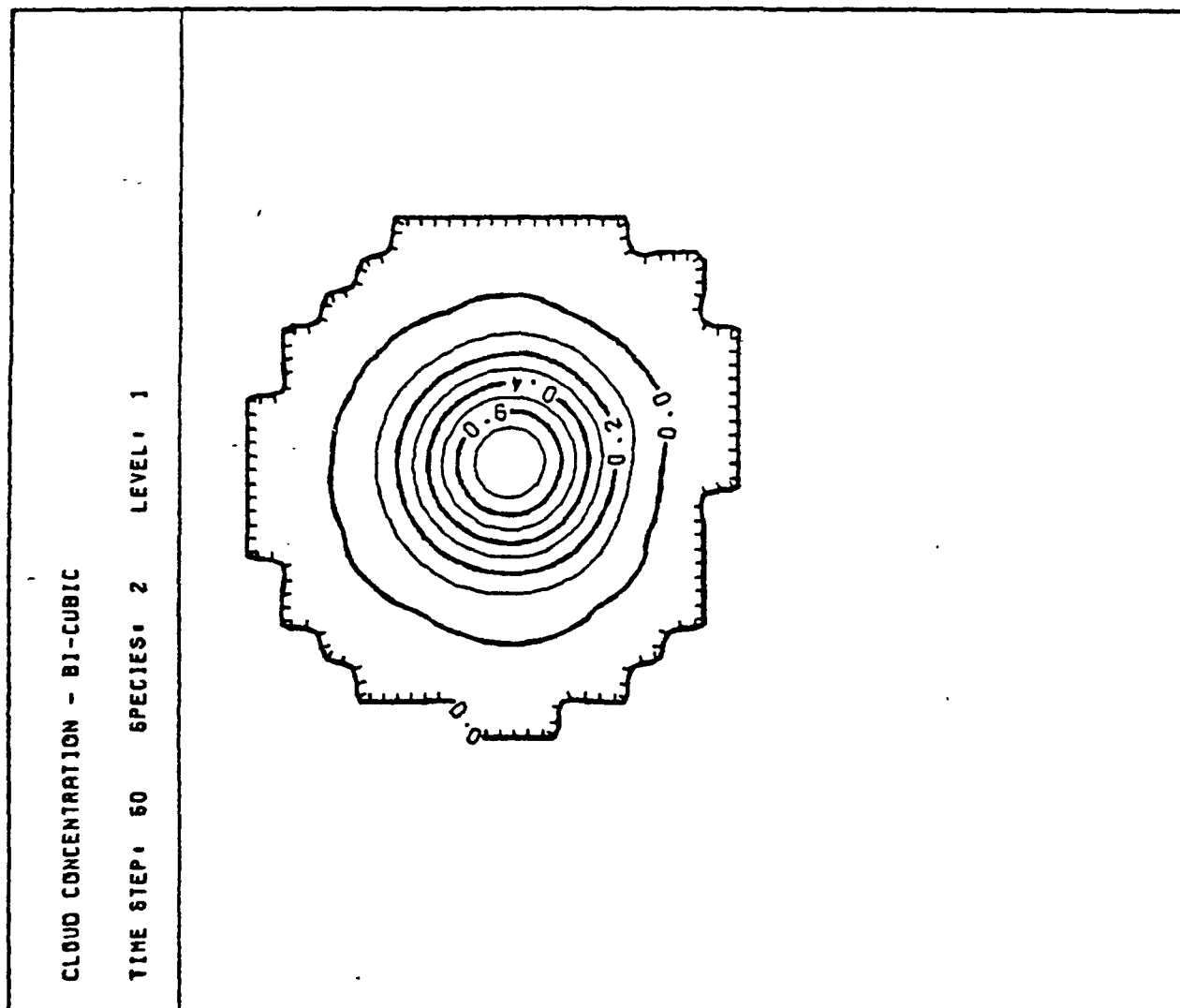


Figure 9-3a. Same as Figure 9-2a using the bicubic scheme.

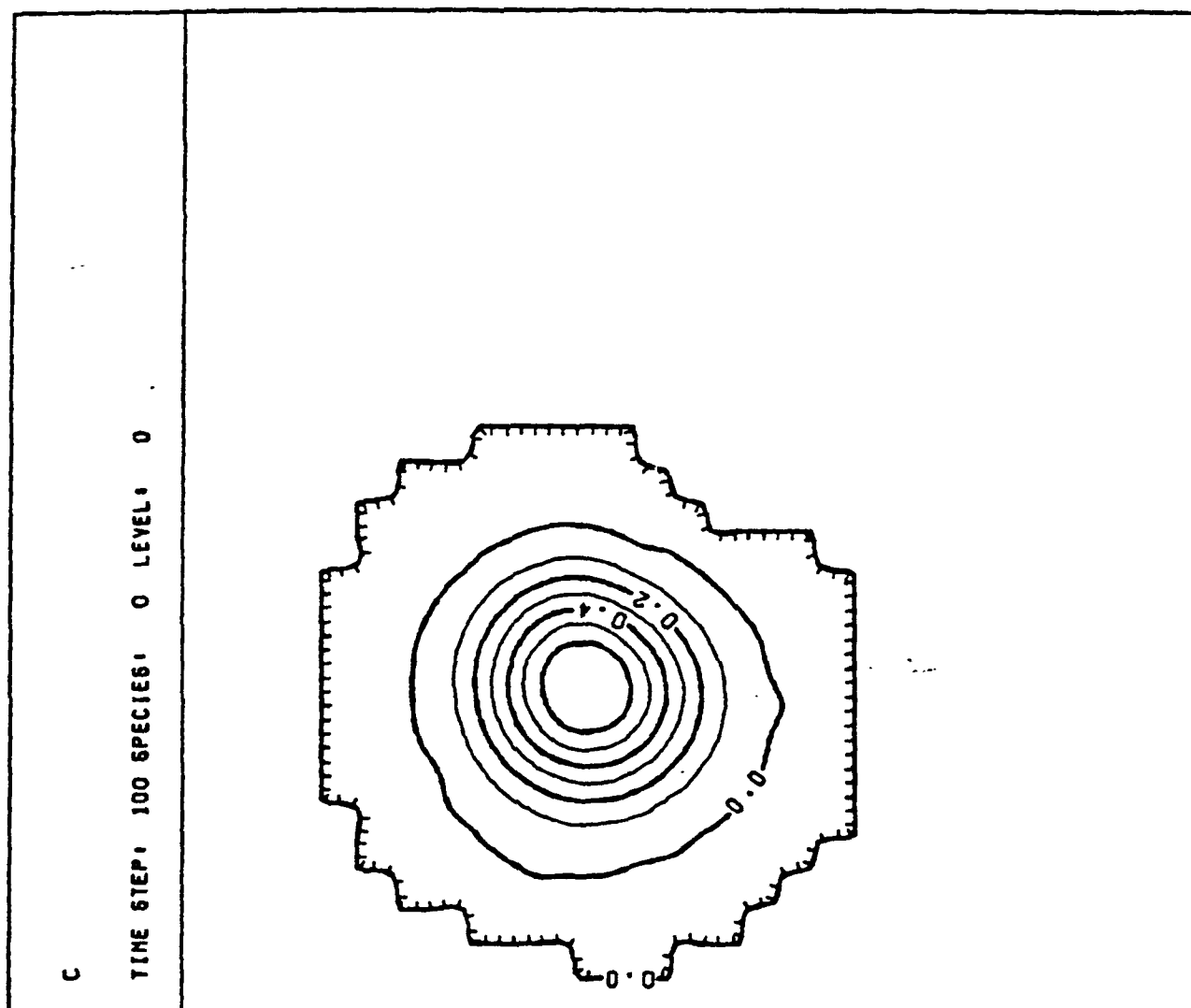


Figure 9-3b. Same as 9-3a, except results are after 100 time steps .

Although the bicubic scheme also generates negative r values, they are of much smaller amplitude and are confined to a ring that completely surrounds the moving cloud. This is apparent in Figures 9-3a,b. More importantly, the size of the domain of negative numbers and the maximum magnitude of the values do not increase with time. In contrast, the crests and troughs of r values generated by the biquadratic scheme increase slowly in magnitude with time and successively more and more crests and troughs are formed. We should add that many tests of difference schemes reported in the literature refer to these negative concentrations as "bad numbers" and refrain from showing them. We include them in this discussion because they can have serious effects in air pollution simulations that treat non-linear chemical reactions.

Another superior feature of the bicubic scheme is its maintenance of axial symmetry of the moving cloud. The biquadratic scheme shows a slight tendency to elongate the cloud along its direction of motion.

The biquadratic excels in its ability to preserve the peak concentration in the cloud. After 100 time steps the highest concentration in the cloud simulated by the biquadratic method is $r_{MAX} \approx 0.8$ whereas the bicubic method gives $r_{MAX} \approx 0.7$. Both schemes preserve total mass to within ± 1 part in 10^4 out to 100 time steps, and apparently indefinitely.

We have found that the accuracy with which the differencing scheme preserves both mass and symmetry is quite sensitive to the accuracy with which the point (\bar{x}, \bar{y}) is specified. Recall that this is the point where a particle located at a given grid point (I, J) at time $t = n\Delta t$ was located at time $t = (n-1)\Delta t$. In the vast majority of advection-diffusion differencing schemes, the point (\bar{x}, \bar{y}) is assumed implicitly to be the point of inter-

section of the straight line of slope v/u that passes through (I, J) and the circle of radius $(u^2 + v^2)^{1/2} \Delta t$ centered at (I, J) . This assumption is good as long as Δt and/or the flow speed are small; but in schemes such as those derived above that allow arbitrarily large values of Δt , the estimation of (\tilde{x}, \tilde{y}) by a simple linear extrapolation can cause significant errors in mass conservation and symmetry preservation. To circumvent these errors, we convert the flow speed (u, v) at each grid point and time step into the corresponding (\tilde{x}, \tilde{y}) array. This is done outside the model using an algorithm of high-order accuracy to evaluate (9-29). The array (\tilde{x}, \tilde{y}) is then used as input to the model, rather than (u, v) .

Another difference between the 2-D schemes derived from the technique introduced above and most of those in current use is the neglect in the latter of cross product terms in the polynomial representation of the dependent variable. Examples of these terms are those with coefficients A_{11} , A_{21} , A_{12} and A_{22} in the biquadratic expansion (9-46) of $\Gamma(\eta, \xi)$. The errors incurred by the neglect of these terms are not revealed by the popular test of advection differencing schemes used in Figures 9-2 and 9-3 that simulates clouds of axially symmetric shapes in a rotating flow, because the cross product terms in question are nonzero only when the cloud is asymmetric. We illustrate this below in simulations of the advection of a cloud of ellipsoidal shape in a rotating flow.

Figure 9-4 shows the results of tests of 3 differencing schemes: the biquintic scheme (Q) derived by the procedure illustrated above with (9-46) replaced by the 36-term biquintic polynomial; the upstream cubic spline scheme (S) reported by Mahrer and Pielke (1978); and the fourth-order flux corrector scheme (Z) of Zalesak (1979). All 3 are explicit schemes. Each of the

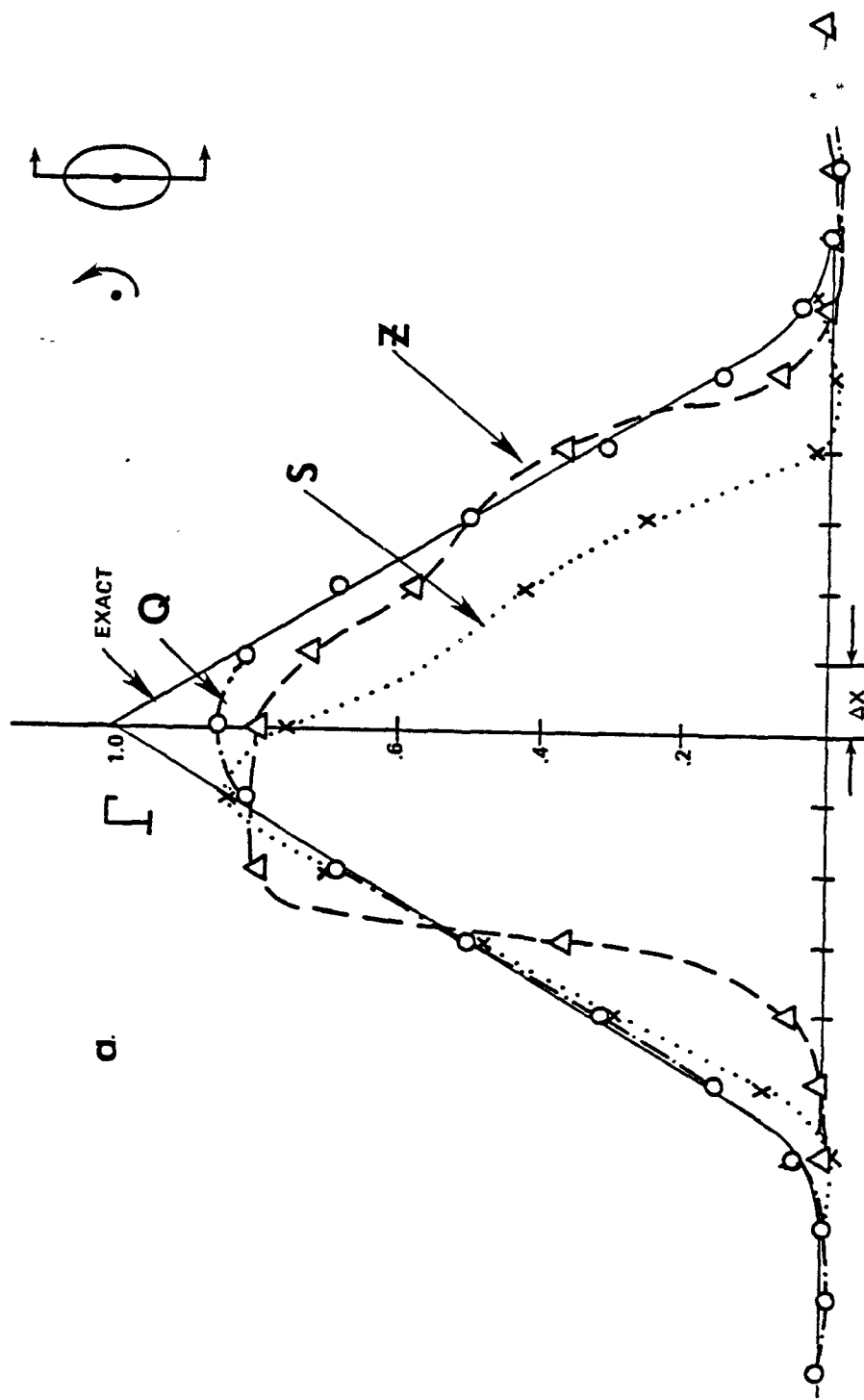


Figure 9-4. Comparison of simulations by 3 differencing schemes of the advection of an ellipsoidal cloud in a rotating flow. Panels a-e display different cross-sections of the cloud (indicated in the upper right corner of each panel) after one complete rotation of the cloud, 100 time steps in the case of schemes Q and S, 150 steps in the case of Z.

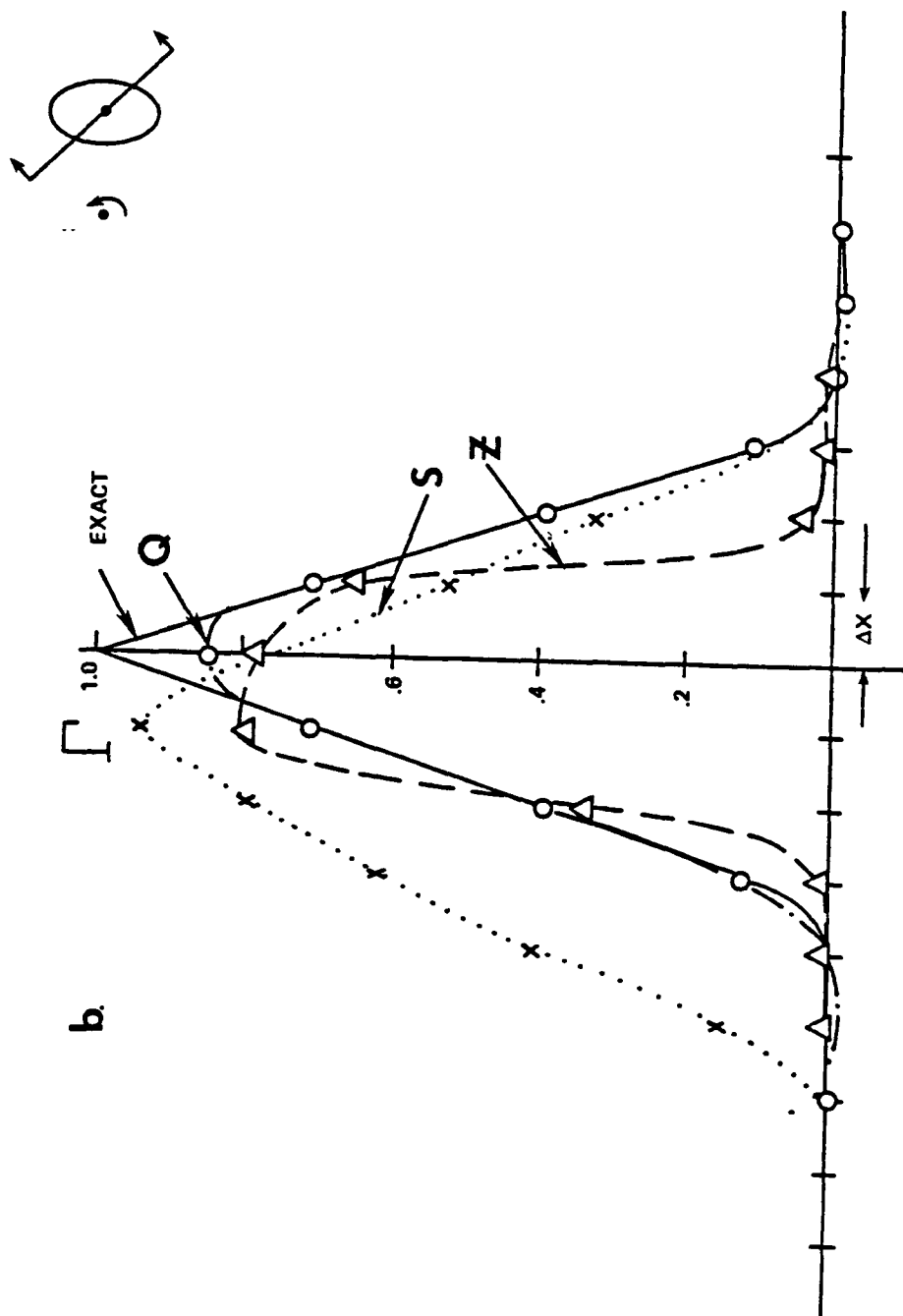


Figure 9-4 continued.

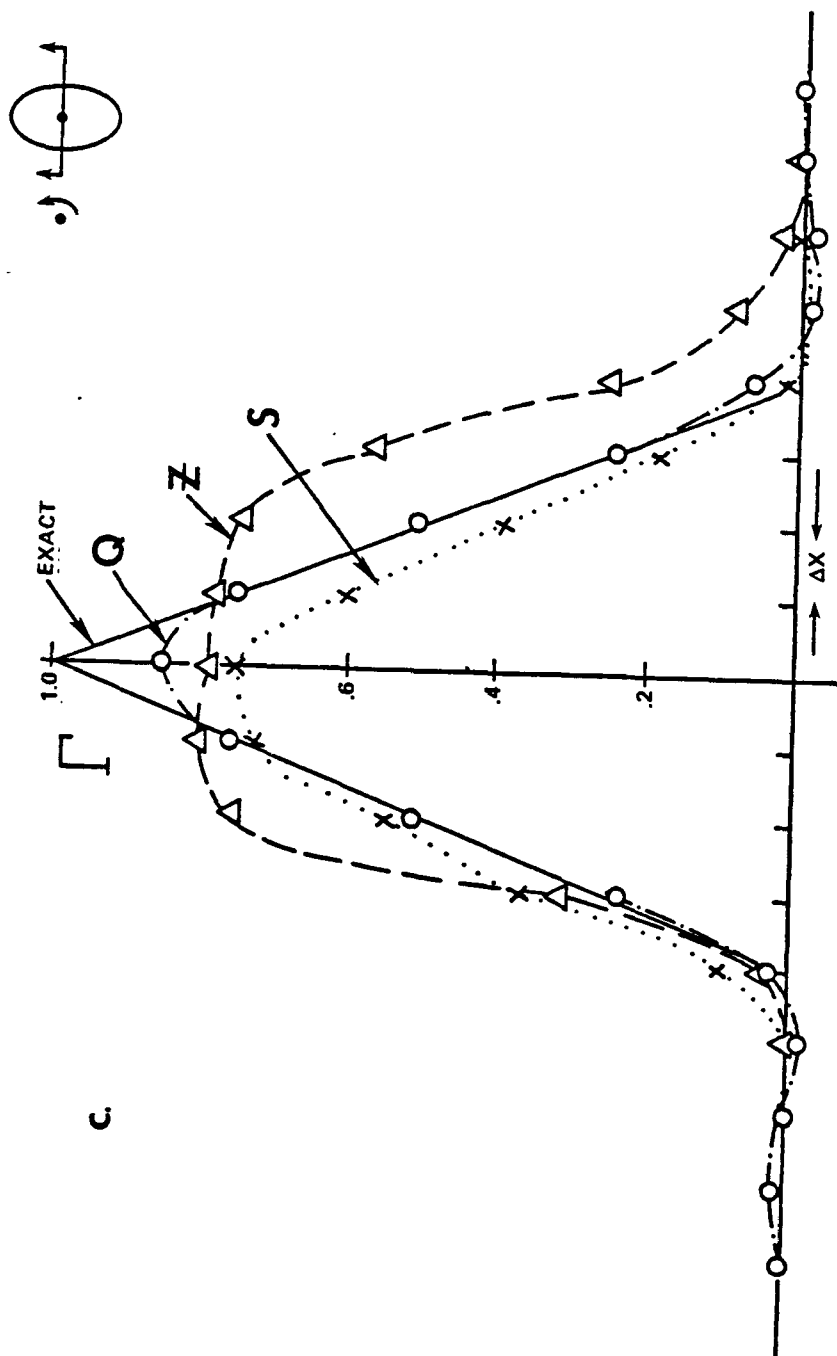


Figure 9-4 continued.

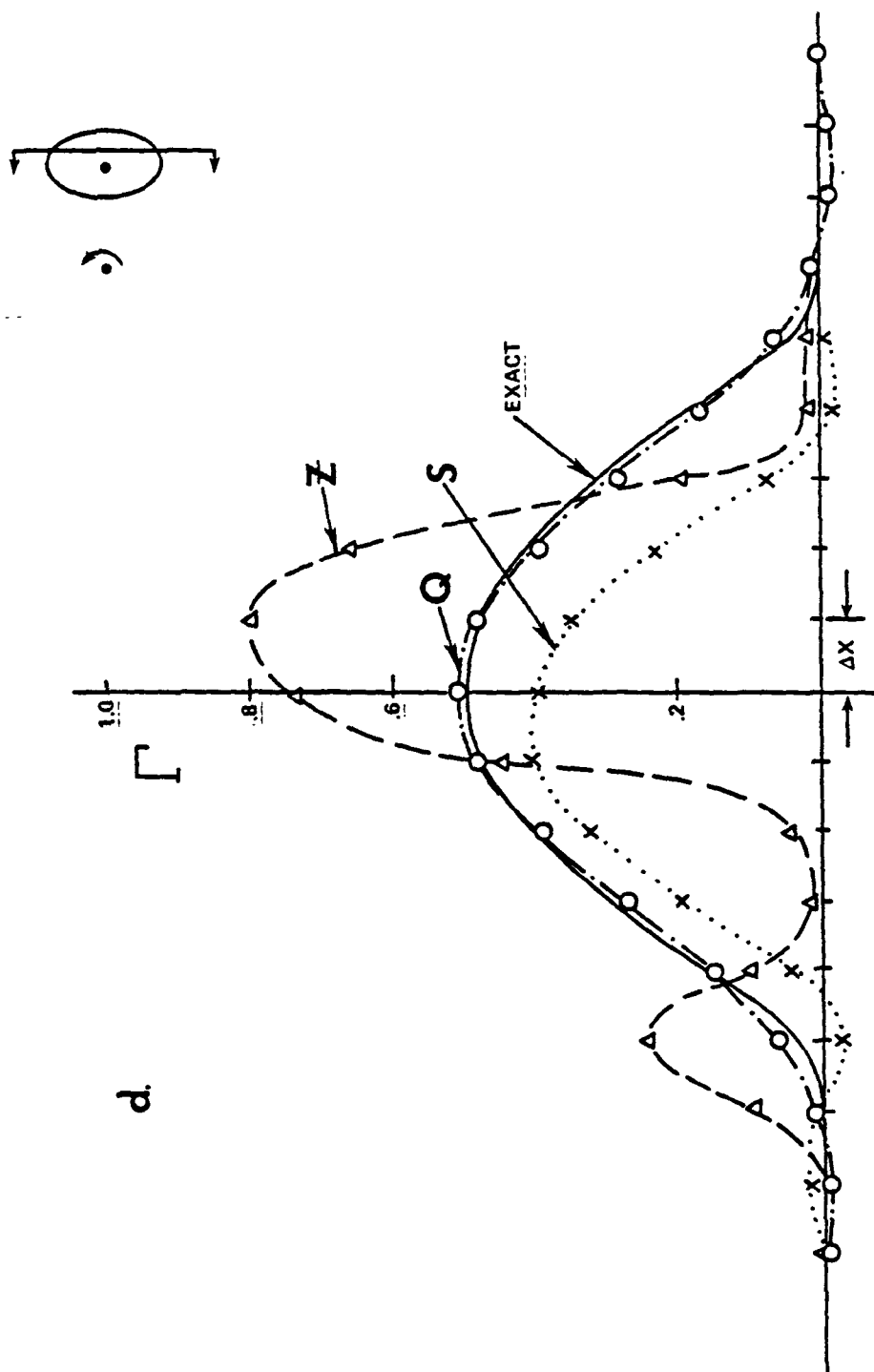


Figure 9-4 continued.

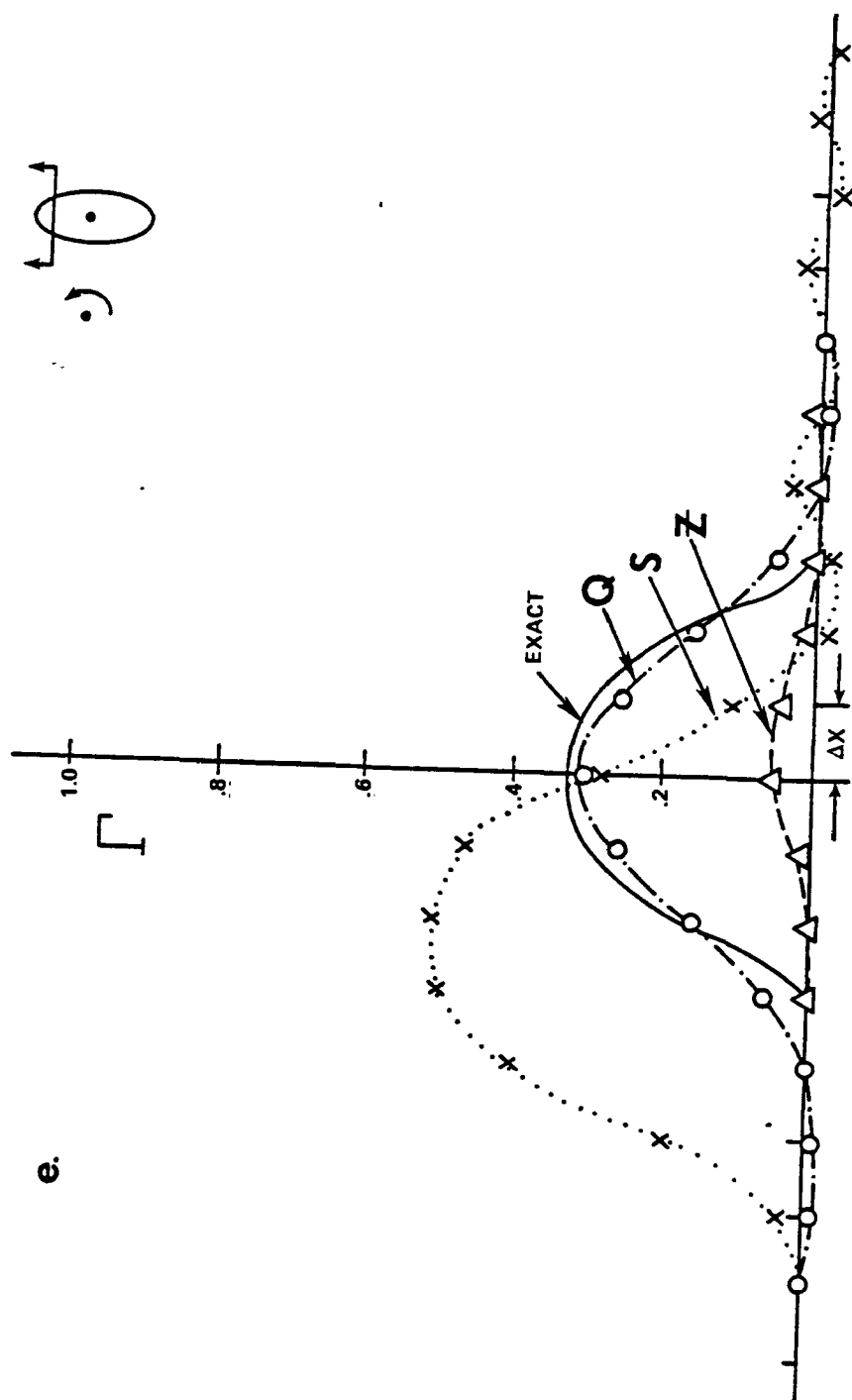


Figure 9-4 completed.

5 panels of Figure 9-4 shows a different cross-section of the cloud (indicated in the upper right corner of each panel) after 1 complete revolution about the axis of fluid rotation (also indicated in Figure 9-4). In the tests of the Q and S schemes, which are unconditionally stable, 1 revolution was completed in 100 time steps. A slower rotational rate was required with the Z scheme to maintain computational stability; therefore in its test 1 revolution marks the completion of 150 time steps.

The results presented in Figure 9-4 show clearly the superior ability of the biquintic scheme to preserve symmetry, shape, phase, amplitude and other important properties. The upstream cubic spline distorts the shape and orientation of the simulated cloud but the errors are somewhat smaller than those generated by the Zalesak scheme (Z). The errors generated by both of these schemes raise the question of whether either could provide a viable basis for simulating advection in regional models of photochemical pollutants, where the chemical reaction rates are nonlinear functions of concentration.

The principal asset of the Zalesak scheme is that it preserves the positive definite property of concentration. In both the Q and S schemes, negative concentrations are produced. However, it is apparent from Figure 9-4 that to maintain positive amplitudes, the Z scheme induces sizeable, non-symmetrical errors whose effects in some applications, such as simulating photochemical pollutants, are larger than those incurred in schemes like the Q and S schemes simply by setting negative amplitudes to zero. The maximum negative values generated by the biquintic scheme are about 3 percent of the peak amplitude of the cloud, depending on the width of the cloud relative to the grid dimensions, Δx , Δy .

The computer time requirements of each of the 3 schemes are summarized in Table 9-1. The time shown for the biquintic scheme is based on the optimized code, mentioned earlier; and it includes simulation of both advection and diffusion. The S and Z schemes treat advection only.

TABLE 9-1. COMPUTER TIME REQUIREMENTS FOR THE Q, S AND Z SCHEMES

Scheme	CPU time (UNIVAC 1182) per grid point per time step
Biquintic (Q)	$8.8 \cdot 10^{-4} \text{ s}^*$
Upstream cubic spline (S)	$7.0 \cdot 10^{-4} \text{ s}$
Zalesak fourth order flux corrector (Z)	$3.0 \cdot 10^{-4} \text{ s}$

* Advection and diffusion combined. S and Z schemes treat advection only.

Solution of the $\hat{\gamma}_n$ Equations, (9-17)

If the time interval Δt that we use as the time step in solving the Γ equation is subdivided into periods small enough that changes in γ'_n , the "chemistry variable", are negligible, then within each of these subintervals we can treat Equation (9-17) which govern $\hat{\gamma}_n$ in each of the 3 layers $n=1,2,3$ as a system of linear, ordinary differential equations. We should point out here that with the grid cell sizes we anticipate, the time scale Δt of the horizontal transport and diffusion process is much larger than that of vertical mixing, which is implicit in the coefficients b_{nm}^{**} of the $\hat{\gamma}_n$ equation; and that both time scales are generally larger than that of the fastest chemical reaction processes described in the γ'_n equations (9-24).

With the concentration $\langle c \rangle_n$ split into the 3 phenomenological components Γ_n , $\hat{\gamma}_n$ and γ'_n , these intrinsic differences in time scales can be handled separately and, moreover, locally in the simulations. This permits optimal efficiency in solving the governing equations because those phenomena that are changing slowest can be treated with large time steps, faster phenomena can be simulated using smaller time steps. And in regions of the modeling domain where approximate equilibrium prevails among the various phenomena, larger time steps can be employed than in those areas where transient processes are taking place.

Rather than approach the solution of Equation (9-17) by finite difference methods, we propose instead to exploit the pseudo-linear character of these equations during the subintervals in Δt to obtain analytic solutions. Aside from the obvious advantage of precision that the analytic solutions afford, there is the added asset that time steps can be chosen as large as the

chemistry variable γ'_n will allow. We pointed out earlier that during nighttime hours when vertical fluxes among the model layers are negligible, large gradients in material concentration can arise. Once vertical mixing begins following sunrise, large transient fluxes of material result as concentration levels proceed toward the well-mixed state. These transients could cause computational instability in numerical solutions of (9-17); but by using the analytic solution, we can use time steps of arbitrary length without adverse effects. We will demonstrate this feature later.

Detailed mathematical descriptions of each of the coefficients b_{nm} that enter into the definition (9-19) of the coefficients b_{nm}^{**} of the $\hat{\gamma}_n$ equations (9-17) are given in Appendix C. Also provided there are expressions for the inhomogeneous terms g_n that appear in (9-17). For notational convenience we will represent (9-17) here by

$$\left. \begin{aligned} \frac{\partial x}{\partial t} + D_1 x + D_2 y &= G_1 \\ \frac{\partial y}{\partial t} + E_1 x + E_2 y + E_3 z &= G_2 \\ \frac{\partial z}{\partial t} + F_1 x + F_2 y + F_3 z &= G_3 \end{aligned} \right\} \quad (9-55)$$

First, we look for solutions of the homogeneous equations, (9-55), with $G_1 = G_2 = G_3 = 0$, of the form

$$x = k_x e^{\lambda t}, \quad y = k_y e^{\lambda t}, \quad z = k_z e^{\lambda t} \quad (9-56)$$

Substituting these into the homogeneous equations, expanding and collecting terms we obtain

$$\left. \begin{aligned} k_x(\lambda + D_1) + k_y D_2 &= 0 \\ k_x E_1 + k_y(\lambda + E_2) + k_z E_3 &= 0 \\ k_x F_1 + k_y F_2 + (\lambda + F_3)k_z &= 0 \end{aligned} \right\} \quad (9-57)$$

This system of equations has a solution only if

$$\begin{vmatrix} \lambda + D_1 & D_2 & 0 \\ E_1 & \lambda + E_2 & E_3 \\ F_1 & F_2 & \lambda + F_3 \end{vmatrix} = 0 \quad (9-58)$$

Expanding this determinant we obtain the characteristic equation

$$\lambda^3 + p\lambda^2 + q\lambda + r = 0 \quad (9-59)$$

whose roots are the eigenvalues of (9-55). Here

$$p = F_3 + E_2 + D_1 \quad (9-60)$$

$$q = E_2 F_3 - E_3 F_2 + D_1 F_3 + D_1 E_2 - D_2 E_1 \quad (9-61)$$

$$r = D_1(E_2 F_3 - E_3 F_2) - D_2(E_1 F_3 - E_3 F_1) \quad (9-62)$$

Due to the physical nature of the system that (9-55) represents, all 3 of the roots of (9-59) must be real and negative.

The characteristic equation (9-59) can be solved rather easily. First we use Newton's iterative method to find the root nearest zero. With this technique the estimate of a given root after n iterations is

$$\lambda_n^* = \lambda_{n-1}^* - \frac{f(\lambda_{n-1}^*)}{f'(\lambda_{n-1}^*)} \quad (9-63)$$

where $f(\lambda)$ represents the left side of (9-59) and $f'(\lambda) = df/d\lambda$. Starting

(9-63) at $\lambda^* = 0$ to find the root nearest 0 we find from (9-59) and (9-63)

$$\lambda_1^* = \lambda_0^* - r/q = -r/q \quad (9-64)$$

With only 4 more iterations of (9-63) we obtain an estimate of 1 root of (9-59) that is accurate to 8 significant figures. Let us call this result λ_1 , i.e., $\lambda_1^* = \lambda_1$. Then the remaining 2 roots λ_2 and λ_3 are found by synthetic division of (9-59) to be

$$\lambda_2 = \frac{1}{2} [- (p + \lambda_1) + \sqrt{(p + \lambda_1)^2 - 4q - 4\lambda_1(p + \lambda_1)}] \quad (9-65)$$

and a similar expression for λ_3 except for a minus sign before the square root term.

Now for each eigenvalue λ_n there is a system of equations (9-57) for the components of the eigenvector \underline{k} . For example, the components of the eigenvector associated with λ_1 satisfy the equations

$$\left. \begin{aligned} k_{x_1}(\lambda_1 + D_1) + k_{y_1}D_2 &= 0 \\ k_{x_1}E_1 + (\lambda_1 + E_2)k_{y_1} + k_{z_1}E_3 &= 0 \\ k_{x_1}F_1 + k_{y_1}F_2 + (\lambda_1 + F_3)k_{z_1} &= 0 \end{aligned} \right\} \quad (9-66)$$

We can choose one component of this system arbitrarily. If we pick

$$k_{x_1} = -1 \quad (9-67)$$

then

$$k_{y_1} = \frac{\lambda_1 + D_1}{D_2} \quad (9-68)$$

$$k_{z_1} = \frac{1}{F_3 + \lambda_1} [F_1 - k_{y_1}F_2], \quad (9-69)$$

provided that D_2 and $(F_3 + \lambda_1)$ are not zero

Through a similar process we obtain k_{x_2} , k_{x_3} , k_{y_2} , etc. Thus, the general form of the solution of the homogeneous system (9-55) is

$$\left. \begin{aligned} x &= v_1 x_1 + v_2 x_2 + v_3 x_3 \\ y &= v_1 y_1 + v_2 y_2 + v_3 y_3 \\ z &= v_1 z_1 + v_2 z_2 + v_3 z_3 \end{aligned} \right\} \quad (9-70)$$

where $x_1 = k_{x_1} e^{\lambda_1 t}$, $y_1 = k_{y_1} e^{\lambda_1 t}$, etc; and the v_n 's are constants determined by the initial conditions on (x, y, z) . Following Kaplan (1962) we can solve the inhomogeneous system (9-55) using (9-70) with the v_n 's treated as time dependent variables. Substituting (9-70) into (9-55) and making use of the fact that (9-70) is the solution of the homogeneous system (9-55) we get

$$\left. \begin{aligned} x_1 \frac{dv_1}{dt} + x_2 \frac{dv_2}{dt} + x_3 \frac{dv_3}{dt} &= G_1 \\ y_1 \frac{dv_1}{dt} + y_2 \frac{dv_2}{dt} + y_3 \frac{dv_3}{dt} &= G_2 \\ z_1 \frac{dv_1}{dt} + z_2 \frac{dv_2}{dt} + z_3 \frac{dv_3}{dt} &= G_3 \end{aligned} \right\} \quad (9-71)$$

Solving this system first for dv_1/dt we obtain

$$\frac{dv_1}{dt} = \frac{G_1}{K} e^{-\lambda_1 t} \quad (9-72)$$

where

$$G_1 = G_1(k_{y_2} k_{z_3} - k_{z_2} k_{y_3}) + G_3(k_{x_2} k_{y_3} - k_{x_3} k_{y_2}) \quad (9-73)$$

and

$$\begin{aligned} K = & k_{x_1} [k_{y_2} k_{z_3} - k_{z_2} k_{y_3}] - k_{x_2} [k_{y_1} k_{z_3} - k_{z_1} k_{y_3}] \\ & + k_{x_3} [k_{y_1} k_{z_2} - k_{z_1} k_{y_2}] \end{aligned} \quad (9-74)$$

Hence, from (9-72)

$$v_1 = \int \frac{dv_1}{dt} dt = \begin{cases} -\frac{1}{\lambda_1} \frac{G_1}{K} e^{-\lambda_1 t} & , \text{ if } \lambda_1 \neq 0 \\ \frac{G_1 t}{K} & , \text{ otherwise} \end{cases} \quad (9-75)$$

Solving for v_2 and v_3 in a similar manner and substituting the results into (9-70) we obtain finally for the general solution of (9-55)

$$x = \sum_{i=1}^3 [C_i k_{xi} e^{\lambda_i t} + \frac{1}{K} k_{xi} G_i U_i] \quad (9-76)$$

with similar expressions for y and z except with k_{yi} and k_{zi} replacing k_{xi} .

In this equation

$$U_i = \begin{cases} -\frac{1}{\lambda_i} & , \text{ if } \lambda_i \neq 0 \\ t & , \text{ otherwise} \end{cases} \quad (9-77)$$

and the C_i 's are constants that are evaluated by setting $t = 0$ in (9-76) and solving the resulting set of equations with x , y , and z assigned their initial ($t = 0$) values. We will not write the expressions here for these constants nor will we discuss any of the operational aspects of determining the k 's that enter in (9-76) in special situations (such as the case of double roots of the characteristic equation). We have developed a computer code for evaluating (9-76) which we use in the regional model to solve the $\hat{\gamma}_n$ equations (9-17). Below we illustrate some results of exercises performed with this code which, in essence, constitutes a $3\frac{1}{2}$ layer, 1-dimensional diffusion model.

Returning to our original notation, we can express Equation (9-17) in the concise form

$$\frac{d\hat{\underline{\gamma}}}{dt} + \underline{B}\hat{\underline{\gamma}} = \underline{G} \quad (9-78)$$

where $\hat{\underline{\gamma}} = (\hat{\gamma}_1, \hat{\gamma}_2, \hat{\gamma}_3)$, \underline{B} is a 3x3 matrix whose elements are the coefficients of (9-17), and $\underline{G} = (G_1, G_2, G_3)$. Figure 9-5 shows solutions we have derived for 3 sample cases. The first, depicted in Figure 9-5a, is the case of no sources, $\underline{G} = 0$, no material sinks, and layers of equal thickness. There is vertical mixing between each of the 3 layers but mixing across the interface between layers 2 and 3 is only one-half as strong as across the surface between layers 1 and 2. Starting with initial values $\hat{\gamma}_1 = \hat{\gamma}_3 = 0$, $\hat{\gamma}_2 = 10$, the evolution of $\hat{\underline{\gamma}}(t)$ is as shown in the Figure. After a time $t \approx 15$, layers 1 and 2 are well mixed, but the concentration in layer 3 is smaller reflecting the weaker mixing between layers 2 and 3. In the limit as $t \rightarrow \infty$, the material initially present in layer 2 is equally partitioned among the 3 layers, as is evident in the $\hat{\underline{\gamma}}$ values shown for time $t = 500$.

Incidentally, the curves shown in Figure 9-5(a), (b) and (c) were obtained by recursive application of the algorithm we developed above for solving (9-78). That is, we solve (9-78) for $\hat{\underline{\gamma}}$ at $t = 1$ using the initial conditions. This result is used as the initial condition in a second application of the algorithm in which we solve for $\hat{\underline{\gamma}}$ at time $t = 2$. It is not difficult to show that this second value of $\hat{\underline{\gamma}}$ is equivalent to the solution of (9-78) at time $t = 2$ using the given value of $\hat{\underline{\gamma}}$ at $t = 0$ as initial condition. The use of a small time step like $\Delta t = 1$ would be essential in solving (9-78) by finite difference methods under the conditions given in Figure 9-5(a) to reproduce accurately the $\hat{\gamma}_n$ values in the interval $0 < t < 10$ where changes are occurring most rapidly. In fact, since $d\hat{\gamma}_2/dt = 1.5$

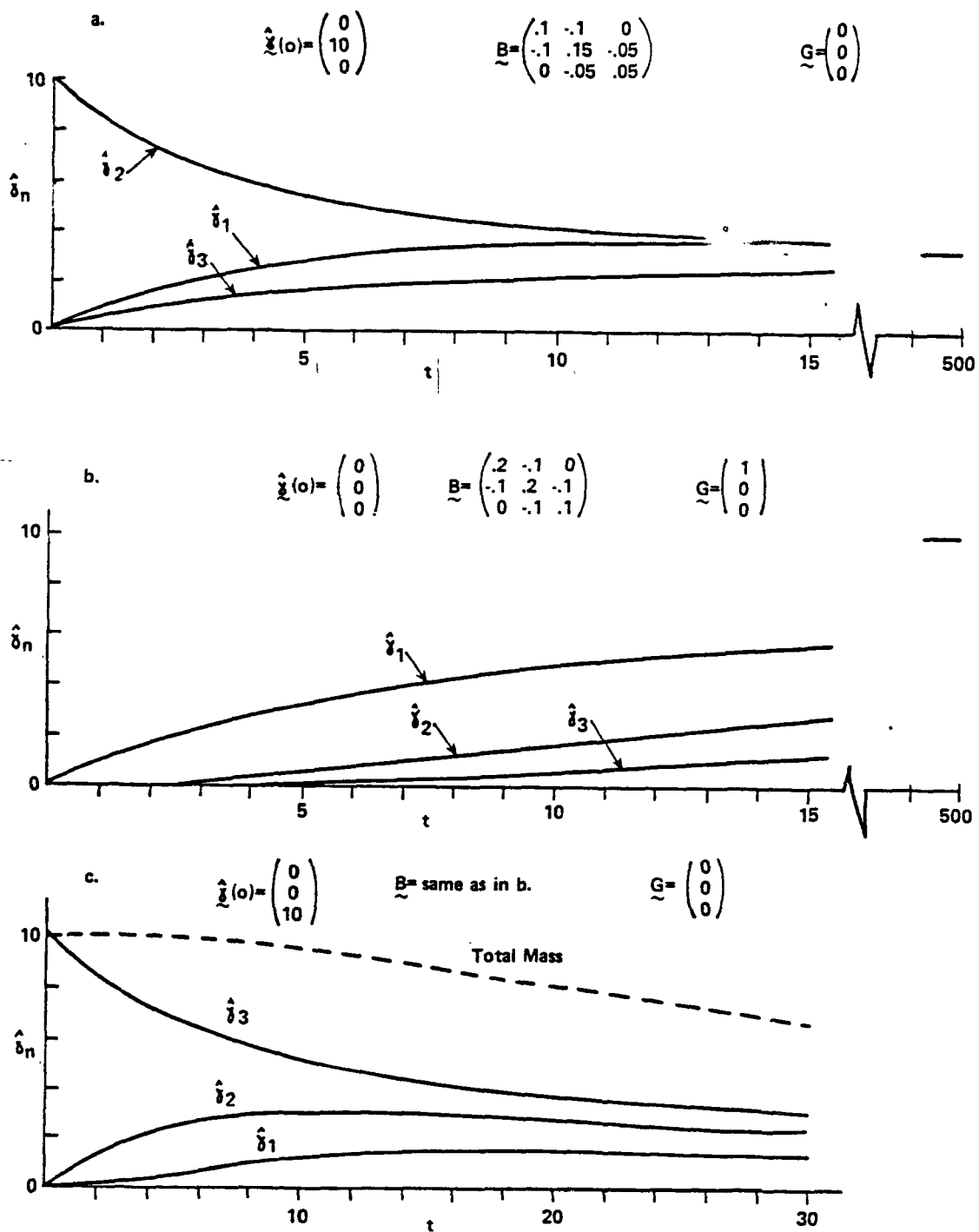


Figure 9-5. Sample solutions of the $\hat{\underline{y}}$ equation (9-78) .

initially, a time step larger than about 7 in a finite difference solution of (9-78) would produce negative values of $\hat{\gamma}$ and possibly computational instability. Using the analytic solution one can obtain exact solutions for arbitrary values of t with essentially a single iteration of the algorithm. Of course, more computations are required than in a single time step of a numerical solution technique, but the total computer time requirements are certainly comparable, and the flexibility and accuracy provided by the analytic method are most valuable.

In the second sample calculation presented in Figure 9-5(b), a source of unit strength is located in layer 1 and there is also material deposition in this layer (deposition rate = $0.1\hat{\gamma}_1$). Mixing of equal strength occurs between each of the layers and initially no material is present. The solution $\hat{\gamma}(t)$ shown in the figure displays the expected behavior, with $\hat{\gamma}_1 > \hat{\gamma}_2 > \hat{\gamma}_3$ due to the source in layer 1. The steady-state is reached in this system when the concentration $\hat{\gamma}_1$ has become large enough that the deposition rate $0.1\hat{\gamma}_1$ is equal to the source emission rate $G_1 = 1$. Our algorithm gives the correct steady-state solution $\hat{\gamma}_1 = \hat{\gamma}_2 = \hat{\gamma}_3 = 10$, as indicated in the figure for $t = 500$.

The final calculation shown in Figure 9-5(c) is for the same case just presented except instead of a material source, we begin with a puff of concentration 10 initially in layer 3. The results show that $\hat{\gamma}_1$ rises from a value of 0 initially to a peak value of about 1.4 at time $t = 20$ and then declines after that. The total mass of material present, indicated by the dashed line in the figure, is almost constant until $t = 5$, but after that it begins a rather rapid decline as material filters into layer 1 and is subsequently removed by deposition.

Using the 3 case studies just described and others, we have validated the accuracy of the algorithm we have developed above for use in solving the $\hat{\gamma}_n$ equations, (9-17). This algorithm is currently operational in our regional model.

Solution of the $\gamma'_{(\alpha)n}$ Equations (9-24)

Since the $\hat{\gamma}$ and γ' equations (9-17) and (9-24) are coupled, they must be solved simultaneously. (By contrast the Γ equation (9-5) is virtually independent of both $\hat{\gamma}$ and γ' .) The method we developed above for solving (9-17) gives $\hat{\gamma}$ at the end of time intervals of arbitrary length provided that the parameters b_{nm}^{**} and G_n that enter (9-17) are approximately constant during each interval. Both of these parameters are functions of γ' , [see (9-19) and (9-55)], so the time interval used to evaluate $\hat{\gamma}_n$ is determined by the rate of change of γ'_n .

The system of equations (9-24) that governs $\gamma'_{(\alpha)n}$ [recall that the subscript (α) refers to the pollutant species] is nonlinear. Despite its relatively simple form this system is particularly difficult to handle numerically; because being representative of the chemical reactions that occur among air pollutants, some eigenvalues of the system are 10^8 times larger than others. We develop below a numerical technique that appears to be able to handle this particular system. It is computationally stable; it does not produce negative concentrations, as most numerical schemes do when the constants $k_{\alpha ij}$ have greatly disparate values; and it provides easy control over the accuracy of the solutions.

To develop this method we first write (9-24) in the equivalent form

$$\frac{\partial \gamma'_\alpha}{\partial t} = \sum_{i=1}^I k_{\alpha i} \gamma'_\alpha \gamma'_i + \sum_{\substack{i,j=1 \\ (i \neq \alpha \neq j)}}^I k_{\alpha ij} \gamma'_i \gamma'_j \quad (9-79)$$

where I represents the total number of chemical species present. For notational convenience we have dropped the layer reference subscript n from $\gamma'_{(\alpha)n}$ and use the subscript to refer to the pollutant species. The first summation on the right side of (9-79) represents all reactions of the type



These reactions destroy species α by transforming it into different species ℓ and m . It follows then that $k_{\alpha\alpha i}$ is negative.

The last term on the right side of (9-79), which by design does not contain γ'_α , represents all reactions of the type



These reactions produce species α from other pollutant species and hence $k_{\alpha ij}$ is positive. Having noted these aspects of the summation terms in (9-79) let us now write this equation in the more abbreviated form

$$\frac{\partial \gamma'_\alpha}{\partial t} + P_\alpha \gamma'_\alpha = Q_\alpha \quad (9-82)$$

where

$$P_\alpha = - \sum_{i=1}^I k_{\alpha\alpha i} \gamma'_i \quad (9-83)$$

$$Q_\alpha = \sum_i \sum_{\substack{j=i \\ (i \neq \alpha \neq j)}}^I k_{\alpha ij} \gamma'_i \gamma'_j \quad (9-84)$$

Consider now a time interval $t_0 \leq t \leq t_1$ for which the values $\gamma'_i(t_0)$ are known for all $i = 1, 2, \dots, I$ pollutants. And let $P_{\alpha 0}$ and $Q_{\alpha 0}$ be the values obtained from (9-83) and (9-84), respectively, using the given values of γ'_i at t_0 . If P_α and Q_α were constant in (t_0, t_1) , Equation (9-82) would have the solution

$$\gamma'_\alpha(t) = Q_{\alpha 0}/P_{\alpha 0} + [\gamma'_\alpha(t_0) - Q_{\alpha 0}/P_{\alpha 0}] \exp [-P_{\alpha 0}(t - t_0)] \quad (9-85)$$

Obviously the degree to which this expression approximates the general solution of (9-82) is determined by the rate at which P_α and Q_α are changing in (t_0, t_1) .

Suppose that from the set of solutions (9-85) for one pollutant we determine a time t_1 , say, such that no value $\gamma'_i(t_1)$ differs from its initial value $\gamma'_i(t_0)$ by more than some given small fraction λ , say 1 percent (We will elaborate on this procedure later.) Using the $\gamma'_i(t_1)$ values obtained from (9-85) we can define $P_{\alpha 1}$ and $Q_{\alpha 1}$ from (9-83, 84) just as we defined $P_{\alpha 0}$ and $Q_{\alpha 0}$ before. Treating $P_{\alpha 1}$ and $Q_{\alpha 1}$ constants and using the γ'_i values at t_1 as initial conditions for (9-82) we obtain from (9-85)

$$\gamma'_\alpha(t_2) = Q_{\alpha 1}/P_{\alpha 1} + [\gamma'_\alpha(t_1) - Q_{\alpha 1}/P_{\alpha 1}] \exp [-P_{\alpha 1}(t_2 - t_1)] \quad (9-86)$$

where t_2 is chosen such that none of the $\gamma'_\alpha(t_2)$ exceeds $\gamma'_i(t_1)$ by a fraction larger than λ . Continuing this process forward in time we obtain an approximation of the general solution of (9-82) at discrete time intervals.

We have tested this method for use in the regional model and we have found it to perform well. However, in simulating air pollution chemistry where the reaction rates cover a wide range of values, the computer time required by this technique can become quite large unless the λ parameter is chosen in a particular way. To elaborate on the definition of this term and its selection, we note first that in (9-85) or (9-86),

$$Q_\alpha/P_\alpha \equiv \xi_\alpha \quad (9-87)$$

is the asymptotic or steady-state value of γ'_α , which may be larger than,

smaller than, or equal to the initial value

$$\gamma'_\alpha(t_0) \equiv \gamma'_{\alpha 0} \quad (9-88)$$

As we noted earlier, (9-85) is a good approximation of the solution of (9-82) only for times t such that

$$\Delta\gamma'_i \equiv |\gamma'_i(t) - \gamma'_i(t_0)| \leq \lambda\gamma'_i(t_0) \quad (9-89)$$

where λ is a small fraction. The "smallness" of λ is determined by what we define a "close" approximation of the solution of (9-82) to be.

The limit on t imposed by (9-89) can be found by substituting (9-85) into (9-89) for $\gamma'_i(t)$. We get

$$\Delta\gamma'_i = |\gamma'_i(t_0) - \xi_i[1 - \exp(-P_{i0}(t - t_0))]| \leq \lambda\gamma'_i(t_0) \quad (9-90)$$

or

$$1 - \exp(-P_{i0}(t - t_0)) \leq \frac{\lambda\gamma'_i(t_0)}{|\gamma'_i(t_0) - \xi_i|} \equiv F_i \quad (9-91)$$

If $F_i \geq 1$ then any value of $t \geq t_0$ satisfies (9-90); but when $F_i < 1$, we require

$$t_1 - t_0 \leq -\ln(1 - F_i)/P_{i0} \quad (9-92)$$

Thus, a sufficient condition for (9-85) to be a close approximation of the solution of (9-82) for all I species in the interval $t_0 \leq t \leq t_1$ is that t_1 satisfy

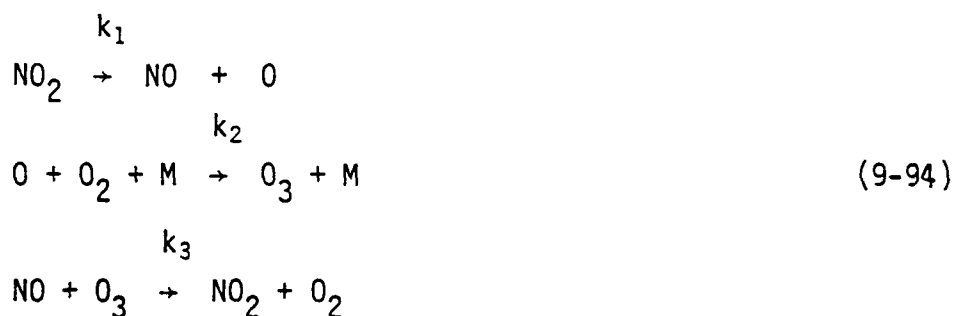
$$t_1 = t_0 + \min_I \{ -\ln(1 - F_i)/P_{i0} \} \quad (9-93)$$

We should add here that in evaluating F_i using (9-91), $\lambda\gamma'_i(t_0)$ is replaced

by $\lambda \xi_i$ if $\gamma_i^!(t_0) < \xi_i$.

In the studies we have performed to date with this method of solving (9-82) we have found that the time intervals $\Delta t_n = t_n - t_{n-1}$ given by (9-93) are unnecessarily small when the same value of λ is used for all species. Our available evidence is that λ can be made much larger for pollutant species like oxygen atom that are present in extremely small concentration than for the more plentiful species like NO, O₃, etc.

For example, we used the scheme above to simulate the 4-species mechanism



with rate constants

$$\begin{aligned}
 k_1 &= (21/36) \cdot 10^{-2} \text{ s}^{-1} \\
 k_2(\text{O}_2)(\text{M}) &= \frac{1}{15} \cdot 10^6 \text{ s}^{-1} \\
 k_3 &= (4/9) \cdot 10^{-1} \text{ ppb}^{-1} \text{ s}^{-1}
 \end{aligned}$$

Note that the effective rate constant $k_2(\text{O}_2)(\text{M})$ is about 10^8 times larger than k_1 .

We solved the rate equations for this system

$$\frac{d\text{NO}}{dt} = k_1(\text{NO}_2) - k_3(\text{O}_3)(\text{NO})$$

etc, using a value $\lambda = .1$ for each species. The initial conditions were chosen arbitrarily as NO = 100 ppb, NO₂ = 500 ppb, O₃ = 300 ppb, O = 10^{-5} ppb.

The results are shown in Figure 9-6a. We repeated this simulation using the same initial conditions but with $\lambda = 0.1$ for NO, NO₂, and O₃ and $\lambda = 0.4$ for oxygen atom, O. The results obtained in this calculation for $t = 100$ were within approximately 0.1 percent of the values obtained in the first run (shown in Figure 9-6a); yet the computer time required was only 2/3 that required in the first case. The time difference was due to the fact that 18 time steps were needed to reach $t = 100$ with $\lambda = 0.1$ for all 4 species whereas only 12 steps were required when the λ value assigned to oxygen atom was relaxed to 0.4. In the former case the first 7 of the 18 time steps were smaller than 0.001 s. During these 7 steps oxygen atom concentration increased gradually (by 10 percent increases) from its initial value of 10^{-5} ppb to $4.06 \cdot 10^{-5}$ ppb. During these 7 steps the concentrations of O₃, NO and NO₂ were virtually unchanged from their initial values. Once the O concentration had reached $4.06 \cdot 10^{-5}$ ppb it was within 10 percent of its equilibrium value for the NO, NO₂ and O₃ concentrations existing at that time and thus infinitely large subsequent steps were permissible "with respect to O." Consequently, control of the time step size then shifted to NO, NO₂ and O₃ at this point and, due to their slower reaction rate, the remaining time steps were larger than 1 s. The actual time intervals are indicated by the arrows in Figure 9-6a. Also shown is the sum (NO + NO₂) which, according to (9-93), should remain constant. The scheme maintains this property to within a few percentage points depending on the value of λ chosen.

The interesting feature of the simulation is that when the value of λ used for oxygen atom was increased from 0.1 to 0.4, with the other 3 λ values held the same, the model used only 1 sub-millisecond time step initially, rather than 7, yet in doing so it committed no error (the values of O at $t = 1.027$ are identical in the 2 cases).

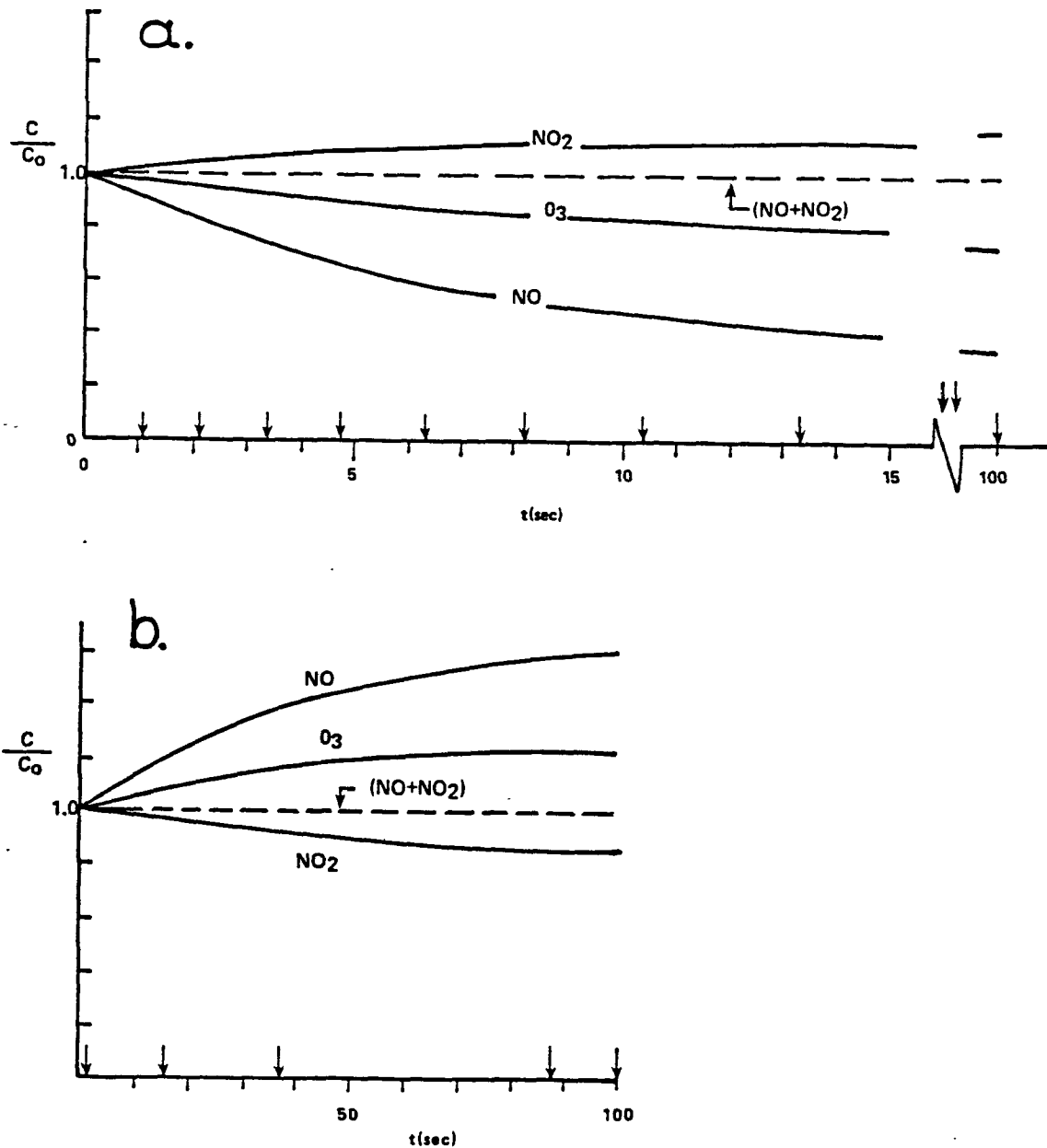


Figure 9-6. Temporal behavior of the reaction system (9-94) for initial species concentrations (a) $\text{NO} = 100 \text{ ppb}$, $\text{NO}_2 = 500 \text{ ppb}$, $\text{O}_3 = 30 \text{ ppb}$, $\text{O} = 10^{-5} \text{ ppb}$; and (b) one tenth the values used in (a). Arrows indicate the time steps used by the model to arrive at concentrations at $t = 100 \text{ sec}$.

As a further check of the effect of letting λ vary with the species, we performed a second pair of simulations as above but with initial conditions 1/10th those used in the first set -- $\text{NO} = 10 \text{ ppb}$, $\text{NO}_2 = 50 \text{ ppb}$, $\text{O}_3 = 30 \text{ ppb}$, $\text{O} = 10^{-6} \text{ ppb}$. The results of this experiment with $\lambda = 0.1$ for all 4 species are depicted in Figure 9-6b. The values obtained with $\lambda = 0.1$ for NO , NO_2 and O_3 and $\lambda = 0.4$ for oxygen atom were within 1 percent of the values derived in the first example at $t = 100 \text{ s}$. However, with this set of initial concentrations, the simulation that used $\lambda = 0.4$ for oxygen atom took only 5/11 the computer time needed with λ set to 0.1 for all species. This reduction in machine time is considerably larger than that realized in the first pair of experiments where different initial concentrations were used. The reason is that with smaller initial concentrations of NO , NO_2 and O_3 , the rates of change of these species are considerably reduced (compare Figures 9-6a and b) and thus a larger fraction of the iterations required to reach time $t = 100$ are dominated by the rapid variations in oxygen atoms. Incidentally, it is interesting to note in Figure 9-6 that due to the nonlinear character of the chemistry, the temporal behavior of all of the species is reversed when the initial concentrations are all divided by 10.

Having found that the performance of our solution technique is much more sensitive to the behavior of some species than others, we restructured the method to achieve maximum execution efficiency. This work was performed through applications of the scheme to the 23 species kinetic mechanism reported by Demerjian and Schere (1979). As a result of this work, the technique presented above for solving the γ' Equations (9-24) was modified and it now has the following form:

1. Compute preliminary estimates $P_{\alpha 0}^*$, $Q_{\alpha 0}^*$ of the decay and production coefficients (9-83, 84) using the known values of $\gamma'_{\alpha 0} = \gamma'_{\alpha}(t_0)$.
2. Compute the sum C_{ON} of the concentrations of NO, NO₂ and O₃ at time t_0 :

$$C_{ON} = [NO]_0 + [NO_2]_0 + [O_3]_0$$

Note that $[NO]_0 = \tau_{(NO)} \gamma'_{(NO)}_0$, etc. (cf. 9-3)

3. Determine the time t_1 using (9-93) but with the function $\min\{ \overset{I}{} \}$ replaced by $\min\{ \overset{K}{} \}$, where K denotes the subset of the I species whose concentrations $[i]_0$ at t_0 satisfy

$$[i]_0 \geq C_{ON}/100$$

4. Using the values $P_{\alpha 0}^*$, $Q_{\alpha 0}^*$ from Step 1 and the $\gamma'_{\alpha 0}$, compute preliminary estimates $\gamma'_{\alpha 1}^* = \gamma'_{\alpha}(t_1)$ using (9-85)
5. Using the $\gamma'_{\alpha 1}^*$ values from Step 4 and (9-83, 84), compute $P_{\alpha 1}^*$, $Q_{\alpha 1}^*$
6. Compute corrected, final estimates of $P_{\alpha 0}$, $Q_{\alpha 0}$ by

$$P_{\alpha 0} = P_{\alpha 1}^*$$

$$Q_{\alpha 0} = (Q_{\alpha 0}^* + Q_{\alpha 1}^*)/2$$

(These expressions are the result of empirical findings rather than theoretical considerations.)

7. Compute the final estimates of $\gamma'_{\alpha 1}$ using the $P_{\alpha 0}$ and $Q_{\alpha 0}$ from Step 6 and the $\gamma'_{\alpha 0}$
8. Return to Step 1 and repeat the steps above to obtain at $\gamma'_{\alpha 2}$, etc.

In Part III of this report we will present detailed comparisons of the performance of this scheme with that of the well-known Gear routine. We will show that the solutions of (9-24) given by the technique above are within about 1 percent of those given by the Gear method for each of the 23 species in the Demerjian-Schere mechanism over 24 h simulations. The method developed above achieves this level of accuracy with about $\frac{1}{2}$ the computer time required by the Gear method. If the control parameter λ in the scheme is increased until the maximum differences between the generated solutions and those given by Gear are of the order of 25 percent, the execution time is about $\frac{1}{5}$ the Gear routine requirement. This difference in machine times is due chiefly to the fact that the method above is in essence a 2-step scheme whereas Gear is multi-stepped. In our regional model where the $\hat{\gamma}$ and γ' equations are solved alternately over short time intervals, the need for multiple values of γ' by the Gear method to produce solutions within each subinterval results in a large computational "overhead".

SECTION 10

SUMMARY OF MODEL EQUATIONS

For convenience we summarize below the basic forms of the governing equations in each of the model's 4 layers.

Layer 1:

$$\begin{aligned}
 & \frac{\partial \langle C \rangle_1}{\partial t} + \langle C \rangle_1 \frac{\partial \ln V_1}{\partial t} + \mu_\lambda \langle u \rangle_1 \frac{\partial \langle C \rangle_1}{\partial \lambda} + \mu_\phi \langle v \rangle_1 \frac{\partial \langle C \rangle_1}{\partial \phi} \\
 & + \mu_\lambda \langle u'c' \rangle_1 \frac{\partial \ln V_1}{\partial \lambda} + \mu_\phi \langle v'c' \rangle_1 \frac{\partial \ln V_1}{\partial \phi} \\
 & + \mu_\lambda \frac{\partial \langle u'c' \rangle_1}{\partial \lambda} + \mu_\phi \frac{\partial \langle v'c' \rangle_1}{\partial \phi} \\
 & + \frac{A}{V_1} [+ F_{0,1} - F_{1,1}] = \langle R \rangle_1 + \langle S \rangle_1
 \end{aligned}$$

where

$$\mu_\lambda = \frac{1}{a \cos \phi}$$

$$\mu_\phi = \frac{1}{a}$$

a = earth radius at MSL (in meters)

λ = longitude

ϕ = latitude

$$A = a^2 (\Delta\phi\Delta\lambda) \cos\phi$$

$\Delta\phi, \Delta\lambda$ = latitude, longitude grid cell dimensions
 = constants ($\Delta\phi = \frac{1}{6}^\circ$ $\Delta\lambda = \frac{1}{4}^\circ$)

$$V_1(\lambda, \phi, t) = a^2 \cos \phi \int_{\lambda - \Delta\lambda/2}^{\lambda + \Delta\lambda/2} \int_{\phi - \Delta\phi/2}^{\phi + \Delta\phi/2} \text{MAX} \{0, [z_1(\lambda', \phi', t) - \text{MAX} [\hat{z}_T(\lambda', \phi'), z_0(\lambda', \phi', t)]]\} d\phi' d\lambda'$$

$$\left. \begin{array}{l} \langle u'c' \rangle_1 \\ \langle v'c' \rangle_1 \end{array} \right\} \text{ subgrid scale fluxes of } c \text{ (see Section 7)}$$

$\langle R \rangle_1$ = all chemical, rainout and washout processes.

$\langle S \rangle_1$ = all emissions of c in Layer 1 (includes stacks and surface sources above nighttime radiation inversion).

$\langle u \rangle_1, \langle v \rangle_1$ = layer averaged horizontal wind components

(u = east-west component), (v = north-south component).

$$F_{1,1} = (1 - \sigma_{T1}) [(\langle c \rangle_1 - \langle c \rangle_2) \omega_{1m} + \langle c \rangle_1 \omega_1]$$

β = deposition velocity of species c

$\sigma_{T1}(\lambda, \phi, t)$ = fraction of surface H_1 penetrated by terrain

$$\omega_1 = \frac{\psi_c \bar{w}_c}{1 - \sigma_{T1}} + \frac{z_1}{2} \left[1 + \text{erf} \left(\frac{w_m - \bar{w}_{D1}}{\sqrt{2} \sigma_{w_1}} \right) \right]$$

$$\omega_{1m} = - \frac{\sigma_{w_1}}{\sqrt{2\pi}} \exp \left(- \frac{\bar{w}_{R1}^2}{2 \sigma_{w_1}^2} \right) + \frac{\bar{w}_{R1}}{2} \left[1 - \text{erf} \left(\frac{\bar{w}_{R1}}{\sqrt{2} \sigma_{w_1}} \right) \right]$$

$$\bar{w}_{R1} = \begin{cases} \bar{w}_{D1} - \dot{z}_1, & \text{neutral and unstable conditions;} \\ -\bar{\eta}_1, & (= \text{given inversion layer depth growth rate}), \text{ stable} \end{cases}$$

\bar{w}_{D1} = mean vertical velocity on H_1 (terrain induced component excluded)

σ_{w1} = rms vertical turbulence on H_1 (= 0 in stable cases)

w_m = threshold of cumulus "root" updraft velocity on H_1

$\dot{z}_1 = \partial z_1 / \partial t$

$\psi, \sigma_c, \bar{w}_c$ (see Layer 2 equations)

$$\text{erf}(x) = \frac{2}{\sqrt{\pi}} \int_0^x e^{-t^2} dt$$

$$F_{o,1} = (\sigma_{T0} - \sigma_{T1}) \beta < c >_1 + (1 - \sigma_{T0}) F_o$$

σ_{T0} = fraction of surface H_o in given grid cell penetrated by terrain

$F_o =$

Ozone:

$$F_o(O_3) = <O_3>_1 w_{-\lambda_-} - O_3 w_{+\lambda_+} (1 - \xi)(1 - \alpha)$$

$$- (1 - \alpha) \cdot \begin{cases} 0, & \text{if } \tilde{S}_{NO} > v \xi O_3 \\ \frac{O_3 v^2 \xi - \tilde{S}_{NO} v}{\beta_{O_3} + v}, & \text{otherwise} \end{cases}$$

Nitric Oxide:

$$F_o(NO) = <NO>_1 w_{-\lambda_-} - NO w_{+\lambda_+} (1 - \xi)(1 - \alpha)$$

$$- (1 - \alpha) \cdot \begin{cases} \frac{\tilde{S}_{NO} + v \xi (NO - O_3)}{1 + \beta_{NO}/v}, & \text{if } \tilde{S}_{NO} > v \xi O_3 \\ \frac{v \xi NO}{1 + \beta_{NO}/v}, & \text{otherwise} \end{cases}$$

Nitrogen Dioxide:

$$F_0(\text{NO}_2) = \langle \text{NO}_2 \rangle_1 w_- \lambda_- - \text{NO}_2 w_+ \lambda_+ (1 - \xi)(1 - \alpha) - (1 - \alpha) \cdot \begin{cases} \frac{\nu \zeta (\text{NO}_2 + \text{O}_3) + \tilde{S}_{\text{NO}_2}}{1 + \beta_{\text{NO}_2}/\nu} & , \text{ if } \tilde{S}_{\text{NO}} > \nu \zeta \text{O}_3 \\ \frac{\nu \zeta \text{NO}_2 + \tilde{S}_{\text{NO}} + \tilde{S}_{\text{NO}_2}}{1 + \beta_{\text{NO}_2}/\nu} & , \text{ otherwise} \end{cases}$$

all other species, χ .

$$F_0(\chi) = \langle \chi \rangle_1 w_- \lambda_- - \chi w_+ \lambda_+ (1 - \xi)(1 - \alpha) - (1 - \alpha)(\nu \zeta \chi + \tilde{S}_\chi)(1 + \beta_\chi/\nu)^{-1}$$

$$\alpha = \frac{\psi \sigma_c}{w_+ \lambda_+ (1 - \sigma_{T_0})} \left[- \frac{\bar{w}_2 - \bar{w}_c}{1 - \sigma_c} - f\theta/\Delta\theta \right]$$

See Layer 0 equations for specification of O_3 , NO , NO_2 , χ , w_+ , λ_+ , etc.

Layer 2:

$$\begin{aligned} \frac{\partial}{\partial t} \langle c \rangle_2 + \langle c \rangle_2 \frac{\partial \ln V_2}{\partial t} + \mu_\lambda \langle u \rangle_2 \frac{\partial \langle c \rangle_2}{\partial \lambda} + \mu_\phi \langle \dot{v} \rangle_2 \frac{\partial \langle c \rangle_2}{\partial \phi} \\ + \mu_\lambda \langle u' c' \rangle_2 \frac{\partial \ln V_2}{\partial \lambda} + \mu_\phi \langle v' c' \rangle_2 \frac{\partial \ln V_2}{\partial \phi} + \mu_\lambda \frac{\partial}{\partial \lambda} \langle u' c' \rangle_2 \\ + \mu_\phi \frac{\partial}{\partial \phi} \langle v' c' \rangle_2 + \frac{A}{V_2} [+ F_{1,2} - F_{2,2}] \\ = \langle R \rangle_2 + \langle S \rangle_2 \end{aligned}$$

$$V_2(\lambda, \phi, t) = a^2 \cos \phi \int_{\lambda - \Delta\lambda/2}^{\lambda + \Delta\lambda/2} \int_{\phi - \Delta\phi/2}^{\phi + \Delta\phi/2} \{ z_2(\lambda', \phi', t) - \text{MAX} [\hat{z}_T(\lambda', \phi') z_1(\lambda', \phi', t)] \} d\phi' d\lambda'$$

$$\left. \begin{array}{l} \langle u'c' \rangle_2 \\ \langle v'c' \rangle_2 \end{array} \right\} \text{ subgrid scale fluxes of } c \text{ (see Section 7)}$$

$\langle R \rangle_2$ = all chemical, rainout and washout processes in Layer 2

$\langle S \rangle_2$ = source emissions in Layer 2 (if any)

$\langle u \rangle_2, \langle v \rangle_2$ = Layer 2 averaged winds.

$$F_{2,2} = \frac{\sigma_c(\bar{w}_2 - \bar{w}_c)}{1 - \sigma_c} (\bar{c}_c - \langle c \rangle_2) + \langle c \rangle_2 \frac{\partial \bar{z}_2}{\partial t} - \frac{f_\theta}{\Delta\theta} [- (1 - \sigma_c) \langle c \rangle_3 - \sigma_c \bar{c}_c + \langle c \rangle_2]$$

$$F_{1,2} = \sigma_{T1} \beta \langle c \rangle_2 + (1 - \sigma_{T1}) [\langle c \rangle_1 w_1 + (\langle c \rangle_1 - \langle c \rangle_2) w_{1m} + (\langle c \rangle_2 - \langle c \rangle_1) \bar{w}_{D1}]$$

w_1, w_{1m} , see Layer 1; \bar{w}_{D1} , see (4-44c)

σ_c = fractional area coverage of cumulus clouds

\bar{w}_c = mean upward velocity in cumulus clouds

$\frac{f_\theta}{\Delta\theta}$ = turbulent entrainment rate of inversion air into mixed layer

\bar{w}_2 = mean vertical velocity (mean of both terrain induced component w_{T2} and divergent component w_{D2})

$\frac{\partial \bar{z}_2}{\partial t} = \dot{z}_2$ = local time rate of change of mixed layer top

$$\bar{c}_c = (1 - \psi) \langle c \rangle_2$$

ψ = fraction of cloud air from surface layer

$$0 \leq \psi \leq 1 \text{ and } \psi \leq w_+ \lambda_+ (1 - \sigma_{T0}) / (V_c \sigma_c)$$

$$V_c = - \frac{\bar{w}_2 - \bar{w}_c}{1 - \sigma_c} - f_\theta / \Delta\theta$$

$c, c', \xi, w_+, \lambda_+$ = See Layer 0 equations

Layer 3:

$$\begin{aligned} \frac{\partial \langle c \rangle_3}{\partial t} + \langle c \rangle_3 \frac{\partial \ln V_3}{\partial t} + \mu_\lambda \langle u \rangle_3 \frac{\partial \langle c \rangle_3}{\partial \lambda} + \mu_\phi \langle v \rangle_3 \frac{\partial \langle c \rangle_3}{\partial \phi} \\ + \mu_\lambda \langle u'c' \rangle_3 \frac{\partial \ln V_3}{\partial \lambda} + \mu_\phi \langle v'c' \rangle_3 \frac{\partial \ln V_3}{\partial \phi} \\ + \mu_\lambda \frac{\partial \langle u'c' \rangle_3}{\partial \lambda} + \mu_\phi \frac{\partial \langle v'c' \rangle_3}{\partial \phi} + \frac{A}{V_3} [F_{2,3} - F_{3,3}] = \langle R \rangle_3 \end{aligned}$$

$$V_3(\lambda, \phi, t) = a^2 \cos \phi \int_{\lambda - \Delta\lambda/2}^{\lambda + \Delta\lambda/2} \int_{\phi - \Delta\phi/2}^{\phi + \Delta\phi/2} [z_3(\lambda', \phi') - z_2(\lambda', \phi', t)] d\phi' d\lambda'$$

$z_2(\lambda, \phi, t)$ = mixed layer top

$z_3(\lambda, \phi, t)$ = model top

$\left. \begin{array}{l} \langle u'c' \rangle_3 \\ \langle v'c' \rangle_3 \end{array} \right\}$ subgrid scale flux of c (see Section 8)

$\langle R \rangle_3$ = all chemical (wet and dry) rainout and washout processes

$\langle u \rangle_3, \langle v \rangle_3$ = layer averaged winds

$$F_{2,3} = \sigma_c \left[\frac{\bar{w}_2 - \bar{w}_c}{1 - \sigma_c} + f\theta/\Delta\theta \right] (\bar{c}_c - \langle c \rangle_3) + \langle c \rangle_3 \frac{\partial \bar{z}_2}{\partial t}$$

$$F_{3,3} = \begin{cases} \langle c \rangle_3 \frac{\partial z_3}{\partial t} & , \text{ if } \overline{dH_3}/dt \leq 0 ; \\ (c_\infty - \langle c \rangle_3) \overline{dH_3}/dt + \langle c \rangle_3 \frac{\partial z_3}{\partial t} & , \text{ otherwise} \end{cases}$$

c_∞ = concentration of species c above z_3

$\overline{dH_3}/dt$ = given volume flux through model top surface

$$\bar{c}_c = (1 - \psi) \langle c \rangle_2 + \psi [\xi c' + (1 - \xi) c]$$

where c' and c are defined with the Layer 0 variables.

Layer 0:

$$\langle O_3 \rangle_0 = (1 - \zeta) O_3 + \zeta O_3'$$

$$O_3 = \frac{w_{-}\lambda_{-}\langle O_3 \rangle_1}{w_{+}\lambda_{+} + (1 - \zeta)\beta_{O_3}}$$

$$O_3' = \begin{cases} 0, & \text{if } \tilde{S}_{NO} > v\zeta O_3 \\ \frac{O_3 v - \tilde{S}_{NO}/\zeta}{\beta_{O_3} + v}, & \text{otherwise} \end{cases}$$

$$\langle NO \rangle_0 = (1 - \zeta) NO + \zeta NO'$$

$$NO = \frac{w_{-}\lambda_{-}\langle NO \rangle_1}{w_{+}\lambda_{+} + (1 - \zeta)\beta_{NO}}$$

$$NO' = \begin{cases} \frac{\tilde{S}_{NO}/\zeta + v(NO - O_3)}{\beta_{NO} + v}, & \text{if } \tilde{S}_{NO} > v\zeta O_3 \\ \frac{vNO}{\beta_{NO} + v}, & \text{otherwise} \end{cases}$$

$$\langle NO_2 \rangle_0 = (1 - \zeta) NO_2 + \zeta NO_2'$$

$$NO_2 = \frac{w_{-}\lambda_{-}\langle NO_2 \rangle_1}{w_{+}\lambda_{+} + (1 - \zeta)\beta_{NO_2}}$$

$$NO_2' = \begin{cases} \frac{NO_2 v + O_3 v + \tilde{S}_{NO_2}/\zeta}{\beta_{NO_2} + v}, & \text{if } \tilde{S}_{NO} > v\zeta O_3 \\ \frac{NO_2 v + (\tilde{S}_{NO} + \tilde{S}_{NO_2})/\zeta}{\beta_{NO_2} + v}, & \text{otherwise} \end{cases}$$

Species χ other than O_3 , NO , and NO_2 :

$$\langle \chi \rangle_0 = (1 - \zeta)\chi + \zeta\chi'$$

$$\chi = \frac{w_- \lambda_- \langle \chi \rangle_1}{w_+ \lambda_+ + (1 - \zeta) \beta_\chi}$$

$$\chi' = \frac{\chi v + \tilde{S}_\chi / \zeta}{\beta_\chi + v}$$

Parameters:

$$\lambda_+ = \frac{1}{2} \left[1 - \operatorname{erf} \left(\frac{z_0}{\sqrt{2} \sigma_{w_0}} \right) \right]$$

$$\lambda_- = 1 - \lambda_+$$

$$w_- = -z_0 - \frac{\sigma_{w_0}}{\sqrt{2\pi}} \exp \left(-\frac{z_0^2}{2\sigma_{w_0}^2} \right)$$

$$+ \frac{z_0}{2} \left[1 - \operatorname{erf} \left(\frac{z_0}{\sqrt{2} \sigma_{w_0}} \right) \right]$$

$$w_+ = w_- - \dot{z}_0$$

$$v = u^* \text{ (plume entrainment velocity)}$$

$$\xi = \frac{v \zeta}{w_+ \lambda_+}$$

$$\zeta = \text{plume volume fraction}$$

$$\sigma_{w_0} = \text{rms vertical turbulent velocity on } H_0$$

REFERENCES

- Artoz, M. A. and J. C. Andre, (1980): "Similarity Studies of Entrainment in Convective Mixed Layers", Bound. Layer Meteor., Vol. 19, pp 51-66.
- Batchelor, G. K., (1950): "Application of the Similarity Theory of Turbulence to Atmospheric Diffusion", Quart. J. Roy. Meteor. Soc., Vol. 76, pp 133-146.
- Binkowski, F. S., (1979): "A Simple Semi-Empirical Theory for Turbulence in the Atmospheric Surface Layer, Atmos. Environ., Vol. 13, pp 247-253.
- Carras, J. N. and D. J. Williams, (1981): "The Long-range Dispersion of a Plume from an Isolated Point Source", Atmos. Env., Vol. 15, pp 2205-2217.
- Deardorff, J. W., (1974): "Three Dimensional Study of the Height and Mean Structure of a Heated Planetary Boundary Layer", Boundary Layer Meteor., Vol. 7, pp 81-106.
- Deardorff, J.W., and R.L. Peskin, (1970), "Lagrangian Statistics from Numerically Integrated Turbulent Shear Flow," Physics of Fluids, Vol. 13, pp. 584-595.
- Demerjian, K. L. and K. L. Schere, (1979): "Applications of a Photochemical Box Model for Ozone Air Quality in Houston, Texas. Proceedings, Ozone/Oxidants: Interactions with the Total Environment II, Houston, TX, 14-17 Oct. 1979, APCA, Pittsburgh, Pa., pp. 329-352.
- Draxler, R. R., (1976): "Determination of Atmospheric Diffusion Parameters", Atmos. Env. 10:99-105.
- Evans, R.B., (1979) "The Contribution of Ozone Aloft to Surface Ozone Maxima", Doctoral Dissertation, University of North Carolina, School of Public Health, Chapel Hill, NC. 301 pages + viii.
- Godowitch, J. M., J. K. S. Ching, J. F. Clarke, (1979): "Dissipation of the Nocturnal Inversion Layer at an Urban and Rural Site in St. Louis", Preprint Volume, Proceedings of the Fourth Symposium on Turbulence, Diffusion and Air Pollution, Reno, Nevada.
- Gradshteyn, I. S. and I. M. Ryzhik, (1965): Table of Integrals Series and Products, Academic Press, New York.
- Haltiner, G. J., (1971): Numerical Weather Prediction, John Wiley and Sons, New York, New York, p. 54.

- Hamming, R. W., (1962): Numerical Methods for Scientists and Engineers. McGraw Hill Book Co., New York.
- Hay, J. S. and F. Pasquill, (1959): "Diffusion from a Continuous Source in Relation to the Spectrum and Scale of Turbulence", Advances in Geophysics, Vol. 6, Academic Press.
- Henderson, R.G., R.P. Pitter and J. Wisniewski (1980) "Research Guidelines for Regional Modeling of Fine Particulates, Acid Deposition and Visibility", Report of a Workshop held at Port Deposit, MD October 29-November 1, 1979.
- Hunt, J. C. R., W. H. Snyder and R. E. Lawson, (1979): "Flow Structure and Turbulent Diffusion Around a Three-Dimensional Hill", EPA-600/4-78-041, Environmental Protection Agency, Research Triangle Park, North Carolina.
- Kaimal, J. C., J. C. Wyngaard, D. A. Haugen, O. R. Cote, Y. Izumi, S. J. Caughey and C. J. Readings, (1976): "Turbulence Structure in the Convective Boundary Layer", J. Atmos. Sci., Vol. 33, pp 2152-2169.
- Kaplan, W., (1962): "Ordinary Differential Equations", Addison-Wesley Publishing Co., Reading, MA. 534 pages.
- Lamb, R. G., (1976): "Research in Mesoscale Air Pollution Simulation Modeling, Vol. III: Modeling of Microscale Phenomena. Final Report by Systems Application, Inc. to EPA, Contract 68-02-1237.
- Lamb, R. G., W. R. Shu, D. R. Durran, J. H. Seinfeld and L. E. Reid, (1977): "Continued Research in Mesoscale Air Pollution Simulation Modeling, Vol. VI: Further Studies in the Modeling of Mesoscale Phenomena", Draft Final Report to EPA Contract No. 68-02-2216.
- Lamb, R. G., (1971): "Numerical Modeling of Urban Air Pollution", Ph.D dissertation, Department of Meteorology, UCLA, Los Angeles, CA. 289 pages + xvii.
- Lamb, R. G., (1975): "The Calculation of Long Term Atmospheric Pollutant Concentration Statistics Using the Concept of a Macro Turbulence. Proceedings of the IBM Seminar held in Venice. (Available from the author).
- Lamb, R. G. and D. R. Durran, (1978): "Eddy Diffusivity Derived from a Numerical Model of the Convective Planetary Boundary Layer. Il Nuovo Cimento 1C:1-17.
- Lass, H., (1950): Vector and Tensor Analysis, McGraw Hill Book Co., New York, New York, p 54.
- Leith, C. E., (1965): "Numerical Simulation of the Earth's Atmosphere," Methods in Computational Physics, 4: 1-28.
- Lilly, D. K., (1968): "Models of Cloud Topped Mixed Layer Under a Strong Inversion", Quart. J. of Royal Met. Soc., Vol. 94, pp 292-309.

- Lumley, J. L. and H. A. Panofsky, (1964): The Structure of Atmospheric Turbulence, John Wiley and Sons, New York.
- McMahon, R. A. and P. J. Denison, (1979): "Empirical Atmospheric Deposition Parameters - A Survey", Atmos. Environ., Vol. 13, pp 571-585.
- Mahrer, Y. and R. A. Pielke, (1978): "A Test of an Upstream Spline Interpolation Technique for the Advection Terms in a Numerical Mesoscale Model". Mon. Wea. Rev., Vol. 106, pp 818-830.
- Siple, G. W., et al. (1977): "Air Quality Data from the Northeast Oxidant Transport Study", EPA-600/4-77-020, Environmental Protection Agency, Research Triangle Park, North Carolina.
- Taylor, G. I., (1921): "Diffusion by Continuous Movement". Proc. London Math. Soc., Ser. 2, 20:196-202.
- Telford, J. W., A. Vaziri and P. B. Wagner, (1976): "Aircraft Observations in the Planetary Boundary Under Stable Conditions", Boundary Layer Meteorology, Vol. 10, pp 353-377.
- Tennekes, H., (1973): "A Model of the Dynamics of the Inversion Above a Convective Boundary Layer", J. Atmos. Sci., Vol. 30, pp 558-567.
- Thorpe, A. J. and T. H. Guymer, (1977): "The Nocturnal Jet", Quart. J. Royal Met. Soc., Vol. 13, pp 633-653.
- Van der Hoven, I., (1957): "Power Spectrum of Horizontal Wind Speed in the Frequency Range from 0.0007 to 900 Cycles Per Hour", J. of Meteor., Vol. 14, pp 160-164.
- Venkatram, A., (1979): "The Expected Deviation of Observed Concentration from Predicted Ensemble Means". Atmos. Env. 13:1547-1550.
- Wesley, M. L. and B. B. Hicks, (1977): "Some Factors that Affect the Deposition Rates of Sulfur Dioxide and Similar Gases on Vegetation", J. Air Pollutant Control Assoc., Vol. 27, pp 1110-1116.
- Willis, G. E. and J. W. Deardorff, (1974): "A Laboratory Model of the Unstable Planetary Boundary Layer", J. Applied Meteor., Vol. 31, pp 1297-1307.
- Wyngaard, J. C. and O. R. Cote, (1971): "Budgets of Turbulent Kinetic Energy and Temperature Variance in the Atmospheric Surface Layer", J. Atmos. Sci., Vol. 28, pp 190-201.
- Zalesak, S., (1979): "Fully Multidimensional Flux-Corrected Transport Algorithms for Fluids", J. Comp. Physics, 31:335-362.

Appendix A. Transformation of the Governing Equations to Curvilinear Coordinates.

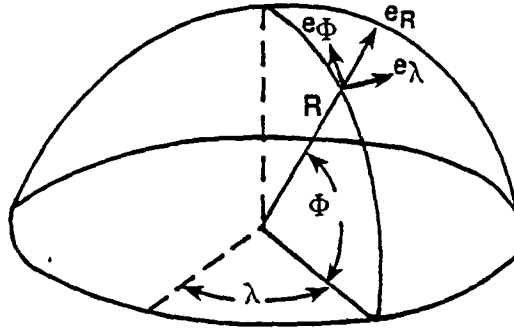


Figure A-1. The curvilinear coordinate system used in the model.

To transform the divergence operator ($\nabla \cdot$) into the coordinates of the frame depicted in Figure A-1 in which the basis vectors \underline{e}_λ and \underline{e}_ϕ are everywhere parallel to latitude and longitude circles, respectively, and in which \underline{e}_R is vertically upward, we use the vector calculus relationship [see Lass (1950)]

$$\nabla \cdot \underline{F} = \frac{1}{h_\lambda h_\phi h_R} \left[\frac{\partial}{\partial \lambda} (h_\phi h_R F_\lambda) + \frac{\partial}{\partial \phi} (h_\lambda h_R F_\phi) + \frac{\partial}{\partial R} (h_\lambda h_\phi F_R) \right] \quad (A-1)$$

where \underline{F} is an arbitrary vector with components (F_λ, F_ϕ, F_R) and h_λ , h_ϕ and h_R are the metric factors that transform the coordinate increments $\Delta\lambda$, $\Delta\phi$, and ΔR into arc lengths ds :

$$\left. \begin{aligned} ds_\lambda &= h_\lambda d\lambda \\ ds_\phi &= h_\phi d\phi \\ ds_R &= h_R dR \end{aligned} \right\} \quad (A-2)$$

In our case it is easy to see from Figure A-1 that

$$\left. \begin{aligned} h_\lambda &= R \cos \phi \\ h_\phi &= R \\ h_R &= 1 \end{aligned} \right\} \quad (A-3)$$

Thus, we find from Equations (A-1) and (A-3) that in the curvilinear frame, divergence of a vector field is given by

$$\text{div } \underline{F} = \frac{1}{R \cos \phi} \frac{\partial F_\lambda}{\partial \lambda} + \frac{1}{R} \frac{\partial F_\phi}{\partial \phi} + \frac{\partial F_z}{\partial z} - \frac{F_\phi}{R} \tan \phi + \frac{2F_z}{R} \quad (\text{A-4})$$

where

$$R = a + z$$

$$\underline{F} = F_\lambda \underline{e}_\lambda + F_\phi \underline{e}_\phi + F_z \underline{e}_R$$

The mass continuity equation

$$\frac{\partial c}{\partial t} + \text{div}(\underline{vc}) = Q \quad (\text{A-5})$$

can now be expressed in curvilinear coordinates using Equation (A-4), where the velocity vector \underline{v} is

$$\underline{v} = u \underline{e}_\lambda + v \underline{e}_\phi + w \underline{e}_R \quad (\text{A-6})$$

In the curvilinear frame we define cell volume averages by

$$\langle F \rangle_j \equiv \frac{1}{V_j} \int_{\lambda-\Delta\lambda}^{\lambda+\Delta\lambda} \int_{\phi-\Delta\phi}^{\phi+\Delta\phi} \int_{z_{j-1}(\lambda,\phi,t)}^{z_j(\lambda,\phi,t)} F(\lambda', \phi', R, t) (R d\phi') (R \cos \phi' d\lambda') dR \quad (\text{A-7a})$$

where the cell volume V_j is defined by

$$V_j = \int_{\lambda-\Delta\lambda}^{\lambda+\Delta\lambda} \int_{\phi-\Delta\phi}^{\phi+\Delta\phi} \int_{z_{j-1}(\lambda,\phi,t)}^{z_j(\lambda,\phi,t)} R^2 \cos \phi' dR d\phi' d\lambda' \quad (\text{A-7b})$$

Since the angular dimensions $(\Delta\lambda, \Delta\phi)$ of the cells we plan to use are small with respect to unity, and since we are concerned with elevations z that are a small fraction of the earth radius a , we can simplify (A-7) to

$$\langle F \rangle_j(\lambda, \phi, t) = \frac{a^2 \cos \phi}{V_j} \int_{\lambda - \Delta \lambda}^{\lambda + \Delta \lambda} \int_{\phi - \Delta \phi}^{\phi + \Delta \phi} \int_{z_{j-1}}^{z_j} F(\lambda', \phi', t) dR d\phi' d\lambda' \quad (A-8)$$

$$V_j(\lambda, \phi, t) = a^2 \cos \phi \int_{\lambda - \Delta \lambda}^{\lambda + \Delta \lambda} \int_{\phi - \Delta \phi}^{\phi + \Delta \phi} \int_{z_{j-1}}^{z_j} dR d\phi' d\lambda' \quad (A-9)$$

Consider now the forms that cell averaged spatial derivatives acquire. For notational convenience we will drop the layer designation subscripts. Let's look first at $\frac{\partial \langle F \rangle}{\partial \lambda}$. From Equation (A-8) we find using Leibniz' theorem

$$\frac{\partial \langle F \rangle}{\partial \lambda} = a^2 \cos \phi \left[\frac{1}{V} (I(\lambda + \Delta \lambda) - I(\lambda - \Delta \lambda)) \right] - \frac{\langle F \rangle}{V} \frac{\partial V}{\partial \lambda}$$

where

$$I(\xi) = \int_{\phi - \Delta \phi}^{\phi + \Delta \phi} \int_{z_1(\xi, \phi')}^{z_2(\xi, \phi')} F(\xi, \phi', R) dR d\phi' \quad (A-10)$$

In a similar fashion we obtain

$$\frac{\partial I}{\partial \xi} = \int_{\phi - \Delta \phi}^{\phi + \Delta \phi} \left[F(\xi, \phi', z_2) \frac{\partial z_2}{\partial \xi} - F(\xi, \phi', z_1) \frac{\partial z_1}{\partial \xi} + \int_{z_1(\xi, \phi')}^{z_2(\xi, \phi')} \frac{\partial F}{\partial \xi} dR \right] d\phi'$$

Integrate this with respect to ξ :

$$\begin{aligned} \int_{\xi - \Delta \xi}^{\xi + \Delta \xi} \frac{\partial I}{\partial \xi} d\xi &= I(\xi + \Delta \xi) - I(\xi - \Delta \xi) = \int_{\xi - \Delta \xi}^{\xi + \Delta \xi} \int_{\phi - \Delta \phi}^{\phi + \Delta \phi} \left[F(\xi', \phi', z_2) \frac{\partial z_2}{\partial \xi'} - F(\xi', \phi', z_1) \frac{\partial z_1}{\partial \xi'} \right] d\phi' \\ &\quad + \int_{\xi - \Delta \xi}^{\xi + \Delta \xi} \int_{\phi - \Delta \phi}^{\phi + \Delta \phi} \int_{z_1(\xi', \phi')}^{z_2(\xi', \phi')} \frac{\partial F}{\partial \xi'} dR d\phi' d\xi' \end{aligned}$$

Letting $\xi = \lambda$ we get

$$I(\lambda + \Delta\lambda) - I(\lambda - \Delta\lambda) = \frac{A}{a^2 \cos \phi} \left[\overline{F(\lambda, \phi, z_2) \frac{\partial z_2}{\partial \lambda}} - \overline{F(\lambda, \phi, z_1) \frac{\partial z_1}{\partial \lambda}} \right] + \frac{V}{a^2 \cos \phi} \left\langle \frac{\partial F}{\partial \lambda} \right\rangle \quad (A-11)$$

where

$$\overline{F(\lambda, \phi, z_n) \frac{\partial z_n}{\partial \lambda}} = \frac{1}{A} \int_{\lambda-\Delta\lambda}^{\lambda+\Delta\lambda} \int_{\phi-\Delta\phi}^{\phi+\Delta\phi} F(\lambda', \phi', z_n) \frac{\partial z_n}{\partial \lambda'} (R_n d\phi') (R_n \cos \phi') d\lambda' \quad (A-12)$$

$$A = \int_{\lambda-\Delta\lambda}^{\lambda+\Delta\lambda} \int_{\phi-\Delta\phi}^{\phi+\Delta\phi} R_n^2 \cos \phi d\lambda' d\phi' \approx a^2 \cos \phi (4\Delta\phi \Delta\lambda) \quad (A-13)$$

and

$$R_n = a + z_n$$

From (A-10) we have

$$I(\lambda + \Delta\lambda) - I(\lambda - \Delta\lambda) = \frac{V}{a^2 \cos \phi} \frac{\partial \langle F \rangle}{\partial \lambda} + \frac{\langle F \rangle}{a^2 \cos \phi} \frac{\partial V}{\partial \lambda}$$

Substituting this into (A-11) we obtain

$$\frac{\partial \langle F \rangle}{\partial \lambda} + \frac{\langle F \rangle}{V} \frac{\partial V}{\partial \lambda} = \frac{A}{V} \left[\overline{F \frac{\partial z_2}{\partial \lambda}} - \overline{F \frac{\partial z_1}{\partial \lambda}} \right] + \left\langle \frac{\partial F}{\partial \lambda} \right\rangle$$

In the governing equation, we have the term

$$\frac{1}{R \cos \phi} \frac{\partial F}{\partial \lambda}$$

From the analyses above we conclude that

$$\left\langle \frac{1}{R \cos \phi} \frac{\partial F}{\partial \lambda} \right\rangle_j = \frac{1}{a \cos \phi} \left[\frac{\partial \langle F \rangle}{\partial \lambda} \right]_j + \frac{\langle F \rangle}{V_j} \frac{\partial V}{\partial \lambda} \Big|_j + \frac{A}{V_j} \left[\overline{F \frac{\partial z}{\partial \lambda}} \Big|_{j-1} - \overline{F \frac{\partial z}{\partial \lambda}} \Big|_j \right] \quad (A-14)$$

Let's now look at the term $\frac{\partial \langle F \rangle}{\partial \phi}$.

From Equation (A-8) and Leibniz' rule,

$$\frac{\partial \langle F \rangle}{\partial \phi} = \frac{a^2 \cos \phi}{V} [I_\phi(\phi + \Delta \phi) - I_\phi(\phi - \Delta \phi)] - \frac{a^2 \sin \phi}{V} \psi - \frac{a^2 \cos \phi}{V^2} \psi \frac{\partial V}{\partial \phi} \quad (A-15)$$

where ψ represents the triple integral in (A-8), and

$$I_\phi(\xi) = \int_{\lambda - \Delta \lambda}^{\lambda + \Delta \lambda} \int_{z_1(\lambda', \xi)}^{z_2(\lambda', \xi)} F(\lambda', \xi, R) dR d\lambda'$$

$$\frac{\partial I_\phi}{\partial \xi} = \int_{\lambda - \Delta \lambda}^{\lambda + \Delta \lambda} \left\{ [F(\lambda', \xi, z_2) \frac{\partial z_2}{\partial \xi} - F(\lambda', \xi, z_1) \frac{\partial z_1}{\partial \xi}] + \int_{z_1}^{z_2} \frac{\partial F}{\partial \xi} dR \right\} d\lambda'$$

Integrating with respect to ξ

$$\int_{\xi - \Delta \xi}^{\xi + \Delta \xi} \frac{\partial I_\phi}{\partial \xi} d\xi = I_\phi(\xi + \Delta \xi) - I_\phi(\xi - \Delta \xi) = \frac{A}{a^2 \cos \phi} \left[\overline{F(\lambda, \phi, z_2) \frac{\partial z_2}{\partial \xi}} - \overline{F(\lambda, \phi, z_1) \frac{\partial z_1}{\partial \xi}} \right] + \frac{V}{a^2 \cos \phi} \left\langle \frac{\partial F}{\partial \xi} \right\rangle$$

where the overbar terms are defined as in (A-12).

Let $\xi = \phi$:

$$I_\phi(\phi + \Delta \phi) - I_\phi(\phi - \Delta \phi) = \frac{A}{a^2 \cos \phi} \left[\overline{F \frac{\partial z_2}{\partial \phi}} - \overline{F \frac{\partial z_1}{\partial \phi}} \right] + \frac{V}{a^2 \cos \phi} \left\langle \frac{\partial F}{\partial \phi} \right\rangle \quad (A-16)$$

Then from (A-15) we obtain

$$\begin{aligned} I_\phi(\phi + \Delta \phi) - I_\phi(\phi - \Delta \phi) &= \frac{V}{a^2 \cos \phi} \frac{\partial \langle F \rangle}{\partial \phi} + \psi \tan \phi + \frac{\psi}{V} \frac{\partial V}{\partial \phi} \\ &= \frac{V}{a^2 \cos \phi} \frac{\partial \langle F \rangle}{\partial \phi} + \tan \phi \frac{V \langle F \rangle}{a^2 \cos \phi} + \frac{\langle F \rangle}{a^2 \cos \phi} \frac{\partial V}{\partial \phi} \end{aligned}$$

Substituting this relationship into (A-16), yields

$$\frac{\partial \langle F \rangle}{\partial \phi} + \langle F \rangle \tan \phi + \frac{\langle F \rangle}{V} \frac{\partial V}{\partial \phi} = \frac{A}{V} \left[\overline{F \frac{\partial Z_2}{\partial \phi}} - \overline{F \frac{\partial Z_1}{\partial \phi}} \right] + \left\langle \frac{\partial F}{\partial \phi} \right\rangle$$

We conclude that on averaging the governing equation the term $\frac{1}{R} \frac{\partial F}{\partial \phi}$ becomes

$$\left\langle \frac{1}{R} \frac{\partial F}{\partial \phi} \right\rangle_j = \frac{1}{a} \left[\frac{\partial \langle F \rangle}{\partial \phi} \right]_j + \langle F \rangle_j \tan \phi + \frac{\langle F \rangle_j}{V_j} \frac{\partial V_j}{\partial \phi} + \frac{A}{V_j} \left(\overline{F \frac{\partial Z_{j-1}}{\partial \phi}} - \overline{F \frac{\partial Z_j}{\partial \phi}} \right) \quad (A-17)$$

Performing the $\langle \rangle$ averaging on the governing equations and using results (A-14), (A-17) and (2-11) we get

$$\left\langle \frac{\partial c}{\partial t} \right\rangle = \frac{\partial \langle c \rangle}{\partial t} + \frac{A}{V} \left[\overline{c \frac{\partial Z_1}{\partial t}} - \overline{c \frac{\partial Z_2}{\partial t}} \right] + \frac{\langle c \rangle}{V} \frac{\partial V}{\partial t}$$

$$\left\langle \frac{1}{R \cos \phi} \frac{\partial u c}{\partial \lambda} \right\rangle = \frac{1}{a \cos \phi} \frac{\partial \langle u c \rangle}{\partial \lambda} + \frac{\langle u c \rangle}{a \cos \phi} \frac{\partial \ln V}{\partial \lambda} + \frac{A}{a V \cos \phi} \left[\overline{u c \frac{\partial Z_1}{\partial \lambda}} - \overline{u c \frac{\partial Z_2}{\partial \lambda}} \right]$$

$$\left\langle \frac{1}{R} \frac{\partial v c}{\partial \phi} \right\rangle = \frac{1}{a} \frac{\partial \langle v c \rangle}{\partial \phi} + \frac{\langle v c \rangle}{a} \tan \phi + \frac{\langle v c \rangle}{a} \frac{\partial \ln V}{\partial \phi} + \frac{A}{a V} \left[\overline{v c \frac{\partial Z_1}{\partial \phi}} - \overline{v c \frac{\partial Z_2}{\partial \phi}} \right]$$

$$\left\langle \frac{\partial w c}{\partial z} \right\rangle = \frac{A}{V} \left[\overline{w c Z_2} - \overline{w c Z_1} \right]$$

$$\left\langle \frac{v c}{R} \tan \phi \right\rangle = \frac{\langle v c \rangle}{a} \tan \phi \approx 0$$

$$\left\langle \frac{2 c w}{R} \right\rangle \approx 0$$

Adding these terms and recalling the form (A-6) of the wind vector \underline{v} , we obtain the governing equations of layer-averaged species concentrations in curvilinear coordinates:

$$\begin{aligned} \frac{\partial \langle C \rangle_j}{\partial t} + \langle C \rangle_j \frac{\partial \ln V_j}{\partial t} + \mu_\lambda \frac{\partial \langle UC \rangle_j}{\partial \lambda} + \mu_\phi \frac{\partial \langle VC \rangle_j}{\partial \phi} + \mu_\lambda \langle UC \rangle_j \frac{\partial \ln V_j}{\partial \lambda} + \mu_\phi \langle VC \rangle_j \frac{\partial \ln V_j}{\partial \phi} \\ + \frac{A}{V_j} \left[\overline{c \frac{dH}{dt}}_j - 1 - c \overline{\frac{dH}{dt}}_j \right] = \langle S \rangle_j + \langle R \rangle_j + \langle W \rangle_j \end{aligned}$$

where

$$\frac{d}{dt} \equiv \frac{\partial}{\partial t} + \mu_\lambda u \frac{\partial}{\partial \lambda} + \mu_\phi v \frac{\partial}{\partial \phi} + w \frac{\partial}{\partial z}$$

$$\mu_\lambda = \frac{1}{a \cos \phi}$$

$$\mu_\phi = \frac{1}{a}$$

and $H_j(\lambda, \phi, t) = z_j(\lambda, \phi, t) - z.$

Appendix B. Criteria for Validity of the Steady-State Assumption
in Layer 0.

We shall investigate here the error incurred by the assumption of steady-state conditions in Layer 0 made in the formulation of the governing equations of this layer in Section 5. Since the meteorological conditions under which the steady-state assumption is most erroneous are those that confine mixing to Layers 1 and 0, we will consider only these 2 layers in the analyses below.

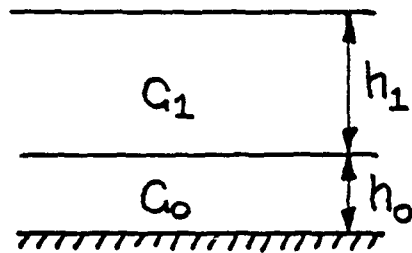


Figure B-1. Two-layer system for analysis of the steady-state mixing assumption.

Figure B-1 shows the two-layer system we will consider. The equations used in the model to describe concentrations c_1 and c_0 in the lowest 2 layers have the form (for inert species)

$$\partial c_1 / \partial t = - (c_1 - c_0) \sigma_w / h_1 \quad (B-1)$$

$$\partial c_0 / \partial t = - \beta c_0 / h_0 + S / h_0 + (c_1 - c_0) \sigma_w / h_0 \quad (B-2)$$

where σ_w is the rms turbulence velocity on surface H_0 which separates the layers. Here we have neglected horizontal transport and sources in Layer 1. The surface deposition process is so slow that no significant error arises in treating it with steady-state approximations, so we shall set the deposition velocity $\beta = 0$ in (B-2). The solution of the resulting equation is

$$c_1(t) = c_1(0) + \frac{St}{h_1} - \frac{h_0}{h_1\sigma_w} (S + \sigma_w\Delta_0)(1 - e^{-\lambda}) \quad (B-3)$$

$$c_0(t) = c_1(0) + \frac{St}{h_1} + (1 - e^{-\lambda})(S/\sigma_w - \frac{Sh_0}{h_1\sigma_w} - \frac{h_0\Delta_0}{h_1}) - \Delta_0 e^{-\lambda} \quad (B-4)$$

where

$$\Delta_0 = c_1(0) - c_0(0) \quad (B-5)$$

$$\lambda = \sigma_w t / h_0 \quad (B-6)$$

and where we have assumed

$$h_1 \gg h_0 \quad (B-7)$$

The corresponding steady-state (i.e., $\partial c_0 / \partial t = 0$) solutions are

$$c_{1ss}(t) = c_1(0) + St/h_1 \quad (B-8)$$

$$c_{0ss}(t) = c_1(0) + S/\sigma_w \quad (B-9)$$

Thus, the error committed in assuming the steady-state in Layer 0 is:

$$\epsilon_1 = c_{1ss} - c_1 = \frac{h_0}{h_1\sigma_w} (S + \sigma_w\Delta_0)(1 - e^{-\lambda}) \quad (B-10)$$

$$\epsilon_0 = c_{0ss} - c_0 = \frac{Sh_0}{h_1\sigma_w} [1 - e^{-\lambda}] + \frac{h_0\Delta_0}{h_1} (1 - e^{-\lambda}) + e^{-\lambda}(\Delta_0 + S/\sigma_w) \quad (B-11)$$

The steady-state solutions will have the largest error during early morning and later afternoon hours in rural areas as σ_w undergoes a rapid change. Suppose that in the hours just before sunrise, σ_w has some small value σ_{w0} and that within 1 time step Δt of the model simulation it jumps to a much larger value σ_w . From (B-8) and (B-9) we get

$$\Delta_0 = S(\Delta t/h_1 - 1/\sigma_{w0})$$

and hence

$$\epsilon_1 = \frac{h_0 S}{h_1 \sigma_w} \left(1 + \lambda \frac{h_0}{h_1} - \frac{\sigma_w}{\sigma_{w0}}\right) (1 - e^{-\lambda}) \quad (\text{B-12})$$

where λ is

$$\lambda = \frac{\sigma_w \Delta t}{h_0} \quad (\text{B-13})$$

and Δt and h_0 are given. We have already assumed that

$$h_1 \gg h_0$$

so if we multiply ϵ_1 by h_1 , we get a measure of the total mass lost or gained ΔM as a result of the steady-state assumption. Using a typical regional scale model time step $\Delta t = 600$ s, $h_0 = 30$ m ($h_1 \geq 300$ m) and a post-sunrise value $\sigma_w \approx 0.3$ m/s, we see that $\lambda \approx 6$ and that

$$\Delta M \approx -h_0 S / \sigma_{w0} \quad (\text{sunrise}) \quad (\text{B-14})$$

After sunrise there is a mass loss from the system equal to the quantity emitted by the sources in the time interval h_0/σ_{w0} required to traverse the depth of Layer 0 moving at a speed σ_{w0} . If $h_0 \approx 30$ and σ_{w0} is only several centimeters per second, ΔM can be quite sizable. However, the source emission rate prior to sunrise is usually a minimum and, moreover, the occurrence of a large increase in σ_w following sunrise occurs only in rural areas where S

is generally quite small. Nevertheless, a constraint on the nighttime depth of Layer 0 should be

$$h_0/\sigma_{w0} \leq \Delta t \quad (\text{nighttime}) \quad (\text{B-15})$$

In the late afternoon the reverse condition arises and σ_w drops abruptly in a short period. Assuming $\sigma_w/\sigma_{w0} \ll 1$ we get

$$\Delta M = S \Delta t \quad (\text{sunset}) \quad (\text{B-16})$$

That is, the system gains mass at sunset equal to the emissions of the sources in 1 time step.

During the nighttime hours when σ_w is increasing slowly,

$$\Delta M \sim \left(\frac{h_0}{h_1} \right) S \Delta t$$

We conclude that the steady-state approximation that we used in formulating the Layer 0 equation is acceptable provided that

$$h_0/h_1 \ll 1$$

and that during nighttime hours

$$h_0/\sigma_{w0} \leq \Delta t$$

where σ_{w0} is the rms vertical velocity fluctuation on surface H_0 and Δt is the model time step.

Appendix C. Explicit Forms of the b and g Matrix Elements b_{nm} , g_n That Enter in the $\hat{\gamma}$ Equation.

The $\hat{\gamma}$ equation (9-17), that describes the vertical material fluxes, source functions, surface deposition and the like contains the matrix b and the vector g , both of which are defined in Equation (9-13). Here we prescribe the exact forms of these two parameters.

Rewriting Equation (9-13) here for reference we have

$$\frac{1}{h_n} [F_{n-1,n} - F_{n,n}] + a_n c_n - S_n = b_{n1} c_1 + b_{n2} c_2 + b_{n3} c_3 - g_n \quad (C-1)$$

where h_n is the thickness of layer n , c_n is the average concentration in that layer, S_n is the emission rate, and $a_n = \partial \ln V_n / \partial t$.

Consider, for example, the Layer 1 equations. From Section 10 we have

$$F_{0,1} - F_{1,1} = (\sigma_{T0} - \sigma_{T1}) \beta c_1 + (1 - \sigma_{T0}) F_0 - (1 - \sigma_{T1}) [\omega_1 c_1 + (c_1 - c_2) \omega_{1m}] \quad (C-2)$$

In the case of ozone, we obtain from Equation (5-50)

$$F_0 (\text{ozone}) = w_{-\lambda_-} c_1 - Q_{O_3} w_{+\lambda_+} (1 - \xi) (1 - \alpha) c_1 + \frac{(1 - U_0)(1 - \alpha)v}{\beta_{O_3} + v} [\tilde{S}_{NO} - v\zeta Q_{O_3} c_1] \quad (C-3)$$

where

$$U_0 = \begin{cases} 1, & \text{is } \tilde{S}_{NO} > v\zeta Q_{O_3} \langle O_3 \rangle_1 \\ 0, & \text{otherwise} \end{cases} \quad (C-4)$$

and

$$Q_x = \frac{w_{-\lambda_-}}{w_{+\lambda_+} + (1 - \zeta) \beta_x} \quad x = O_3, NO, NO_2 \text{ or } x \quad (C-5)$$

Let

$$e_w^x = (\sigma_{T0} - \sigma_{T1})\beta_x - (1 - \alpha_{T1})(w_1 + w_{1m}) \quad (C-6)$$

$$e_o^x = w_{-\lambda_-} - w_{+\lambda_+}(1 - \xi)(1 - \alpha)Q_x \quad (C-7)$$

Then on substituting (C-2, 3 and 4) into (C-1) and noting that

$$a_1 = h_1/h_1$$

and that for ozone the emission rate S in any layer is identically zero, we get

Ozone (O_3)

$$b_{11} = \frac{1}{h_1} [e_w^{O_3} + h_1 + (1 - \sigma_{T0})(e_o^{O_3} - \frac{(1 - U_o)(1 - \alpha)v^2\epsilon Q_{O_3}}{\beta_{O_3} + v})]$$

$$b_{12} = \frac{1}{h_1} (1 - \sigma_{T1})w_{1m} \quad (C-8)$$

$$b_{13} = 0$$

$$g_1 = \frac{-(1 - U_o)(1 - \sigma_{T0})(1 - \alpha)v\tilde{S}_{NO}}{h_1(\beta_{O_3} + v)}$$

In a similar manner we find that for species NO

Nitric Oxide (NO)

$$b_{11} = \frac{1}{h_1} [e_w^{NO} + h_1 + (1 - \sigma_{T0})(e_o^{NO} - \frac{1 - \alpha}{v + \beta_{NO}} v^2\epsilon Q_{NO})]$$

$$b_{12} = \frac{1}{h_1} (1 - \sigma_{T1})w_{1m} \quad (C-9)$$

$$b_{13} = 0$$

$$g_1 = S_1^{NO} + \frac{U_o}{h_1} \frac{(1 - \sigma_{T0})(1 - \alpha)}{v + \beta_{NO}} (v\tilde{S}_{NO} - v^2\epsilon Q_{O_3} <O_3>_1)$$

Nitrogen Dioxide (NO₂)

$$b_{11} = \frac{1}{h_1} [e_w^{NO_2} + h_1 + (1 - \sigma_{TO})(e_o^{NO_2} - \frac{(1 - \alpha)}{v + \beta_{NO_2}} v^2 \epsilon Q_{NO_2})]$$

$$b_{12} = \frac{1}{h_1} (1 - \sigma_{T1}) w_{1m}$$

$$b_{13} = 0$$

$$g_1 = s_1^{NO_2} + \frac{(1 - \sigma_{TO})(1 - \alpha)}{h_1(v + \beta_{NO_2})} [v \tilde{S}_{NO_2} + U_o v^2 \epsilon Q_{O_3} <O_3>_1 + (1 - U_o) v \tilde{S}_{NO}]$$

(C-10)

Species χ (excluding O₃, NO and NO₂)

$$b_{11} = \frac{1}{h_1} [e_w^\chi + h_1 + (1 - \sigma_{TO})(e_o^\chi - \frac{1 - \alpha}{v + \beta_\chi} v^2 \epsilon Q_\chi)]$$

$$b_{12} = \frac{1}{h_1} (1 - \sigma_{T1}) w_{1m}$$

$$b_{13} = 0$$

$$g_1 = s_1^\chi + \frac{(1 - \sigma_{TO})(1 - \alpha)}{h_1(v + \beta_\chi)} v \tilde{S}_\chi$$

(C-11)

All Species

$$b_{21} = \frac{1}{h_2} (1 - \sigma_{T1}) (w_1 + w_{1m} - \bar{w}_{D1})$$

$$b_{22} = \frac{1}{h_2} [h_2 + \sigma_{T1} \beta + (1 - \sigma_{T1}) (\bar{w}_{D1} - w_{1m}) - \dot{z}_2 + \frac{\psi \sigma_c (\bar{w}_2 - \bar{w}_c)}{1 - \sigma_c}$$

$$+ \frac{f\theta}{\Delta\theta} (1 - \sigma_c + \sigma_c \psi)]$$

(C-12)

$$b_{23} = - \frac{f\theta}{h_2 \Delta\theta} (1 - \sigma_c)$$

$$g_2 = s_2$$

Ozone (O_3)

$$b_{31} = \frac{\psi M Q_{O_3}}{h_3} \left[\xi v \frac{1 - U_0}{v + \beta_{O_3}} + 1 - \xi \right]$$

$$b_{32} = \frac{1}{h_3} (1 - \psi) M$$

$$b_{33} = \frac{1}{h_3} (-M + \dot{H}_3 U_3)$$

$$g_3 = \frac{1}{h_3} \left[\frac{\psi M \xi (1 - U_0) \tilde{S}_{NO}}{\xi (v + \beta_{O_3})} + \dot{H}_3 U_3 c_{\infty}^{O_3} \right]$$

(C-13)

Nitric Oxide (NO)

$$b_{31} = \frac{\psi M Q_{NO}}{h_3} \left[\frac{\xi v}{v + \beta_{NO}} + 1 - \xi \right]$$

$$b_{32} = \frac{1}{h_3} (1 - \psi) M$$

$$b_{33} = \frac{1}{h_3} [-M + \dot{H}_3 U_3]$$

$$g_3 = \frac{1}{h_3} \left[\dot{H}_3 U_3 c_{\infty}^{NO} - \frac{\psi M \xi U_0}{v + \beta_{NO}} \left(\frac{\tilde{S}_{NO}}{\xi} - v Q_{O_3} \langle O_3 \rangle_1 \right) \right]$$

(C-14)

Nitrogen Dioxide (NO_2)

$$b_{31} = \frac{\psi M Q_{NO_2}}{h_3} \left[\frac{\xi v}{v + \beta_{NO_2}} + 1 - \xi \right]$$

$$b_{32} = \frac{1}{h_3} (1 - \psi) M$$

$$b_{33} = \frac{1}{h_3} (-M + \dot{H}_3 U_3)$$

(C-15)

$$g_3 = \frac{\dot{H}_3 U_3}{h_3} c_{\infty}^{NO_2} - \frac{\psi M \xi}{h_3 (\nu + \beta_{NO_2})} \left[\frac{\tilde{S}_{NO_2}}{\epsilon} + \nu Q_{O_3} U_{O_3} > 1 + (1 - U_0) \frac{\tilde{S}_{NO}}{\epsilon} \right]$$

Species χ (excluding O_3 , NO and NO_2)

$$b_{31} = \frac{\psi M Q_{\chi}}{h_3} \left[\frac{\xi \nu}{\nu + \beta_{\chi}} + 1 - \xi \right]$$

$$b_{32} = \frac{1}{h_3} (1 - \psi) M \quad (C-16)$$

$$b_{33} = \frac{1}{h_3} [-M + \dot{H}_3 U_3]$$

$$g_3 = \frac{1}{h_3} \dot{H}_3 U_3 c_{\infty}^{\chi} - \frac{\psi M \xi \tilde{S}_{\chi}}{h_3 \epsilon (\nu + \beta_{\chi})}$$

where

$$U_3 = \begin{cases} 1, & \text{if } \dot{H}_3 > 0 \\ 0, & \text{if } \dot{H}_3 \leq 0 \end{cases} \quad (C-17)$$

$$M = \sigma_c \left[\frac{\bar{w}_2 - \bar{w}_c}{1 - \sigma_c} + f\theta/\Delta\theta \right] \quad (C-18)$$

$$\dot{H}_3 = d\bar{H}_3/dt \quad (C-19)$$

We can check the correctness of the coefficients b_{nm} that we have just formulated by determining whether they satisfy certain integral constraints. In particular, in the absence of emissions ($\tilde{S} = S_n = 0$), chemical reactions ($R_n = 0$), and surface deposition ($\beta = 0$), the total mass of pollutant in a vertical column extending through all $3\frac{1}{2}$ layers must be constant. That is,

$$\frac{d}{dt} [h_1\gamma_1 + h_2\gamma_2 + h_3\gamma_3] = 0 \quad (C-20)$$

or

$$h_1 \frac{d\gamma_1}{dt} + h_2 \frac{d\gamma_2}{dt} + h_3 \frac{d\gamma_3}{dt} + \gamma_1 \dot{h}_1 + \gamma_2 \dot{h}_2 + \gamma_3 \dot{h}_3 = 0 \quad (C-21)$$

Since this condition must hold for any combination of values of γ_1 , γ_2 and γ_3 , we find from (9-14) that (C-21) holds in general only if the following three conditions are satisfied:

$$h_1 b_{11} + h_2 b_{21} + h_3 b_{31} - \dot{h}_1 = 0$$

$$h_1 b_{12} + h_2 b_{22} + h_3 b_{32} - \dot{h}_2 = 0 \quad (C-22)$$

$$h_1 b_{13} + h_2 b_{23} + h_3 b_{33} - \dot{h}_3 = 0$$

Consider for example the elements b_{nm} in the equations governing ozone (O_3). From (C-8, 12, and 13) we obtain with the aid of (5-13)

$$h_1 b_{11} + h_2 b_{21} + h_3 b_{31} - \dot{h}_1 = (1 - \sigma_{T0})w_{-\lambda-\alpha} + \psi M Q_{O_3} \quad (C-23)$$

On substituting the expressions for α (5-48), M (C-18), and Q_{O_3} (C-5) we find that the righthand side of (C-23) is identically zero, and hence the first condition in (C-22) is satisfied. In like manner we find that the expressions given above for b_{nm} for all species satisfy the consistency conditions (C-22).

TECHNICAL REPORT DATA <i>(Please read Instructions on the reverse before completing)</i>		
1. REPORT NO.	2.	3. RECIPIENT'S ACCESSION NO.
4. TITLE AND SUBTITLE A REGIONAL SCALE (1000 km) MODEL OF PHOTOCHEMICAL AIR POLLUTION Part 1. Theoretical Formulation		5. REPORT DATE
		6. PERFORMING ORGANIZATION CODE
7. AUTHOR(S) Robert G. Lamb		8. PERFORMING ORGANIZATION REPORT NO.
9. PERFORMING ORGANIZATION NAME AND ADDRESS Same as 12		10. PROGRAM ELEMENT NO. CDWA1A/02-1335 (FY-82)
		11. CONTRACT/GRANT NO.
12. SPONSORING AGENCY NAME AND ADDRESS Environmental Sciences Research Laboratory - RTP, NC Office of Research and Development Environmental Protection Agency Research Triangle Park, North Carolina 27711		13. TYPE OF REPORT AND PERIOD COVERED In-house
		14. SPONSORING AGENCY CODE EPA/600/09
15. SUPPLEMENTARY NOTES		
16. ABSTRACT A theoretical framework for a multi-day 1000 km scale simulation model of photochemical oxidant is developed. It is structured in a highly modular form so that eventually the model can be applied through straightforward modifications to simulations of particulates, visibility and acid rain. The model structure is based on phenomenological concepts and consists of 3 1/2 layers. The interface surfaces that separate the layers are functions of both space and time that respond to variations in the meteorological phenomena that each layer is intended to treat. Among the physical and chemical processes that the model is designed to handle are: horizontal transport; photochemistry and nighttime chemistry of the products and precursors of pollutant reactions; nighttime wind shear, stability stratification and turbulence "episodes" associated with the nocturnal jet; cumulus cloud effects - venting pollutants from the mixed layer, perturbing photochemical reaction rates, etc; mesoscale vertical motion induced by terrain and horizontal divergence of the large scale flow; subgrid scale chemistry processes -- resulting from emissions from sources smaller than the model's grid can resolve; natural sources of hydrocarbons, NO _x and stratospheric ozone; and others. Considerable attention is given to the question of the predictability of pollutant concentrations at long range and to the related problem of parameterization of "mesoscale" diffusion, the design of model "validation" experiments, and the like.		
7. KEY WORDS AND DOCUMENT ANALYSIS		
DESCRIPTORS	b. IDENTIFIERS/OPEN ENDED TERMS	c. COSATI Field/Group
18. DISTRIBUTION STATEMENT RELEASE TO PUBLIC	19. SECURITY CLASS (This Report) UNCLASSIFIED	21. NO. OF PAGES 239
	20. SECURITY CLASS (This page) UNCLASSIFIED	22. PRICE